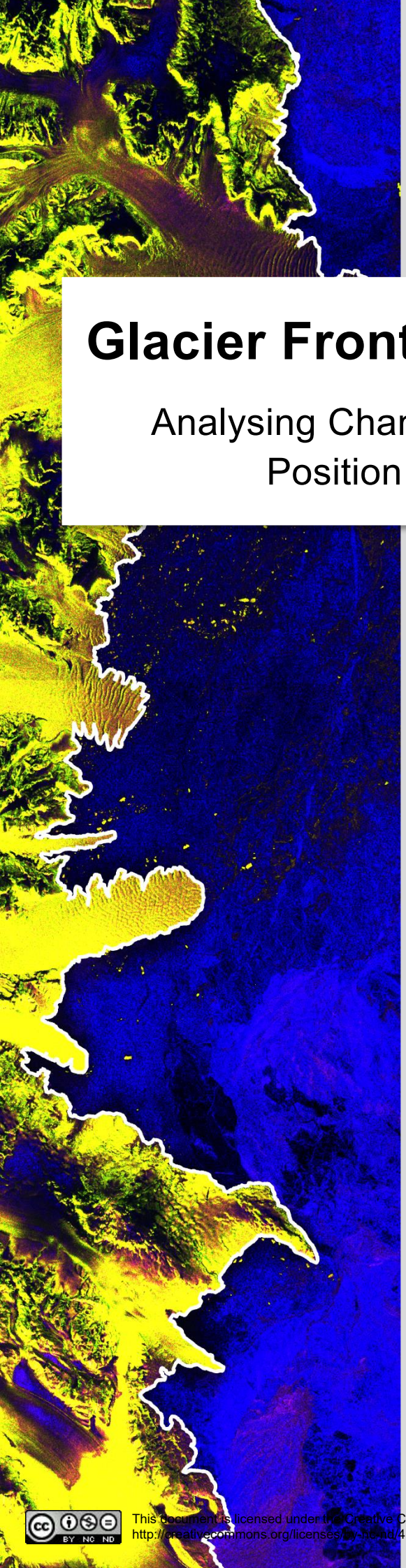

Glacier Front Dynamics of Antarctica -

Analysing Changes in Glacier and Ice Shelf Front Position based on SAR Time Series

Dissertation zur Erlangung der Doktorwürde
der Philosophischen Fakultät der
Julius-Maximilians-Universität Würzburg

vorgelegt von

Celia Amélie Baumhoer

August 2020

Julius-Maximilians-
UNIVERSITÄT
WÜRZBURG

Titelbild: Dual-polarisierte Sentinel-1 Szene (HH, HV, HH/HV) aufgenommen über Victoria Land, Ostantarktis. In weiß ist die automatisch abgeleitete Küstenlinie aufgetragen.

Eingereicht am: 18. August 2020

Von: Celia Amélie Baumhoer

Ort: Lehrstuhl für Fernerkundung der Julius-Maximilians-Universität Würzburg, in Kooperation mit dem Deutschen Fernerkundungsdatenzentrum (DFD) des Deutschen Zentrums für Luft- und Raumfahrt (DLR)

Erstbetreuerin: Prof. Dr. Claudia Künzer

Zweitbetreuer: Prof. Dr. Christof Kneisel

Tag des Kolloquiums: 5. Mai 2021

This dissertation was prepared in the department "Land Surface Dynamics" at the German Remote Sensing Data Center (DFD), Earth Observation Center (EOC) of the German Aerospace Center (DLR), Oberpfaffenhofen, Germany.

“You can have data without information,
but you cannot have information without data.”
— Daniel Keys Moran

Table of Contents

Table of Contents ..... **- 7 -**
Acknowledgments ..... **- 11 -**
English Summary ..... **- 13 -**
Kurzfassung ..... **- 15 -**
Resumen en Español ..... **- 17 -**
Chinese Summary (中文摘要) ..... **- 19 -**
List of Figures ..... **- 21 -**
List of Tables ..... **- 25 -**
List of Abbreviations ..... **- 27 -**
1 Introduction ..... **- 1 -**
1.1 Relevance of Antarctica ..... - 1 -
1.2 The Need for Monitoring Antarctic Glacier and Ice Shelf Front Changes ..... - 5 -
1.3 Research Focus and Objectives ..... - 6 -
1.4 Structure of the Thesis ..... - 9 -
2 Characteristics of Antarctica ..... **- 11 -**
2.1 Physiography ..... - 11 -
2.2 Climatic, Oceanic and Hydrological Setting ..... - 13 -
2.3 Recent Changes in the Antarctic Ice Sheet Mass Balance ..... - 19 -
3 A Review on Antarctic Glacier and Ice Shelf Front Dynamics ..... **- 23 -**
3.1 Background on Calving Front Dynamics ..... - 23 -
3.2 The History of Remote Sensing for Calving Front Mapping ..... - 25 -
3.3 Results of the Literature Review ..... - 26 -
3.3.1 Categorization of Calving Front Studies ..... - 27 -
3.3.2 Geospatial Agglomeration and Coverage of Calving Front Studies ..... - 29 -
3.3.3 Temporal Availability of Calving Front Measurements ..... - 34 -
3.3.4 A Compiled Dataset on Existing Calving Front Change Rates ..... - 35 -
3.4 Summary ..... - 38 -
4 Remote Sensing of Calving Fronts ..... **- 41 -**
4.1 The Potential of Satellite Sensors to Monitor Calving Fronts ..... - 41 -
4.1.1 Spectral Properties of Antarctic Surface Features and Clouds ..... - 42 -
4.1.2 Backscatter Characteristics of Ice Sheets and Sea Ice ..... - 43 -
4.1.3 Applied Optical and SAR Sensors ..... - 45 -
4.2 Existing Methods for Calving Front Extraction ..... - 47 -
4.2.1 Semi-Automatic Approaches ..... - 48 -

4.2.2 Automatic Approaches - 49 -
4.3 Methods to Measure Calving Front Location Change - 51 -
4.4 Summary - 52 -
5 A Novel Methodical Framework for Automatic Calving Front Extraction - 53 -
5.1 Deep Learning for Calving Front Detection - 53 -
5.2 Input Data - 55 -
5.2.1 Sentinel-1 - 55 -
5.2.2 TanDEM-X Polar DEM 90 - 57 -
5.2.3 Training Labels - 57 -
5.2.4 Training and Testing Areas - 58 -
5.3 Methodology - 60 -
5.3.1 SAR Pre-Processing - 62 -
5.3.2 U-Net based Image Segmentation - 62 -
5.3.3 Training the U-Net - 65 -
5.3.4 Post-Processing - 67 -
5.3.5 Time Series Generation - 67 -
5.4 Results - 69 -
5.4.1 Intra-Annual Patterns of Glacier and Ice Shelf Front Fluctuations - 69 -
5.4.1.1 Pine Island Glacier - 69 -
5.4.1.2 Glenzer Glacier - 70 -
5.4.1.3 Amery Ice Shelf - 73 -
5.4.1.4 Denman Glacier - 74 -
5.4.2 Intercomparison - 74 -
5.4.3 Fully-Automated Calving Front Time Series - 76 -
5.4.4 Coastline Extraction Results - 77 -
5.5 Accuracy Assessment - 80 -
5.5.1 Calculating Accuracies - 80 -
5.5.2 Results of the Accuracy Assessment - 81 -
5.5.2.1 Accuracies for Time Series - 81 -
5.5.2.2 Classification Accuracies - 82 -
5.5.2.3 Distance Measured Accuracies - 83 -
5.6 Implementation of *Antarctic*LINES for Circum-Antarctic Processing - 85 -
5.6.1 General Implementation of AntarcticLINES - 85 -
5.6.2 Circum-Antarctic Coastline Extraction - 87 -
5.6.3 The Extracted Coastline 2018 - 88 -
5.7 Discussion - 91 -
5.7.1 Performance - 91 -

5.7.2 Intra-Annual Calving Front Fluctuations ..... - 92 -
5.7.3 Fully-Automated Calving Front Time Series ..... - 94 -
5.7.4 Large-Scale Applicability ..... - 95 -
5.8 Summary ..... - 96 -
6 Environmental Drivers of Calving Front Change ..... - 99 -
6.1 Data Sets ..... - 100 -
6.1.1 Coastlines ..... - 100 -
6.1.2 ERA5 ..... - 100 -
6.1.3 Sea Ice Coverage ..... - 102 -
6.1.4 Sea Surface Temperature ..... - 102 -
6.2 Study Design ..... - 103 -
6.2.1 Calculating Calving Front Change ..... - 103 -
6.2.2 Climate Data Correlation ..... - 104 -
6.3 Results ..... - 105 -
6.3.1 Antarctic Coastal Change ..... - 106 -
6.3.2 Advance and Retreat of Antarctic Glaciers and Ice Shelves ..... - 106 -
6.3.3 Air Temperature ..... - 108 -
6.3.4 Sea Ice Days ..... - 110 -
6.3.5 Sea Surface Temperature ..... - 111 -
6.3.6 Snowmelt ..... - 112 -
6.3.7 Wind Direction ..... - 113 -
6.3.8 Correlation Matrix ..... - 114 -
6.4 Discussion ..... - 116 -
6.4.1 Antarctic Peninsula ..... - 116 -
6.4.2 West Antarctica ..... - 118 -
6.4.3 East Antarctica ..... - 120 -
6.4.4 A Circum-Antarctic Perspective ..... - 122 -
6.5 Summary ..... - 125 -
7 Synthesis & Outlook ..... - 127 -
7.1 Conclusive Findings ..... - 127 -
7.2 Towards the Monitoring of Antarctic Calving Fronts ..... - 132 -
8 References ..... - 135 -
Eidesstattliche Erklärung ..... - 159 -
Curriculum Vitae – C. Baumhoer ..... - 161 -

Acknowledgments

This dissertation would not have been possible without the support and help of many people to whom I would like to express sincere gratitude:

To my mentor and supervisor at the German Remote Sensing Data Center (DFD), at the German Aerospace Center (DLR), Prof. Dr. Claudia Kuenzer, for her constant support and straightforwardness. Without her clear guidance, experience, and forward-thinking attitude it would have never been possible to finish this dissertation within three years. Frequent feedback on all aspects of my work could always bring my research to a higher level. I very much appreciate her commitment to advance my scientific career.

To my supervisors at the University of Wuerzburg, Prof. Dr. Christof Kneisel, and Prof. Dr. Heiko Paeth, for their discussions and feedback on my research and for agreeing to be a referee of this thesis.

To Dr. Andreas Dietz, for his frequent support, advice, and feedback on my work. For creating an open and free working atmosphere allowing independent work within a great team.

To the institute leader of DFD-DLR, Prof. Dr. Stefan Dech, for his keen interest in my work and his advice. I am very thankful for his experience and the willingness to get to the bottom of a research problem by fruitful discussions.

To my colleagues from DFD-DLR, especially Mariel Dirscherl for discussing Antarctic related research, visiting conferences together, proofreading, and her helpful comments. My thanks go to Stefan Mayr for great coffee break discussions and the countless mountain adventures. I very much appreciate the support of Julian Zeidler for maintaining and developing the server infrastructure at DFD-LAX. Furthermore, I would like to thank my colleagues at DLR which accompanied the journey of this PhD: Gustav Grether, Ya-Lun Tsai, Jonas Koehler, Dr. Sebastian Roeßler, Dr. Marco Ottinger, Soner Üreyen, Sophie Reinermann, Aiym Orynbaikyzy, and Thorsten Hoeser. Additional thanks go to Dr. Zhongyang Hu and Dr. Emmanuel Da Ponte for translating the summary of this thesis.

To my wonderful parents Carmen and Christoph Baumhoer, for their motivation and endless trust in my decisions. For the financial security they provided and their never-ending support which should never be taken for granted.

To my brother Cornelius Baumhoer for his support and the great time, we spend together.

To Regina Fleischmann for motivating me to do a PhD, the countless travels all over the world and the best study years we spend together at University. Without her, I would never have taken the path of a scientific career.

To Johannes, for his love, patience, and the ability to always cheer me up even during the most intense stages of this PhD.

Munich, August 2020 Celia Baumhoer

English Summary

The Antarctic Ice Sheet stores ~91% of the global ice volume which is equivalent to a sea-level rise of 58.3 meters. Recent disintegration events of ice shelves and retreating glaciers along the Antarctic Peninsula and West Antarctica indicate the current vulnerable state of the Antarctic Ice Sheet. Glacier tongues and ice shelves create a safety band around Antarctica with buttressing effects on ice discharge. Current decreases in glacier and ice shelf extent reduce the effective buttressing forces and increase ice discharge of grounded ice. The consequence is a higher contribution to sea-level rise from the Antarctic Ice Sheet. So far, it is unresolved which proportion of Antarctic glacier retreat can be attributed to climate change and which part to the natural cycle of growth and decay in the lifetime of a glacier. The quantitative assessment of the magnitude, spatial extent, distribution, and dynamics of circum-Antarctic glacier and ice shelf retreat is of utmost importance to monitor Antarctica's weakening safety band. In remote areas like Antarctica, earth observation provides optimal properties for large-scale mapping and monitoring of glaciers and ice shelves. Nowadays, the variety of available satellite sensors, technical advancements regarding spatial resolution and revisit times, as well as open satellite data archives create an ideal basis for monitoring calving front change. A systematic review conducted within this thesis revealed major gaps in the availability of glacier and ice shelf front position measurements despite the improved satellite data availability. The previously limited availability of satellite imagery and the time-consuming manual delineation of calving fronts did neither allow a circum-Antarctic assessment of glacier retreat nor the assessment of intra-annual changes in glacier front position. To advance the understanding of Antarctic glacier front change, this thesis presents a novel automated approach for calving front extraction and explores drivers of glacier retreat.

A comprehensive review of existing methods for glacier front extraction ascertained the lack of a fully automatic approach for large-scale monitoring of Antarctic calving fronts using radar imagery. Similar backscatter characteristics of different ice types, seasonally changing backscatter values, multi-year sea ice, and mélange made it challenging to implement an automated approach with traditional image processing techniques. Therefore, the present abundance of satellite data is best exploited by integrating recent developments in big data and artificial intelligence (AI) research to derive circum-Antarctic calving front dynamics. In the context of this thesis, the novel AI-based framework "*Antarctic*LINES" (Antarctic G**l**acier and **I**ce Shelf Fro**n**t Tim**e** **S**eries) was created which provides a fully automated processing chain for calving front extraction from Sentinel-1 imagery. Open access Sentinel-1 radar imagery is an ideal data source for monitoring current and future changes in the Antarctic coastline with revisit times of less than six days and all-weather imaging capabilities. The developed processing chain includes the pre-processing of dual-polarized Sentinel-1 imagery for machine learning applications. 38 Sentinel-1 scenes were used to train the deep learning architecture U-Net for image segmentation. The trained weights of the neural network can be used to segment Sentinel-1 scenes into land ice and ocean. Additional post-processing ensures even more accurate results by including morphological filtering before extracting the final coastline. A comprehensive accuracy assessment has proven the correct extraction of the coastline. On average, the automatically extracted coastline deviates by 2-3 pixels (93 m) from a manual delineation. This accuracy is in range with deviations between manually delineated coastlines from different experts.

For the first time, the fully automated framework *Antarctic*LINES enabled the extraction of intra-annual glacier front fluctuations to assess seasonal variations in calving front change. Thereby, for example, an increased calving frequency of Pine Island Glacier and a beginning disintegration of Glenzer Glacier were revealed. Besides, the extraction of the entire Antarctic coastline for 2018 highlighted the large-scale applicability of the developed approach. Accurate results for entire Antarctica were derived except for the Western Antarctic Peninsula where training imagery was not sufficient and should be included in future studies.

Furthermore, this dissertation presents an unprecedented record of circum-Antarctic calving front change over the last two decades. The newly extracted coastline for 2018 was compared to previous coastline products from 2009 and 1997. This revealed that the Antarctic Ice Sheet shrank 29,618±1193 km^2 in extent between 1997-2008 and gained an area of 7,108±1029 km^2 between 2009-2018. Glacier retreat concentrated along the Antarctic Peninsula and West Antarctica. The only East Antarctic coastal sector primarily experiencing calving front retreat was Wilkes Land in 2009-2018. Finally, potential drivers of circum-Antarctic glacier retreat were identified by combining data on glacier front change with changes in climate variables. It was found that strengthening westerlies, snowmelt, rising sea surface temperatures, and decreasing sea ice cover forced glacier retreat over the last two decades. Relative changes in mean air temperature could not be identified as a driver for glacier retreat and further investigations on extreme events in air temperature are necessary to assess the effect of atmospheric forcing on frontal retreat. The strengthening of all identified drivers was closely connected to positive phases of the Southern Annular Mode (SAM). With increasing greenhouse gases and ozone depletion, positive phases of SAM will occur more often and force glacier retreat even further in the future.

Within this thesis, a comprehensive review on existing Antarctic glacier and ice shelf front studies was conducted revealing major gaps in Antarctic calving front records. Therefore, a fully automated processing chain for glacier and ice shelf front extraction was implemented to track circum-Antarctic calving front fluctuations on an intra-annual basis. The large-scale applicability was certified by presenting two decades of circum-Antarctic calving front change. In combination with climate variables, drivers of recent glacier retreat were identified. In the future, the presented framework *Antarctic*LINES will greatly contribute to the constant monitoring of the Antarctic coastline under the pressure of a changing climate.

Kurzfassung

Der antarktische Eisschild speichert ~91 % des globalen Eisvolumens. Ein gänzliches Abschmelzen des Eisschildes hätte global einen Meeresspiegelanstieg von 58,3 Metern zur Folge. Der aktuelle Zerfall von Eisschelfen und der Gletscherrückgang entlang der Antarktischen Halbinsel und Westantarktis verdeutlichen den vulnerablen Status des antarktischen Eisschildes. Gletscherzungen und Eisschelfe säumen die antarktische Küstenlinie und halten die Eisströme Richtung Ozean zurück. Ein Rückzug der Eisschelfe und Gletscher vermindert den Rückhalteeffekt und führt zu zunehmenden Gletscher-Fließgeschwindigkeiten in Richtung Ozean. Der dadurch verursachte Masseverlust trägt zum globalen Meeresspiegelanstieg bei. Bislang ist ungeklärt, welcher Anteil des antarktischen Gletscherrückgangs auf den Klimawandel und welcher auf den natürlichen Kalbungszyklus der Gletscher und Eisschelfe zurückzuführen ist. Aufgrund des vermehrten Zerfalls von Eisschelfen in den letzten Dekaden ist es von großer Wichtigkeit, den Gletscherrückgang zu quantifizieren und dessen Ausmaß, räumlichen Ausdehnung, Verteilung und Dynamik zirkumantarktisch zu erfassen, um mögliche Auswirkungen auf den Meeresspiegelanstieg frühzeitig zu erkennen.

In abgelegenen Regionen wie der Antarktis bietet die Erdbeobachtung optimale Voraussetzungen für das großflächige Kartieren und Beobachten von Gletschern und Eisschelfen. Heute stellt die Fülle an frei-verfügbaren Satellitendaten verschiedener Sensoren, in Kombination mit technischen Neuerungen hinsichtlich der räumlichen und zeitlichen Abdeckung, eine ideale Basis für das Monitoring der Kalbungsfronten dar. Trotz der guten Datenverfügbarkeit hat ein umfassender Literaturüberblick − welcher im Rahmen dieser Dissertation durchgeführt wurde − große Lücken in der Verfügbarkeit von Gletscher- und Eisschelffrontpositionsmessungen festgestellt. Die zuvor limitierte Verfügbarkeit von Satellitendaten und die zeitaufwändige manuelle Ableitung der Küstenlinie machten eine zirkumantarktische Beurteilung des Gletscherrückgangs und die intra-annuelle Analyse von Gletscherfrontpositionen unmöglich. Für ein besseres Verständnis antarktischer Gletscherfrontveränderungen, präsentiert diese Dissertation ein neues, automatisiertes Konzept zur Kalbungsfrontextraktion und untersucht ob klimatische Faktoren für den beobachteten Kalbungsfrontenrückgang verantwortlich sind.

Anhand des Literaturüberblicks konnte festgestellt werden, dass bis dato kein komplett automatisiertes Verfahren für die Gletscherfrontextraktion aus großvolumigen Radarsatellitenbildern bestand. Ähnliche Rückstreuwerte von verschiedenen Eistypen, saisonal veränderliche Rückstreuwerte, mehrjähriges Meereis und Eis-Mélange erschwerten die Entwicklung eines automatisierten Ansatzes mit traditionellen Bildverarbeitungsansätzen. Doch die Neuerungen in den Bereichen „Big Data“ und der künstlichen Intelligenz (KI) ermöglichen es, die heutige Fülle an Satellitendaten für die Ableitung von Kalbungsfronten zu nutzen. Im Rahmen dieser Dissertation wurde das neuartige Framework “*Antarctic*LINES” (Antarctic G**l**acier and **I**ce Shelf Fro**n**t Tim**e** **S**eries) kreiert, welches eine komplett automatisierte, KI-basierte Prozessierungskette für die Gletscherfrontenextraktion von Sentinel-1 Daten beinhaltet. Frei verfügbare Sentinel-1 Daten sind ideal, um derzeitige und zukünftige Veränderungen der antarktischen Küstenlinie zu beobachten, da die Orbitwiederholrate weniger als sechs Tage beträgt und die Bildgebung wetterunabhängig ist. Die entwickelte Prozessierungskette beinhaltet die Vorprozessierung, Maskierung und Zerlegung der Satellitenbilder in kleinere Kacheln. Es wurden 38 Sentinel-1 Szenen genutzt, um die Deep Learning Architektur U-Net für eine Bildsegmentierung zu trainieren. Die trainierten Gewichte des Neuronalen Netzes können

genutzt werden, um Sentinel-1 Szenen in die Klassen Ozean und Eis zu segmentieren. Eine zusätzliche Nachprozessierung ermöglicht noch genauere Ergebnisse durch morphologisches Filtern, bevor die finale Küstenlinie zwischen den beiden Klassen extrahiert wird. Eine umfangreiche Genauigkeitsauswertung hat ergeben, dass die automatisch abgeleitete Küstenlinie im Mittel 2-3 Pixel (93 m) von einer manuell abgeleiteten Küstenlinie abweicht. Diese Genauigkeit ist im Rahmen der durchschnittlichen Abweichungen von manuell abgeleiteten Küstenlinien verschiedener Experten.

Erstmals ermöglicht das Framework AntarcticLINES die automatisierte Extraktion von intra-annuellen Gletscherfrontfluktuationen, um saisonale Variationen in der Kalbungsfrontänderung zu untersuchen. Dadurch konnte beispielsweise eine erhöhte Kalbungsfrequenz des Pine-Island-Gletschers festgestellt werden. Die Extraktion der antarktischen Küstenlinie für 2018 zeigt die mögliche Anwendung der entwickelten Methodik für großräumige Gebiete. Für den Großteil der Antarktis wurden genaue Ergebnisse erzielt, lediglich entlang der westlichen Antarktischen Halbinsel fehlten Trainingsdaten, welche in zukünftigen Studien inkludiert werden sollten.

Darüber hinaus präsentiert diese Dissertation einen bis dato beispiellosen Datensatz zu zirkumantarktischen Veränderungen der Kalbungsfronten über die letzten zwei Jahrzehnte. Die neu extrahierte Küstenlinie für das Jahr 2018 wurde mit früheren Küstenlinienprodukten von 2009 und 1997 verglichen. Dies hat offengelegt, dass der Antarktische Eisschild zwischen 1997 und 2008 eine Fläche von 29,618±1193 km^2 verlor und zwischen 2009 und 2018 eine Fläche von 7,108±1029 km^2 dazugewann. Der Gletscherrückgang konzentrierte sich entlang der Antarktischen Halbinsel und der Westantarktis. Der einzige ostantarktische Sektor, in dem sich simultaner Gletscherrückgang zeigte, war Wilkes Land in den Jahren 2009 bis 2018. Im Anschluss wurden Ursachen für den Antarktischen Gletscherrückgang durch die Korrelation mit Klimavariablen identifiziert. Zunehmende Westwinde, Schneeschmelze, ansteigende Meeresoberflächentemperaturen und zurückgehendes Meereis begünstigten den Gletscherrückgang in den letzten zwei Dekaden. Relative Veränderungen in der durchschnittlichen Lufttemperatur konnten nicht als Ursache für den Gletscherrückgang identifiziert werden und weiter Analysen zu Extremereignissen in der Lufttemperatur sind nötig um Frontveränderungen verursacht durch atmosphärischen Antrieb besser verstehen zu können. Die Verstärkung aller identifizierten Treiber ist eng mit positiven Phasen des Southern Annular Mode (SAM) verbunden. In Anbetracht ansteigender Konzentrationen von Treibhausgasen und dem Ozonrückgang werden positive Phasen des SAMs in Zukunft öfter auftreten, was in Folge den Gletscherrückgang noch weiter vorantreiben kann.

Zusammengefasst wurde im Rahmen dieser Dissertation ein umfassender Literaturüberblick zu existierenden Gletscher- und Eisschelffrontstudien durchgeführt, welcher größere Lücken in Kalbungsfrontstudien aufzeigte. Es wurde eine voll-automatisierte Prozessierungskette entwickelt, um zirkumantarktische Kalbungsfrontpositionen intra-annuell beobachten zu können und die Datenlücken zu schließen. In Kombination mit Klimavariablen wurden treibende Kräfte, die den aktuellen Gletscherrückgang begünstigen, identifiziert. In Zukunft wird das präsentierte Framework *Antarctic*LINES zur konstanten Beobachtung der Antarktischen Küstenlinie eingesetzt, um Veränderungen in Anbetracht eines sich ändernden Klimas zu analysieren.

Resumen en Español

La capa de hielo de la Antártida almacena el 91% del volumen de hielo mundial, lo que equivale a un aumento de 5.8 metros del nivel del mar. Los acontecimientos recientes referentes a la desintegración de las plataformas de hielo y el retroceso de los glaciares a lo largo de la Península Antártica y la Antártida Occidental indican la actual vulnerabilidad de la capa de hielo Antártica. Las lenguas de los glaciares y las plataformas de hielo proveen una banda de seguridad alrededor de la Antártida al crear efectos de refuerzo en la descarga de hielo. Sin embargo la actual disminución de la extensión de los glaciares y las plataformas de hielo reduce los efectos de refuerzo aumentando la descarga de hielo pulverizado contribuyendo directamente al incremento del nivel del mar. Hasta el momento no se ha definido si el retroceso de los glaciares antárticos puede ser atribuido al cambio climático o al ciclo natural de crecimiento y decadencia del tiempo de vida de un glaciar. La evaluación cuantitativa de la magnitud, la extensión espacial, la distribución y la dinámica del retroceso de los glaciares y la plataforma de hielo de la Antártida es de suma importancia para monitorear el debilitamiento de la banda de seguridad de la Antártida. En zonas remotas como la Antártida, la observación de la Tierra proporciona propiedades óptimas para la cartografía, la observación de los glaciares a gran escala y las plataformas de hielo. Actualmente, la variedad de sensores satelitales disponibles, los avances técnicos en cuanto a resolución espacial y tiempos de revisión, así como también los archivos abiertos de datos satelitales crean una plataforma ideal para la vigilancia de los cambios de frente. No obstante, un examen sistemático realizado en el marco de esta tesis reveló importantes vacíos en la disponibilidad de las mediciones de la posición del frente de los glaciares y las plataformas de hielo. Anteriormente la disponibilidad limitada de imágenes satelitales y la parsimoniosa delimitación manual de los partos glaciares no permitían una evaluación circunnacional del retroceso de los glaciares ni la evaluación de los cambios intra-anuales de la posición del frente de los glaciares. Con el fin de incrementar la comprensión de los cambios de frente de los glaciares antárticos, esta tesis presenta un novedoso enfoque automatizado para la extracción de los frentes de parto.

Un examen exhaustivo de los métodos existentes para la extracción del frente de los glaciares determinó la falta de un enfoque totalmente automático por medio de la utilización de las imágenes de radar. Las características similares de retrodispersión de los diferentes tipos de hielo, los valores de retrodispersión cambiantes en función de la estación, el hielo marino plurianual y la combinación de estos factores dificultan la incorporación de un enfoque automatizado con las técnicas tradicionales de procesamiento de imágenes. Por consiguiente, la actual abundancia de datos satelitales es utilizado mediante la integración de recientes avances en la investigación relacionados utilización de grandes base de datos en combinación con inteligencia artificial para derivar la dinámica del frente de parto circunnacional de la Antártida. El enfoque desarrollado se basa en las imágenes de radar de libre acceso Sentinel-1, ya que presenta una fuente de datos ideal para monitorear cambios presentes y futuros en la costa antártica, con tiempos de revisión de menos de seis días y capacidad de obtención de imágenes para todo tipo de clima.

El novedoso marco de trabajo creado AntarcticLINES (Antarctic Glacier and Ice Shelf Front Time Series) proporciona una cadena de procesamiento totalmente automatizada elaborada con el fin de extraer las ubicaciones de los frentes de parto por medio imágenes Sentinel-1. La cadena de procesamiento incluye el pre-procesamiento,

enmascaramiento y mosaico de imágenes Sentinel-1 de doble polarización. Los mosaicos de imágenes comprenden 38 escenas de Sentinel-1 que se utilizaron con el fin de entrenar la arquitectura de aprendizaje profundo U-Net para conseguir la segmentación de imágenes. Los pesos entrenados en la red neuronal pueden ser usados para segmentar cualquier escena de Sentinel 1 en la Antártida en el hielo terrestre y el océano. Durante el post-procesamiento, se aplica el filtrado morfológico para finalmente extraer la frontera entre la capa de hielo y el océano que representa la costa antártica. Una exhaustiva evaluación de precisión demostró la correcta extracción de la línea costera. En promedio, los frentes extraídos automáticamente se desvían 2-3 píxeles (93 m) de las delineaciones manuales. Esto se encuentrz en el rango de las desviaciones entre las líneas costeras delineadas manualmente por diferentes expertos. Por primera vez, un marco de trabajo totalmente automatizado AntarcticLINES permite derivar las fluctuaciones intra-anuales del frente de los glaciares con el fin de evaluar las variaciones estacionales en el cambio del frente de parto. La extracción de todo el litoral antártico referentes al año 2018 evidencia la amplia aplicabilidad del enfoque desarrollado. Actualmente es pposible derivar resultados precisos para toda la Antártida, con excepción de la Península Antártica occidental, donde las imágenes de entrenamiento no fueron suficientes y deberían considerarse para estudios futuros.

Asimismo, esta disertación presenta un registro sin precedentes de los cambios en el frente de parto de la circunnavegación antártica en las últimas dos décadas. La costa extraída para el año 2018 se comparó con los productos costeros anteriores del 2009 y 1997. La capa de hielo antártico se redujo en extensión alrededor de 29618±1193 km2 entre 1997-2008 e incremento en una superficie de 7108±1029 km2 entre 2009-2018. El retroceso de los glaciares fue identificado a lo largo de la Península Antártica y la Antártida Occidental. El único sector costero de la Antártida oriental que experimentó un retroceso simultáneo del frente de parto fue el Wilkes Land entre periodo 2009-2018. Por último, se identificaron los posibles factores que impulsaban el retroceso de los glaciares de la circunnavegación antártica combinando los datos sobre el retroceso de los glaciares con los cambios en las variables climáticas. Se constató que el fortalecimiento de las zonas occidentales, el deshielo, el aumento de las temperaturas de la superficie del mar y la disminución de la cubierta de hielo marino han venido contribuyendo al retroceso de los glaciares en los dos últimos decenios. Los cambios relativos en la temperatura media del aire no pudieron identificarse como factores que impulsen el retroceso de los glaciares. El fortalecimiento de todos los contribuyentes identificados estaba estrechamente relacionado con las fases positivas del Modo Anular Austral (SAM). Con respecto al aumento de los gases de efecto invernadero y el deterioro de la capa del ozono, las fases positivas del SAM se producirán con mayor frecuencia y obligarán a los glaciares a retroceder aún más en el futuro.

Para concluir, en el marco de esta tesis se realizó un examen exhaustivo de los estudios existentes sobre el frente de los glaciares y las plataformas de hielo de la Antártida que reveló que existen importantes vacíos en los estudios referentes al frente de parto de la Antártida. Se puso en marcha un flujo de procesamiento totalmente automatizada para la extracción del frente de los glaciares y las plataformas de hielo a fin de establecer un monitoreo de las fluctuaciones estacionales del frente de parto. La aplicabilidad a gran escala se certificó presentando dos decenios de cambios en los frentes de parto de la circunnavegación antártica. En combinación con las variables climáticas, se identificaron los posibles factores del reciente retroceso de los glaciares. En el futuro, el marco de trabajo presentado AntarcticLINES ayudara contribui al monitoreo constante de la costa antártica amenazada bajo la presión de un clima cambiante.

Chinese Summary (中文摘要)

南极冰盖储存了全球91％的冰量，若全部融化，海平面将上升58.3米。近期，南极半岛和西南极洲冰架的崩解和后退事件表明南极冰盖正处于脆弱状态。冰舌和冰盖通过排冰从而产生了支撑效应，在南极洲外筑起了安全带。然而，由于当前冰川和冰架的后退降低了这一效应，与此同时，陆上的排冰量的增加直接加剧了海平面上升。目前为止，还不能断定南极冰川的退缩是由于气候变化还是在冰川生命周期内的自然增减。定量评估环南极洲的冰川与冰盖后退的规模，空间范围，分布和动态对于监测南极洲日益弱的安全带至关重要。对于像南极洲这样的偏远地区，对地观测是对冰川和冰架大范围制图与监测的最佳选择。如今多种多样的卫星传感器，在时空分辨率上的技术革新，以及卫星数据库的开放为监测崩解创造了理想的基础。但是本文中系统性的文献综述部门表明：在冰川去冰架前缘位置的测量数据的可用性方面存在巨大的研究缺口。以前受制于卫星数据的可用性以及人工描绘的时间成本，难以达成环南极洲的冰川后退评估抑或是冰川前缘位置的年内变化观测。为了深化对南极冰川前缘的变化的理解，本文提出了一种创新的自动的崩解前缘的提取。

对于现存的冰川前缘提取的全面的文献综述指出了基于雷达数据全自动提取方法的短缺。全自动地利用传统图像处理方法进行提取主要存在来自以下几个方面的挑战：不同冰面类型在后向散射信号特征上的相似性，后向散射信号的季节性变化，多年海冰以及混合物的影响。因此，结合大数据以及人工智能研究，本文运用了丰富的卫星数据去提取环南极洲崩解前缘的动态。在监视南极海岸线当前和未来变化的数据集方面，因为开放的哨兵1号雷达图像具备少于六天的重访周期而且可以达到全天候的成像能力，故而其是一个理想数据源。

本文开发了一种名为AntarcticLINES（**A**ntarctic **G**l**a**cier and **I**ce Shelf Fro**n**t Tim**e** **S**eries）的框架，从而为全自动化地利用哨兵1号图像提取崩解前缘位置提供了可能。整个处理链包含了预处理，遮罩，与缝补哨兵1号双极化图像。38景哨兵1号图像块使用在了对U-Net深度学习架构进行图像的语义分割训练。训练好的神经网络权重用在了接下来对哨兵1号数据的南极陆冰与海洋的分割。在后处理过程中，地貌滤波器被运用在了对冰盖与海洋边界的最后区分，用以呈现南极大陆的海岸线。在之后的全面的准确性评估证明了海岸线的正确提取性。自动提取的前缘与人工描绘的前缘的平均偏差在2-3个相元之间（93m）。这个水平达到了不同专家人工描绘结果之间的精度差异。全自动的AntarcticLINES框架首次实现了对年度内对冰川前缘

波动的提取，从而用以评估崩解前缘变化的季节性变化。对2018年度的整个南极海岸线的提取结果突显了该方法的大规模适用性。对于之后的研究，除了训练集合不足的西南极半岛，提取整个南极大陆精确的海岸线使可能的。

此外，本文史无前例地提供了近二十年来环南极大陆的崩解前缘的变化。同时将最新提取的2018年海岸线与之前1997年以及2009年的海岸线产品进行了比较。南极冰盖在1997-2008年之间收缩了29618±1193 km^2，在2009-2018年之间增加了7108±1029 km^2。南极冰川的后退主要集中在南极半岛和南极西部。在2009-2018年期间，威尔克斯地是南极东部沿海唯一的同时间内发生前缘崩解的地区。最后，为了确定了南极洲冰川退缩的潜在驱动因素，本文结合分析了冰川退缩数据与气候变量变化。研究发现在过去的二十年，冰川的后退与西风的增强，冰雪的融化，海温的上升与海冰的缩减有关。平均气温的相对变化，没有被认定为冰川退缩的驱动力。所有确定的驱动因子的加强都与南环空模式（SAM）的正相紧密关联。在温室气体不断增加和臭氧减少的背景下，SAM的正相将更频繁地发生，并在未来迫使冰川进一步退缩。

总而言之，在本论文中，对现有的南极冰川和冰架前缘的研究综述揭示了在环南极洲崩解前缘方面存在主要研究空白。 一种全自动的南极冰川和冰架前缘提取处理链，用在了追踪崩解前缘的季节性波动。对于过去20年的环南极大陆崩解前缘的变化提取结果证明了该方法的大范围适用性。结合气候变量的分析明确了近期冰川退缩的潜在动因。将来，本文提出的AntarcticLINES框架讲促进南极海岸线在气候变化背景下的持续监测。

List of Figures

Figure 1.1: Map of Antarctica visualizing territorial claims and locations of national research facilities ..... - 2 -

Figure 1.2: Cumulative ice sheet mass loss and according sea level contribution from ice sheets between 1992 and 2016. ..... - 3 -

Figure 1.3: Ice shelf features and processes. ..... - 4 -

Figure 2.1: Map of Antarctica showing major ice shelves and glaciers. Climate diagrams for O'Higgins Station on the Peninsula, Casey Station in Wilkes Land and the South Pole ..... - 12 -

Figure 2.2: Topography of Antarctica. TanDEM-X surface elevation model of the Antarctic Ice Sheet (left) and Antarctic bed topography (right) ..... - 13 -

Figure 2.3: Ocean currents around Antarctica. Lines show the southern ocean fronts. Mean surface speed is displayed in the background ..... - 14 -

Figure 2.4: Climatological Parameters of Antarctica. (a) Mean air temperature 2 m above ground derived from ERA5 monthly means data between 1982 and 2019. (b) Surface meltwater production between 1999 and 2009 from Trusel et al. ..... - 16 -

Figure 2.5: Air temperature trend between 1982 and 2019 calculated based on ERA5 hourly data on single levels ..... - 17 -

Figure 2.6: Mass loss of the Antarctic Ice Sheet and ice shelves. (a) Elevation change of the Antarctic Ice Sheet between 1992 and 2017 (Shepherd *et al.* 2019). (b) Ice discharge of the Antarctic Ice Sheet and mass budget between 2008 and 2015 (Gardner *et al.* 2018). ..... - 20 -

Figure 2.7: (a) Mass loss share between ice shelf melting and iceberg calving (Rignot *et al.* 2013). (b) Thickness change of ice shelves and glacier tongues between 1994 and 2012 (Paolo *et al.* 2015b). ..... - 21 -

Figure 3.1: Various ice fronts in SAR (a-g) and optical (h-k) remote sensing imagery. ..... - 24 -

Figure 3.2: Pie charts summarizing main study topics (a), research motivation (b), studied glacial features (c) and first author nationalities identified by the systematic review. ..... - 27 -

Modified after Baumhoer et al. (2018). ..... - 27 -

Figure 3.3: Geospatial distribution and coverage of calving front studies. (a) Geospatial distribution, (b) number of studies per individual glacier and ice shelf, and (c) spatial coverage of coastline studies. ..... - 30 -

Figure 3.4: Maximum observation length in years for available calving front data. ..... - 35 -

Figure 3.5: Example for calculating overall change rates for one glacier. The above table includes measurements of different studies (A-D) for different time frames. None of the studies cover the example period between 1980 and 2010. To calculate the change rate from 1980 to 2010 the available annual rates of different studies were averaged for each year (blue column). The overall annual change rate is the average of all values per year (orange line). ..... - 36 -

Figure 3.6. Circum-Antarctic pattern of annual calving front change rates. ..... - 38 -

Figure 4.1: Reflectance spectra of Antarctic surface features and clouds in the visual and near-infrared spectrum. ..... - 43 -

Figure 4.2: Exemplary appearance of radar glacier facies during austral summer (upper part) and winter (lower part). (a) Overview of Ronne Entrance with George V Ice Shelf. (b) Front of Stange Ice Shelf with perennial sea ice and open water in summer and with entire sea ice cover in winter. (c) Glacier radar facies nearby Ronne Entrance in summer and winter. ..... - 45 -

Figure 4.3: Pie chart (left) of proportions of used data sources and bar plot (right) of most frequently used sensors. Aerial imagery is an optical source of data. “Other” includes maps and further optical sensors. ..... - 45 -

Figure 4.4: Different techniques to measure calving front dynamics. Distance-based methods measure from one fixed point to the front (a). Higher accuracy is reached by using the average of several lines (b). Area (orange/blue) can only be measured to a reference line (orange) and the front (red). This can be a fixed box (c), which is relative to the grounding line or coastline of a specific year. ..... - 51 -

Figure 5.1: Exemplary EW acquisition coverage within two weeks in 2015 from Sentinel-1A (left) and in 2019 (right). Since the launch of Sentinel-1B a denser coverage with dual-polarized acquisitions exists. Though, not all coastal areas are acquired regularly every six days as planned by ESA ..... - 56 -

Figure 5.2: Sentinel-1 acquisition modes over Antarctica before May 2017 (a) and after (b). Note the shift from single-polarized to dual-polarized imaging. ..... - 56 -

Figure 5.3: Creating Labels. (a) Initial Senintel-1 scene, (b) overlaid by the manually delineated vector shapefile and (c) final rasterized label. ..... - 58 -

Figure 5.4: Training and test areas over Antarctica. ..... - 59 -

Figure 5.5: AntarcticLINES workflow for training and testing the automated calving front extraction framework. DEM: digital elevation model, S1: Sentinel-1, GRD EW: Extra wide swath Level-1 ground range detected S1 product. ..... - 61 -

Figure 5.6: U-Net architecture with four down-sampling encoder blocks separated by red arrows and four up-sampling decoder blocks with green arrows. Skip connections are indicated by black arrows and dropout by yellow ones. Image sizes and number of feature channels are given in black numbers. ..... - 63 -

Figure 5.7: Simplified convolution and max-pooling example for a four-channel image (white) and a 3x3 kernel (yellow). The complete filter is depicted in green and the convoluted feature in blue. The 2x2 max-pooling is shown in red with a final condensed feature in orange. ..... - 64 -

Figure 5.8: Filters with decreasing size from 780, 390, 195, 97 to 48 pixels. Filter size decreases from left to right whereas the number of filters increases from 32, 64, 128, 256 to 512. For clearness, only a few exemplary filters are shown. ..... - 65 -

Figure 5.9: Prediction results on selected validation tiles. Manual reference labels are given in the lower line. Very accurate results were achieved except for the very low contrast glacier front on the left. ..... - 66 -

Figure 5.10: Glenzer Glacier during melt season in January (left) and after melt season in February (right). Displayed for the same backscatter coefficient range in both images. ..... - 68 -

Figure 5.11: Glacier front fluctuations of Pine Island Glacier from February 2015 (red) to April 2020 (dark blue) in the upper panel. The lower panel displays cumulative calving front position changes relative to February 2015. Dates are monthly averages or exact when the date was given. ..... - 70 -

Figure 5.12: Retreating front of Glenzer Glacier with the iceberg trapped at the former pinning point. ..... - 71 -

Figure 5.13: Crevasse opening at Glenzer Glacier from 2015 to March 2020 shortly before break up. ..... - 72 -

Figure 5.14: Calving front fluctuation of Amery Ice Shelf. The iceberg D-28 which calved in September 2019 is still visible in the picture. The ice shelf front change is given for the northern part of Amery Ice Shelf (1) and the southern part (2). ..... - 72 -

Figure 5.15: Glacier front advance of Denman Glacier since February 2015. Steady calving front advance (upper panel) and cumulative frontal change in meters (lower panel). ..... - 73 -

Figure 5.16: Comparison of glacier front changes for Amery Ice Shelf, Pine Island Glacier, Denman Glacier, and Glenzer Glacier ..... - 74 -

Figure 5.17: Calving front time series of Getz Ice Shelf. (a) Continuous advance of the DeVicq Glacier. (b) Part of a stable coastline. (c) Front of the Beakley Glacier showing a calving event. Front of Getz 1 with wrong delineation in (d) and calving event in (e). ..... - 75 -

Figure 5.18: Calving front fluctuations in meters at Getz Ice Shelf relative to May 2017. Not the erroneously extracted front of Getz 1. All fronts advanced except the one of Beakley Glacier. ..... - 76 -

Figure 5.19: Calving front extraction results for Shackleton Ice Shelf (A) with detailed display of Roscoe Glacier (A1) and Denman Glacier (A2). (B) Results for Wilkes Land with detailed presentation of Moskow University Ice Shelf (B1) and DeHaven Glacier (B2). ..... - 78 -

Figure 5.20: Results for the area around the former Wordie Ice Shelf (C) and Oates Land (D). Detailed displays of Hariot Glacier (C1) and the Wordie Bay (C2) covered by mélange. For Oates Land detailed displays of Rennick Ice Shelf (D1) and McLeod Glacier (D2) are presented. ..... - 79 -

Figure 5.21: Schematic representation of transect measurements at Mawson Glacier. Point of measurement is the intersection between each transect and the glacier front. . - 80 -

Figure 5.22: Comparison of the ADD coastline (orange) with the manual expert delineation (blue) and the automatically extracted one (turquoise). The ADD coastline includes fast ice areas over Swinburne Ice Shelf (A), at Land Glacier (B), and Sulzberger Ice Shelf (C). Background: Sentinel-1 Copernicus data 2018. ..... - 84 -

Figure 5.23: Implementation of AntarcticLINES. A methodical framework for automatic calving front extraction. Copyright for icons belongs to corresponding companies. ..... - 86 -

Figure 5.24: Antarctic coastline split into 18 zones. The amount and polarization of available Sentinel-1 scenes are indicated. ..... - 88 -

Figure 5.25: Automatically extracted coastline (black) in winter 2018 underlaid by the manually corrected coastline (orange). Enlarged views of the Antarctic Peninsula (a), Pine Island Bay (b), Dronning Maud Land (c), Oates Land (d), Kemp Land, and Amery Ice Shelf (e). ..... - 89 -

Figure 5.26: Exemplary displays of the extracted coastline 2018 for the Antarctic Peninsula (a-c), Pine Island Bay (d,e), Ross Ice Shelf (f), David Glacier (g), Mertz Glacier (h), Kemp Land (i), Hayes Glacier (j) and a part of Larsen D (k). ..... - 90 -

Figure 6.1: Two decades of Antarctic coastal change from 1997 to 2018. Map in the center: Overview of entire Antarctica. Enlarged displays (counter-clockwise) for Larsen Ice Shelf, Pine Island Bay, George V Land, Wilkes Land, Shirase Bay, and Dronning Maud Land. ..... - 105 -

Figure 6.2: Glacier and ice shelf extent changes between 1997-2008, 2009-2018, and 1997-2018. ..... - 108 -

Figure 6.3: Absolute (upper) and relative (lower) air temperatures over the Antarctic continent in summer (Oct-Mar) and winter (Apr-Sep). ..... - 109 -

Figure 6.4: Sea ice days around the Antarctic continent measured during April to October for each year. Absolute sea ice days (upper panel) and relative mean sea ice days compared to the long-term mean (lower) per year. Also, the difference of mean annual sea ice days between both decades is given. ..... - 110 -

Figure 6.5: Sea surface temperature of the Southern Ocean from October to March. Absolute sea surface temperature (upper panel) and relative changes to the long-term mean (lower panel). ..... - 112 -

Figure 6.6: Mean absolute snowmelt in mm water equivalent per day between 1997-2008 and 2009-2018 (upper panel) and relative to the long-term mean (1982-1996). The enlarged panels show absolute and relative snowmelt amount over the Antarctic Peninsula ..... - 113 -

Figure 6.7: Zonal (West to East) wind speed (m/s) during summer months Dec-Feb. Positive absolute wind speed indicates dominating westerlies, negative speed dominating easterlies. Relative changes show changes in wind speed compared to the long-term mean. ..... - 114 -

Figure 6.8: Correlation between glacier and ice shelf change and the analysed climate variables winter/summer air temperature, snowmelt, sea ice days, summer sea surface temperatures, and zonal wind speed. Colour and circle size indicate the correlation coefficient. ..... - 115 -

Figure 6.9: Southern Annular Mode (SAM) since 1960. Values are given for the annual SAM (blue), SAM during summer (orange), and a 5-year moving average for the annual SAM (red). The dashed grey lines indicate the investigated periods 1997/08 and 2009/18, as delimited by the available coastline data. For SAM during summer (Dec-Feb), the beginning of austral summer (hence December) indicates the year of the peak. ..... - 117 -

List of Tables

Table 3.1: Available coastline Products for Antarctica based on remote sensing data. ..... - 34 -

Table 4.1: Comparison of advantages and disadvantages for calving front location (CFL) extraction in optical and SAR imagery. ..... - 42 -

Table 4.2: List of most relevant optical and SAR space-borne instruments for calving front mapping. ..... - 46 -

Table 4.3: Advantages and disadvantages of different CFL mapping techniques. ..... - 48 -

Table 4.4: Comparison of automatic (A) and semi-automatic (SA) calving front extraction approaches. ..... - 50 -

Table 5.1: Calving front change rates per year with mean standard deviation and R-square of linear regression for each calving front time series. ..... - 77 -

Table 5.2: Error calculation for the Getz time series with five manual reference coastlines. The distance to the reference coastlines is presented as the absolute mean of the measured transect values. ..... - 82 -

Table 5.3: Error calculation for the Getz time series with five manual reference coastlines. The distance to the reference coastlines is presented as the median of the measured transect values ..... - 82 -

Table 5.4: Classification performance for all training and test sites (June 2018). Highest and lowest values are indicated in bold. ..... - 83 -

Table 5.5: Distance measured errors (in meters) along transects for frontal and stable coastline sections as well as the entire study region. An estimate for the difference between two manually delineated coastlines is given with the ADD (Antarctic Digital Database) coastline (mean error). A/F is the averaged width of the enclosed area between the automated and manual delineated coastline for each study region. ..... - 83 -

Table 6.1: Summary of processed climate variable data sets. ..... - 103 -

Table 6.2: Area change rates in glacier and ice shelf front extent between 1997 and 2018 (upper table). Total lost and gained ice shelf/glacier area per decade (lower table). ..... - 107 -

List of Abbreviations

A/F	Area divided by calving front length
ABW	Antarctic Bottom Water
ACC	Antarctic Circumpolar Current
ADD	Antarctic Digital Database
AIS	Antarctic Ice Sheet
ALOS	Advanced Land Observing Satellite
AntarcticLINES	Antarctic Ice Shelf and Glacier Front Time Series
AOI	Area of Interest
AP	Antarctic Peninsula
ARGON	A series of reconnaissance satellites
ASAR	Advanced Synthetic Aperture Radar
ASF	Antarctic Slope Front
AVHRR	Advanced Very High Resolution Radiometer
CDW	Circumpolar Deep Water
CFL	Calving Front Location
CIA	Central Intelligence Agency
CNN	Convolutional Neural Networks
CONMAP	Council of Managers of National Antarctic Programs
CV	Computer Vision
DEM	Digital Elevation Model
DISP	Declassified Intelligence Satellite Photographs
DLR	German Aerospace Center
DMSP	Defense Meteorological Satellite Program
DSAS	Digital Shoreline Analysis System
EAIS	East Antarctic Ice Sheet
ENSO	El Nino/Southern Oscillation
Envisat	Environmental Satellite
ERS	European Remote Sensing Satellite
ESA	European Space Agency
EW	Extra Wide Swath
FCN	Fully Convolutional Network
GEE	Google Earth Engine
GEEDiT	Google Earth Engine Digitization Tool
GeoFarm	Server Processing Infrastructure at DLR
GPT	Graph Processing Tool
GPU	Graphical Processing Unit
GRD	Ground Range Detected
H	Horizontal

IDA	Internal Data Access
IPY	International Polar Year
IW	Interferometric Wide-Swath
LIMA	Landsat Image Mosaic of Antarctica
LR	Learning Rate
MAMM	Modified Antarctic Mapping Mission
MOA	Modis Mosaic for Antarctica
MODIS	Moderate-resolution Imaging Spectroradiometer
NOAA	National Oceanic and Atmospheric Administration
NSIDC	National Snow and Ice Data Center
PALSAR	Phased Array type L-band Synthetic Aperture Radar
PF	Polar Front
Px	Pixels
RAM	Random Access Memory
RAMP	Radarsat Antarctic Mapping Project
RARE	Ronne Antarctic Research Expedition
ReLU	Rectified Linear Units
REMA	Reference Elevation Model for Antarctica
SAF	Subantarctic Front
SAM	Southern Annular Mode
SAR	Synthetic Aperture Radar
SAT	Secretariat of the Antarctic Treaty
SCAR	Scientific Committee on Antarctic Research
SCI	Science Citation Index
SCL	Single Look Complex
SH	Southern Hemisphere
SMB	Surface Mass Balance
SNAP	Sentinel Application Platform
SPOT	Satellite Pour l'Observation de la Terre
SPRI	Scott Polar Research Institute
SST	Sea Surface Temperature
US	United States
USGS	United States Geological Survey
V	Vertical
WAIS	West Antarctic Ice Sheet
WTK	Well Known Text
w. eq.	Water equivalent

CHAPTER 1

1 Introduction

The current state of the Antarctic Ice Sheet (AIS) is alarming. Mass loss of the Antarctic Ice Sheet accelerated rapidly over the last two decades (IMBIE 2018, Rignot *et al.* 2019). Along the Antarctic Peninsula, 87 % of glaciers retreated and 7 out of 12 ice shelves in the area of the Antarctic Peninsula disintegrated (Cook & Vaughan 2010). Grounding lines retreated significantly along the WAIS (West Antarctic Ice Sheet) and in parts of the Wilkes Land (Konrad *et al.* 2018). Ice sheet flow is accelerating along the Antarctic Peninsula and West Antarctica (Pritchard & Vaughan 2007, Rignot *et al.* 2002), and ice shelves are thinning (Paolo *et al.* 2015, Rignot *et al.* 2013). Ice sheet elevation decreased most intense in West Antarctica, the Antarctic Peninsula, and Wilkes Land (Shepherd *et al.* 2019) where ice discharge significantly increased (Gardner *et al.* 2018).

1.1 Relevance of Antarctica

For our society, the greatest relevance of Antarctica is the potential of the AIS to raise global sea-levels significantly. The AIS stores 91% of the global ice volume (Swithinbank *et al.* 1988) equivalent to a sea-level rise of 58.3 meters. Therefore, the Antarctic Ice Sheet holds the most uncertain potential to raise global sea level (Vaughan *et al.* 2013). Although the complete melt of the Antarctic Ice Sheet is very unlikely, it will still significantly contribute to global sea-level rise in the 21st century with up to 1 meter depending on emission scenario and uncertainties in ice sheet dynamics (DeConto & Pollard 2016). Most recent measurements revealed an Antarctic sea level contribution of 7.6 ± 3.9 millimeters measured between 1992 and 2017 based on altimetry (IMBIE 2018). Calculations based on ice thickness and velocity data calculated a sea level contribution of 13.9 ± 2.0 millimeters (1979-2017). The contribution is very unevenly distributed. Single glaciers, like Pine

Island, account for 13 % of Antarctica's contribution (Rignot *et al.* 2019) and other parts like the East Antarctic Ice Sheet (EAIS) do not significantly lose mass at present (IMBIE 2018). Mass loss of the Antarctic Ice Sheet is situated at the Antarctic coastline which is fringed by innumerable glaciers and ice shelves. Ice shelves along the coastline cover an area of 1.56×10^6 km^2 (Rignot *et al.* 2013). The number of Antarctic glaciers is so far unknown and ranges roughly between 2752 (Radić *et al.* 2014) and 3274 (Vaughan *et al.* 2013) glaciers.

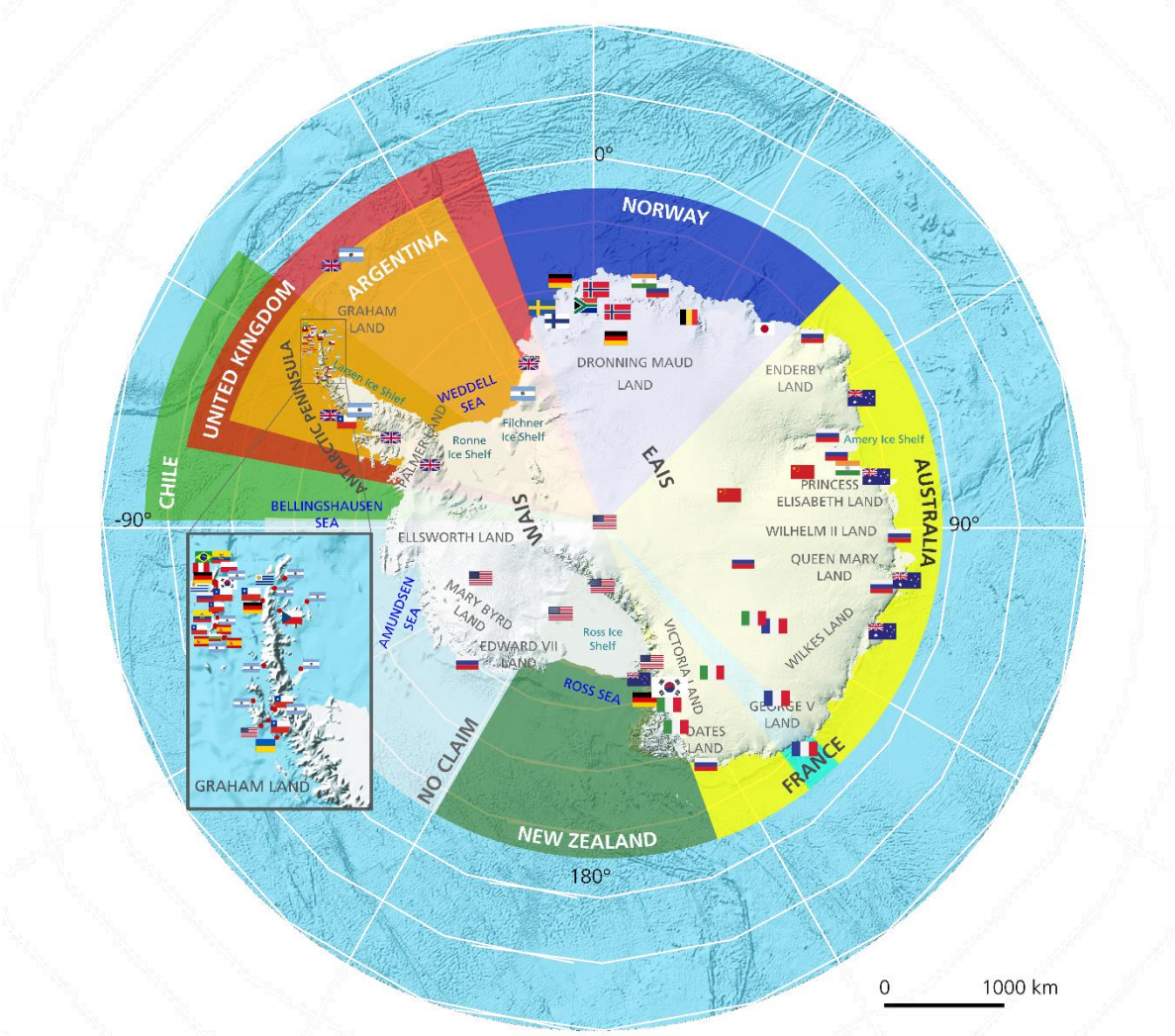

Figure 1.1: Map of Antarctica visualizing territorial claims and locations of national research facilities (flags). Data: Territorial Boundaries: Australian Antarctic Data Center; Research Facilities (as of March 2017): Council of Managers of National Antarctic Programs (COMNAP). Modified after Baumhoer et al. (2018).

Besides the cryosphere, Antarctica offers valuable resources such as metallic and non-metallic minerals, coal, and fossil fuels (Rose & McElroy 1987, Wright & Williams 1974). The global competition on natural resources did not yet reach Antarctica as their extraction is still too cost-intensive and the Antarctic Treaty preserves the status quo of territorial claims which might change with globally depleting natural resources (Naylor *et al.* 2008). The Antarctic Treaty covers the Antarctic territory from 60°S to the South Pole

(ATCM 2017) including the highest elevation of 4897 m at Vinson Massif (Swithinbank 1993). 12 states signed the Antarctic treaty with 7 countries claiming land (Dodds 2010). Currently, Antarctica holds about 112 open research facilities run by 30 different nations (see Figure 1.1) (CONMAP 2020).

Not only the worldwide struggle for natural resources might put pressure on Antarctica but even more a changing climate. Especially because of intensified temperature rise in Polar Regions, also known as polar amplification (Holland & Bitz 2003, Stuecker *et al.* 2018). The ecosystem of the WAIS and the Antarctic Peninsula (AP) is put under pressure by warming temperatures (Bindoff *et al.* 2013). Additionally, the emerging human impact puts even more pressure on this fragile ecosystem through illegal fishing activities, whaling, exploitation for bioprospecting purposes, and a growing tourism industry (Swithinbank 1993, Dodds 2010, Bindoff *et al.* 2013). Changes in the Antarctic ecosystem can have global impacts on sea level, climate, biochemical cycles, thermohaline circulation, and radiation budget which might furthermore trigger teleconnections not yet fully understood.

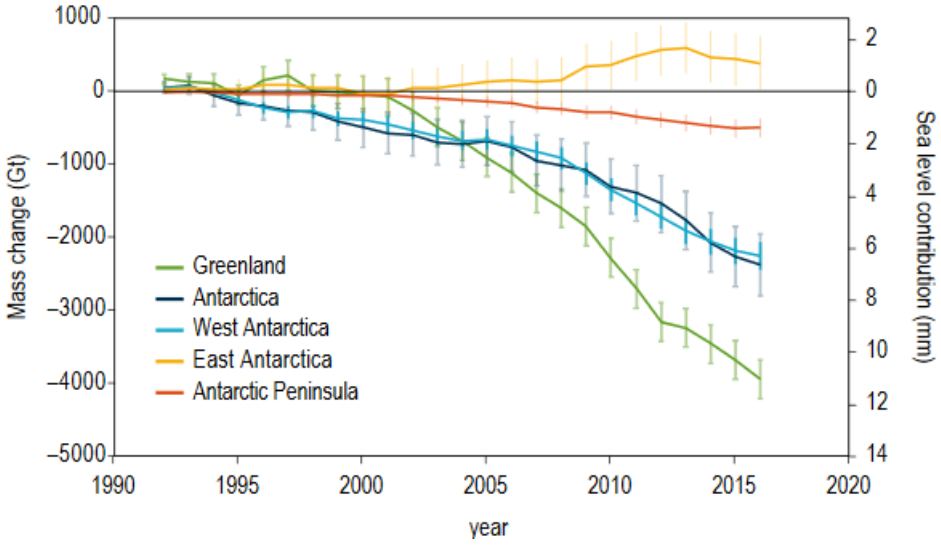

Figure 1.2: Cumulative ice sheet mass loss and according sea level contribution from ice sheets between 1992 and 2016. Antarctic data: IMBIE (2018). Greenland data: Bamber et al. (2018). Source: Meredith et al. (In press.)

Global sea-level rise is still the strongest concern as it will affect more than half of the most populated cities located at the coast (Hanson *et al.* 2011). In 2050, economic loss through floods at coastal cities will double to US$1 trillion per year just by adding sea-level rise scenarios (Hallegatte *et al.* 2013). Current global sea-level rise contribution is highest by mountain glaciers with 0.92 ± 0.39 mm/year (1961-2016) (Zemp *et al.* 2019), followed by the Greenland Ice Sheet with 0.42 ± 0.04 mm/yr (1992-2018) (IMBIE 2020) and Antarctica 0.36 ± 0.05 mm/yr (1979-2017) (Rignot *et al.* 2019) (see Figure 1.2). Already in 2100, the mass loss of the Antarctic Ice Sheet could exceed contributions from the

Greenland Ice Sheet and mountain glaciers and ice caps (depending on the scenario) (Bamber *et al.* 2019, Pfeffer *et al.* 2008). More accurate estimations will require a better understanding of ice dynamics of the Antarctic Ice Sheet. Especially in consideration of the recent acceleration of the sea level contribution by the WAIS since 2007 (IMBIE 2018, Rignot *et al.* 2019) and the certainty that single glaciers like Pine Island or Thwaites retreat quickly with the ability to rise sea levels significantly. Pine Island and Thwaites Glacier alone have contributed to a global sea-level rise of 4.8 mm since 1979 which is almost the double amount of the contribution from the entire Antarctic Peninsula (Rignot et al., 2019).

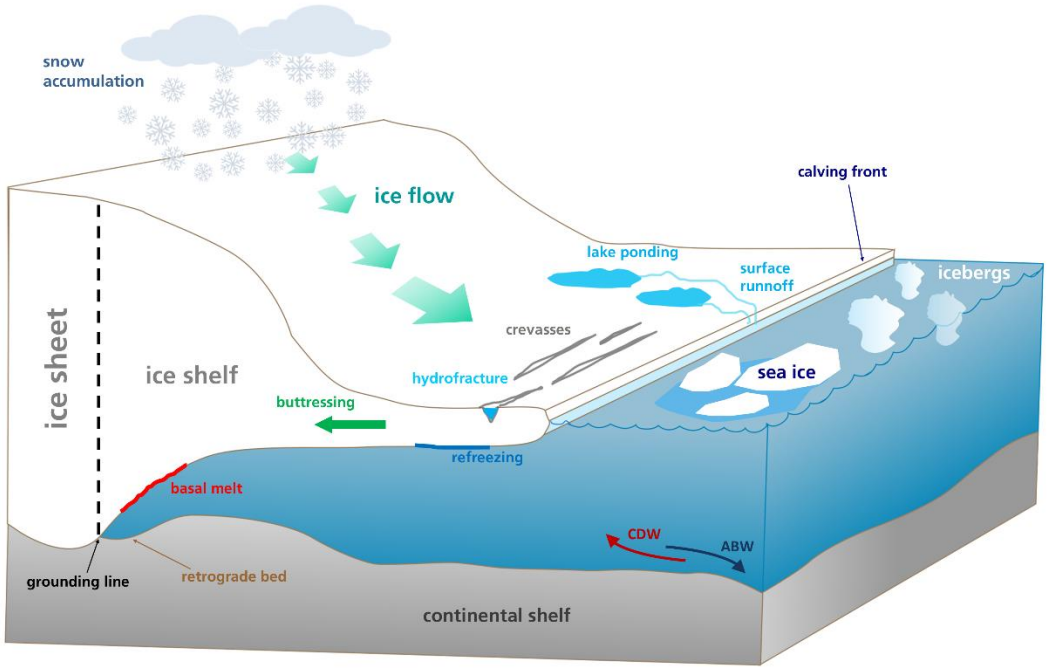

Figure 1.3: Ice shelf features and processes. CDW: Circumpolar Deep Water, ABW: Antarctic Bottom Water.

Accurate predictions on sea-level rise require the monitoring of outlet glaciers and ice shelves as they are responsible for Antarctica's ice discharge (Depoorter *et al.* 2013, Kusahara & Hasumi 2013). Calving of icebergs and melting underneath the ice shelves almost equally account for mass loss of the Antarctic Ice Sheet (Depoorter *et al.* 2013, Liu *et al.* 2015) whereas loss through a negative surface mass balance is proportional small (Rignot *et al.* 2019). Recent thinning and acceleration of outlet glaciers along West Antarctica and the Antarctic Peninsula increased the ice discharge of the Antarctic Ice Sheet within the last decades (Smith *et al.* 2020, IMBIE 2018, Pritchard & Vaughan 2007, Shepherd *et al.* 2019). These changes are attributed to the retreat, disintegration and thinning of ice shelves and glacier tongues (Scambos *et al.* 2004, Royston & Gudmundsson 2016, De Rydt *et al.* 2015). Ice shelves and glacier tongues create a safety band around Antarctica building buttressing effects on ice flow velocities and ice discharge (Fürst *et al.* 2016, Gagliardini *et al.* 2010, De Rydt *et al.* 2015). The safety band can weaken if the ice

shelf extent decreases due to calving front retreat. “Frontal retreat starts with the formation of a crevasse originating from a strain rate surpassing the yield stress of ice (Mosbeux *et al.* 2020a). For ice shelves and floating glacier tongues, the calving position evolves where crevasses develop into through-cutting fractures (rifts). These ice shelf rifts can propagate further into the ice front or intersect with other rifts, resulting in a tabular iceberg calving event (Benn *et al.* 2007, Joughin & MacAyeal 2005), where the extent of the ice shelf and the size of the iceberg are defined by the rift location (Lipovsky 2020, Walker *et al.* 2013, Mosbeux *et al.* 2020a). Further boundary conditions such as fjord geometry (Catania *et al.* 2018, Alley *et al.* 2008),ice rises and rumples (Matsuoka *et al.* 2015), and bed topography (Hughes 1981) influence the stability of the calving margin” (Baumhoer *et al.* 2021). Additionally, rift development can be affected by several external factors such as surface melt, ponding, basal melt, hydrofracture, iceberg collision and stabilizing sea ice and fast ice. Figure 1.3 shows the cross-section of an ice shelf with processes and parameters impacting ice shelf stability and ice sheet dynamics.

A majority of glaciers along the Antarctic Peninsula retreated and ice shelves disintegrated such as the Larsen A, Larsen B, Wordie, and Wilkins Ice Shelf (Cook *et al.* 2016, Cook & Vaughan 2010). Along West Antarctica, strong retreat (especially of Pine Island and Thwaites Glacier) is observed (Rignot 2002) whereas glacier fronts along the EAIS are stable except for Wilkes Land (Miles *et al.* 2016). Drivers of calving front retreat are manifold and still much discussed. Increasing air temperatures, warming ocean temperatures by upwelling Circumpolar Deep Water (CDW), the formation of melt ponds, hydrofracture, increased runoff, and decreasing sea ice are mostly connected to disintegration and glacier retreat but strongly vary along regions and glaciers (Cook *et al.* 2016, Cook *et al.* 2005, Wouters *et al.* 2015, Scambos *et al.* 2017, Miles *et al.* 2016).

1.2 The Need for Monitoring Antarctic Glacier and Ice Shelf Front Changes

Up to now, many of the involved processes relevant for sea-level rise and atmospheric and oceanic circulation are poorly understood, not to mention their interactions and positive (e.g. albedo reduction due to loss of floating ice) as well as negative feedbacks (e.g. mass gain due to increasing precipitation over the AIS) (Slater *et al.* 2021, Bromwich *et al.* 2011, Kennicutt *et al.* 2015). This led the Scientific Committee on Antarctic Research (SCAR) to the development of the Antarctic and Southern Ocean Science Horizon Scan. The result of this scan was the identification of 80 questions out of 955 proposed by several experts to manifest the future directions of Antarctic research (Kennicutt *et al.* 2015).

Focusing on sea-level rise and hence ice sheet stability many questions emerged regarding ice-ocean interactions as: “The influence of large-scale atmospheric and oceanic

processes on the melting of ice shelves and ice sheet margins is likewise ill-defined" (Kennicutt *et al.* 2015, p. 8). So far, several studies investigated on the basal melt on ice shelves and the resulting mass loss (Shepherd *et al.* 2010, Paolo *et al.* 2015, Pritchard *et al.* 2012, Rignot *et al.* 2013, Fürst *et al.* 2016). Glacier and ice shelves are in direct interaction with the atmosphere and ocean and hence sensitive to changes in environmental conditions (Vaughan & Doake 1996, Kim *et al.* 2001, Domack *et al.* 2005, Wouters *et al.* 2015). Changes in glacier and ice shelf extent can also be part of the natural cycle of glacier decay and growth (Hogg & Gudmundsson 2017, De Rydt *et al.* 2019). Even though many disintegration events have been mapped with remote sensing imagery (Braun *et al.* 2009, Cook & Vaughan 2010, Doake *et al.* 1998) over the last decades the circum-Antarctic state of glaciers and ice shelves has not yet been mapped, and coastal change analyses often do not provide sub-decadal information. Lack of information on calving front changes led to the simplification and underrepresentation of calving in mass loss estimates. For example, circum-Antarctic changes in ice shelf extent and ice sheet margins are estimated by calculating the calving flux (ice discharge at a steady defined calving front) as a proxy (Depoorter *et al.* 2013, Rignot *et al.* 2013) and the buttressing effect of ice shelves were neglected in modelling ice-ocean interactions (Schoof 2007). Just recently, the study by Wuite et al. (2019) revealed the strong underestimation of calving when using flux gates as a proxy. This means the actual share of mass loss between basal melt and calving might not be equally shared as previously thought.

A continent-wide study is still needed to understand the influence of large-scale oceanic and atmospheric processes on ice sheet mass balance (Kennicutt *et al.* 2015). An important mass loss component of ice sheets is iceberg calving from glacier and ice shelves margins (Benn *et al.* 2007). Huge calving events might reduce the buttressing force of floating ice in front of margins resulting in accelerating ice streams of the ice sheet. In order to better understand ice sheet/ice shelf interactions on a continental scale, the fluctuation of the ice sheet margin may yield valuable information on ice sheet mass loss under changing environmental conditions. Generating a data set through mapping continental-wide glacier and ice shelf fronts at a high temporal resolution from satellite imagery would reveal current changes in Antarctic calving front dynamics. This data set could reveal unusual glacier retreat and ice shelf disintegration events being an important indicator for the health of the Antarctic Ice Sheet.

1.3 Research Focus and Objectives

In past warmer epochs, the Antarctic Ice Sheet has been the primary contributor to sea-level rise and is seen as a major contributor for future increasing sea levels in the context of global warming (DeConto & Pollard, 2016). As outlined above, warming temperatures induce increased mass loss of the Antarctic Ice Sheet resulting in global

consequences as sea-level rises as well as the atmospheric and oceanic circulation is affected (Kennicutt *et al.* 2015, Rignot *et al.* 2013, Depoorter *et al.* 2013). This highlights the need for studying Antarctica's mass balance and understanding all involved processes and their interactions in order to quantify future sea-level rise which is of high societal relevance due to the exposure of coastal cities to floods (Hanson *et al.* 2011, Hallegatte *et al.* 2013). If the AIS would melt entirely, the global sea level would rise 58.3 m (Vaughan *et al.* 2013). Today, the sea level contribution of the Antarctic Ice Sheet is very little with 7.6 ± 3.9 mm (1992-2017) calculated from recent altimeter measurements. The contribution is likely to increase in the future (IMBIE 2018). The magnitude of sea-level rise is directly linked to the mass balance of the Antarctic Ice Sheet. A negative mass balance is influenced through two major mass loss components – surface melt and losses through ice dynamical discharge. For Antarctica, the surface melt can be seen as a minor issue as an increase of surface mass balance due to future increased snowfall is predicted (Hanna *et al.* 2013). Therefore, ice dynamical discharge through ice streams remains a major ablation process mainly regulated by buttressing ice shelves, ice thickness, and bed topography at the grounding line (Schoof, 2007). Antarctica is fringed by glaciers and ice shelves through which ice flows into the ocean. At the coastline, ice mass loss happens either through basal melt at the bottom of ice shelves or through iceberg calving (Depoorter *et al.* 2013, Rignot *et al.* 2013). For comprehensive sea level projections, it is of major importance to quantify contributions through ice dynamics, but the influences of atmospheric and oceanic processes on ice shelf melting and calving front position cause huge uncertainties (Kennicutt *et al.* 2015). So far, several studies investigated the basal melt on ice shelves and the resulting mass loss (Paolo *et al.* 2015, Rignot *et al.* 2013, Depoorter *et al.* 2013). Nevertheless, the rapid disintegration of ice shelves and the fluctuations of ice sheet margins have been studied at several regional examples (Cook & Vaughan 2010, Cook *et al.* 2005, Rack & Rott 2004, Rott *et al.* 1998, Ferrigno & Gould 1987) but circum-Antarctic changes in ice shelf extent and ice sheet margins are so far estimated by a proxy (Depoorter *et al.* 2013, Rignot 2002) and the buttressing effects of ice shelves are neglected in modelling ice-ocean interactions (Schoof 2007).

In this context, the primary goal of this thesis is to advance the understanding on calving front location change along the Antarctic coastline and to establish a comprehensive circum-Antarctic knowledge base with a special focus on seasonal fluctuations of glacier and ice shelf fronts and the identification of coastal areas where glacier retreat dominates.

Data availability on Antarctic calving fronts is closely connected to satellite data availability and the time-consuming manual delineation of fronts (Baumhoer *et al.* 2018). Since the launch of the Sentinel Copernicus mission, satellite data over the Antarctic coastline exists year-round and continuously. But to use this valuable satellite archive a robust algorithm is needed to replace the time-consuming manual ice front delineation.

Therefore, the further goal of this dissertation is to create a transferable and fully automated workflow for Antarctic calving front extraction which is transferable in space and time. This allows the continuous monitoring of glacier and ice shelf front changes with Sentinel-1 data and advances the understanding of circum-Antarctic calving front retreat in relation to changing environmental conditions.

Based on these two overall goals, several research questions are addressed in this dissertation. First of all, a sound review is performed in order to assess the data availability of glacier and ice shelf front positions along the Antarctic coastline. The already available measurements will be used to get a circum-Antarctic picture of past changes in the calving front location.

Research Question 1:

What is the relevance of Antarctic glacier and ice shelf fronts? Which calving and disintegration events were observed in the past? How good is the circum-Antarctic data availability of glacier and ice shelf front positions?

Thereafter, the opportunities to use satellite data for large scale coastal monitoring are assessed. Already existing methods for front extraction are reviewed.

Research Question 2:

What is the potential of earth observation for the assessment of Antarctic calving fronts? What are the advantages and challenges of remote sensing-based calving front studies? Which methods exist to extract calving fronts and what technical innovations can be achieved by integrating big data and artificial intelligence approaches?

As no fully-automated workflow for Antarctic calving front extraction exists, a novel deep learning approach is developed to be applied on Sentinel-1 data.

Research Question 3:

How can dense Sentinel-1 time series support the monitoring of calving front fluctuations? How can deep learning be used to automatically extract Antarctic glacier and ice shelf fronts? How can a novel fully-automated framework for circum-Antarctic calving front extraction be implemented that is transferable in space and time?

The implemented processing workflow is used to assess changes in Antarctic calving front dynamics. A special focus are seasonal fluctuations of calving fronts and the circum-Antarctic pattern of calving front change over the last two decades to identify driving forces of glacier retreat.

Research Question 4:

Which different patterns in intra-annual calving front fluctuations can be observed? Which circum-Antarctic patterns of glacier and ice shelf front change occurred over the last two decades and what were potential driving forces?

In order to answer the questions above the following research objectives are formulated:

1) Conduct a comprehensive review on existing Antarctic glacier and ice shelf front studies including a data availability study.
2) Review existing methods and develop an automated calving front extraction algorithm for Sentinel-1 satellite data.
3) Implement a fully automated processing chain to track seasonal calving front fluctuations.
4) Identify current patterns in Antarctic glacier and ice shelf front changes, as well as seasonal variations, and investigate driving forces of terminus retreat.

1.4 Structure of the Thesis

This thesis consists of seven chapters which are outlined below.

CHAPTER 1: gives a brief background on the Antarctic Ice Sheet and its relevance for our society. It also emphasizes the importance of glacier and ice shelf fronts for Antarctic ice dynamics and explains the need for glacier and ice shelf front monitoring. Furthermore, research questions, objectives, and the general structure of this thesis are described.

CHAPTER 2: focuses on the physical properties of the Antarctic Ice Sheet. Besides topography also the climatic and hydrological setting is explained.

CHAPTER 3: introduces principals of calving front dynamics. A comprehensive review of existing data sets and studies related to calving front extraction is provided. Finally, the content of all revised studies is presented in several maps covering the entire ice sheet.

CHAPTER 4: provides a background on remote sensing of calving fronts. Different kinds of remote sensing data are introduced and already existing methods for glacier front delineation are reviewed. Additionally, different methods to measure glacier terminus fluctuations are introduced.

CHAPTER 5: presents the novel developed framework *Antarctic*LINES for the automatic extraction of calving fronts. A focus on convolutional neural networks for remote sensing data is set before explaining the developed method. The workflow for the automatic extraction of calving fronts is presented in brief detail and the entire processing chain is described. Intra-annual fluctuations of selected glaciers are presented and an accuracy assessment is performed. Finally, the large-scale applicability of the developed framework is demonstrated by extracting the Antarctic coastline for 2018.

CHAPTER 6: focuses on the identification of potential drivers for Antarctic calving front change. Two decades of glacier and ice shelf front fluctuations are presented in connection to changes in climate variables.

CHAPTER 7: shortly summarizes the entire thesis and presents the conclusive findings with respect to the research questions and objectives. Furthermore, opportunities for future developments are highlighted.

CHAPTER 2

2 Characteristics of Antarctica

Antarctica (see Figure 2.1) is a continent of superlatives breaking records in temperature, wind speed, and aridity (Gossart *et al.* 2019). The Antarctic territory stretches between 60°S and the South Pole (SAT 2020). The continent covers an area of 14.2 million km^2 (8.3 % of global landmass) which is 1.4 times larger than Europe. Despite the size of the continent, Antarctica is only inhabited by 4,400 researchers and technicians in summer and 1,100 in winter (CIA 2020, Vaughan *et al.* 2013). They are housed in one of seasonal or year-round 112 research stations run by 31 different countries (CONMAP 2020). The Antarctic Treaty was established in 1959 to create a mechanism for governing Antarctica and maintain a status quo on the 7 territorial claims by the United Kingdom, Chile, Argentina, France, Australia, New Zealand, and Norway (Dodds 2010). Today, 54 parties signed the Antarctic Treaty and enabled the successful implementation of legal instruments over the last sixty years (Dodds 2010, SAT 2020). Without this strong governance of Antarctica, exploitation by mining, illegal fishing, whaling, territorial claims, and tourism would exist without any regulations (Dodds 2010). The Antarctic Treaty proves to be an important part of Antarctica ensuring environmental protection, conservation, and sustainable actions on the Antarctic continent.

2.1 Physiography

The Antarctic Ice Sheet stores ~91 % (Swithinbank *et al.* 1988) of the global ice mass with the potential to raise global sea level by 58.3 meters (Vaughan *et al.* 2013). The Antarctic continent is covered by 13.9 million km^2 ice (Fox & Cooper 1994) of which 1.56 million km^2 are of floating ice shelves and glacier tongues (Rignot *et al.* 2013). Ice-free areas are located on the Antarctic Peninsula, in Victoria Land and in parts of Wilkes Land.

The coastline of Antarctica has a length of 43,449 km whereof 75 % consist of ice shelf fronts (Rignot *et al.* 2013) draining 80 % of Antarctica's grounded ice (Pritchard *et al.* 2012).

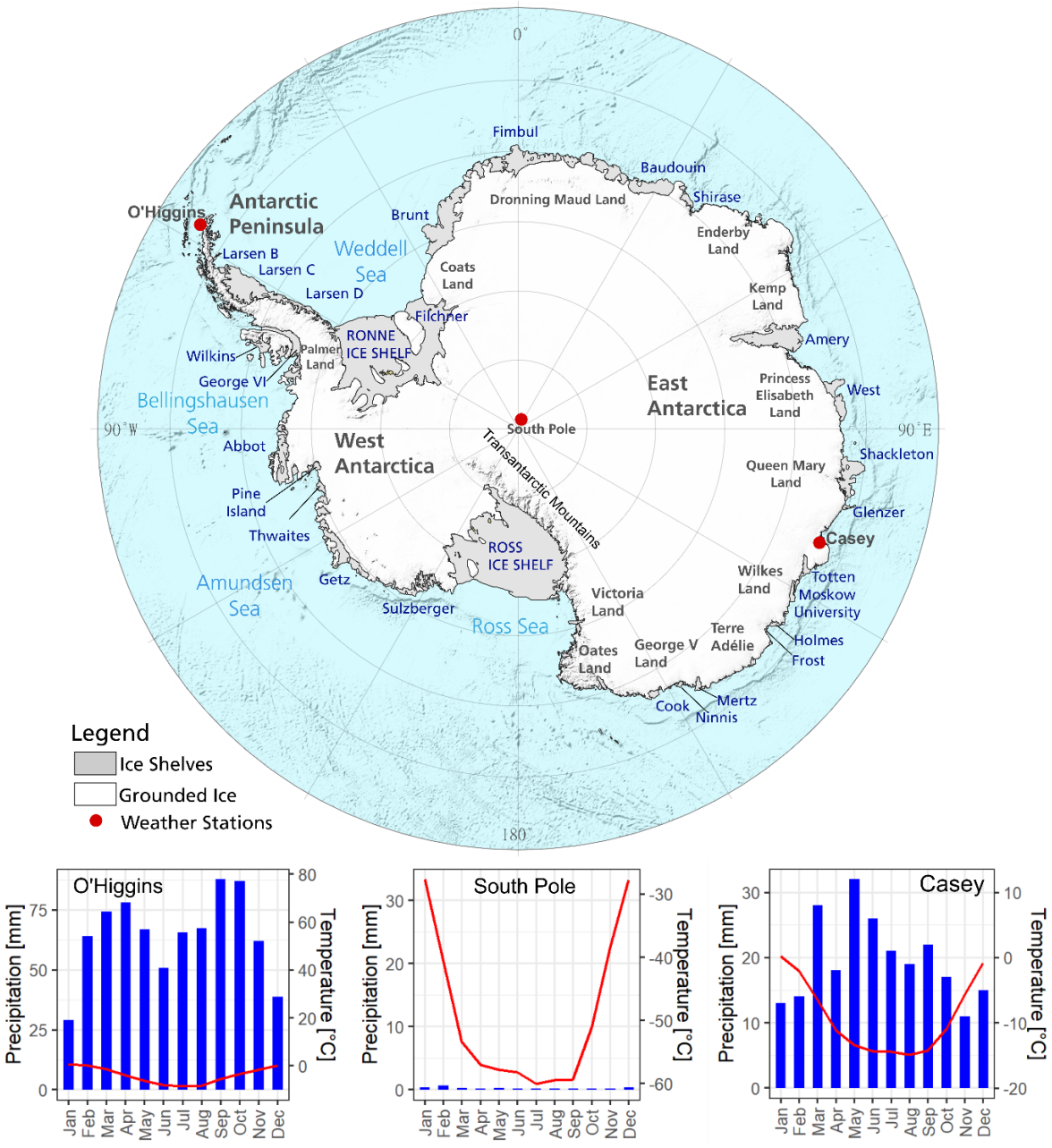

Figure 2.1: Map of Antarctica showing major ice shelves and glaciers. Climate diagrams for O'Higgins Station on the Peninsula, Casey Station in Wilkes Land and the South Pole. Data: DWD (2020).

The continent is covered by kilometers of ice reaching a maximum thickness of 4897 m in Astrolabe Subglacial Basin (see Figure 2.2) (Fretwell *et al.* 2013). On average, the ice thickness of the Antarctic basin is 2126 m (Fretwell *et al.* 2013). The bed elevation of Antarctica varies between the highest mountain at Vinson Massif with 4892 m (see Figure 2.2) (Swithinbank 1993) and the deepest point at Bentley Subglacial with -2870 m below the WAIS (Fretwell *et al.* 2013). Antarctica is divided into three main regions as displayed in Figure 2.1: The Antarctic Peninsula with a steep mountain range, many small outlet glaciers and the huge

Larsen ice shelves on the eastern side. West Antarctica including Ronne and the western Ross Ice Shelf is characterized by a very low lying bed elevation with wide areas below sea level (Hughes 1981, Fretwell *et al.* 2013). The Transantarctic Mountain Range separates the WAIS from the larger EAIS covered by a thick layer of ice. The EAIS is characterized by smaller outlet glaciers between Victoria and Wilkes Land whereas in the East and North ice shelves dominate the coastline. On the EAIS, the South Pole is located at 90° 0′ 0″ S marked by the US American Amundsen Scott station (CONMAP 2020). Deposits of Antarctica's natural resources are not well documented, probably to avoid illegal mining activities. Potential resources are iron, noble metals (copper, gold, silver), manganese nodules, coal and oil (Rose & McElroy 1987, Wright & Williams 1974). A geological map of Antarctica is provided by Tingey (1991) holding information on different rock units. The Antarctic continent has deposits of various rocks including sedimentary, volcanic and metamorphic rocks.

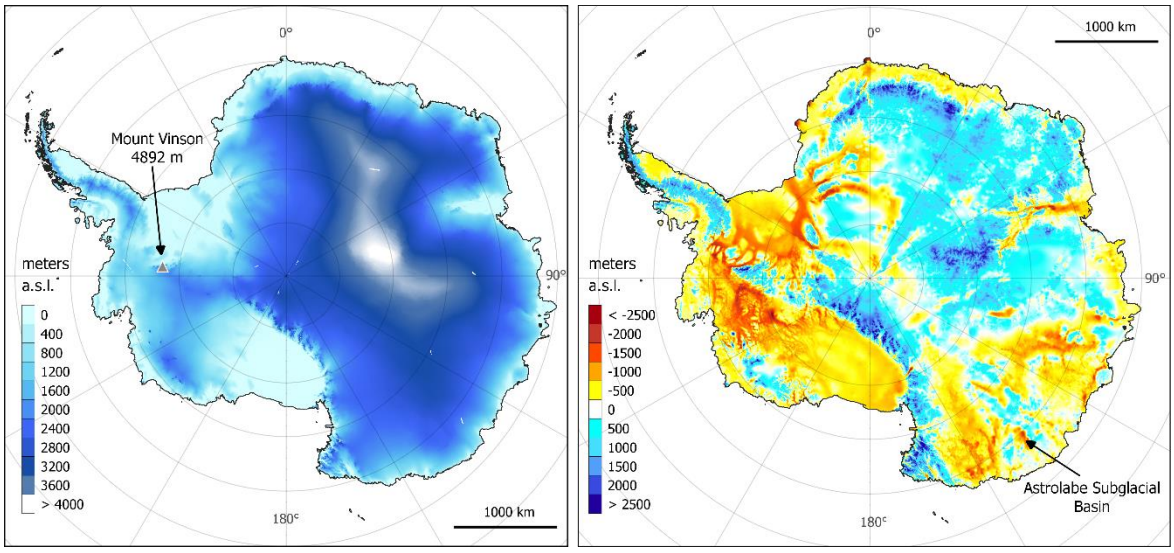

Figure 2.2: Topography of Antarctica. TanDEM-X surface elevation model of the Antarctic Ice Sheet (left) and Antarctic bed topography (right) after Fretwell et al. (2013). Red areas are below sea level, blue areas above.

2.2 Climatic, Oceanic and Hydrological Setting

Antarctica is the coldest continent on earth (Turner *et al.* 2009a, Gossart *et al.* 2019). The Antarctic Circumpolar Current (ACC) keeps Antarctica cool as it creates a boundary between warm subtropical ocean water and the cooler ocean close to the Antarctic continent (see Figure 2.3). Equally important for the Antarctic climate is the Southern Annular Mode (SAM) influencing the Antarctic climate through fluctuations in the mid-to-high-latitude atmospheric pressure gradient (Jones *et al.* 2016).

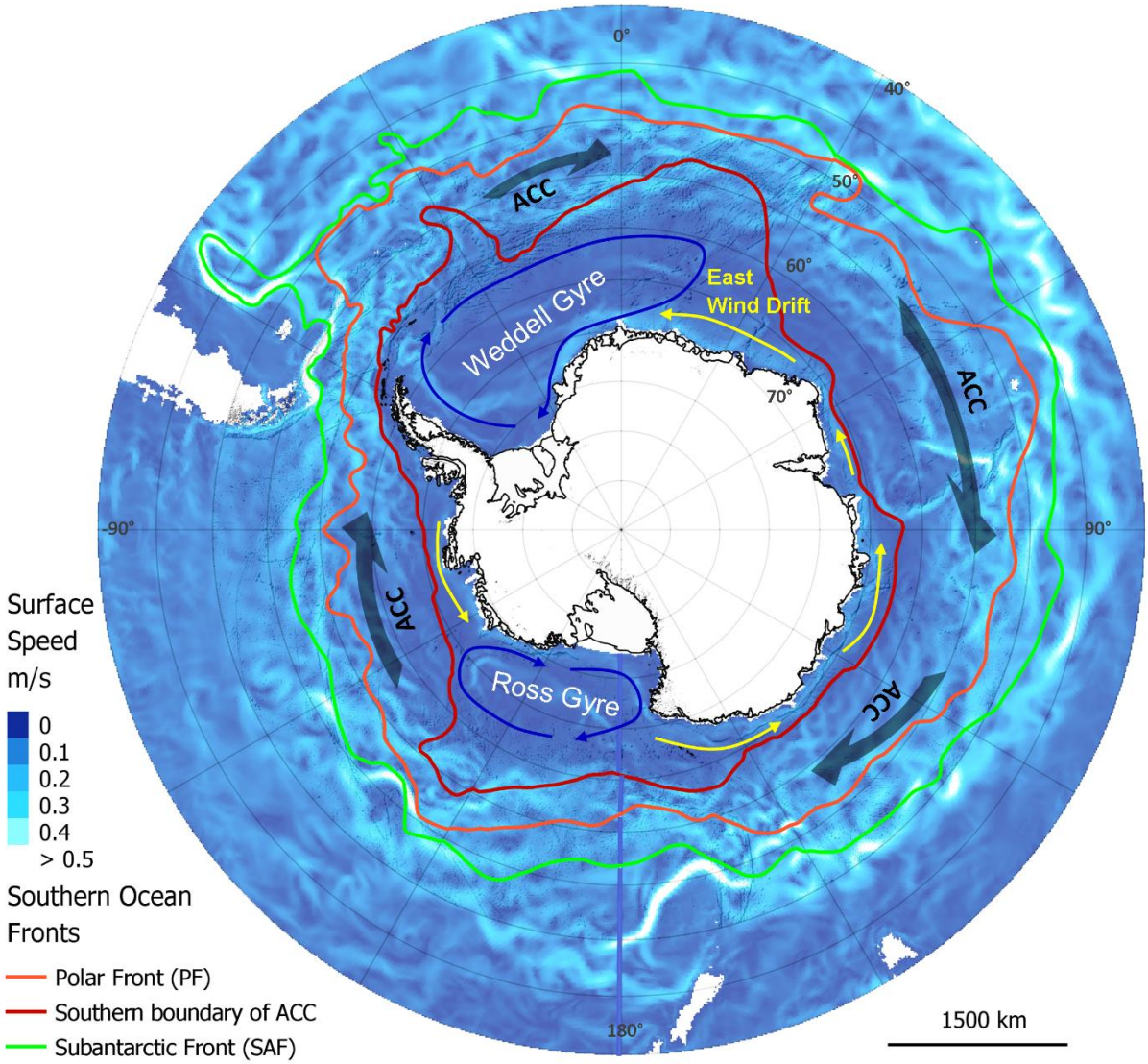

Figure 2.3: Ocean currents around Antarctica. Lines show the southern ocean fronts. Mean surface speed is displayed in the background. Data: Malzloff et al. (2010) & ADD (2020). ACC: Antarctic Circumpolar Current.

Positive phases of SAM strengthen and move the westerly wind belt driving the ACC poleward. This not only affects changes in air temperature but also the distribution and timing of precipitation (Jones *et al.* 2016, Marshall 2007). Positive phases of SAM lead to warmer temperatures on the Antarctic Peninsula and cooling over the inner continent (Marshall 2007). There is growing evidence that ozone depletion, tropical sea surface temperature and increasing CO_2 concentrations strengthen positive SAM years (Thompson *et al.* 2011, Raphael *et al.* 2016, Clem *et al.* 2017). The second major influence of the Antarctic climate and circulation variability is the El Nino/Southern Oscillation (ENSO). Teleconnections between changes in tropical and mid-latitude sea surface temperatures and the Antarctic climate exist (Turner 2004, Clem *et al.* 2016). For example, La Nina events strengthen the Amundsen Sea Low (regional atmospheric circulation in the Amundsen Sea

Embayment) which leads to warming air temperatures and a reduction in sea ice at the Western Antarctic Peninsula and in the Amundsen Sea (Raphael *et al.* 2016, Clem *et al.* 2016, Jones *et al.* 2016). Recently, it was found that SAM strongly influences the climate of the Antarctic Peninsula during summer and autumn whereas ENSO influences the climate during austral winter and spring (Clem *et al.* 2016).

In general, it is very challenging to assess trends and anthropogenic influences on the Antarctic climate as in-situ data are rare and date back to the 1950s at best (Turner 2004, Jones *et al.* 2016). In 2020, only 57 automatic weather stations exist on the entire ice sheet (AMRC 2020) and climate reanalysis data and geological records (e.g. ice cores, isotopes) oftentimes offer the only opportunity to analyze the climate of the AIS in a holistic way (Jones *et al.* 2016, Gossart *et al.* 2019, Steig *et al.* 2013). Exemplary for the high variability of the Antarctic climate, three climate diagrams for O'Higgins (AP), the South Pole and Casey (EAIS) station are presented in Figure 2.1. The Antarctic climate is divided into four seasons: summer (Dec, Jan, Feb), autumn (Mar, Apr, May), winter (Jun , Jul, Aug) and spring (Sep, Oct, Nov). In the following, state-of-the-art knowledge as well as recent trends of the Antarctic climate and hydrology is presented.

Wind

The wind system over Antarctica forms due to the temperature gradient between the equator and the South Pole. Air flows poleward from the subtropical high pressure zone at 30°S to the low pressure at 60-65°S and is forced by the Coriolis Force. This forms the mid-latitude westerly winds. Those strong winds of the Southern hemisphere (SH) drive the ACC clockwise around Antarctica creating ocean upwelling (also known as the Antarctic Divergence) (Turner *et al.* 2009b). Within the ACC, strong changes in water density exist which create the Polar and Subantarctic Front (see Figure 2.3). Additionally, closer to the Antarctic coastline, a belt of easterly winds (East Wind Drift) exists due to high pressure over the Antarctic continent creating the Antarctic Coastal Current (see Figure 2.3). This much narrower wind belt is of importance as it circulates the ice shelf fronts leading to deep convection and the creation of Antarctic Bottom Water (ABW). The newly formed dense water from the continental shelf is transported by the easterlies to the Antarctic Slope Front (ASF) where warm CDW approaches the surface and ABW is formed (Jacobs 1991). Hence, the Antarctic Slope Front is the boundary between ABW and CDW. Since 1979, easterly winds have not weakened on average throughout the year as previously thought (Hazel & Stewart 2019). Only during the seasonal cycle, a significant poleward shift and strengthening of westerlies could be observed at the Antarctic coastline during summer. This shift allows upwelling of warm CDW onto the continental shelf and enhances basal melt below ice shelves (Hazel & Stewart 2019).

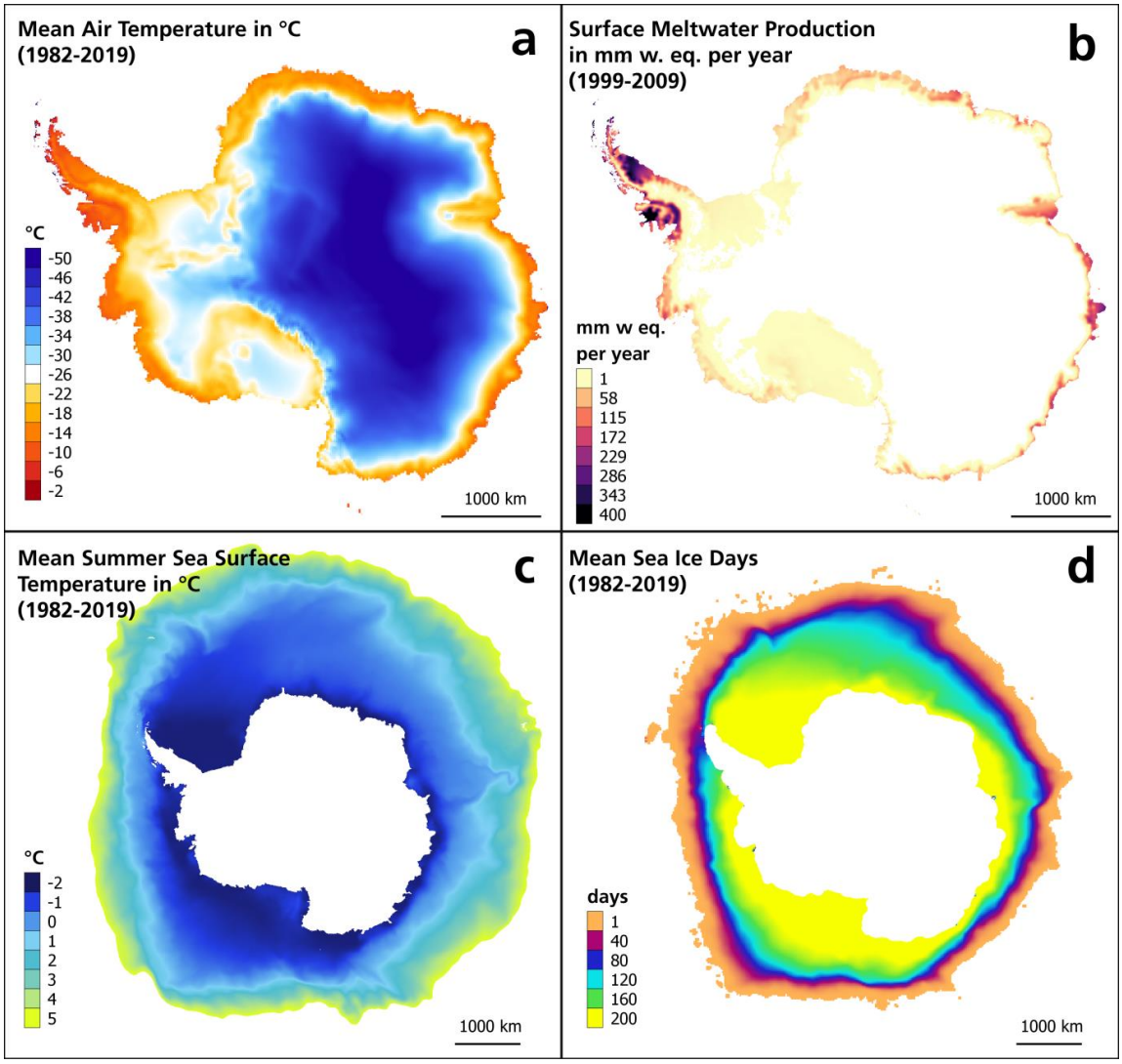

Figure 2.4: Climatological Parameters of Antarctica. (a) Mean air temperature 2 m above ground derived from ERA5 monthly means data between 1982 and 2019. (b) Surface meltwater production between 1999 and 2009 from Trusel et al. (2013). (c) Mean summer sea surface temperature based on ERA5 monthly means data between 1982 and 2018. (d) Mean sea ice days between 1982 and 2018 (Apr-Oct) calculated based on data from EUMETSAT OSI SAF (Lavergne *et al.* 2019). ERA5: C3S (2017).

Temperature

The lowest ever measured air temperature was recorded in Antarctica at Lake Vostok with -89.2°C in July 1983 (Turner *et al.* 2009a). Recent satellite measurements could prove even lower temperatures of < -90°C occurring more frequently on the upper East Antarctic ice divide with a record low of -94°C. Between 1982 and 2019, the average temperature of the Antarctic Ice Sheet was -33.03°C (based on monthly means) with large regional differences. This data was calculated using ERA5 reanalysis data based on a 9 km grid. The mean distribution of temperature between 1982 and 2019 is displayed in Figure 2.4a. Temperature trends in Antarctica vary strongly between seasons and regions. The Antarctic Peninsula is a hotspot of temperature increase. At Faraday Station, the mean annual temperature increased by 2.8°C between 1951 to 2000 (Turner *et al.* 2016). Since then the

Antarctic Peninsula entered a cooling phase. During 1979-1997, a warming of 0.32 °C per decade in mean annual surface air temperature was measured for the AP whereas cooling was apparent between 1999-2014 with -0.47 °C per decade (Turner *et al.* 2016). A recent study by Bozkurt et al. (2020) found that the cooling trend only exists during summer (approx. -0.4°C per decade) whereas in autumn, a warming trend of up to 1.2°C per decade on the Larsen C Ice Shelf existed (measured between 1991-2015). It is assumed that this decadal cooling happened due to extreme natural internal variability and not due to global drivers of temperature change.

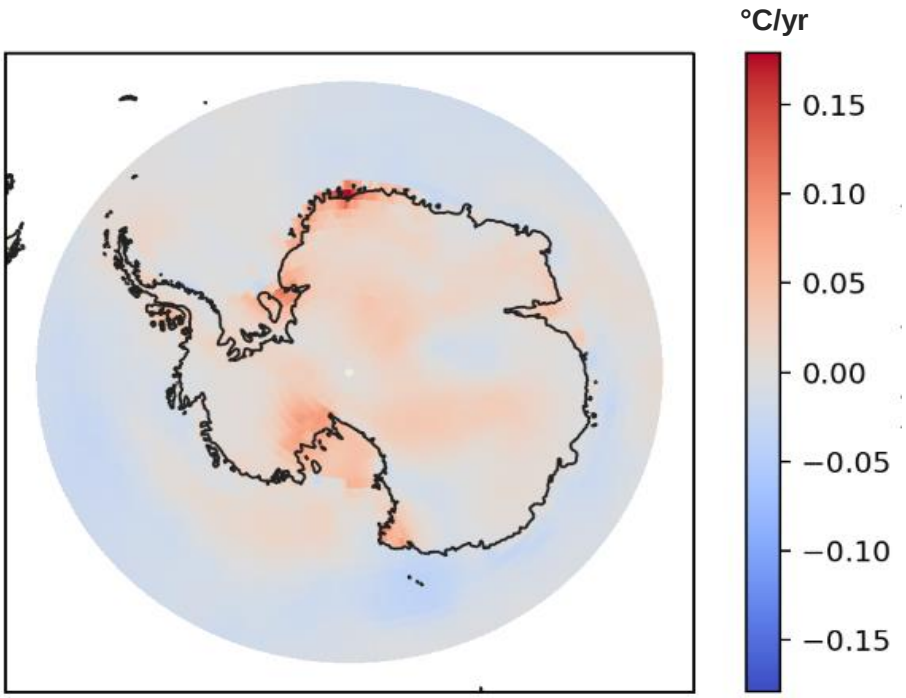

Figure 2.5: Air temperature trend between 1982 and 2019 calculated based on ERA5 hourly data on single levels. Data: C3S (2017).

Central West Antarctica also belongs to the fastest warming regions on earth with an increase of annual temperatures by 2.4±1.2°C between 1985 and 2010 and particular warming during summer (Bromwich *et al.* 2013). The entire WAIS warmed by 0.1°C per decade between 1957 to 2006 with peaks during winter and spring (Steig *et al.* 2009). The pressure on West Antarctica is twofold. During El Nino episodes, surface melt increases and weakens the ice shelves from above. Melt from below increases in phases of positive SAM years as stronger westerlies bring warm CDW to the bottom of ice shelves and glacier tongues (Deb *et al.* 2018). Air temperature trends over the EAIS are less clear. Comiso (2000) calculated a slight cooling trend over East Antarctica between 1979 and 1998. Using longer time series and larger data sets yields evidence that also temperatures over EAIS increased (Steig *et al.* 2009). Especially, warming was measured during spring based on station data between 1957 and 2016. But this warming trend was still lower in magnitude than for West Antarctica and the Peninsula (Jones *et al.* 2019). Temperature trends for

Antarctica calculated with ERA5 data between 1982 and 2019 are displayed in Figure 2.5. A clear warming trend for entire Antarctica is apparent except for small parts at Adélie and Prince Elisabeth Land.

Precipitation/Snowfall

The spatial distribution and magnitude of Antarctic precipitation is mainly influenced by the variation of the southern baroclinic annular mode, the SAM, and the two Pacific-South American teleconnection patterns (Marshall *et al.* 2017). Between the 1950s and 2006, no increase in snowfall was measured based on observations, ice core data and model simulations (Monaghan 2006). A more recent study by Medley and Thomas (2019) found an increase in snow accumulation on the Antarctic Ice Sheet within the twentieth century based on reanalysis and ice core data. Over the EAIS, a continuous increase in snow accumulation was detected until 1957 with a slight decreasing trend afterwards. Snow accumulation over the Antarctic Peninsula accelerated during the 20th century. Over West Antarctica, the accumulation gain in the western part equals out the loss over the eastern part (Medley & Thomas 2019). Projections on future precipitation patterns simulate increases due to rising air temperatures ranging from +5 to 7.4 %/°C (Palerme *et al.* 2017, Frieler *et al.* 2015, Winkelmann *et al.* 2012).

Sea Ice Extent

Recent developments in the Antarctic sea ice extent contradict previous trends (Meredith *et al.* In press.). Between 1979 and 2015, a significant positive trend in sea ice cover existed (Comiso *et al.* 2017). But three consecutive years of record low sea ice extent present a turning point. Including the most up-to-date sea ice measurements, no significant trend on total annual sea ice cover exists (Ludescher *et al.* 2019, Meredith *et al.* In press.). Only regional and seasonal analyses reveal significant decreases in sea ice cover along the Antarctic Peninsula during autumn and in February for the Amundsen and Bellingshausen Sea (Ludescher *et al.* 2019). Early satellite records may also point to an overall decrease in sea ice extent since the 1960s (Gallaher *et al.* 2014). Previous increases in sea ice are attributed to internal variability (Gagné *et al.* 2015) whereas sea ice decrease happened due to ocean and atmospheric forcing (Meredith *et al.* In press., Ludescher *et al.* 2019). Future projections of sea ice extent are unreliable as several anthropogenic forcings and complex ocean and atmosphere interactions do not allow such analysis with low uncertainty (Meredith *et al.* In press.). Mean sea ice days measured between 1982 and 2019 are displayed in Figure 2.4.

2.3 Recent Changes in the Antarctic Ice Sheet Mass Balance

Mass balance is a good measure to assess the long-term health of the Antarctic Ice Sheet. The ice sheet gains mass by the accumulation of snow compacting over time and transforming to ice. The ice merges into ice streams flowing seawards and building floating ice tongues and ice shelves. Mass loss can either happen at the ice sheet surface through surface melt generating runoff. Or mass is lost at the coastline where icebergs calve and ice shelves melt from below through basal melt. Runoff is the major mass loss component for the Greenland Ice Sheet whereas Antarctica only loses mass by calving and basal melt (Rignot *et al.* 2013). The Mass Balance (MB) of an ice sheet can be formulated as follows:

$$MB = SMB - D$$

The Surface Mass Balance (SMB) is the net accumulation between precipitation, sublimation and surface runoff and D the solid ice discharge to the ocean (Rignot *et al.* 2013, Gardner *et al.* 2018).

Remote sensing offers various techniques to estimate ice sheet mass balance via gravimetry, altimeter measurements and the input-output method, also known as the budget method (Hanna *et al.* 2013). Figure 2.6a shows the average rate of elevation change between 1992 and 2017 based on altimeter measurements (Shepherd *et al.* 2019). Clear volume loss can be observed for the WAIS especially at Pine Island Bay and Totten Glacier at Wilkes Land. Measurements based on the input-output method to calculate ice discharge are depicted in Figure 2.6b.

The difference between snow accumulation and ice discharge at the grounding line demonstrates the strong ice loss in West Antarctica, on the Peninsula and in Wilkes Land (but of slighter magnitude) between 2008 and 2015. A positive mass balance exists along Dronning Maud Land (Gardner *et al.* 2018). Figure 2.7a illustrates the share of mass loss through calving (2007/2008) and basal melt (2003-2008). Mass loss by basal melt is mainly located at the Bellingshausen and Amundsen Sea whereas calving dominates along East Antarctica (Rignot *et al.* 2013). This pattern is also apparent in more recent published thickness change rates of ice shelves and corresponding volume changes by Paolo et al. (2015) (see Figure 2.7b). Strong thinning of ice shelves occurs along the Antarctic Peninsula and on the WAIS whereas slight gains exist for East Antarctica between 1994 and 2012.

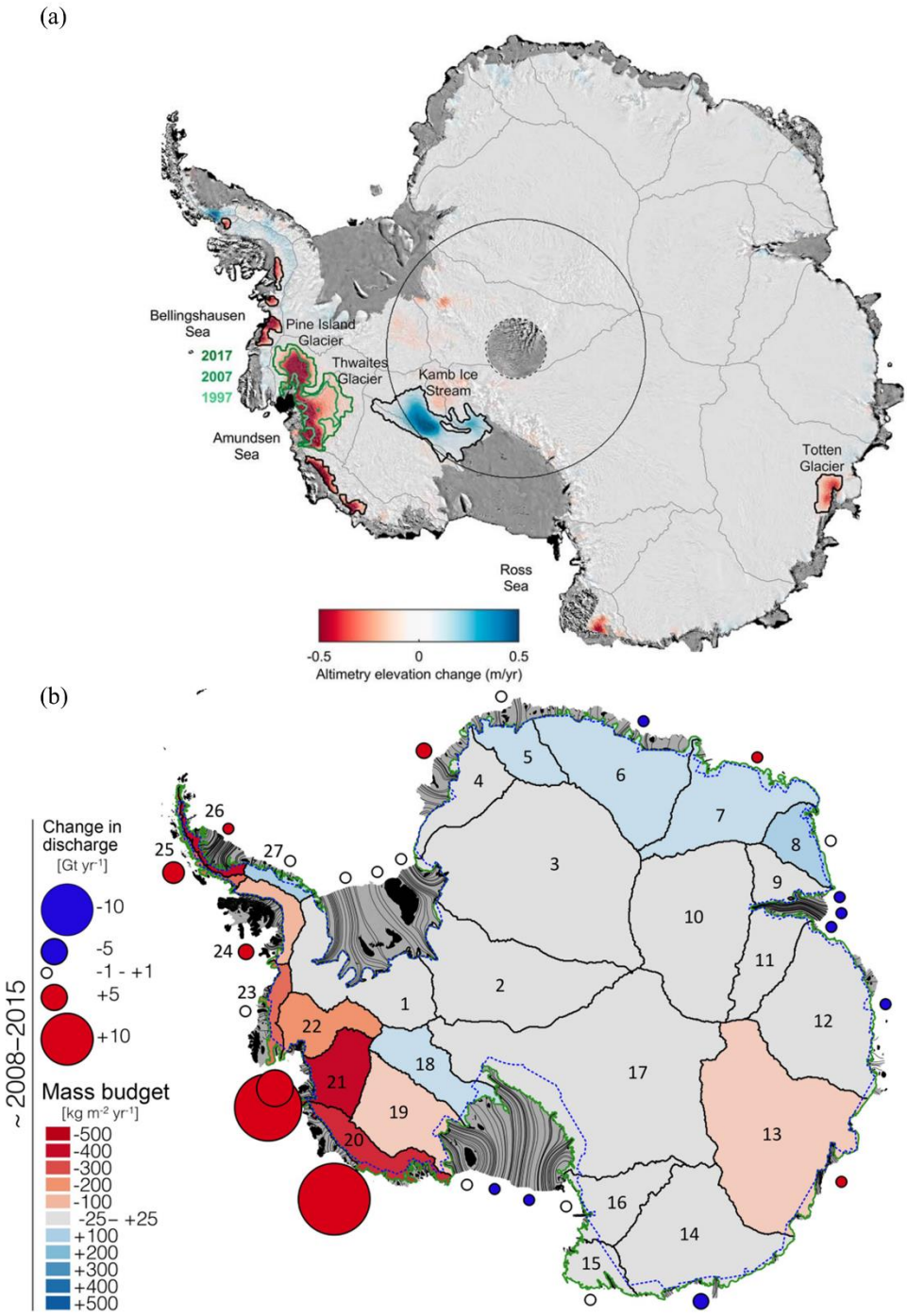

Figure 2.6: Mass loss of the Antarctic Ice Sheet and ice shelves. (a) Elevation change of the Antarctic Ice Sheet between 1992 and 2017 (Shepherd *et al.* 2019). (b) Ice discharge of the Antarctic Ice Sheet and mass budget between 2008 and 2015 (Gardner *et al.* 2018).

The ice mass loss in West Antarctica even accelerated since 2003 by about 70%. Most recently published state-of-the-art publications on the mass balance of the Antarctic Ice Sheet raised new questions. The IMBIE Team (2018) calculated a mass gain of 5±46 Gt per year for the EAIS (1992-2017) whereas Rignot et al. (2019) measured a mass loss of -41.6 Gt per year (1979-2017) based on the mass budget method. Consistent is only the

overall agreement that the entire Antarctic Ice Sheet is losing mass at a rate between -130.4 Gt/yr (Rignot *et al.* 2019) and -109±56 Gt/yr (IMBIE 2018).

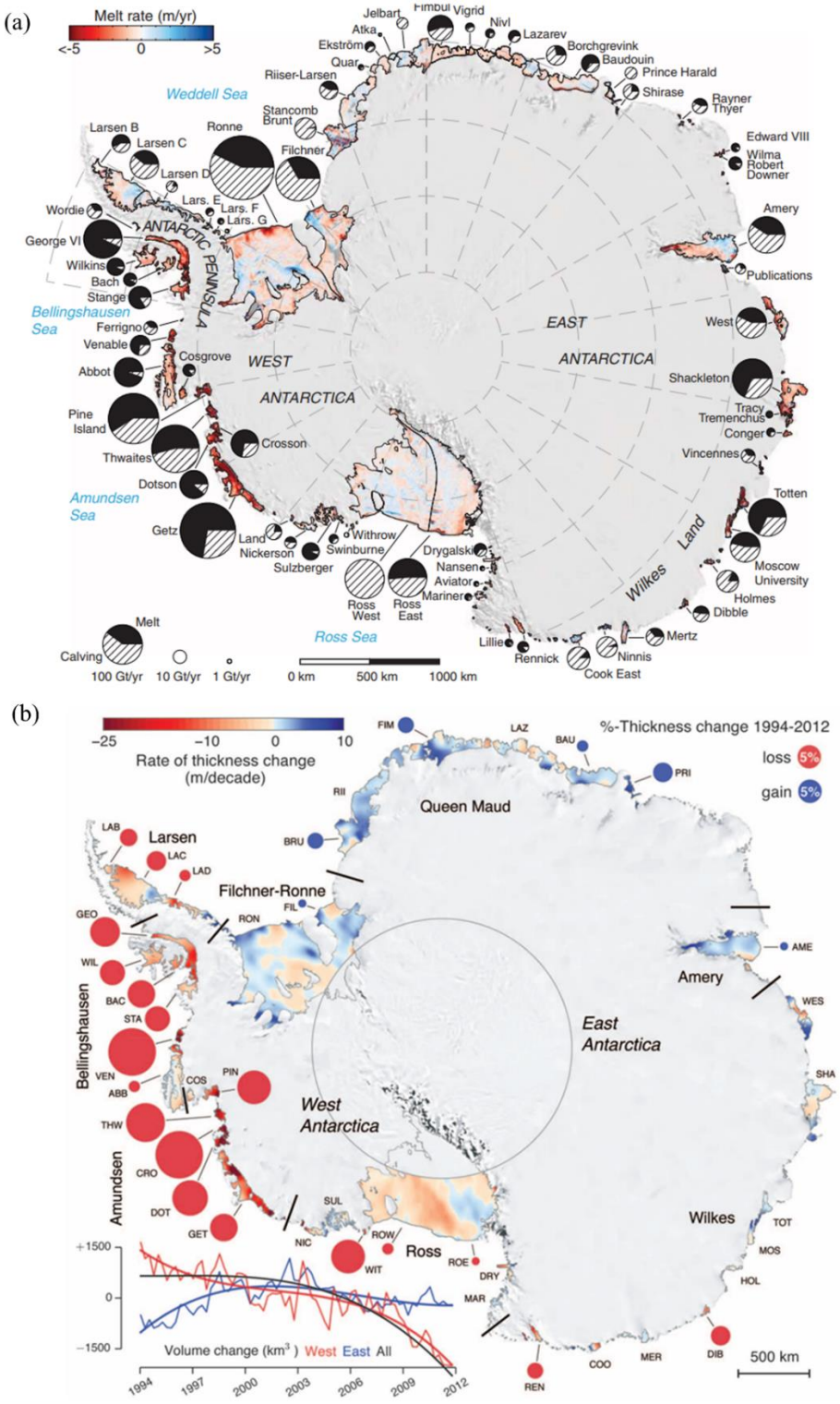

Figure 2.7: (a) Mass loss share between ice shelf melting and iceberg calving. From Rignot et al. (2013). Reprinted with permission from AAAS. (b) Thickness change of ice shelves and glacier tongues between 1994 and 2012. From Paolo et al. (2015). Reprinted with permission from AAAS.

CHAPTER 3

3 A Review on Antarctic Glacier and Ice Shelf Front Dynamics*

The following chapter provides a comprehensive review on glacier and ice shelf front dynamics. The first part introduces basic information on calving front terminology and calving processes. Further on, a short introduction into the history of glacier and ice shelf front studies in relation to remote sensing imagery is provided. Finally, a systematic literature review based on over 100 publications is presented. The results of the review include the spatial and temporal availability of Antarctic glacier and ice shelf front studies. Furthermore, a compiled data set of all existing Antarctic calving front positions measurements is presented.

3.1 Background on Calving Front Dynamics

The calving front is defined as the border between ice sheet and ocean (Nicholls *et al.* 2009). As ice shelves and glaciers are the floating extensions of the ice sheet, they belong to the ice mass on land. In contrast, sea ice and fast ice (multi-year sea ice fastened to land) form from ocean water and do not belong to the ice sheet. All mentioned ice types can have a very similar appearance in remote sensing imagery (depending on season and sensor) and can complicate the immediate detection of the calving front (Bindschadler 1998). Additionally, the delineation of calving fronts is challenging due to icebergs at the glacier front. Sometimes it is difficult to assess whether a piece of ice has already broken off or is still connected to the glacier tongue.

* Parts of this chapter are based on: Baumhoer, C. A., Dietz, A. J., Dech, S., & Kuenzer, C. (2018). Remote sensing of Antarctic glacier and ice-shelf front dynamics - A review. Remote Sensing, 10(9), 1445.

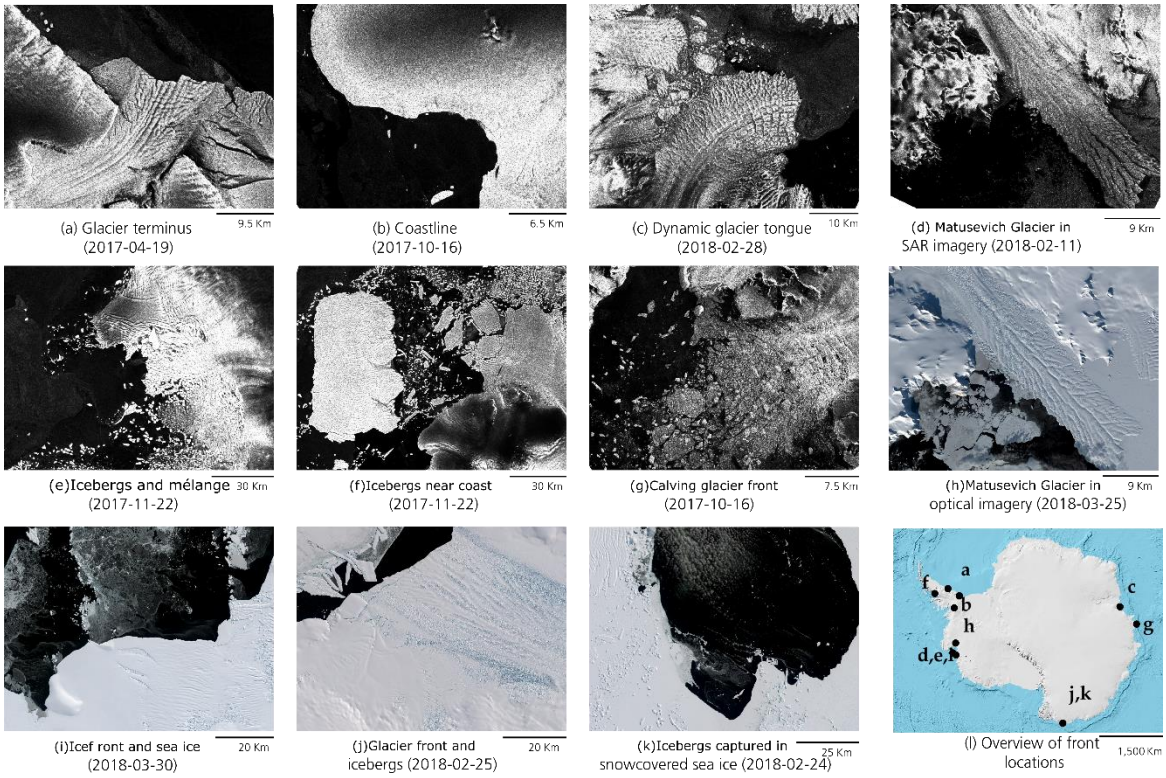

Figure 3.1: Various ice fronts in SAR (a-g) and optical (h-k) remote sensing imagery. Copernicus Sentinel Data 2017/18. Modified after Baumhoer et al. (2018)

Sometimes, icebergs are enclosed in a mixture of slightly frozen sea ice and snow creating ice mélange in front of a glacier after calving (Robel 2017). This can further complicate glacier terminus detection. Examples of different terminus types and their appearance in remote sensing imagery are given in Figure 3.1.

When speaking about calving fronts and their changing position various terms exists. “Front” can be substituted with terminus (Miles *et al.* 2013, Bassis 2011), margin (Fountain *et al.* 2017), calving front (Wesche *et al.* 2013) or barrier (Zwally *et al.* 2002). Taken together the shorter term calving front location (CFL) can be used as proposed by Baumhoer et al. (2018). In contrast to the Greenland Ice Sheet, glaciers and ice shelves of Antarctica not always have solid defined borders. Therefore, the term “coastal change” is often related to calving front change (Ferrigno *et al.* 1998, Williams *et al.* 1995) or changes in ice shelf extent (Bindschadler 1998).

Calving fronts are of great importance for ice sheet dynamics for several reasons. First of all, the calving front location is the periphery of the ice sheet and in direct contact with the ocean. Hence, ice shelves and glaciers are sensitive indicators of environmental change (Wouters *et al.* 2015). Second, calving is a very complex process which can either trigger increased ice flow velocities or can be the result of changes in internal ice dynamics (Benn *et al.* 2007). Last but not least, it is crucial to bear in mind that calving and retreating glacier fronts can be part of the natural cycle of growth and decay of glaciers but also the reaction

to changing environmental conditions (Hogg & Gudmundsson 2017). To make accurate predictions of Antarctic Ice Sheet dynamics and sea level contributions, it is essential to improve the understanding of iceberg calving and the driving forces behind glacier retreat (Luckman *et al.* 2015, Miles *et al.* 2017, Hill *et al.* 2018, Liu *et al.* 2015, DeConto & Pollard 2016, Baumhoer *et al.* 2018).

3.2 The History of Remote Sensing for Calving Front Mapping

Investigating on the effects of climate change on Antarctica's ice sheet has long been of keen interest but faced several challenges as suitable data was missing (Mercer, 1978; Swithinbank, 1980). This changed when for the first time satellite missions acquired imagery over Antarctica and the first observations of iceberg calving and ice shelf front changes on satellite imagery were made by Popham and Samuelson (1965). With the availability of AVHRR and Landsat imagery the first studies on changes of ice shelf extent and flow velocities were published. The dynamic characteristics of West Antarctica's coastline were discovered by Ferrigno and Gould (1987) and Wiliams et al. (1982) based on satellite imagery. But cloud cover, few available satellites and the lack of light during polar night reduced the available scenes to a minimum. Hence, in the beginning only case studies on some specific glaciers and ice shelves were possible. For example, Ferrigno and Gould (1987) used Landsat and NOAA imagery for the year 1986 to study calving events on the Filchner and Larsen Ice Shelves and Thwaites Glacier. They assessed how those events changed Antarctica's coastline.

The first mosaic of entire Antarctica was processed based on AVHRR imagery from the NOAA satellites for a map with 1 km spatial resolution. Unfortunately, cloud cover, geolocation issues and the availability of only 40 usable scenes allowed only a rough and inaccurate mosaic (Merson, 1989). Nevertheless, the front line positions of several glaciers and ice shelves were pictured for the first time for entire Antarctica. To better assess ice sheet dynamics on entire Antarctica, a long-term coastal mapping project of USGS and the Scott Polar Research Institute was started in the 1990s. This was recommended by SCAR (The Scientific Committee on Antarctic Research) and the Polar Research Board of National Council to map coastal change of Antarctica on the basis of 24 regional maps (Williams, et al., 1995). The first official map was published in 1991 based on NOAA and Landsat imagery, and a second modified map followed in 1996. Still, severe geolocation errors were apparent with a mean root square error of 2.5 km (Williams, et al., 1995). One of the first encompassing studies using this data was published by Ferrigno (1998) and highlighted the very dynamic nature of Antarctica's coastline. This study detected several calving events and glacier front advances. However, no clear trend for retreating or advancing fronts (between the 70s and 90s) was detected for the studied area.

The maps were improved over the years by adding additional imagery from following Landsat missions and Radarsat imagery to complete the Coastal-Change and Glaciological Maps of Antarctica map series of USGS. Within this project glacier and ice shelf fronts were mapped for each decade back to the 40s (if aerial imagery was available). Valuable information on coastal change and changing front line positions over the last decades until 2004/2009 (depending on region) were provided by accompanying pamphlets delivered with each map.

Direct comparison on ice shelf extent changes became easier with the two Radarsat mosaics produced in the framework of the Antarctic Mapping Project (RAMP). A high-resolution coastline extracted from a Radarsat mosaic from 1997 was published by Liu and Jezek (2004b). This milestone increased the resolution from 1: 1 000 000 on the USGS maps to 20-times higher resolution of 1: 50 000, and cloud cover was no issue anymore due to the usage of SAR imagery. Still, the automatically extracted coastline had to be manually adjusted. In 2000, the same methodology was applied for a second Radarsat mosaic to extract the coastline again and compare changes as suggested in the frame work of the MAMM (Modified Antarctic Mapping Mission). Shortly after, a coastline on a 125m grid was manually extracted from a mosaic of MODIS imagery for the years 2004 and 2009 (Scambos, et al., 2007). In 2007, old ARGON imagery from 1963 was processed to prolong the time series of coastal change (Kim, et al., 2007).

The most up to date coastline is provided by the Antarctic Digital Database (ADD) where different scientists manually update the coastline frequently by mostly optical imagery. Hence, only partial coverage of updated data is available. All in all, the Antarctic coastline has been studied in the past and annual comparisons of ice shelf extents exist. But due to limited remote sensing data and time consuming manual delineation, there is a lack of intra-annual time series of glacier front retreat as well as circum-Antarctic calving front change products do not yet exist.

3.3 Results of the Literature Review

For a systematic literature review on Antarctic glacier and ice shelf front analysis, 114 relevant SCI (Science Citation Index) papers were identified. The criterion for publication selection was the analysis or mapping of Antarctic calving fronts based on airborne and/or satellite remote sensing data. For each study, information on the following topics was extracted: used input data, applied sensors, study topic, research motivation, studied glacial features, applied methodology and spatial location of the study region. Additionally, if rates of glacier terminus retreat or advance had been mentioned, they would have been added to a circum-Antarctic data set on calving front location changes which is

presented at the end of this chapter. Prior to that, the spatial and temporal coverage of all reviewed studies is presented.

3.3.1 Categorization of Calving Front Studies

To identify major reasons for calving front mapping and analysis all studies were categorized regarding study topic, research motivation and author nationality. Additionally, the number of studies analyzing glaciers, ice shelves or the entire coastline was assessed. The results are displayed in Figure 3.2. Figure 3.2a visualizes that one quarter of the assessed studies just mapped changes in glacier and ice shelf extent. The other quarter specifically investigated glacier retreat or ice shelf collapse.

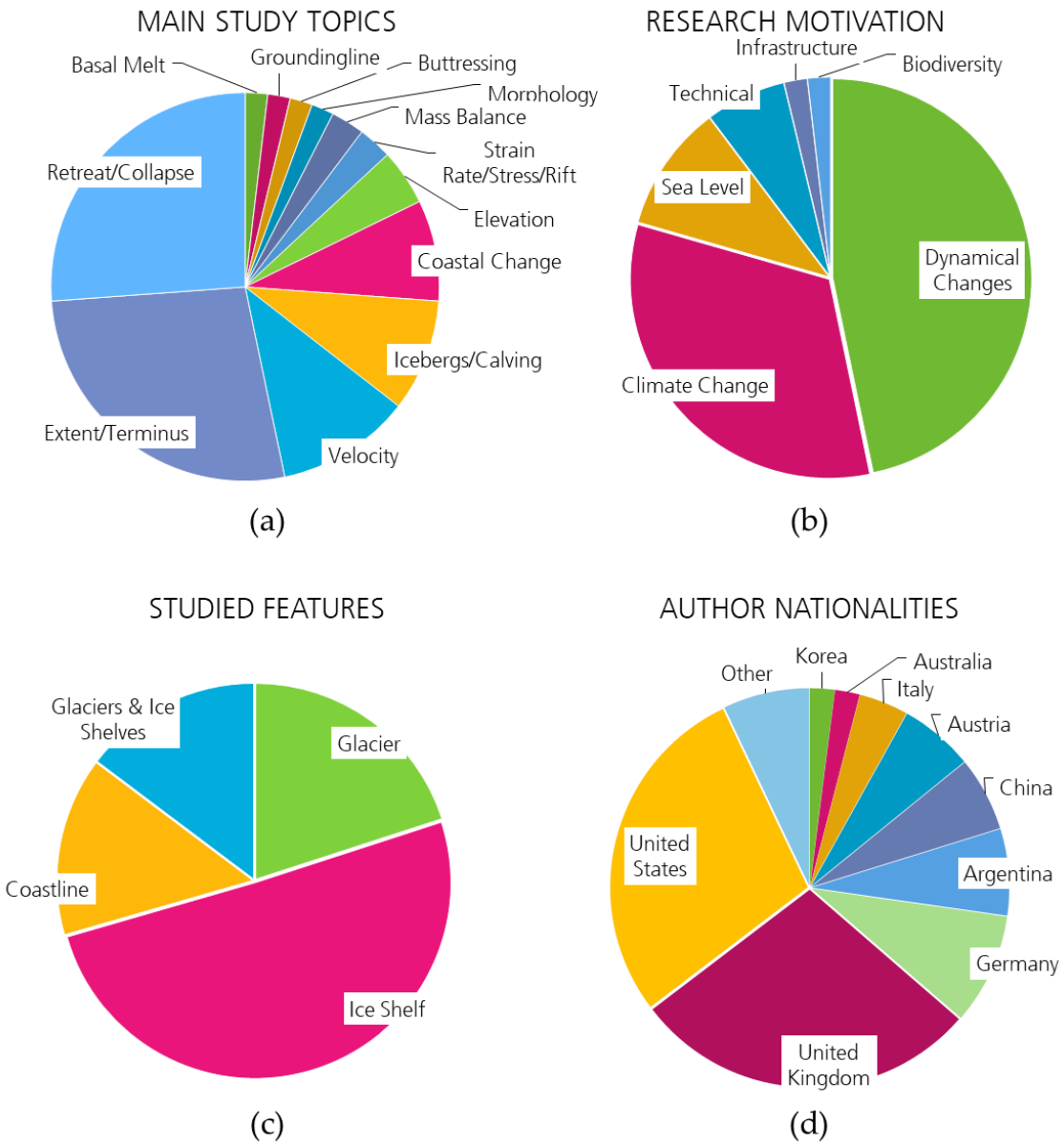

Figure 3.2: Pie charts summarizing main study topics (a), research motivation (b), studied glacial features (c) and first author nationalities identified by the systematic review. Modified after Baumhoer et al. (2018).

The other half of the studies was split into several smaller proportions assessing front locations in combination with velocity measurements, iceberg calving, and coastal change. Only a minor part of the studies combined grounding line movement, buttressing effects, mass balance, basal melt, and elevation changes with fluctuations in CFL. The great number of studies that solely investigated single glaciers or the coastline position in one satellite scene comprise early studies. At that time, the processing of satellite and airborne images was still expensive and data availability limited (Williams *et al.* 1995, Frezzotti *et al.* 1998, Ferrigno *et al.* 1998). In recent years, however, satellite image availability, better processing capabilities, and numerous data sets allowed much more complex study topics such as buttressing effects, velocity changes, and basal melt (Massom *et al.* 2018, Goldberg *et al.* 2009, Robel 2017).

The research motivation of half of the assessed studies was the understanding of ice dynamical changes (see Figure 3.2b). The authors tried to link changes in glacier and ice shelf extent with ice sheet dynamics to better understand calving processes. One third linked CFL no longer solely to ice sheet dynamics but climate change. Especially in the earlier studies, rising air temperatures were thought to cause calving front retreat (Cook *et al.* 2005, Mercer 1978). A smaller part of the studies assessed the glacier terminus position regarding infrastructure or biodiversity. For example, the calving of Brunt Ice Shelf could have affected the British research station Halley (Anderson *et al.* 2014). For seven percent of the studies, only the technical aspect of calving front extraction from satellite imagery was the study motivation. This included algorithm development with image recognition techniques.

From all assessed studies, the majority (50 %) studied solely ice shelves. Glaciers were only assessed in one-fifth of the studies (see Figure 3.2c). Glaciers and ice shelves together were studied in 16 % of the publications and the entire coastline in 14 %. The high number of ice shelf studies can be explained with a strong interest in ice shelf disintegration events (Doake *et al.* 1998, Braun *et al.* 2009) and basal melt weakening the ice shelves tremendously (Albrecht & Levermann 2014, Massom *et al.* 2015, Schodlok *et al.* 2016).

The last pie chart in Figure 3.2d displays the first author nationality off all 114 reviewed papers. The main proportions of authors were from the UK or the United States. British studies were numerous due to the long history of Antarctic research by the British Antarctic Survey. Especially Cook, Vaughan, and Pritchard were significant contributors (Cook *et al.* 2016, Vaughan & Doake 1996, Pritchard *et al.* 2012). Various studies from the United States were performed within the USGS coastal change mapping project by Ferrigno and Williams (Williams *et al.* 1995, Ferrigno *et al.* 2004) and Scambos from the University of Colorado (Scambos *et al.* 2000). In the late 1990s and early 2000s, the Austrians with the research group of Rack and Rott in cooperation with the Argentinian research group led by Skvarca dominated the research field of calving front change. During

this period, also calving front studies were frequently published by Frezzotti and Polizzi from Italy (Frezzotti & Polizzi 2002, Frezzotti 1997). More recently, Chinese and German scientists started to publish on ice shelf and glacier extent changes.

3.3.2 Geospatial Agglomeration and Coverage of Calving Front Studies

One main intention of this review was to locate spatial gaps in the mapping and analysis of glacier and ice shelf front change. The spatial availability of calving front studies is displayed in Figure 3.3. Three different maps are presented to visualize all different kinds of calving front and coastal change studies. The spatial agglomeration of calving front studies is displayed in the heat map of Figure 3.3a. Each glacier or ice shelf analyzed in the reviewed studies was included in the data set once per study. The heat map highlights a high amount of studies within a radius of 100 km in red whereas fewer available studies are indicated in blue. Hotspots of calving front mapping were located along the Antarctic Peninsula, King George Island and Victoria Coast (Cook & Vaughan 2010, Fountain *et al.* 2017, Lovell *et al.* 2017, Cook *et al.* 2016, Lee *et al.* 2008, Rückamp *et al.* 2011, Simões *et al.* 1999). The common nature of all three mentioned hotspots is the occurrence of many smaller outlet glaciers. This is in contrast to ice shelves which were mainly studied individually (Braun *et al.* 2009, Friedl *et al.* 2018, Fricker *et al.* 2002). Outlet glaciers were often mapped together in order to identify their individual calving front movement by having similar environmental conditions. Marine terminating glaciers are very sensitive to ocean and atmospheric forcing which made them an important and very dynamic study feature for climate change impact studies (Fountain *et al.* 2017, Lovell *et al.* 2017, Cook *et al.* 2005, Cook *et al.* 2016, Davies *et al.* 2012).

Besides the spatial distribution also the spatial coverage of calving front studies strongly varied. All of the reviewed studies were assigned to one of the following classes:

- Local case studies focusing on one glacier or ice shelf
- Regional studies covering CFL changes over a smaller coastal section
- Circum-Antarctic studies covering the entire Antarctic coastline

Local case studies accounted for 63% of the reviewed studies whereas regional and circum-Antarctic studies were conducted in only 27% and 10% of the cases, respectively.

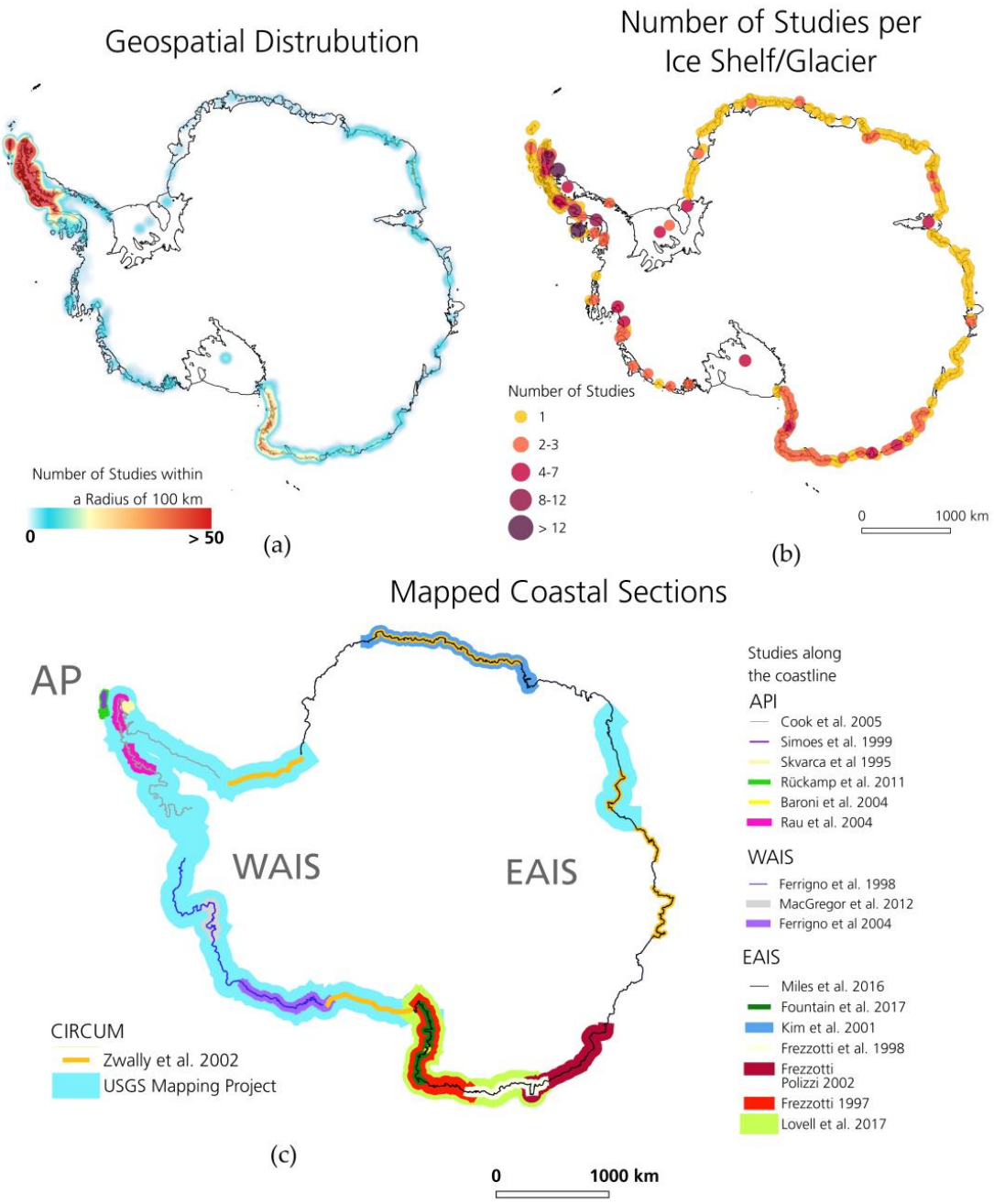

Figure 3.3: Geospatial distribution and coverage of calving front studies. (a) Geospatial distribution, (b) number of studies per individual glacier and ice shelf, and (c) spatial coverage of coastline studies. AP: Antarctic Peninsula, EAIS: East Antarctic Ice Sheet, WAIS: West Antarctic Ice Sheet. Modified after Baumhoer et al. (2018).

Local Calving Front Studies

Spatial disparities in glacier and ice shelf front studies were clearly apparent (see Figure 3.3b). Local calving front studies were concentrated on a few glaciers and ice shelves. Larsen B Ice Shelf leads the statistic with 27 studies. Frequent publications (number in brackets) were available for Wilkins (12), Larsen A (12), Larsen Inlet (11) and

Prince Gustav Ice Shelf (10). The interest in the Larsen Ice Shelf is connected to the previous disintegration events reported for Larsen A Ice Shelf in 1995 and Larsen B Ice Shelf in 2002 (Glasser & Scambos 2008, Royston & Gudmundsson 2016). Detailed studies tried to assess the causes of disintegration as well as the resulting consequences through reduced buttressing (De Rydt *et al.* 2015, Glasser & Scambos 2008). This is especially of interest for the future behavior of the still remaining Larsen C Ice Shelf where a major calving event took place in 2017 (Hogg & Gudmundsson 2017). Wilkins Ice Shelf was a great example of how increased satellite imagery availability enabled the frequent mapping of a disintegration event. Since the 1990s, Wilkins experienced retreat before detaching from Charcot Island in 2008/09 resulting in a partial collapse (Rankl *et al.* 2017).

The two biggest ice shelves of Antarctica (Ronne-Filchner and Ross) are well studied. Calving was the major ablation process for both and break up events resulted in very large icebergs (Keys *et al.* 1998, Wuite *et al.* 2019, Ferrigno *et al.* 2005). The most studied glacier fronts of West Antarctica belonged to Pine Island and Thwaites Glacier. Pine Island and Thwaites were of major importance as they are located on a retrograde bed and retreat of the grounding line can self-reinforce further retreat (Dutrieux *et al.* 2014, Seroussi *et al.* 2017). Both glaciers showed the largest mass losses for single Antarctic glaciers, and their basins hold enough mass to significantly contribute to global sea-level rise (Rignot *et al.* 2019). Studies around Pine Island Bay were less frequent as mass loss was less severe at those glaciers and ice shelves (IMBIE 2018). Well studied glacier and ice shelf fronts in East Antarctica were Aviator (4), Mertz (6), Glaciar de Franciase (6), and Amery Ice Shelf (4). Little less studied was Shackleton Ice Shelf, Shirase Bay, and Victoria Land. Gaps in calving front information existed at Wilkes, Dronning Maud, Enderby, and Queen Mary Land. Many studies for Amery Ice Shelf with regular calving cycles as well as for the characteristic Mertz Glacier Tongue existed (Fricker *et al.* 2002, Giles 2017). In the past, the assumption of a relatively stable EAIS may have led to little research activity on calving fronts in that region (Shepherd *et al.* 2012). But recently a paradigm shift took place highlighting the potential vulnerability of EAIS and asking for more detailed studies in East Antarctica (Rignot *et al.* 2019).

Regional Calving Front Studies

Regional calving front studies have often been used to identify links between glacier and ice shelf fluctuations and changes in the environmental boundary conditions (Fountain *et al.* 2017, MacGregor *et al.* 2012, Miles *et al.* 2016, Cook *et al.* 2016). Figure 3.3c summarizes all studies covering a specific area along the coastline. The coastline of the Antarctic Peninsula was well studied and covered by several analyses. Very comprehensive studies were published by Cook et al. (2010, 2016, 2005) over the last years analyzing the far reaching calving front retreat since the 1940s regarding atmospheric and oceanic

forcing. Most of the glaciers of the Western Antarctic Peninsula retreated except for the northernmost coast due to the cooler ocean conditions in the Bransfield Strait Water (Cook *et al.* 2016). Similar patterns were observed by Rau et al. (2004). Glaciers of the northern Trinity Peninsula were more or less stable whereas the Eastern Antarctic Peninsula (including James Ross Island) and the southern Western Antarctic Peninsula were dominated by glacier retreat. Ice shelves along the Antarctic Peninsula did not show such a uniform behavior. Some had stable or advancing fronts over the entire observation period whereas others retreated or disintegrated completely (Cook & Vaughan 2010). Ice shelves were subject to forcing reaching from rising air and ocean temperatures to foehn winds and strong surface melt, lake drainage, and ponding (Leeson *et al.* 2017, Leeson *et al.* 2020, Walker & Gardner 2017, Scambos *et al.* 2000, Cape *et al.* 2015).

The coastline of the WAIS was less well studied. Regional studies only exist from Ferrigno et al. (2004, 1998) and MacGregor et al. (2012) covering Pine Island Bay. Clear trends in retreat were observed for Pine Island and Thwaites Glacier. The pattern of retreat differentiated between advance and major calving events for Pine Island Glacier and almost continuous retreat of Thwaites Glacier (MacGregor *et al.* 2012). For the remaining coastline, no strong trends in front position change were observed since the 1970s. The major ice shelves Abbot, Getz, and Sulzberger were relatively stable with little change. Between the 1970s and early 1990s, a slight overall advance for Marie Byrd and Ellsworth Land was observed (Ferrigno *et al.* 1998) whereas the fronts of Sulzberger and the eastern Getz Ice Shelf receded between 1972 and 1997 (Ferrigno *et al.* 2004).

Regional studies along East Antarctica varied in space where areas around Victoria Land, Oates Coast, and George V Coast were covered by several studies. In contrast, most parts of Wilkes, Coats, and Enderby Land were only covered by one study (Miles *et al.* 2016). Calving front changes along Victoria Land and also George V and Oats Land were attributed to internal ice dynamics and glacier type instead of changing boundary conditions. Between 1955 and 2015, no clear trend in calving front fluctuations along Victoria Land was observed and changes did not correlate with sea ice and air temperature changes. This led to the conclusion that the different glacier types were the reason for retreat and advance (Fountain *et al.* 2017). This was also confirmed by Lovell et al. (2017). Frezzotti et al. (1997, 2002, 1998) did not observe any trend in CFL along Victoria Land. Oates and George V Land were characterized by a cyclic behavior switching between retreat and advance. Calving fronts of Dronning Maud Land retreated between 1963 and 1997 with most retreat happening until 1975 (Kim *et al.* 2001). The overall retreat was also observed by Zwally et al. (2002) between 1983 and 1986 for Dronning Maud Land.

The most comprehensive study on glacier terminus changes along East Antarctica was published by Miles et al. (2016). They assessed calving front change since the 1970s in decadal time steps. This extensive study revealed that glaciers and ice shelves switched

from retreat (1972-1990) to advance (1990-2012) which lead to the assumption of a cyclic calving behavior of East Antarctic glaciers and ice shelves. The only exception was Wilkes Land where calving fronts retreated over the entire observation period (Miles *et al.* 2016).

Circum-Antarctic Calving Front Studies

To this day, no circum-Antarctic glacier and ice shelf front change study exists (Baumhoer *et al.* 2018). The only possibility to analyze pan-Antarctic changes in CFL is to compare different coastline products of Antarctica. The first complete coastline of Antarctica was mapped by the US spy satellite ARGON in 1963 (Kim *et al.* 2007). This first mosaic of satellite imagery is a great source of calving front information. Nevertheless, consisting of almost not overlapping scenes and very limited acquisitions many areas were cloud covered including broad sections of the WAIS. The Landsat era beginning in 1973 enabled the monitoring of the Antarctic coastline. Still, cloud-free imagery was limited. Initiated by the USGS and SPRI (Scott Polar Research Institue), the Coastal-Change and Glaciological Maps of Antarctica project started in 1990. First map templates were published in 1997 with encompassing studies revealing the very dynamic nature of Antarctica's glaciers and ice shelves (Frezzotti *et al.* 1998, Swithinbank *et al.* 1997). Today, 10 maps have been published including additional satellite imagery and airborne data to assess calving front change.

The first continuous coastline of Antarctica was created by cloud independent radar data in the context of RAMP. A high-resolution coastline was extracted from Radarsat mosaics in 1997 and 2000 (Liu & Jezek). Continuous coastlines from optical satellite imagery were created with MODIS imagery for the years 2004, 2009, and 2014 based on mosaics with a resolution of 125 m (Scambos *et al.* 2007). An additional coastline was delineated from ALOS Palsar and Envisat ASAR data (2008/09) in the context of the International Polar Year (IPY). The most up to date Antarctic coastline is provided by the Antarctic Digital Database (ADD). Manual partly updates (based on all kinds of satellite and airborne imagery) are regularly added. Hence, the ADD coastline is a composition of different resolutions, authors as well as dates and not consistent in mapping standards. All available coastline products are listed in Table 3.1. Even though nowadays several coastline products exist, they cannot directly be used to assess calving front changes. Several factors cause inconsistency in the data such as different approaches of front extraction (manual and semi-automatic), the subjectivity in front delineations, different spatial resolutions, and differences in optical and radar imagery. Hence, deviations between the coastline products cannot be related solely to calving front change.

Table 3.1: Available coastline Products for Antarctica based on remote sensing data. Modified after Baumhoer et al. (2018)

Product	Provider	Year	Description	Access
ADD Coastline	ADD	2002 – today	Most up to date product. Parts of the coastline are frequently updated by various authors. Fronts are delineated from different remote sensing products.	www.add.scar.org
ADD Coastal Change	ADD	1843 -2008	Front fluctuations for all glaciers on the Antarctic Peninsula. Based on the USGS mapping project	www.add.scar.org
Mosaic of Antarctica 2014 (MOA 2014)	NSIDC[1]	2014	Coastline manually delineated from MODIS mosaic 2014	https://nsidc.org/data/nsidc-0730#
Mosaic of Antarctica 2009 (MOA 2009)	NSIDC[1]	2009	Coastline manually delineated from MODIS mosaic 2009.	http://nsidc.org/data/NSIDC-0593
Mosaic of Antarctica 2004 (MOA 2004)	NSIDC[1]	2004	Coastline manually delineated from MODIS mosaic 2004.	http://nsidc.org/data/nsidc-0280#
RAMP AMM-1 (Antarctic Mapping Mission)	BPCRC[2]	1997	Coastline of RADARSAT Mosaic 1997.	http://research.bpcrc.osu.edu/rsl/radarsat/data/
RAMP MAMM (Modified Antarctic Mapping Mission)	BPCRC[2]	2000	Coastline of RADARSAT Mosaic 2000 (Jezek 2002a).	http://research.bpcrc.osu.edu/rsl/radarsat/data/
Antarctic Boundaries MEaSURE V2	NSIDC[1]	2008-2009	Coastline extracted from ALOS PALSAR and ENVISAT ASAR during the International Polar Year.	http://nsidc.org/data/NSIDC-0709
Coastal-Change and Glaciological Maps of Antarctica	USGS	1843-2009	Maps with different front positions mainly AP and WAIS.	https://pubs.usgs.gov/imap/2600/

1 National Snow and Ice Data Center; 2 Byrd Polar Climate Research Center, 3Climate Change Initiative

3.3.3 Temporal Availability of Calving Front Measurements

The temporal availability of calving front measurements was limited by existing observations as well as available cloud-free satellite and airborne acquisitions (Baumhoer *et al.* 2018). Variations in the absolute observation length are displayed in Figure 3.4. The observation length was calculated between the first and last year of available CFL records. Longest observations span a period of 170 years for Ross Ice Shelf, followed by Mertz Glacier (103 years), and the characteristic glacier tongues of Victoria Land like Mackay (113), Nordenskjöld (107), Campbell (103), Ninnis (97) and Harbord (107). These earliest observations reach back to the first ship expeditions to Antarctica and are just approximate front positions (Ross 1847). Good temporal coverage of Antarctic CFLs exists for the Antarctic Peninsula based on airborne images acquired during the RARE (Ronne Antarctic Research Expedition) in 1947. The longest observations in West Antarctica exist for Pine Island Glacier. Especially for the ice shelves Abbot, Getz and Sulzberger shorter records dominate as (besides Landsat images since the 1970s) no cloud-free images existed over

the WAIS. East Antarctica has a long record of glacier and ice shelf front locations in Victoria Land and parts of Oates and George V Land. Also calving fronts of Brunt and Amery Ice Shelf were mapped during ship expeditions with records over 75 years. All other parts have been well covered since the 70s by Landsat imagery published by Miles et al. (2016). Only gaps in the eastern Dronning Maud Land and Wilkes Land exist due to limited image availability.

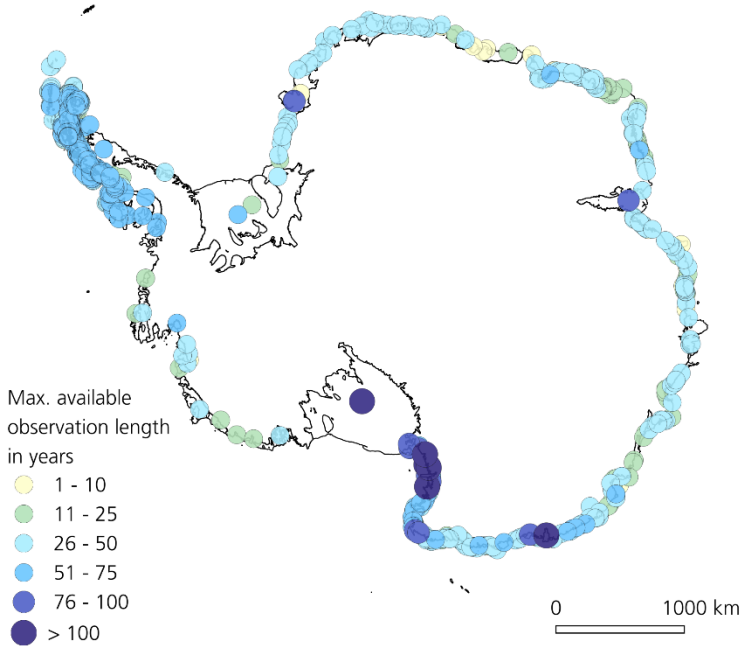

Figure 3.4: Maximum observation length in years for available calving front data. Modified after Baumhoer et al. (2018).

Besides the observation length of calving front change, also the interval of mapping is crucial. As stated by Baumhoer et al. (2018): "The very dynamic nature of glacier tongues and ice-shelf fronts requires a regular monitoring of front positions, as changes between phases of retreat and advance may occur within a few years". Very long observation intervals allow to asses long-term trends in calving front change without disturbances of shorter-term calving cycles (Miles *et al.* 2016). Frequent mapping intervals are needed when studying detailed ice dynamics or monitoring disintegration events (Kussul *et al.* 2017, Wang *et al.* 2016). During the review process, the lack of annual or sub-annual calving front studies was ascertained. Especially image availability was connected to the temporal availability of calving front measurements.

3.3.4 A Compiled Dataset on Existing Calving Front Change Rates

One aim of this review was to collect all available measurements on Antarctic calving front change and compile them to one circum-Antarctic data set. This approach faced several challenges as measurement gaps existed due to limited satellite imagery

availability, measurements cover different time periods and different methods were used to track glacier front changes. Therefore, two time periods covered by the majority of all reviewed studies were chosen (1972/75 to 1988/95 and 2001/ to 2009/2015). The beginning of the Landsat era was chosen as starting point as earlier no measurements for the East Antarctic Ice sheet exist as already mentioned by Miles et al. (2016). Start and end points lie within a short time span as the measurement lengths of different studies varied. If several studies were available for the same glacier or ice shelf, the measurements were averaged. Figure 3.5 explains in more detail how average change rates were calculated. Only area and distance measurements had to be kept separately as they could not be converted to the other without information on glacier width.

Study	Start	End	Annual Change Rate
A	1980	1990	2
B	1990	2010	4
C	1995	2000	5
D	2000	2010	3

Study/ Year	A	B	C	D	Overall Change Rate
1980	2				2
1981	2				2
1982	2				2
1983	2				2
1984	2				2
1985	2				2
1986	2				2
1987	2				2
1988	2				2
1989	2				2
1990	2	4			3
1991		4			4
1992		4			4
1993		4			4
1994		4			4
1995		4	5		4.5

Study/ Year	A	B	C	D	Overall Change Rate
1995		4	5		4.5
1996		4	5		4.5
1997		4	5		4.5
1998		4	5		4.5
1999		4	5		4.5
2000		4	5	3	4
2001		4		3	3.5
2002		4		3	3.5
2003		4		3	3.5
2004		4		3	3.5
2005		4		3	3.5
2006		4		3	3.5
2007		4		3	3.5
2008		4		3	3.5
2009		4		3	3.5
2010		4		3	3.5
					3.24

Figure 3.5: Example for calculating overall change rates for one glacier. The above table includes measurements of different studies (A-D) for different time frames. None of the studies cover the example period between 1980 and 2010. To calculate the change rate from 1980 to 2010 the available annual rates of different studies were averaged for each year (blue column). The overall annual change rate is the average of all values per year (orange line).

The compiled data set is presented in Figure 3.6. Circles are proportional to the magnitude of measured distance changes and diamonds to area change. Blue colors indicate advance whereas red colors retreat. Darker colors imply higher annual change rates. The compiled data set includes more retreating glaciers between 1972/75 and 1988/58 and more advancing glaciers between 2000/01 and 2009/15. Besides this overall trend, local differences exist. Along the Antarctic Peninsula glaciers retreated at the same magnitude

during both observation time frames. Ice shelf retreat was more pronounced in the 1970s and 1980s compared to the later time period. The earlier strong retreat was attributed to the strong retreat of the Prince Gustav, Larsen A, Larsen, Larsen C, Wilkins, Wordie and George VI ice shelves. Later, only the Larsen B, Larsen C and Wilkins ice shelves retreated further. The Larsen D Ice Shelf was the only exception at the Peninsula with a clearly advancing front (see Figure 3.6e).

Measurements for West Antarctica were rare due to reduced scene availability. Studies focused mostly on Pine Island Bay but available studies could not be used for the compiled data set as they did not span the selected calculation time frames. During 1972/75 and 1988/95, the Dotson and Crosson Ice Shelf retreated whereas Abbot and Getz Ice Shelf were stable. The Pine Island Glacier slightly advanced at that time. It should be mentioned that glaciers in the Pine Island Bay are very dynamic (MacGregor *et al.* 2012) and the stable measured front position probably moved in-between but just ended at the same position as it started over the time of observation.

Along Victoria Land, the southernmost glaciers advanced between 1972/75 and 1988/95 whereas the ones along the northern coast slightly retreated. During the later time period, the reversed pattern was apparent. Investigations on boundary conditions and glacier types revealed that those changes were rather attributed to glacier geometry than to a changing climate (Lovell *et al.* 2017, Fountain *et al.* 2017). In the 70s and 80s also the nearby George V and Oates Land had retreating fronts that mostly started to advance later on. This stands in contrast to Wilkes Land where glaciers during both observation periods retreated. This retreat was in line with the negative mass balance (Gardner *et al.* 2018). Miles et al. (2016) found out that a strong decrease in sea ice days was the most probabilistic driver for retreat. At the EAIS, the two big ice shelves Amery and Shackleton advanced over the entire time period whereas smaller shelves and glaciers switched between retreat and advance. Along Kemp and Enderby Land glaciers retreated in the earlier time frame and started to re-advance between 2000/1 and 2009/15. Dronning Maud Land had more retreating ice shelves in the 70s and 80s that started to re-advance until 2009/15. Only a small amount of ice shelves like Leningradbukta and Trolltunga retreated between 2000/01 and 2009/15.

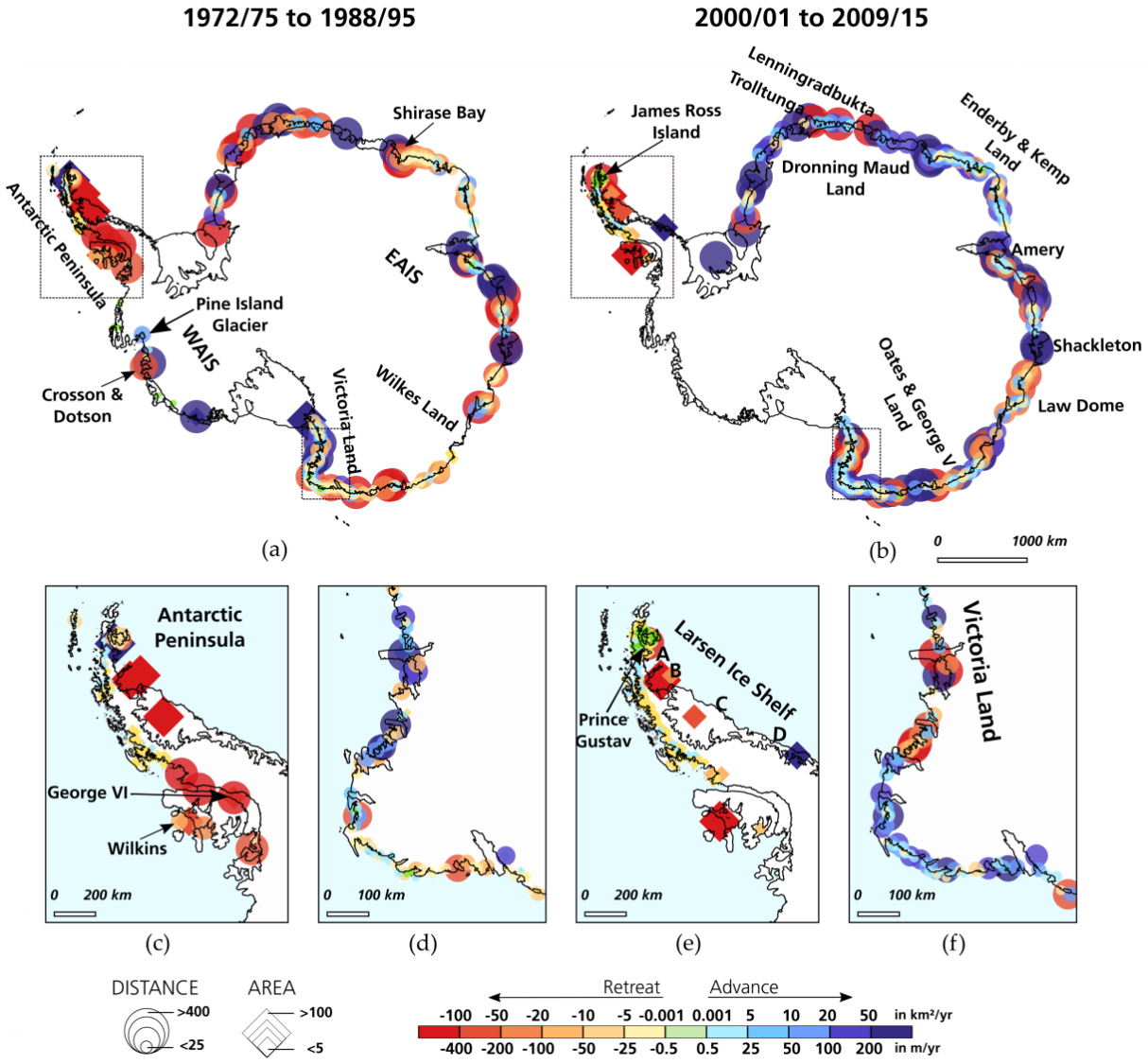

Figure 3.6. Circum-Antarctic pattern of annual calving front change rates. Red colors show retreating calving fronts, whereas blue colors show advancing glacier and ice shelves. Colored dots indicate measurements by distance, and diamonds indicate measurements by area. The map (a) shows advancing and retreating fronts between 1972/75 and 1988/95. Magnified views of advance and retreat are presented in (c) for the Antarctic Peninsula and (d) for Victoria Land. Advance and retreat between 2000/01 and 2009/15 is presented in (b) with magnified views in (e) and (f) of Antarctic Peninsula and Victoria Land. Modified after Baumhoer et al. (2018).

3.4 Summary

This review emphasized the importance of calving fronts for accurate sea level projections due to buttressing effects. They were most often studied to analyse glacier retreat and ice shelf disintegration with regards to ice dynamics and climate change. Remote sensing imagery was essential to map and analyse glacier and ice shelf front fluctuations. For early studies in the 1970s and 1980s studies were limited by image availability. Calving front studies concentrated on the Antarctic Peninsula and Victoria

Land with gaps along West Antarctic, Wilkes, and Dronning Maud Land. Frequent studies on specific ice shelves were mostly conducted in relation to disintegration events. Taken all reviewed studies together, every part of the Antarctic coastline was at least analyzed once, even though, the results covered different time frames and could not be used directly for a circum-Antarctic calving front assessment. Maximum observation lengths were closely connected to image availability. Over the Antarctic Peninsula, good coverage of airborne imagery exist since 1947. The Antarctic coastline was first mapped completely in 1963 by ARGON imagery but frequent observations started with the Landsat era in the 70s. Our compiled data set revealed a strong retreating trend along the Antarctic Peninsula since the 1970s. The WAIS was lacking suitable long-term studies even though the extreme mass loss in this region would require them. Along East Antarctica glaciers and ice shelves had an overall retreat phase between 1972/75 and 1988/95 and an advancing phase between 2000/01 and 2015. The only exception was Wilkes Land showing constant glacier retreat.

To conclude, “standardized and high-interval measurements of calving fronts would revolutionize our understanding of glacier and ice shelf dynamics, contribute to more sophisticated ice sheet models by replacing steady-state calving front assumptions, and allow better identification of the boundary conditions driving calving front change.” (Baumhoer *et al.* 2018).

Chapter 4

4 Remote Sensing of Calving Fronts*

This chapter highlights the opportunities, potentials, and challenges of earth observation for mapping, monitoring, and analysing Antarctic glacier and ice shelf fronts. Moreover, the characteristics and suitability of optical and Synthetic Aperture Radar (SAR) sensors are discussed and existing methods for calving front extraction and frontal change measurement are introduced.

4.1 The Potential of Satellite Sensors to Monitor Calving Fronts

Space-borne remote sensing supports the mapping of the Antarctic coastline, tracking of coastal change, and monitoring of fluctuatuating calving fronts for selected glaciers and ice shelves. The great advantage of earth observation for glacier and ice shelf front mapping is the large-scale spatial coverage as well as the option for continuous monitoring. On-site expeditions are be too time- and cost-intensive for a comparable amount of in-situ measurements. To extract glacier and ice shelf fronts from optical and SAR imagery, a comprehensive knowledge of spectral and physical properties of glacial features is required. The boundary between land and ocean has to be extracted to determine the accurate frontal position. This may be challenging for Antarctic glaciers and ice shelves due to snowmelt (Liu *et al.* 2006, Fahnestock *et al.* 1993) and changes in seasonal sea ice coverage (Kwok *et al.* 1992, Bogdanov *et al.* 2005, Ressel *et al.* 2015). Additionally, sea ice and ice sheet backscatter characteristics and reflectance spectra vary throughout the year making the classification more challenging (Wesche & Dierking 2012, König *et al.*

* Parts of this chapter are based on: Baumhoer, C. A., Dietz, A. J., Dech, S., & Kuenzer, C. (2018). Remote sensing of Antarctic glacier and ice-shelf front dynamics - A review. Remote Sensing, 10(9), 1445.

2001). The advantages and disadvantages of optical and SAR imagery are summarized in Table 4.1.

Table 4.1: Comparison of advantages and disadvantages for calving front location (CFL) extraction in optical and SAR imagery. Modified after Baumhoer et al. (2018).

Variable	Optical	SAR
Accuracy	High spatial accuracy and often higher resolution	Lower spatial accuracy
Data Availability	Low scene availability due to polar night and heavy cloud cover	High scene availability due to light independence and penetration of clouds
Snow & Clouds	Similar reflectance of snow and clouds for some wavelengths	Penetration of clouds and thin snow cover
Ice	Different spectral bands allow separation of ice features. Separation of shelf ice and fast ice sometimes challenging due to snow cover.	Change of backscatter values during the year (glacier facies) Different ice types might have similar backscatter values
Additional	Even for non-experts fronts are easy to distinguish	Wind roughening of the ocean surface. High contrast for water-ice boundary Shadow, Layover, incident angle, penetration depth.

4.1.1 Spectral Properties of Antarctic Surface Features and Clouds

Optical satellite imagery reveals the entire beauty of Antarctica. Ice shelf fronts and glacier termini can be easily defined visually. The low reflectance of the ocean builds a high contrast to bright snow and ice. Depending on age, fresh snow reflects up to 80-90 % of the radiation in the visible spectrum. The reflected portion decreases as the snow gets older and grain sizes increase due to melting and refreezing (Dietz *et al.* 2012). Whereas snow and glacier ice are distinguishable in the visual spectrum, the differentiation of perennial sea ice and shelf ice can be very ambiguous in the case of snow cover. A classification of different features occurring in Antarctic satellite imagery is possible if different wavelengths are considered.

Figure 4.1 displays the reflectance properties of different cloud, snow, and ice types. The separation of snow and clouds can be very difficult within shorter wavelengths especially regarding ice clouds. Best results can be obtained for the reflectance decline of snow towards the short-wave infrared (Dietz *et al.* 2012). Sometimes, difficulties arise for the delineation of shelf ice and long-term sea ice due to snow cover (Scambos *et al.* 2007) or the spectral similarity of both ice types (Klinger *et al.* 2011). The reflectance spectra of ice can even change within a few days during the spring melt season in Arctic regions (König *et al.* 2001). A huge issue of optical imagery is that during bad weather periods or polar night no acquisitions are available. This limits data availability to summer months and nice weather periods.

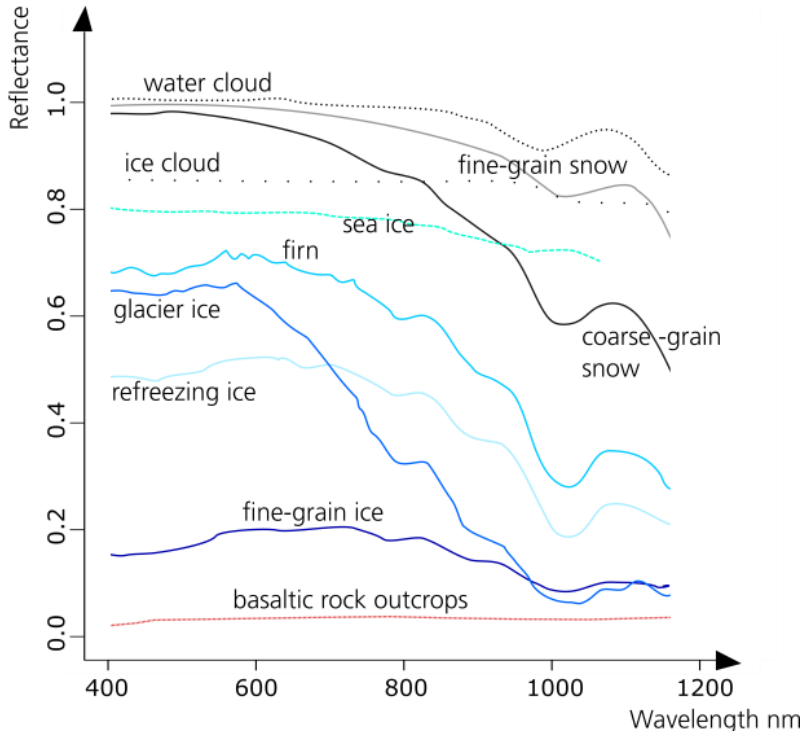

Figure 4.1: Reflectance spectra of Antarctic surface features and clouds in the visual and near-infrared spectrum. Data: Tedesco (2014), Zeng et al. (1984), and Gao et al. (1998). Modified after Baumhoer et al. (2018).

4.1.2 Backscatter Characteristics of Ice Sheets and Sea Ice

SAR satellite sensors are very valuable for Antarctic research as the active emitted signal penetrates clouds and is independent of solar illumination. Year-round image acquisition is possible allowing a constantly growing image archive. Nevertheless, radar imagery is not as simple to interpret as optical imagery as the physical properties of the surface influence the radar backscatter (for comparison see Figure 3.1). The border between water and shelf ice is easily distinguishable during calm weather periods in austral summer without sea ice as long as no surface melt exists (for example Figure 4.2a). Calm water builds a plain surface and the emitted signal is reflected in a rectangular angle away from the sensor. Therefore, water appears dark in the imagery (Liu & Jezek 2004a). Wind roughening of the sea surface leads to signal scattering and the contrast between land and ocean diminishes as water no longer appears black but in diffuse grey (Mason & Davenport 1996). Frontal delineation becomes even more challenging during the year as backscatter intensities for different ice classes are often ambiguous during different seasons. Backscatter values for sea ice, shelf ice, and the ice sheet itself vary, as can be seen in Figure 4.2. The radar backscatter of ice consists of the interaction between surface and volume scattering of the snowpack as well as the scattering at the ice interface itself (Liu *et al.* 2006). Depending on water content through snowmelt, the dielectric component varies and backscatter characteristics change throughout the year (Fahnestock *et al.* 1993). Figure 4.2c visualizes the seasonal change of backscatter values over the different glacier

facies. The ice sheet can be divided into different radar glacier zones with different backscatter intensities approximately reflecting the glacier facies (Braun *et al.* 2009). The dry snow zone covers the greatest part of the ice sheet in high elevations where no surface melt occurs. The radar signal penetrates deeply into the snowpack where low volume scattering occurs due to the small grain size of fresh snow. Hence, little backscatter occurs and the dry snow zone appears relatively dark in the imagery (Fahnestock *et al.* 1993). The percolation zone below creates a high contrast to the dry snow zone as refrozen meltwater builds a rough surface with pipes and lenses. Here, surface scattering is high due to a frozen surface causing high backscatter appearing very bright in the imagery (Partington 1998). The appearance of the wet snow zone below depends on seasonal temperature changes and is highly fluctuating. During austral winter, dry snow conditions lead to intermediate backscatter due to frozen conditions, but as soon as melt begins the dielectric properties change. Low backscatter is apparent when melt water in the snow pack reduces penetration depth of the signal (Fahnestock *et al.* 1993, Rau *et al.* 2000). The lowest bare ice zone varies strongly in backscatter and extent during the year. In winter, the backscatter is lower than the one of firn in the wet snow zone. The boundary between the wet snow zone and bare ice zone is also visible in summer when the wet radar snow zone appears darker due to snowmelt and the ice brighter as surface scattering appears (Fahnestock *et al.* 1993, König *et al.* 2001). This changes with fresh snowfall. When melt occurs, the backscatter of ice is similar to the one of the wet snow zone. If the snow is dry, the backscatter depends on the ice below. The same applies to sea ice as the backscatter intensity strongly varies depending on salinity, air content, snow cover, brine inclusions, and temperature (Kwok *et al.* 1992). Sea ice has very different backscatter characteristics depending on the state of development throughout the year, as can be seen in Figure 4.2. It starts with the formation of grease ice getting more solid and forming nilas and pancake ice (Comiso & Steffen 2001). With increasing age of the ice, the salinity decreases allowing deeper penetration of the radar signal and enhanced volume scattering appears (Wesche & Dierking 2012). This can be particularly problematic when it comes to calving front extraction as the structure and thus the backscatter characteristics of perennial sea ice, fast and shelf ice are oftentimes very similar (Bindschadler 1998). But exactly between both ice types, the front has to be extracted. Additionally, after calving events, ice mélange develops as a mix of sea ice, icebergs and firn making it very difficult to distinguish the calving front from fast ice. Even visually, the front is difficult to detect as the ice gradually fractures and no clear boundary is apparent (Moon & Joughin 2008, König *et al.* 2001).

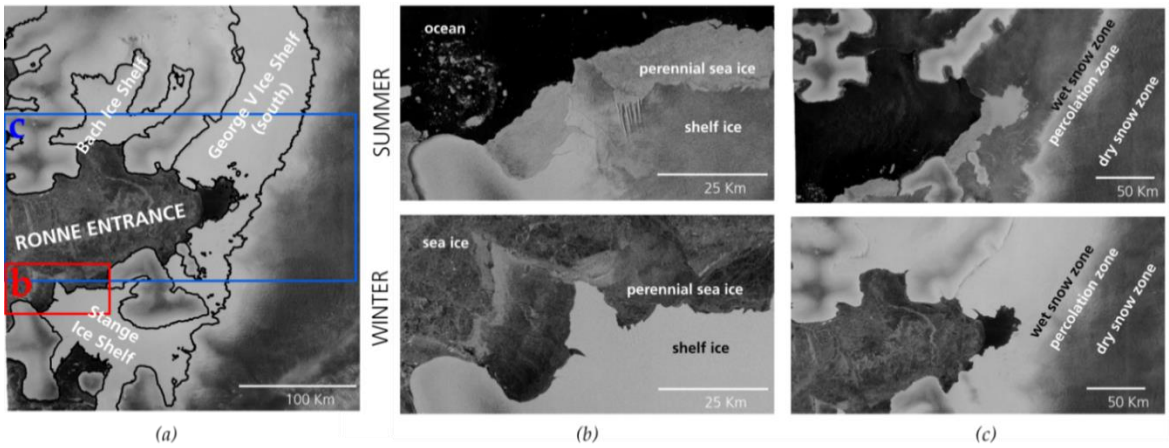

Figure 4.2: Exemplary appearance of radar glacier facies during austral summer (upper part) and winter (lower part). (a) Overview of Ronne Entrance with George V Ice Shelf. (b) Front of Stange Ice Shelf with perennial sea ice and open water in summer and with entire sea ice cover in winter. (c) Glacier radar facies nearby Ronne Entrance in summer and winter. Copernicus Sentinel-1 Data 2019. Summer: 2018-04-01; Winter: 2018-08-25. Modified after Baumhoer et al. (2018).

4.1.3 Applied Optical and SAR Sensors

Above, the advantages and disadvantages of calving front extraction from optical and SAR imagery were explained. This section summarizes which data sources and satellite sensors were frequently used for Antarctic calving front mapping based on 104 reviewed publications. For calving front studies, three major data sources were applied: optical and radar (airborne and space-borne) imagery as well as Antarctic maps. Those often included historical calving front records from ship expeditions and flight campaigns. Figure 4.3 displays the proportions of used image sources for calving front studies. Based on the reviewed calving front studies, 50 % of all publications used optical imagery as a data source. In one-third of the studies, SAR sensors were applied and only one-sixth used historical maps to derive calving front information (see Figure 4.3a).

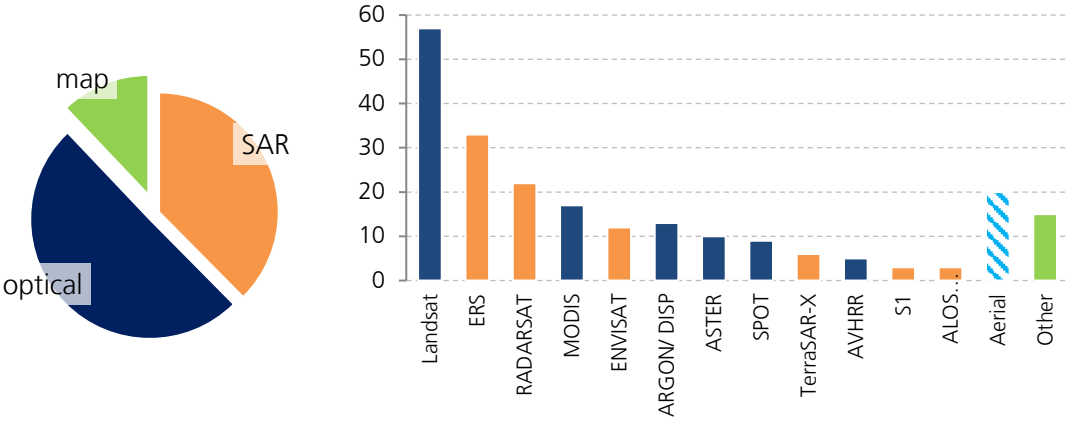

Figure 4.3: Pie chart (left) of proportions of used data sources and bar plot (right) of most frequently used sensors. Aerial imagery is an optical source of data. “Other” includes maps and further optical sensors. Modified after Baumhoer et al. (2018).

Optical imagery might be easier to handle for non-remote sensing scientists but image availability is always restricted by cloud cover and polar darkness. As only a limited amount of studies uses SAR data, there seems to be great potential for future applications focusing on regular and continuous monitoring for calving front mapping.

All major applied sensors are listed in Table 4.2. For the 12 most applied satellite missions, the frequency of use is displayed in Figure 4.3 (right panel). Landsat was the most commonly applied satellite mission for calving front mapping for good reasons. Continuous time-series since the 1970s until today (Landsat-8) and freely available medium resolution optical imagery facilitated the access. ERS and Radarsat were the most frequently applied radar satellite missions.

Table 4.2: List of most relevant optical and SAR space-borne instruments for calving front mapping.

Satellite platform	Sensor	Sensor Type	Spatial Resolution	Revisit Time	Launch Date	Status	Swath width [km]
Worldview-3	WV110	optical	0.31-1.8m	1-3.7d	2014	operational	13.1
Landsat-8	OLI	optical	15/30m	16 d	2013	operational	185
Quickbird	BGIS 2000	optical	0.55-2.44m	1.4-2.8d	2001	inactive 2015	16.8
Landsat-7	ETM+	optical	15/30m	16 d	1999	operational	185
Landsat-5	TM	optical	30m	16 d	1984	inactive 2011	185
Landsat-4	TM	optical	30m	16 d	1982	inactive 1993	185
Landsat-3	RBV	optical	40m	18 d	1978	inactive 1983	185
Landsat-2	RBV	optical	80m	18 d	1975	inactive 1983	185
Landsat-1	RBV	optical	80m	18 d	1972	inactive 1978	185
Sentinel-3A/B	OLCI	optical	300m	2 d	2016/18	operational	1270
KH-5 Argon	Camera	optical	140m	-	1961/64	inactive	556
Terra/Aqua	MODIS	optical	250/500m	1-2d	1999/2002	operational	2330
Sentinel-2A/B	MSI	optical	10-20m	5d	2015/2017	operational	290
TerraSAR-X	TerraSAR-X	SAR	1-18m	11d	2007	operational	100
Radarsat-1	RadarSat-1	SAR	8-100m	24d	1995	inactive 2003	500
ERS-1/2	AMI	SAR	30 m	35 d	1991	inactive 2000/11	100
Seasat	SAR	SAR	25 m	17 d	1978	inactive 1978	100
Sentinel-1A/B	SAR-C	SAR	10-40m	12	2014/16	operational	250
Radarsat-2	RadarSat-2	SAR	3-100m	24d	2007	operational	500

ERS was identified as a valuable data source as it was one of the first operational SAR missions in space. ERS was launched in the early 1990s and was followed by ERS-2 and Envisat. The newer Envisat mission even allowed frequent 3-day mosaics of Antarctica with a 1 km spatial resolution (Caspar *et al.* 2007). The imagery of the Radarsat satellites

were often used because of the two medium resolution 30 m satellite mosaics from 1997 and 2000 (Liu & Jezek 2004a). Low resolution MODIS satellite imagery with 250 or 500 m spatial resolution was the second most applied optical sensor. Its low spatial resolution is compensated by the daily revisit cycle allowing for a higher probability of cloud-free images(Kuenzer *et al.* 2014). Very interesting is the frequent use of ARGON imagery from the US Declassified Intelligence Satellite Photographs (DISP). This imagery is low in resolution and highly cloud covered. Yet, with the correction of geolocation errors by Kim et al. (2007), it is a valuable data source dating back to 1963. More costly and access restricted high resolution imagery from SPOT, TerraSAR-X and Worldview (category "other") were used less often as they are only suitable for local-scale studies. Optical as well as SAR data from the Sentinel mission were used only scarcely which is connected to their recent launch dates in 2015 and 2014, respectively. An abundance of data exists but the covered time period is still short. Several studies also used different data sources from optical and radar sensors in combination (e.g. Ferrigno et al. (2004)) as data availability often limited glacier and ice shelf front tracking. A combination of different data sources can be used to map front positions more frequently and increase data availability (Baumhoer *et al.* 2018).

4.2 Existing Methods for Calving Front Extraction

This section summarizes existing methods for calving front extraction based on reviewed calving front studies applying traditional image processing techniques. Commonly, glacier and ice shelf fronts are delineated manually, either from satellite scenes or from airborne imagery. This technique was applied in about 85 % of the reviewed calving front studies whereas 7 % used automatic or semi-automatic methods and 8 % used existing data sets. Manual delineation was even used for the complex USGS coastal change project (Williams *et al.* 1995) and most parts of the MODIS coastline products (Scambos *et al.* 2007). Both were very time-intensive projects due to manual work. To speed up glacier front delineation in times of fast-growing satellite archives and an unprecedented abundance of imagery, automated approaches from the field of shoreline or coastline extraction were applied to the Antarctic coastline. Coastline extraction algorithms needed modifications as additional challenges arose for the coastline of Antarctica. Seasonal variations in sea ice and glacier ice as well as snow cover were only some of the additional challenges. Different attempts have been made to simplify calving front extraction. For example, Liu et al. (2015) developed a simplistic classification approach for pre-delineation and manual adjustment afterwards. Also, automatic approaches for MODIS (Seale et al. 2011) and Radarsat (Liu & Jezek 2004b) imagery exist. Nevertheless, a manual correction was necessary to achieve the accuracy of an entirely manual delineation. Overall, no fully-automatic method for glacier and ice shelf front extraction exists that achieves accuracies

of a manual delineation (Baumhoer *et al.* 2018). Manual delineations from different experts deviate on average between 38 m (Zhang *et al.* 2019a) and 92.5 m (Mohajerani *et al.* 2019). In the case of the ADD coastline product created by contributions from several people, the inaccuracy can be even higher. The advantages and disadvantages of manual, semi-automatic, and fully automated approaches are summarized in Table 4.3.

In the following, a review of existing semi- and fully automated approaches is presented. The key parameters of each reviewed approach are summarized in Table 4.4.

Table 4.3: Advantages and disadvantages of different CFL mapping techniques. Modified after Baumhoer et al. (2018).

	Manual	Semi-Automatic	Automatic
Advantages	Applicable for every image type Quick for single glaciers Very accurate and precise Even “difficult” fronts can be mapped by experts	Less manual work Mapping of large regions is possible	Quick even for a high amount of scenes Monitoring possible
Disadvantages	Time-consuming Subjectivity of the observer Expert knowledge for difficult fronts necessary Not suitable for large-scale application	Still manual post-processing necessary Restricted to one sensor Expert knowledge for difficult fronts necessary	Not always accurate Long duration for algorithm development Only applicable for one sensor Computational cost is high

4.2.1 Semi-Automatic Approaches

The first semi-automatic approach for Antarctic ocean features was developed by Wu and Liu (2003). They extracted features like the ice edge (border between sea ice and ocean), polar lows, as well as glacier and ice shelf fronts from a very limited amount of Radarsat imagery. Wu and Liu (2003) used traditional edge detection methods in image processing such as greyscale histograms, texture analysis and wavelet transforms. For parameterization a lot of manual work was necessary and the detected fronts were very generalized and rough. A much more promising approach was developed by Liu and Jezek (2004b, 2004a). The authors developed a method to almost automatically extract the Antarctic coastline from the Radarsat Antarctic mosaic created in 1997. They developed a complex workflow for calving front extraction with the key element being adaptive thresholding. First, images were pre-processed with a Lee filter for speckle reduction and an anisotropic diffusion algorithm for edge enhancement. Afterwards, regions of high variance were chosen for calculating the adaptive threshold for land and water classification. For areas of high variance, a histogram was calculated consisting of a bi-modal Gaussian distribution (two peaks for land and water class, valley for the border). The optimal threshold for separating land and water was calculated based on the bi-modal

distribution. In case of no strict border between two classes, the Canny Edge Detector supported edge detection. Final post-processing allowed hole filling and the extraction of a vector file along the coastline. This approach was already highly automated and manual corrections were only necessary for areas of mélange and fast ice as well as for merging the different parts of the coastline (Liu & Jezek 2004b, Liu & Jezek 2004a). Nevertheless, it was only optimized for the radiometrically corrected and balanced Radarsat image mosaic not allowing coastline extraction for single scenes. Besides those traditional approaches, also simplistic approaches to generate a rough pre-classification existed. This made the subsequent manual work less time consuming (Liu *et al.* 2015, Miles *et al.* 2017) just made the manual delineation as efficient as possible (Lea 2018). For example, Liu et al. (2015) used an object-based watershed segmentation approach for a rough separation into land and ocean of each satellite image. Afterwards, manual correction and delineation were applied. A similar approach was presented by Miles et al (2017) where a rough separation of each scene into land and ocean was achieved by a pixel-based classification. This reduced the manual work as about 65% of the coastline imagery was already classified automatically. A completely different but worth mentioning approach was developed by Lea (2018). He made delineation extremely simple and time-efficient by programming the GEEDiT tool in Google Earth Engine (GEE). The user can select a study area and the time period for delineation. Automatically, Landsat and/or Sentinel scenes are presented for delineation. Cloudy scenes can be skipped and successfully delineated fronts can be tracked and downloaded as shapefile.

4.2.2 Automatic Approaches

Due to the difficulties mentioned in Section 4.1, not many fully automatic approaches for calving front extraction exist. The first approach was developed for optical and SAR data by Sohn and Jezek (1999). On a small amount of imagery, they applied edge-enhancement techniques for further adaptive thresholding. Region growing, edge detection as well as edge following were implemented to further improve the results. Tested on only a small region of the Antarctic coastline, they faced classification errors in areas of thin snow. Areas with difficult sea ice and mélange conditions were not tested (Sohn & Jezek 1999). More recently, an approach based on the Canny Edge Detector and edge tracing was published by Krieger and Floriciocu (2017). They tested their approach for two radar scenes (TerraSAR-X and Sentinel-1) of the Greenlandic glacier Zahcariae Isstroem with very difficult mélange conditions. Their approach performed with deviations of 159 and 246 m compared to a manually delineated expert coastline (Krieger & Floricioiu 2017).

A fully automated approach for the Landsat Mosaic of Antarctica (LIMA) was created by Klinger et al. (2011). They used the initial coastline of the Radarsat mosaic (Liu & Jezek 2004a) and applied an active contours algorithm to fit an initial already existing

coastline to the one of the newer LIMA mosaic. Due to intense computational costs, the area of coastal change had to be restricted to 2 km which does not cover larger break-up events. Additionally, the active contours approach was never finished for entire Antarctica as computation was too expensive (Klinger *et al.* 2011). The most promising automated approach exists only for the east Greenlandic coastline. Seale at al. (2011) processed 10 years of MODIS imagery to extract calving front time series. A multi-temporal analysis allowed the identification of areas with changing glacier fronts. Edge detection was applied by the Sobel operator and a brightness gradient.

Table 4.4: Comparison of automatic (A) and semi-automatic (SA) calving front extraction approaches. Modified after Baumhoer et al. (2018).

Study	A / SA	Based on	Image Processing Techniques	Test Area	Years & Amount of Data	Error	Difficulties
Sohn & Jezek 1999	A	ERS-1 SPOT	Edge Enhancement, Texture Features Local Thresholding, Edge Detection with Robert's Operator	100 x 100 km 37.5x37.5 km Jakobshavn Glacier	1988 + 1992 2 Scenes	2-3 pixels 200 m	Lakes and outwash plains Sensor inaccuracies Thin Snow
Seale et al. 2011	A	MODIS	Cloud masking Edge Detection with Sobel's Operator + Brightness Gradient Removal of wrong data points via time-series	32 glaciers 26802 fronts Greenland	2000-2009 105,536 Scenes	1.2 % of data points wrong	Polar night & clouds Sensor inaccuracies Direction of scene
Klinger et al. 2011	A	LIMA Mosaic	Initial Coastline + classification with nearest neighbor 3 snake models with different parameters and edge detectors	12 % of Antarctic coastline	1999-2003	6 % of sections had to be corrected 12.1 % false negative 13.7 false positive 1.5 pixel or 380 m	Initial coastline needed Sea ice to shelf ice boundary No greater change than 2 km allowed Manual post-processing necessary
Krieger & Floricioiu 2017	A	TerraSAR-X Sentinel-1	Canny Edge Detection Shortest Path between Edge candidates	Zachariae Isstroem	2016+ 2017 2 Scenes	Mean Distance between Expert and Automatic 246 m+ 159 m	End and start point have to be specified for each glacier More diverse test areas are required
Liu & Jezek 2004a	A	Landsat 7 RADARSAT	Pre-Segmentation Segmentation Post-Segmentation	212x226 km 409.6x409.6 km	1 Scene 1 Scene	One pixel (compared to visual interpretation)	Fast ice, sea ice and wet snow Fixing Errors in ArcGIS For optical imagery perfect
Wu & Liu 2003	SA	RADARSAT	Feature Detection Wavelet Transform Edge Detection Texture for Classification	Bering sea 400 x 400 km	2000 1 Scene	-	Also detects ice edge Parameterization Static thresholds No error calculation
Liu et al 2016	SA	Envisat ASAR	Object-based classification Watershed Segmentation Manual Modifications	Circum-Antarctic	2005-2011	Visually corrected	Manual work afterwards
Liu & Jezek 2004a Liu et al 2004b	SA	RADARSAT Mosaics AMM & MAMM	Lee filter for edge enhancement and speckle reduction Segmentation with local adaptive threshold Canny Edge Detector Manual editing and merging	Circum-Antarctica	1997 + 2000 Entire Mosaic	130 m (DEM) Visually Corrected Version available	Wind roughened Sea Sea ice Orthorectification
Miles et al. 2017	SA	Envisat, ASAR	Pixel-Based Classification Polygon generation	Coastal Section	Monthly Scenes 2002-2012	45 % had to be manually corrected	Only 65 % were automatically mapped precisely

1 Landsat Image Mosaic of Antarctica, 2 Antarctic Mapping Mission, 3 Modified Antarctic Mapping Mission.

This technique allowed a large-scale analysis of Greenlandic glaciers but still had some drawbacks. Cloud cover and polar night reduced image availability drastically. Additionally, images had to be turned in glacier flow direction and classification inaccuracies occurred over glacier ice and sea ice. The low resolution of MODIS imagery (250-500 m) made the front delineation more difficult and required glaciers moving more than the coarse pixel size to actually track glacier front changes (Seale *et al.* 2011).

4.3 Methods to Measure Calving Front Location Change

A wide range of methods exists to measure calving front change. Change can either be measured by distance or area. Both approaches deliver accurate results but the results cannot be compared directly without information on glacier width. Therefore, it is essential to choose the right measurement technique. Figure 4.4 displays available measurement methods. The most common and quickest approach is to measure frontal change along a center flow line. One fixed point at the glacier is chosen from which a line is drawn to the front along the glacier flow direction (Skvarca *et al.* 1999, Bevan *et al.* 2012). Changes in distance from the previously selected point are measured and indicate glacier change. This simplistic method delivers fast results but leaves out changes along the lateral parts of the front. Especially for glaciers changing unequally over the entire front, the sample lines method is more useful. To measure changes across the entire frontal width, several lines can be drawn along the glacier flow direction with a fixed spacing in-between. A smaller spacing delivers more accurate results but requires more effort. For overall glacier change, the mean or median distance changes of all sample lines can be calculated. For example, this method was applied in the USGS coastal change map templates (Williams *et al.* 1995, Ferrigno *et al.* 2009) or in the study by Fountain et al. (2017).

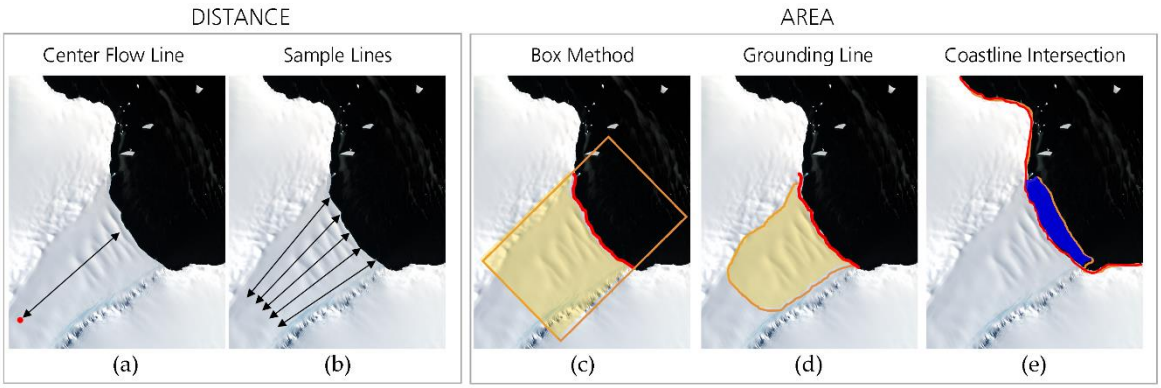

Figure 4.4: Different techniques to measure calving front dynamics. Distance-based methods measure from one fixed point to the front (a). Higher accuracy is reached by using the average of several lines (b). Area (orange/blue) can only be measured to a reference line (orange) and the front (red). This can be a fixed box (c), which is relative to the grounding line or coastline of a specific year. Modified after Baumhoer et al. (2018).

Glacier dynamics can also be assessed by measuring the change in ice shelf and glacier extent. Very common is the box method where a rectangular box is drawn along the glacier. Area loss or gain within the box accounts for calving front retreat or advance. Also, modified versions of the box method exist with curved boxes which can yield more accurate results (Lea *et al.* 2014). The box method was used in many studies such as Fukuda et al. (2014), Miles et al (2013), and Moon and Joughin (2008). Instead of using a bounding box, also the grounding line can be used for measuring the reference area (Frezzotti & Polizzi 2002). Here, it is important to use the same grounding line for reference as the location may have changed over time. Frontal changes relative to the basin area can be assessed by using the glacier basing size as reference area (Davies *et al.* 2012). For large-scale applications, the area change between two coastline delineations can be measured not accounting for single glacier change but overall coastal change (Liu *et al.* 2015, Kim *et al.* 2001). A sound review on methods for calculating calving front change is provided by Lea et al. (2014).

4.4 Summary

This chapter highlighted the potentials of remote sensing for calving front mapping. Optical and radar satellite sensors can be used for glacier front delineation with specific advantages and drawbacks. Optical imagery is easy to use but image availability is restricted by polar night and cloud cover. Continuous glacier front time series can be created from radar data which require complex pre-processing and a good knowledge of the backscatter characteristics of ice. In 85 % of all reviewed studies, the calving front position was manually extracted from optical or SAR imagery. 7 % of the studies used (semi-)automatic approaches which faced several challenges not allowing the development of a fully automated method for circum-Antarctic glacier and ice shelf front extraction. Hence, a novel approach for automatizing calving front extraction is required.

To assess calving front dynamics, changes in the calving front position have to be measured. Area and distance-based approaches exist. Depending on study design and glacier geometry, either distance measurements using several sample lines or area measurements with the box method are commonly applied. Overall coastal change can be measured by comparing the area difference between coastline products.

Chapter 5

5 A Novel Methodical Framework for Automatic Calving Front Extraction*

This chapter introduces *Antarctic*LINES (**Antarctic** Glac**i**er and **I**ce Shelf Fro**n**t Tim**e** Serie**s**) which is a novel methodical framework for automatic calving front extraction. Up today, intra-annual time-series of glacier and ice shelf front change do not exist as calving front extraction could not be automatized nor was sufficient satellite imagery available over the Antarctic coastline (Baumhoer *et al.* 2018). *Antarctic*LINES combines recent developments in the artificial intelligence community with weekly acquired Sentinel-1 data over the Antarctic coast to create monthly time series of calving front fluctuations. In the following, the implementation of deep learning approaches for coastline applications and their applicability for glacier front studies are reviewed. The specifications and availability of Sentinel-1 data are outlined. Further on, the methodical framework is described in detail and a comprehensive accuracy assessment is presented. Finally, calving front extraction results for intra-annual glacier front dynamics and the extraction of the Antarctic coastline for 2018 highlight the spatial and temporal transferability of *Antarctic*LINES.

5.1 Deep Learning for Calving Front Detection

Recent developments in earth observation towards data-intensive science and growing computational power accelerate the use of machine learning techniques to solve

* Parts of this chapter are based on: Baumhoer, C. A., Dietz, A. J., Kneisel, C., & Kuenzer, C. (2019). Automated Extraction of Antarctic Glacier and Ice Shelf Fronts from Sentinel-1 Imagery Using Deep Learning. *Remote Sensing*, *11*(21), 2529.

image recognition challenges (Zhu *et al.* 2017). Advancements in computer vision (CV) demonstrate that especially deep learning approaches often outperform traditional image processing techniques (Liu *et al.* 2018). Machine learning is characterized by algorithms that are designed to learn features from labelled training data (Hoeser & Kuenzer 2020). Deep learning is part of machine learning and consists of neural networks with more than two hidden layers. Adding hidden layers to a neural network makes the network deeper and enables it to learn more feature representations (Zhu *et al.* 2017). For applications on visual imagery most commonly fully convolutional networks (FCN) are used. Convolutional neural networks (CNN) convolve input features with a learned filter to minimize the input features while extracting the maximum of information. The network is called "fully" as the output of one hidden layer is connected to the neurons of the next layer (Long *et al.* 2015). CNNs can solve a palette of image processing tasks such as image recognition, image segmentation, object detection and instance segmentation (a combination of all previous three) (Hoeser & Kuenzer 2020). For classification tasks in remote sensing, especially semantic segmentation has proven to be a successful approach. Semantic segmentation segments the image into several classes where for each pixel the class is defined based on contextual and pixel information (Long *et al.* 2015, Audebert *et al.* 2016, Liu *et al.* 2018). This approach faces several challenges when applied on large-scale remote sensing imagery (Maggiori *et al.* 2017), but recently developed deep learning architectures are also suitable for large-scale applications (Y Li *et al.* 2018). For example, good results for crop type and sea ice classification from satellite imagery were achieved (Kussul *et al.* 2017, Wang *et al.* 2016). Especially for coastline extraction applications, best results were obtained by U-Net based architectures (R. Li *et al.* 2018). The U-Net is one of the most popular used encoder-decoder architectures (Hoeser & Kuenzer 2020) which was first introduced by Ronneberger et al. (2015). It was initially designed for medical cell segmentation in low contrast gray scale imagery. The key feature of the U-Net is its U-like shape built by five encoder and decoder blocks. Within the encoder block, the imagery is down sampled by two adjacent 3x3 convolutions creating 1024 feature maps at the deepest layer. For the decoder part, skip connections are used to transfer detailed local information from the encoder to the high level semantic information of the decoder until the original image size is reached (Hoeser & Kuenzer 2020, Ronneberger *et al.* 2015). This approach is highly useful for glacier and ice shelf front extraction as not only pixel information, but also spatial information is used for image classification. Up to now, calving front extraction with U-Net-based architectures has been performed by Mohajerani et al. (2019) and Zhang et al. (2019b) (both for Greenland).

Mohajerani et al. (2019) did first comparisons between common edge detection techniques compared to CNN derived ones. They tested their U-Net based approach on four selected Greenlandic glacier fronts in Landsat imagery. The CNN derived front was

detected with a mean deviation of 96.3 m (approx. 2 pixels) and outperformed traditional edge detection techniques. Drawbacks of this first small study were the down sampling of the image resolution, necessary alignment of the image in glacier flow direction and the prediction on a three-pixel wide front line. The study by Zhang et al. (2019b) concentrated on high resolution time series of glacier front movement of Jakobshavn Isbrae Glacier (Greenland). A very dense time series of glacier front fluctuations could be created with a mean deviation of 104 m (17.3 pixels) compared to manual delineations. Those results highlight the potential of a CNN-based approach for calving front detection with SAR imagery. Still, it should be considered that those results were obtained by training on only one single glacier with a bunch of training images (75 scenes training-validation versus 84 test images on one single glacier). In contrast to the two mentioned studies above, this thesis targets a large-scale approach for Antarctic calving front detection. The methodical framework and applied input data are explained in the following.

5.2 Input Data

For training the neural network, a sufficient amount of data is necessary. Sentinel-1 data with manually created labels is used for training. The elevation information from the TanDEM-X elevation model is used as additional support for an indication of high altitude areas. The data specifications are explained in the following.

5.2.1 Sentinel-1

The ESA (European Space Agency) developed a new family of satellite missions called the Sentinels. Sentinel-1A and Sentinel-1B are a constellation of two radar imaging satellites identical in construction. The Sentinel satellites ensure continuity as Sentinel-1C and 1D will be launched to continue the Sentinel-1 mission. Both radar imaging sensors operate at C-band with 5.4GHz and a wavelength of 5.6 cm (ESA 2012). Sentinel-1A was launched in 2014 and was complemented by Sentinel-1B in 2016. This increased the 12 days revisit time to six days or even less in Polar Regions (ESA 2020c) (see Figure 5.1).

One major application for Sentinel-1 is the monitoring of the polar environment (e.g. sea ice) making it a great data source for calving front extraction (ESA 2012). Sentinel-1 data is available as a single look complex (SLC) and ground range detected (GRD) files. Whereas SLC data contain the phase and raw data, the GRD files require less pre-processing steps as they are already multi-looked and projected to ground range (ESA 2020c). For this study, GRD products were used because of the following three reasons: phase information was not necessary, the data availability of GRD products is higher, and the data volume smaller than for SLC products. The radar imaging sensor has different acquisition modes with a high-resolution 10 m IW (interferometric wide-swath) mode and a lower resolution EW (extra wide-swath) mode. Over the Antarctic coastline, dual-

polarized EW images in HH and HV polarization exist whereas the IW mode only provides single-polarized imagery (ESA 2012). As several polarizations are essential for classifying different ice types (Ressel *et al.* 2015, Moen *et al.* 2013, Wesche & Dierking 2014) the 40 m EW mode was selected for training.

Additionally, better coverage over the Antarctic coastline exists for EW mode acquisitions. Figure 5.2 displays the coverage with different acquisition modes over the Antarctic Ice Sheet. It should be noted that before May 2017 almost no dual-pol acquisitions existed for Antarctica. Since mid of 2017, the acquisition plans were adapted and EW dual-pol data is widely available except for parts along the Bellingshausen Sea (see Figure 5.1).

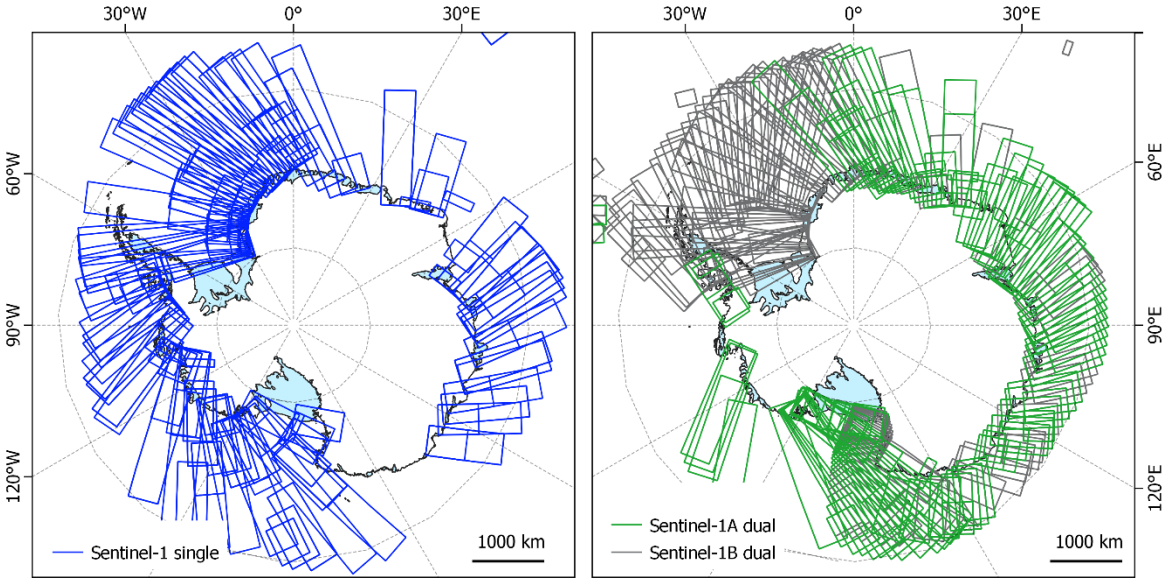

Figure 5.1: Exemplary EW acquisition coverage within two weeks in 2015 from Sentinel-1A (left) and in 2019 (right). Since the launch of Sentinel-1B a denser coverage with dual-polarized acquisitions exists. Though, not all coastal areas are acquired regularly every six days as planned by ESA (2020b). Shapefiles from ESA (2020a).

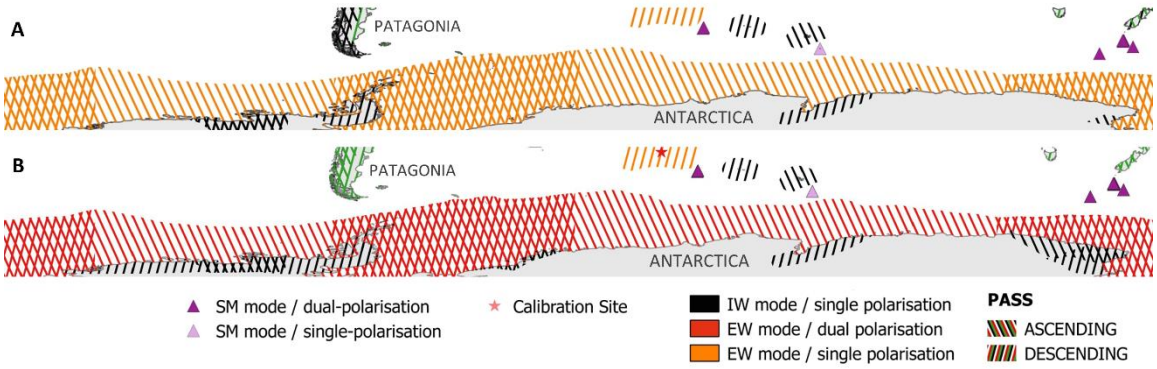

Figure 5.2: Sentinel-1 acquisition modes over Antarctica before May 2017 (a) and after (b). Note the shift from single-polarized to dual-polarized imaging. SM: Stripmap mode. Modified after ESA (2020b).

Nevertheless, the data coverage and spatial resolution of Sentinel-1 is superior to previous satellite missions. Especially optical imagery from Landsat and MODIS is often affected by cloud cover or polar night which limits data availability. In case dual-pol EW data is missing for one month, single-pol data can be used instead.

5.2.2 TanDEM-X Polar DEM 90

For calving front extraction, elevation information is helpful as backscatter characteristics of the higher Antarctic Ice Sheet are as low as over the ocean. In high altitudes, the ice sheet surface appears black in radar imagery due to a thick cover of dry snow. A digital elevation model (DEM) is needed to distinguish the ocean from the higher ice sheet. The TanDEM-X Polar DEM 90 was selected as it is freely available at a resolution of 90 m. Two other freely available DEMs exist for Antarctica but are less applicable. The CryoSat-2 DEM spatial resolution is too low with 1 km (Slater *et al.* 2018) and the REMA (Reference Elevation Model of Antarctica) DEM created with stereophotogrammetry is high in spatial resolution (better than 10 m) (Howat *et al.* 2019) but has several no data areas unsuitable for a pan-Antarctic application.

The Antarctic TanDEM-X was acquired between April 2013 and November 2014. The final version TanDEM-X Polar DEM 90 was edited as icebergs and sea ice created noisy measurements over the ocean. To exclude those noisy areas the DEM was clipped to the coastline of Antarctica by a thresholding approach based on elevation and amplitude values. A manual correction afterwards ensured accurate results. Hence, the glacier and ice shelf front positions of the DEM date back to 2013-2014. As the elevation information is only needed for the higher ice sheet and the open ocean it is negligible if the front positions are not at the same position as the acquired Sentinel-1 scene. The DEM has a high vertical resolution deviating in the worst case ± 5 m over the higher ice sheet. But it should be mentioned that in the developed approach most of the higher ice sheet areas are masked out by a coastline buffer. In low elevations, the vertical accuracy is below one meter (Rizzoli *et al.* 2017).

5.2.3 Training Labels

Training a supervised machine learning algorithm requires ground truth labels. In-situ measurements of glacier and ice shelf front positions are very rare concentrating on early ship expeditions in the 19th century (Ross 1847). Therefore, manually delineated calving fronts from experts need to be used as training data. For Sentinel-1 data only very limited manually delineated calving fronts exist in the Antarctic Digital Database. This amount is not sufficient for training a neural network. At least this data can be used for validation later on.

Consequently, new labels were created for this thesis which was a challenging task on SAR imagery, as this requires a lot of expert knowledge. Calving front delineation is a very subjective task that can be best explained by comparing different coastline products. For example, when comparing the coastline of the Radarsat mosaic (Liu & Jezek 2004b) versus the MODIS coastline (Scambos *et al.* 2007) greater deviations exist in areas of mélange, icebergs trapped in sea ice, blue ice areas and fast ice areas. This can be explained by differences in spatial resolution, the subjective view of the scientist and different appearances in optical and radar imagery. Additional sources of satellite imagery as well as a firm definition of the calving front were used to annotate labels with high accuracy. The calving front was defined as the border between ocean and ice sheet including floating ice tongues and shelves. As soon as ice was broken off and no longer connected to the glacier/ice shelf, an iceberg formed which was considered as ocean. To get a better impression of the Antarctic coastline, previously published coastline products from MODIS, Radarsat, USGS coastal change maps, and the ADD were used as a reference for former front positions. Additionally, in difficult areas (e.g. blue ice areas), optical imagery was used for comparison from Landsat, Sentinel-2, Bing Maps, and Google Earth. Very valuable information for fast ice areas could be obtained from the TanDEM-X elevation model. Fast ice is thinner than glacier ice and hence lower in elevation. As fast ice exists over several years, areas of fast ice often stayed the same location since the acquisition of the DEM.

The labels were created by drawing a vector polygon over the land ice area based on the pre-processed Sentinel-1 scenes. This polygon was then rasterized at the same resolution as the satellite image and classes were assigned (1 for land ice, 0 for ocean and background). An exemplary label is displayed in Figure 5.3.

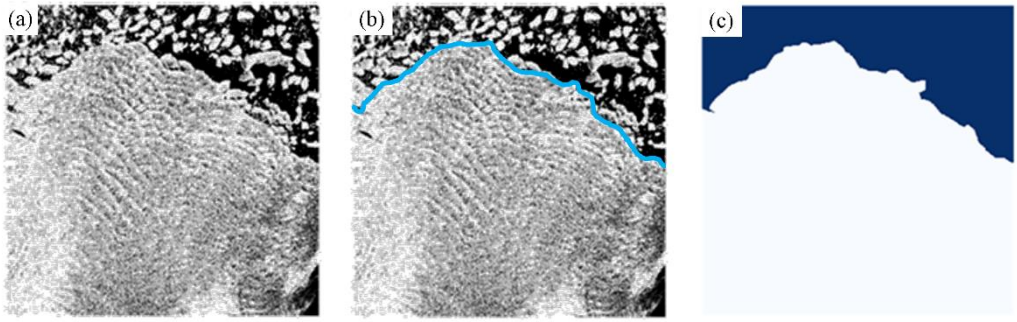

Figure 5.3: Creating Labels. (a) Initial Senintel-1 scene, (b) overlaid by the manually delineated vector shapefile and (c) final rasterized label.

5.2.4 Training and Testing Areas

To train the CNN, 38 Sentinel-1 scenes were selected over four training sites depicted in Figure 5.4. The training areas cover the Sulzberger Ice Shelf with scenes from 20 different dates to cover the different backscatter characteristics throughout the year.

Shackleton Ice Shelf (6), Wilkes Land (6), and Victoria Land (6) were added to train the model on different shapes and backscatter characteristics from more diverse ice types. In the following, the different glaciological specifications are described briefly.

The calving fronts around the Sulzberger Ice Shelf were slowly moving with about 10-200 m/yr belonging either to the 60 km wide Nickerson or 100 km Sulzberger Ice Shelf. An exception was the glacier terminus of Land Glacier moving faster with about 1.6 km/yr (Ferrigno *et al.* 2004, Rignot *et al.* 2011). The terminus was difficult to determine because myriads of small icebergs agglomerated at the claving front and were trapped in fast ice. One of the biggest ice shelves along East Antarctica is the Shackleton Ice Shelf with a length of 400 km (Stephenson & Zwally 1989). Whereas the ice shelf itself was slowly moving the fast flowing outlet glacier Denman is nearby. Often, sea ice conditions changed along the ice shelf front which made it a good and dynamic training area. The coast along Wilkes Land consists of many smaller outlet glaciers recently showing signals of retreat (Miles *et al.* 2016, Miles *et al.* 2017). The glaciers were characterized by ridged glacier tongues, countless icebergs and mélange. This made it difficult to determine the glacier front. Also Victoria Land is fringed with several outlet glaciers but with completely different shapes. Glaciers along Victoria Land are outlet glaciers often building long glacier tongues like the Drygalsky Ice Tongue.

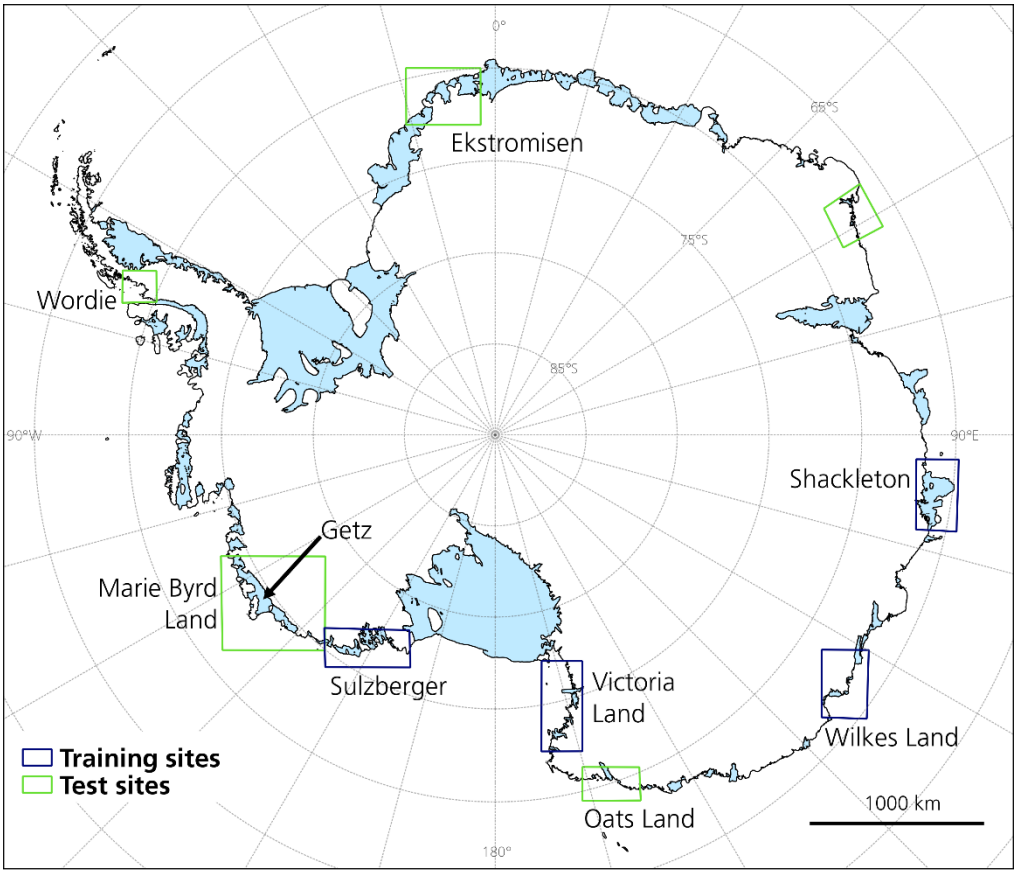

Figure 5.4: Training and test areas over Antarctica. Modified after Baumhoer et al. (2019)

Besides the described training areas, also satellite scenes for testing were required. For the selection of those satellite scenes, two strategies were pursued. First, scenes over the training areas that were not used during the training process were used to test the temporal transferability. Second, additional test areas were selected to test the spatial transferability of the developed approach on other glaciers and ice shelves.

The further test regions are depicted in Figure 5.4 and described in the following. Ekstromisen Ice Shelf is located at Dronning Maud Land far away from any training areas. Dronning Maud Land is characterized by several larger ice shelves separated by ice rises. The Ekstromisen Ice Shelf was a good representative of the morphology of ice shelves along Dronning Maud Land. The disintegrated Wordie Ice Shelf is located at the Western Antarctic Peninsula with a steep rock coastline and mélange in front of the outlet glaciers. The developed framework was tested along Oates Land as very different glacier and ice shelf shapes, as well as rock coastline, are dominant in this sector. Finally, a part of Marie Byrd Land was selected to test the performance on fast ice areas.

The novel created framework *Antarctic*LINES was specially designed to generate time series of calving front fluctuations. To test for time series generation the Getz Ice Shelf was selected which is located at Marie Byrd Land. It is the largest ice shelf along West Antarctica with an area of 33,395 km^2 (Jacobs *et al.* 2013). The Getz Ice Shelf was chosen for testing as little is known about the current front fluctuations of the Getz Ice Shelf (Baumhoer *et al.* 2018), even though, Getz Ice Shelf experienced higher mass loss rates (-67.6±12 Gt/yr) between 2003 and 2008 compared to all other ice shelves of West Antarctica (Rignot *et al.* 2013). "Basal melt accounts for about three quarter of the mass loss and calving for one quarter (Rignot *et al.* 2013) but can vary as Getz is subject to changeable ocean forcing conditions (Jacobs *et al.* 2013). Between 2008 and 2013/2015 the glacier flow of glaciers feeding the Getz Ice Shelf increased by 10 to 100 m/yr at the grounding line (6% increase of discharge) (Gardner *et al.* 2018). The grounding line itself of the Getz Ice Shelf retreated 100–200 m per year between 2010 and 2016 (Konrad *et al.* 2018). Taken together, those factors indicate that the Getz Ice Shelf is exposed to changing environmental conditions" (Baumhoer *et al.* 2019). The effect of changing environmental conditions on the front of the Getz Ice Shelf is still unresolved (Baumhoer *et al.* 2018).

5.3 Methodology

In the context of this thesis, a novel, reliable and versatile applicable framework for automatic glacier and ice shelf front extraction was developed. The framework is called *Antarctic*LINES (**Antarctic** Glac**i**er and **I**ce Shelf Fro**n**t Tim**e** Serie**s**). The deep learning based workflow was designed for Sentinel-1 dual-polarized EW imagery in GRD format but could easily be adapted for other image sources and formats. In short, the workflow

consisted of three main parts (pre-processing, training, and post-processing) with subsequent accuracy assessment. The developed workflow is illustrated in Figure 5.5.

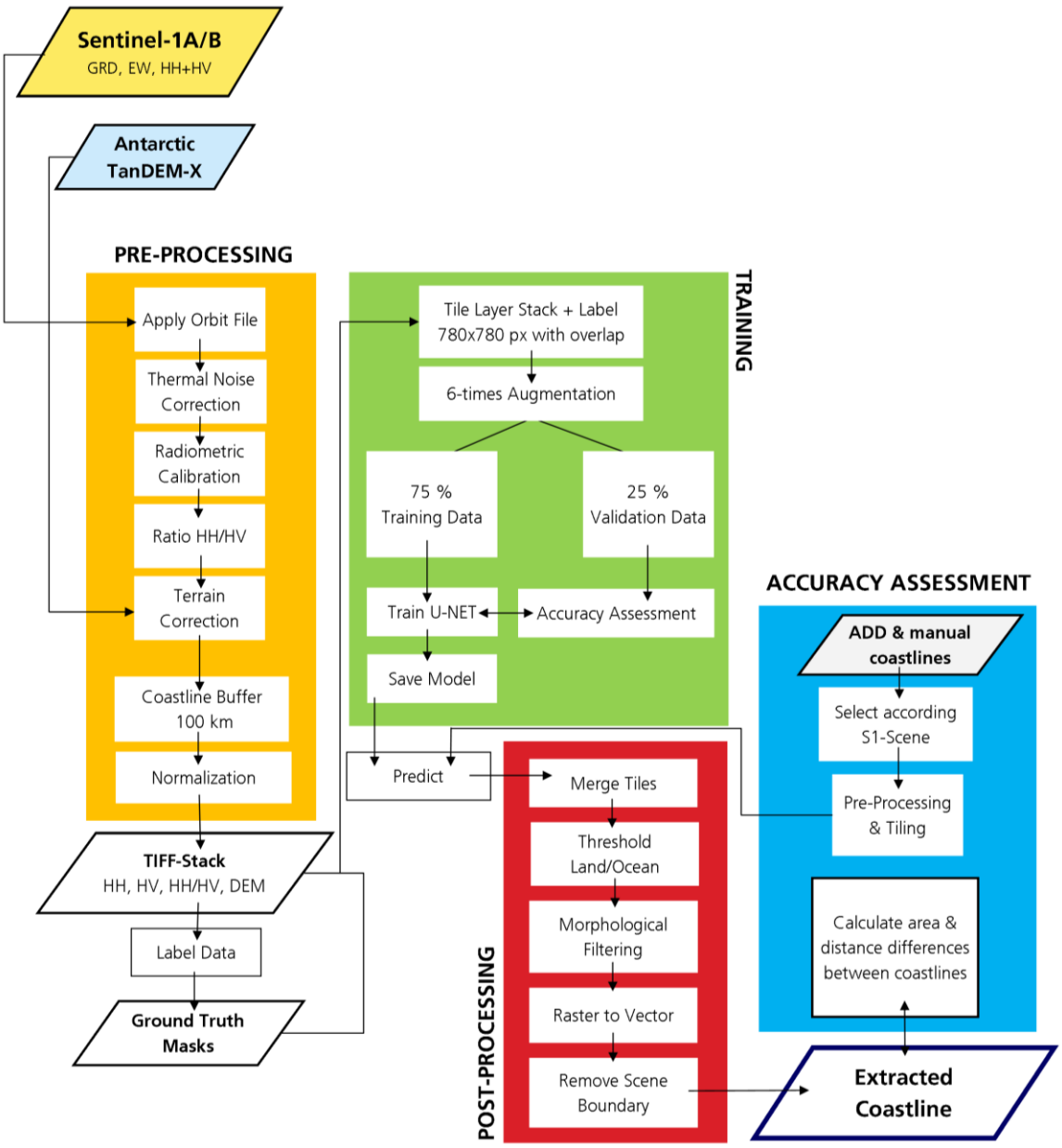

Figure 5.5: AntarcticLINES workflow for training and testing the automated calving front extraction framework. DEM: digital elevation model, S1: Sentinel-1, GRD EW: Extra wide swath Level-1 ground range detected S1 product. Modified after Baumhoer et al (2019).

First, Sentinel-1 data were pre-processed and put together to a four-layer stack consisting of different polarizations and elevation information. For training, labels were created based on the layer stack before tiling all scenes into smaller patches. After training, the learned weights of the neural network were stored to use them later for prediction (deep learning jargon for “classification”). The stored weights were used for testing the approach on additional Sentinel-1 scenes. Within the post-processing step, the scene patches were merged again and the class output was thresholded for a binary water and ice mask.

Morphological filtering was applied to remove small false classifications before creating vector shapefiles from the raster output. The accuracy of the final extracted calving fronts was tested against manually delineated fronts within the accuracy assessment step.

5.3.1 SAR Pre-Processing

The Sentinel-1 data was downloaded from the Alaska Satellite Facility (https://search.asf. alaska.edu/#/) and the Sentinel Scientific Data Hub (https://scihub. copernicus.eu). The ESA SNAP (Sentinel Application Platform) software (Version 6.0) was used for pre-processing Sentinel-1 EW GRD data including the following steps:

- Apply Orbit File
- Thermal noise removal
- Radiometric calibration
- Geometric terrain correction
- Creating layer stack
- Coastline buffer mask

"The Orbit File is applied to update satellite position and satellite velocity for more accurate orbit state vectors. Afterwards, thermal noise is reduced by the thermal noise removal. Radiometric calibration converts the backscatter intensity to the backscatter coefficient sigma nought. Now, the pixel values represent the backscatter of the reflecting surface and make a comparison between different scenes possible. Usually, speckle filtering is applied afterwards but we decided to forgo this step as it might reduce the appearance of edges" (Baumhoer *et al.* 2019). The terrain correction with the TanDEM-X 90 m removed signal distortions due to topography. A four-layer stack was created from the polarizations HH and HV, the DEM, and the ratio between HH and HV. To reduce the data amount, a 50 km buffer at each side of the initial MOA 2014 (MODIS Mosaic of Antarctica 2014) coastline was created to mask the layer stack. This buffer ensured coverage of even large calving events (like the Larsen C A-68 iceberg) but still minimized the data volume to speed up processing.

5.3.2 U-Net based Image Segmentation

The core feature of the presented framework was the modified neural network called U-Net. The basic architecture was based on the publication by Ronneberger et al. (2015) with modifications to suit the requirements for calving front extraction. Modifications included:

- Starting with 32 feature channels increasing to 512 (instead 64 to 1024)
- Increasing the input tile size from 512 to 780 pixels

- Four input channels instead of grey scale imagery
- Including dropout to prevent overfitting

The final implemented U-Net is visualized in Figure 5.6. The network was fed with 780x780 pixel tiles having four input channels. These channels included the HH and HV polarization, a ratio of both, and elevation information of the TanDEM-X Polar DEM 90. Using four instead of one input channel increased the information content on which the model segmented the image. The tile size was selected to be as big as possible by still matching GPU limitations.

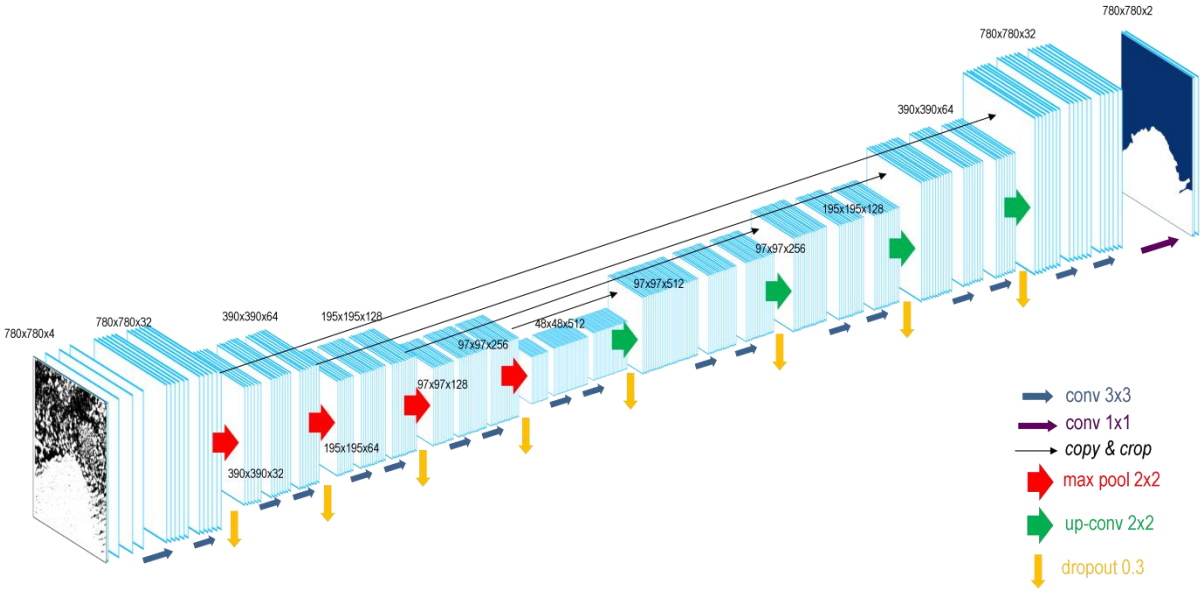

Figure 5.6: U-Net architecture with four down-sampling encoder blocks separated by red arrows and four up-sampling decoder blocks with green arrows. Skip connections are indicated by black arrows and dropout by yellow ones. Image sizes and number of feature channels are given in black numbers. Source: Baumhoer et al. (2019)

Bigger tile sizes allowed the network better knowledge about the spatial context. A size of 780 pixels was the maximum tile size to fit into the GPU by a batch size of two. “For training, each of the input tiles is convoluted by a 3 x 3 kernel with stride 1. The kernel consists of a 3 x 3 matrix of randomly initialized weights which gets updated during the training process using the Adam optimizer in TensorFlow 1.12 with the default learning rate of 0.001, the default cost function categorical cross-entropy and the activation function ReLU (rectified linear units)” (Baumhoer *et al.* 2019). The convolution and pooling process can be best explained on basis of Figure 5.7. The figure shows a simplified encoder block with one convolution only. Each channel of the input image got convoluted by a 3x3 kernel. The weights of this kernel were learned, hence, they adapted during the training process. The kernel shifted one pixel (this means “stride 1”) at a time and calculated a new value until the convoluted feature was complete. To prevent shrinking of the image through convolution, zero padding was applied (not shown in the example). This means a border of zero values was created around the image to compensate for the shrinkage during the

convolution. For each image channel, one kernel with specific weights was learned. A set of learned kernels can be called a filter.

Feeding big image tiles through a CNN requires high computational power and storage. To save both, the image has to decrease in size but the informational content has to be enhanced by increasing the number of filters. Therefore, besides convolution also pooling was applied. During max-pooling the maximum value of four neighbouring pixels was taken to decrease the image size by enhancing the image content (see Figure 5.6 and Figure 5.7).

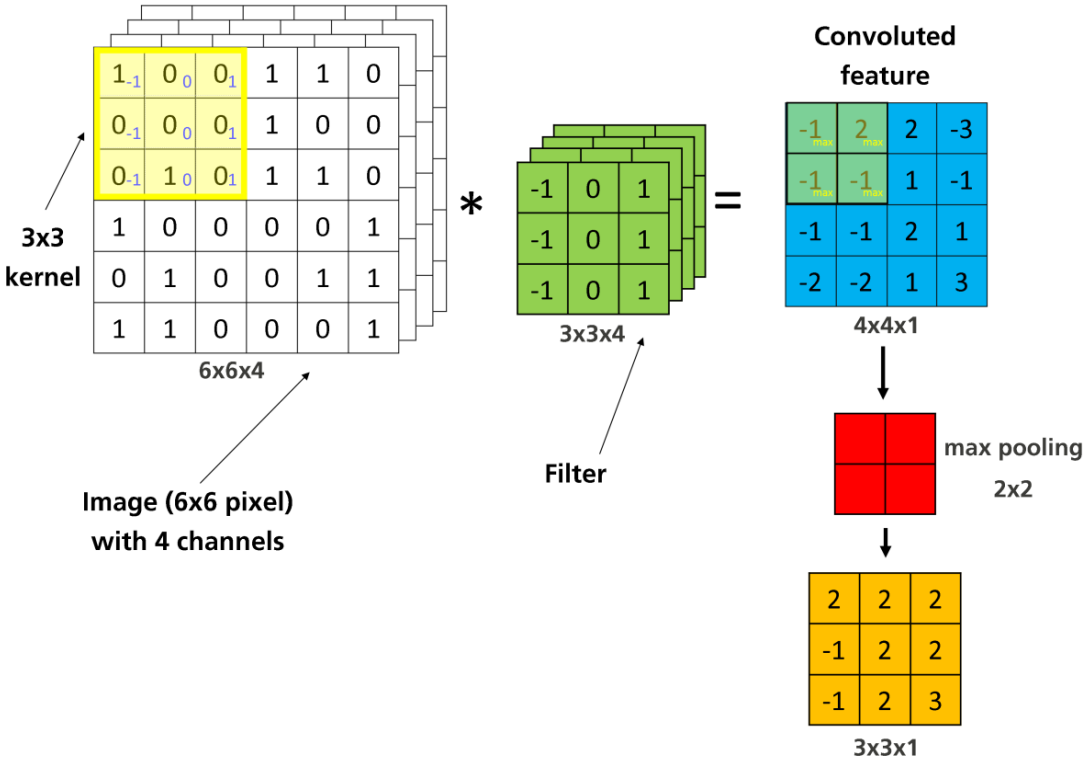

Figure 5.7: Simplified convolution and max-pooling example for a four-channel image (white) and a 3x3 kernel (yellow). The complete filter is depicted in green and the convoluted feature in blue. The 2x2 max-pooling is shown in red with a final condensed feature in orange.

After pooling, dropout with 0.3 was applied to prevent overfitting. This means after each block 30 % of the learned weights were randomly excluded to avoid the model to over fit on the training data. The value of 0.3 was empirically derived as dropout with 0.0, 0.2 and 0.5 decreased the model performance. In this case, four encoding blocks were used and at the lowest level, 512 filters of sizes 48x48 pixels were created. During the up-sampling block, the extracted information for image segmentation had to be increased again to fit the final image label size. The densified semantic information was up-sampled by a 2x2 convolution. To combine the very local information of the encoder block with the semantic information of the decoder block, skip connections were used. Those skip connections allow information transfer between encoder and decoder to finally label the input image

pixel-wise with the semantic information. The last 32 feature maps were reduced to two feature maps by a 1x1 convolution with a Sigmoid activation function. The final outputs were two semantic labels of the sizes 780x780 pixels. For each class (ocean and land ice) one label with prediction probabilities between 0 and 100 % was created. The entire U-Net consisted of 7.8 million trainable parameters.

5.3.3 Training the U-Net

For training the U-Net, all 38 scene stacks of the training data needed to be normalized and tiled into 780x780 patches. After pre-processing each scene was cropped to the data extent determined by the 100 km buffer around the initial coastline. The no-data areas were set to zero. First, the scene intensity of each scene was rescaled between the 2nd and 98th percentile to enhance the contrast. For normalization the mean and standardization over all input scenes were calculated. Normalization was necessary to scale each feature in the same range to keep gradients of the loss function in control. Z-score normalization x' was applied channel-wise. To center the data the mean μ of all training scenes was subtracted from the input scene x and then divided by the standard deviation of all scenes σ for standardization:

$$x' = \frac{x - \mu}{\sigma}$$

After normalization, each scene was tiled with a 200-pixel overlap to avoid border noise and to increase the training data. Training data was further increased by augmentation. All tiles including parts of the calving front were augmented six-times by rotating 90, 180, and 270 degrees as well as flipping and mirroring the tiles.

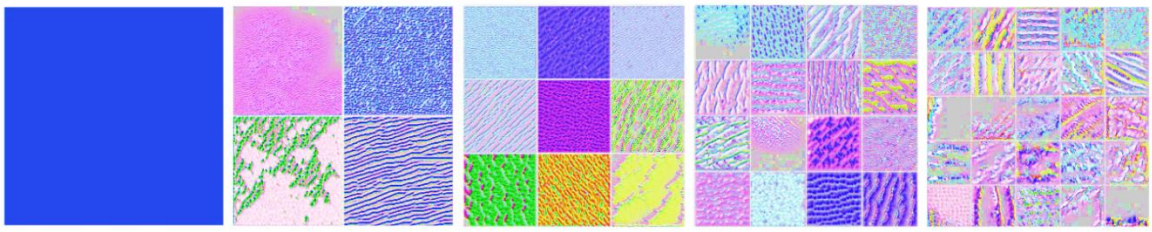

Figure 5.8: Filters with decreasing size from 780, 390, 195, 97 to 48 pixels. Filter size decreases from left to right whereas the number of filters increases from 32, 64, 128, 256 to 512. For clearness, only a few exemplary filters are shown. Modified after Baumhoer et al. (2019).

The training on the calving front was intensified by including 600 % (achieved by augmentation) of tiles from the glacier front, only 30 % of tiles from the image border areas and 90 % of the tiles covering only one class (ocean/land ice). This created a final number

of 19,576 patches of which 25 % were randomly used for validation. Validation in the sense of deep learning means to monitor the training process. The training was stopped when the classification accuracy of the validation tiles drops in comparison to the classification accuracy of the training tiles. Additionally, the calculated loss during each training epoch for training and validation tiles should not start to go apart. Otherwise, overfitting is expectable. The network was trained at a GeForce GTX 1080 GPU (12 GB RAM) with batch sizes of two for 30 epochs. This means all training patches were presented to the network 30-times before overfitting started. The weights which were learned during the training process are presented visually as complete filters in Figure 5.8. From left to right the image size decreases from 780 to 48 but the filter amount increased from 32 to 512. In the beginning, the filter was only sensitive to specific image channels whereas after several convolutions higher-level features (e.g. ice structures) were recognized. The final trained network produced classification accuracies of 98.14 % for training and 98.16 % for validation patches. A few examples of predictions on validation tiles compared to the hand-labeled image are given in Figure 5.9.

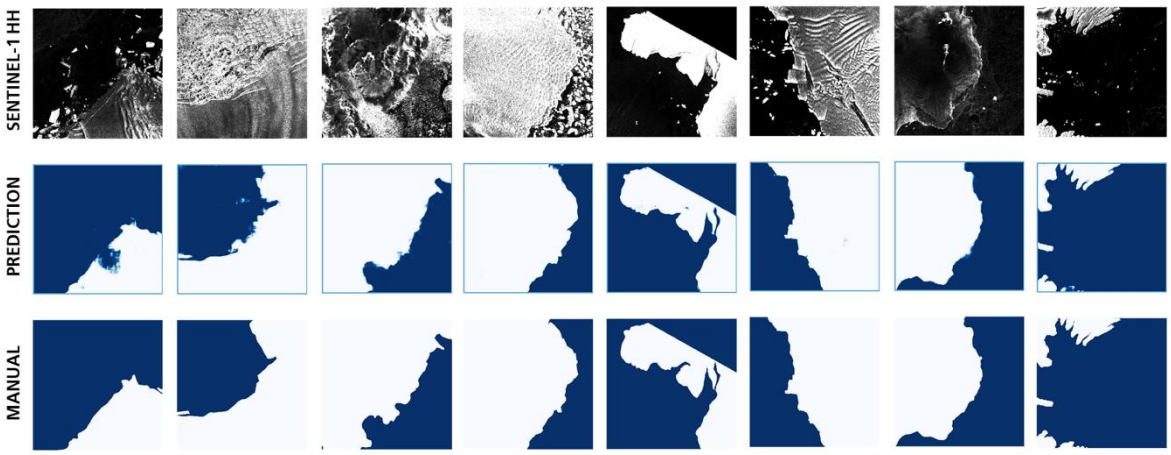

Figure 5.9: Prediction results on selected validation tiles. Manual reference labels are given in the lower line. Very accurate results were achieved except for the very low contrast glacier front on the left.

Afterwards the *Antarctic*LINES framework was adapted for HH single-polarized scenes in order to cover coastal sectors where no dual-polarized scenes were available. For the single-polarized adaption, the U-Net was trained for the same regions as described in Figure 5.4 but only for the HH polarized channel. The classification and validation accuracies decreased slightly with an accuracy of 97.75 % and 97.72 %, respectively. To minimize the slightly worse results especially over the higher ice sheet areas with low backscatter the post-processing was improved for HH scenes with DEM-support. This means all areas higher than 110 m in the DEM were fused with the classification result of the U-Net and automatically classified as ice sheet. The value of 110 m was empirically defined as the grounding line of Antarctic ice shelves lies above this value. Note that the

elevation of 110 m refers to the TanDEM-X Polar DEM 90 elevation model based on ellipsoidal heights relative to the WGS84 ellipsoid in the WGS84-G1150 datum and the sea surface has a negative elevation. Hence, ice shelf fronts were often higher than 110 m and still fully included.

5.3.4 Post-Processing

Post-processing was essential to reassemble the classified satellite scene, minimize errors by morphological filtering, and to create vector shapefiles from the raster labels. For each scene, all raster tiles with prediction probabilities were merged. In overlapping regions, the mean prediction probability was calculated. A binary mask was created from the prediction probabilities by a threshold of 0.5. Every pixel with a 50 % probability of being land ice was classified as such. Morphological filtering was applied to the binary mask by first filling holes in the ice class and afterwards closing islands in the water class. This allowed minimizing wrong classifications especially at patch borders where the neural network could not distinguish whether a piece of ice is still connected to land or already an iceberg. The backscatter of both features is the same and only the spatial context allows distinguishing between them. Additionally, the tile size of 780 x 780 pixels was not always big enough to get the full spatial context. Hence, during post-processing, those errors were eliminated by morphological filtering on the entire scene. After creating two self-contained classes, the raster was converted into a vector polygon. The polygon over the ice class was clipped with a coastline buffer shapefile slightly thinner (98 km wide) than the initial mask shapefile in the pre-processing step to remove border areas of the shapefile. Finally, the remaining polygon was converted into a line shapefile only containing the extracted calving front.

5.3.5 Time Series Generation

The framework *Antarctic*LINES was designed to create calving front time series for glaciers and ice shelves. To create a calving front time series over a selected glacier, a polygon shapefile over the area of interest was needed. This defined the download area for Sentinel-1 scenes. Pre-selection of scenes e.g. by also selecting the relative orbit and/or frame or only one scene per month was used to reduce the processing time. All selected scenes were fed to the pre-trained weights of the U-Net to segment each scene into land ice and ocean. Additionally, to the extracted coastline per scene also monthly, seasonal, semi-annual, and annual mean coastline positions were calculated to create more robust results. For this step, the prediction probabilities for all scenes within the selected time frame (e.g. the summer coastline is a merge of all scenes between December and February) were merged by calculating the mean of the segmentation results. This was especially useful in areas where strong surface melt occurred during summer. During summer, surface melt can reduce the backscatter of the glacier ice and make a calving front delineation impossible

even for manual delineations by experts. As an example see Figure 5.10 with the Glenzer Glacier during summer and winter.

Taking a seasonal or annual mean of the segmentation results balanced out the invisible fronts during summer. For sure, the averaging of front positions also reduced the frequency of available glacier front position measurements. Hence, the selection of the calving front product (daily, annual, etc.) depended on the study design and study region.

For example, for glaciological analysis during calving events very dense glacier front time series were required. Here, daily or monthly derived calving fronts were selected and manually checked for accuracy. If fronts were extracted with slight inaccuracies (e.g. due to mélange or melt) they were corrected manually in the shapefile. In case of strong surface melt, even manual corrections were not possible and the fronts for those months were excluded.

In case a monthly or seasonal calving front time series was sufficient and a fully-automated approach was envisaged, a quality threshold for incorrect front positions was implemented. The outlier detection removed "extreme front positions with a distance greater than the one and a half times of the upper interquartile range plus the 90%-quantile" (Baumhoer *et al.* 2019). This threshold removed extreme values in the calving front time series.

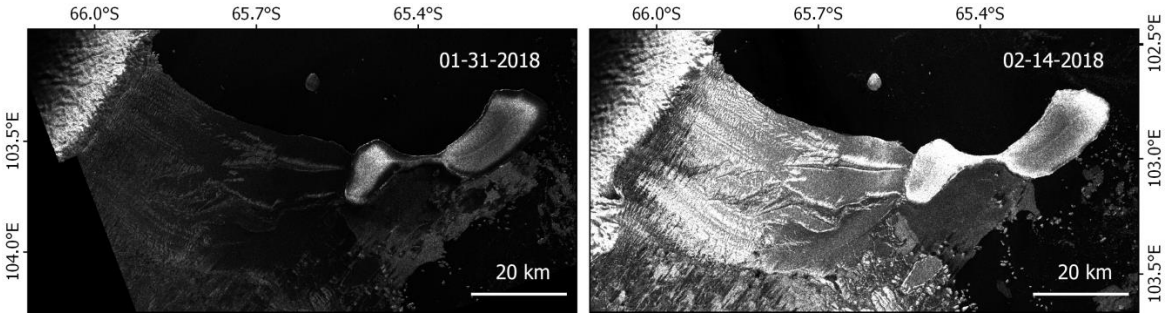

Figure 5.10: Glenzer Glacier during melt season in January (left) and after melt season in February (right). Displayed for the same backscatter coefficient range in both images. Copernicus Sentinel-1 data 2018.

Distance changes in calving front positions were calculated with the Digital Shoreline Analysis System (DSAS). Along the glacier or ice shelf, a base line perpendicular to the glacier flow was drawn. Along this line transects with 500 m spacing were automatically created by the DSAS software. The transect intersections with the front positions were used to calculate the distance from the baseline to each front position with the sample lines method (see Section 4.3). For time series generation an R script was programmed to handle different time series operations. The calculated absolute distances were transformed into mean or median calving front change rates with R. Additionally, the programmed R script provided the optional outlier detection, the plotting of calving front changes, and the calculation of linear regression. The linear regression can be an indicator of the consistency

of frontal advance or retreat if the R^2 is high. For low R^2 values, a calving event occurred or the quality of the extracted coastline was low (Baumhoer *et al.* 2019).

5.4 Results

In this section, the calving front extraction results for different areas of application are presented. First, intra-annual time series of four selected glaciers and ice shelves demonstrate the applicability of *Antarctic*LINES for glaciological calving front studies. Visual corrections of the extracted coastlines enabled densest time series to monitor calving front behavior and the timing of calving events. The second part of this section includes results of the fully-automatic calving front extraction with outlier detection to automatically remove wrong classification results due to melt or mélange. Finally, the extraction of the Antarctic coastline at selected sites is presented.

5.4.1 Intra-Annual Patterns of Glacier and Ice Shelf Front Fluctuations

Seasonal patterns of calving front fluctuations were derived for four glaciers and ice shelves. All four had very different patterns of advance and/or retreat signalizing differences in glacier morphology, glacier health and calving cycle. In the following, calving front time series are presented for Pine Island Glacier, Amery Ice Shelf, Denman Glacier and Glenzer Glacier.

5.4.1.1 Pine Island Glacier

The glacier front of the Pine Island Glacier experienced phases of advance interrupted by four major calving events since February 2015 (see Figure 5.11). The strongest calving front retreat occurred between mid-July 2015 and November 2015 with an average retreat of 15.9 km along the center line. Unfortunately, this calving event could not be timed exactly as the scene coverage was limited in the early stages of Sentinel-1 during this time period. Later calving events were dated very accurately. In September 2017, the front retreated on average 8.3 km and again 9.2 km in October 2018. The most recent calving event in February 2020 caused an average glacier front retreat of 11.6 km. After the calving event in October 2018, the eastern shear margin started to disintegrate slowly before the next calving event in February 2020. During previous retreats, the front rather broke up along a straight line. Early signs of calving were visible by slowly developing crevasses, even though the time between first evidence of crevasse development and calving varied strongly. For calving in 2015, the crevasse existed at least 5 months (no earlier acquisitions were available). For the other events in 2017, 2018 and 2020, the time between first signs of crevassing and calving was 12, 2, and 9 months, respectively. Between calving events, the front advanced with a steady rate of 12.2 m/day (on average). Slight variations accounted for ± 2 m/day on a random pattern which could also be attributed to measurement

inaccuracies. Despite recurring phases of advance, Pine Island Glacier lost a total of 24 km at the glacier tongue since February 2015.

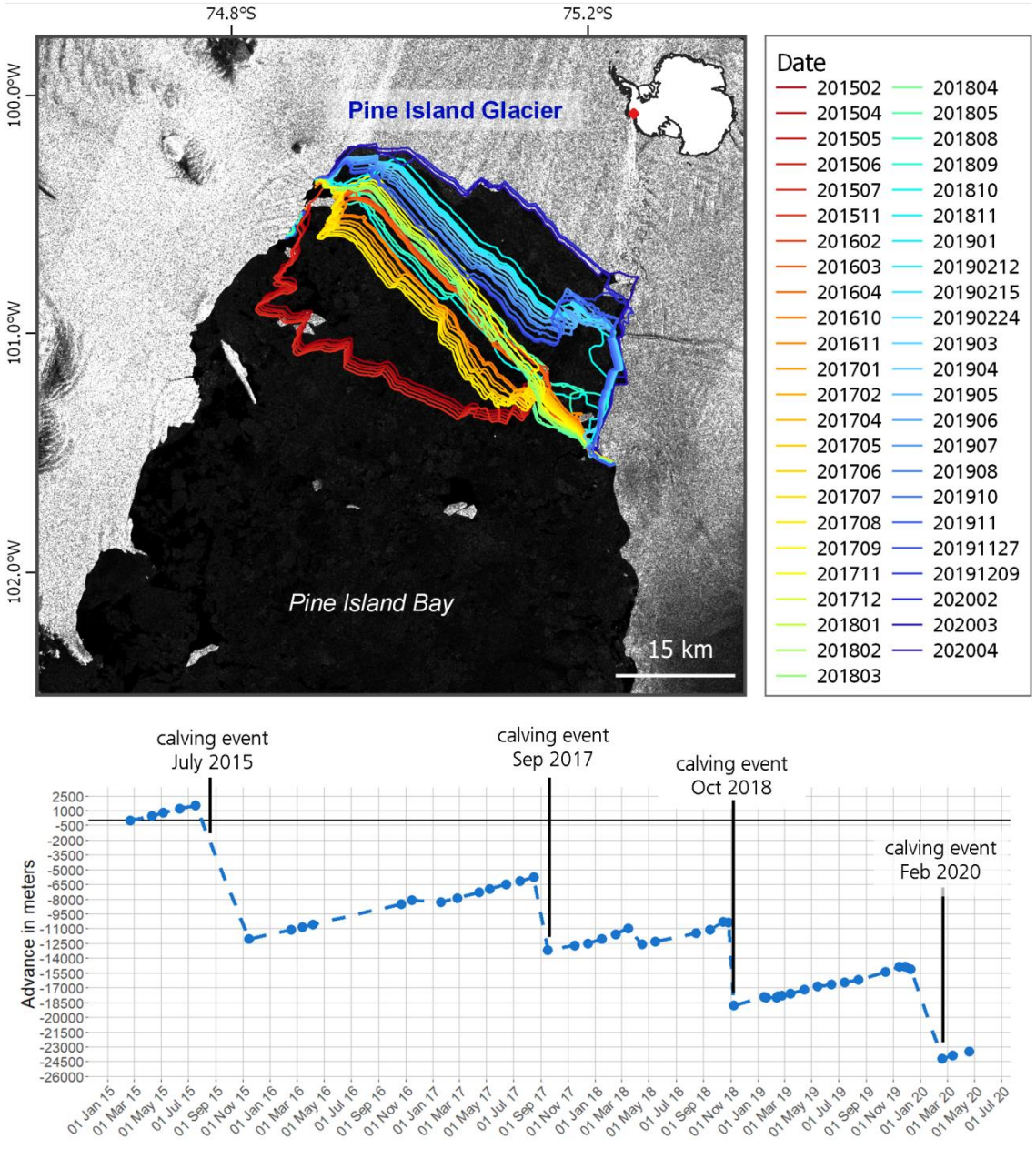

Figure 5.11: Glacier front fluctuations of Pine Island Glacier from February 2015 (red) to April 2020 (dark blue) in the upper panel. The lower panel displays cumulative calving front position changes relative to February 2015. Dates are monthly averages or exact when the date was given. Sentinel-1 Copernicus Data April 2020.

5.4.1.2 Glenzer Glacier

Glenzer Glacier had an almost steady front advancing on average with 0.75 m/day between February 2015 and December 2017. A first calving event occurred in April 2018 with an average front retreat of 1.2 km after heavy melt visible in the SAR Sentinel-1 scenes. A further event occurred one year later between March and May 2019 where 120

m of the front were lost (see Figure 5.12). Afterwards, the glacier front kept steady again but a clear crevasse opening had been visible since September 2016.

The crevasse existed already at least since February 2015 but did not widen at this stage (see Figure 5.13). In April 2020, the crevasse opened up and an iceberg calved which was trapped at a little island has been a former pinning point of Glenzer Glacier (see Figure 5.12). The calving event in April 2020 was the most severe with a median retreat of 4.2 km. The remaining ice bridge between Glenzer Glacier and the opposite island remained with a width of 5.7 km.

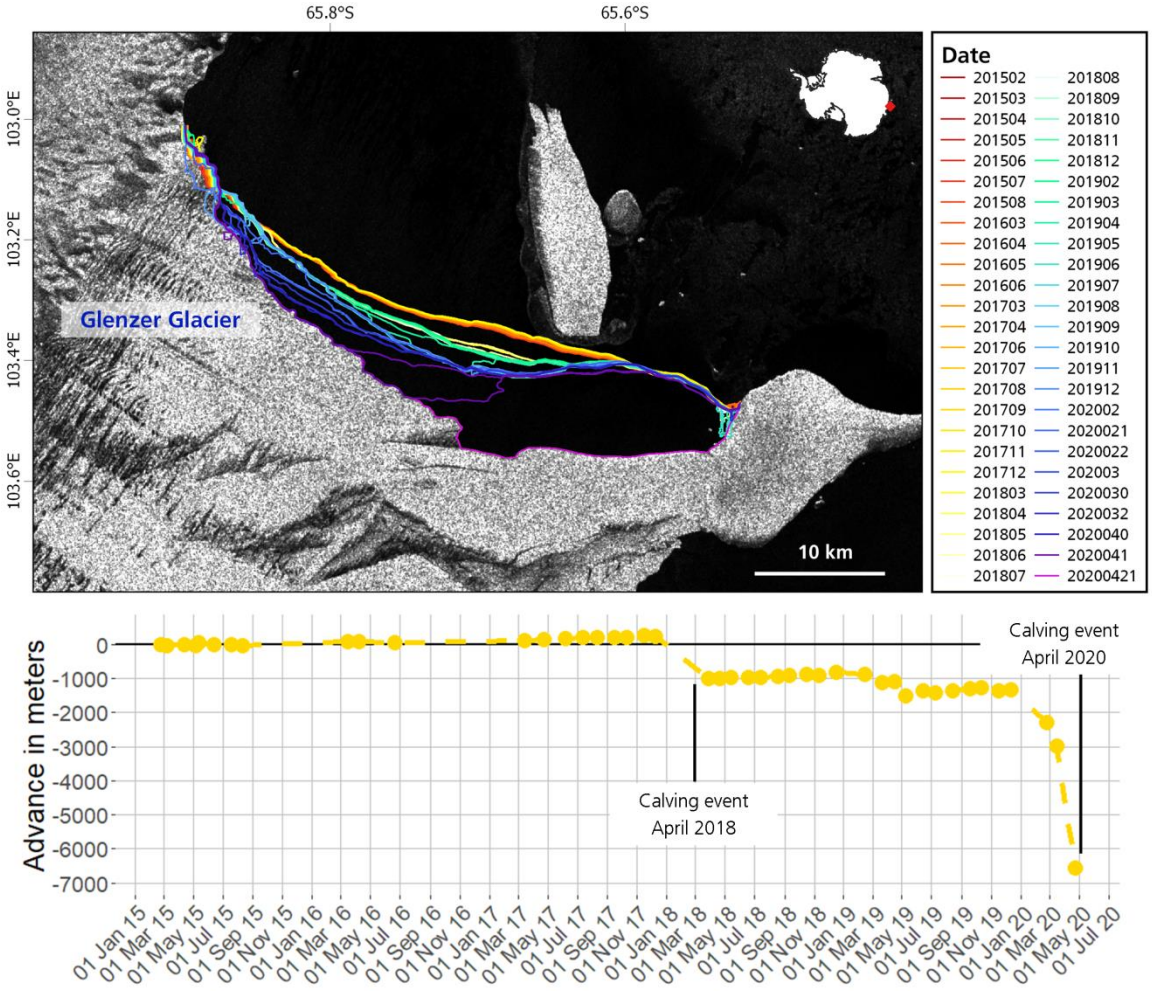

Figure 5.12: Retreating front of Glenzer Glacier with the iceberg trapped at the former pinning point. Sentinel-1 Copernicus Data April 2020.

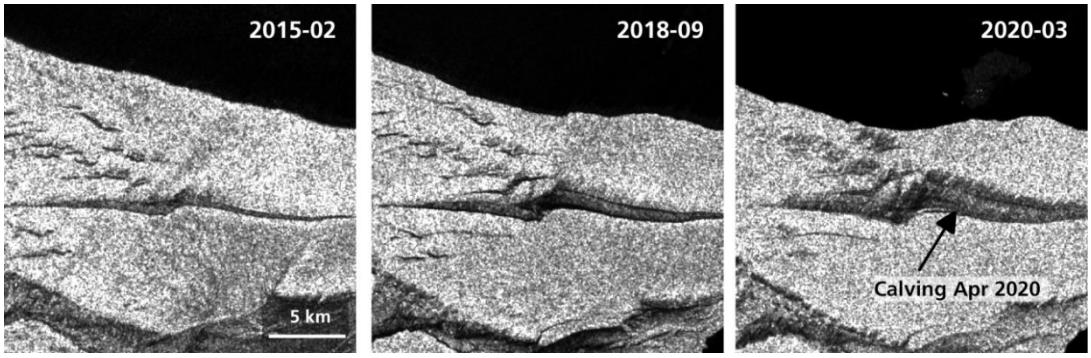

Figure 5.13: Crevasse opening at Glenzer Glacier from 2015 to March 2020 shortly before break up.

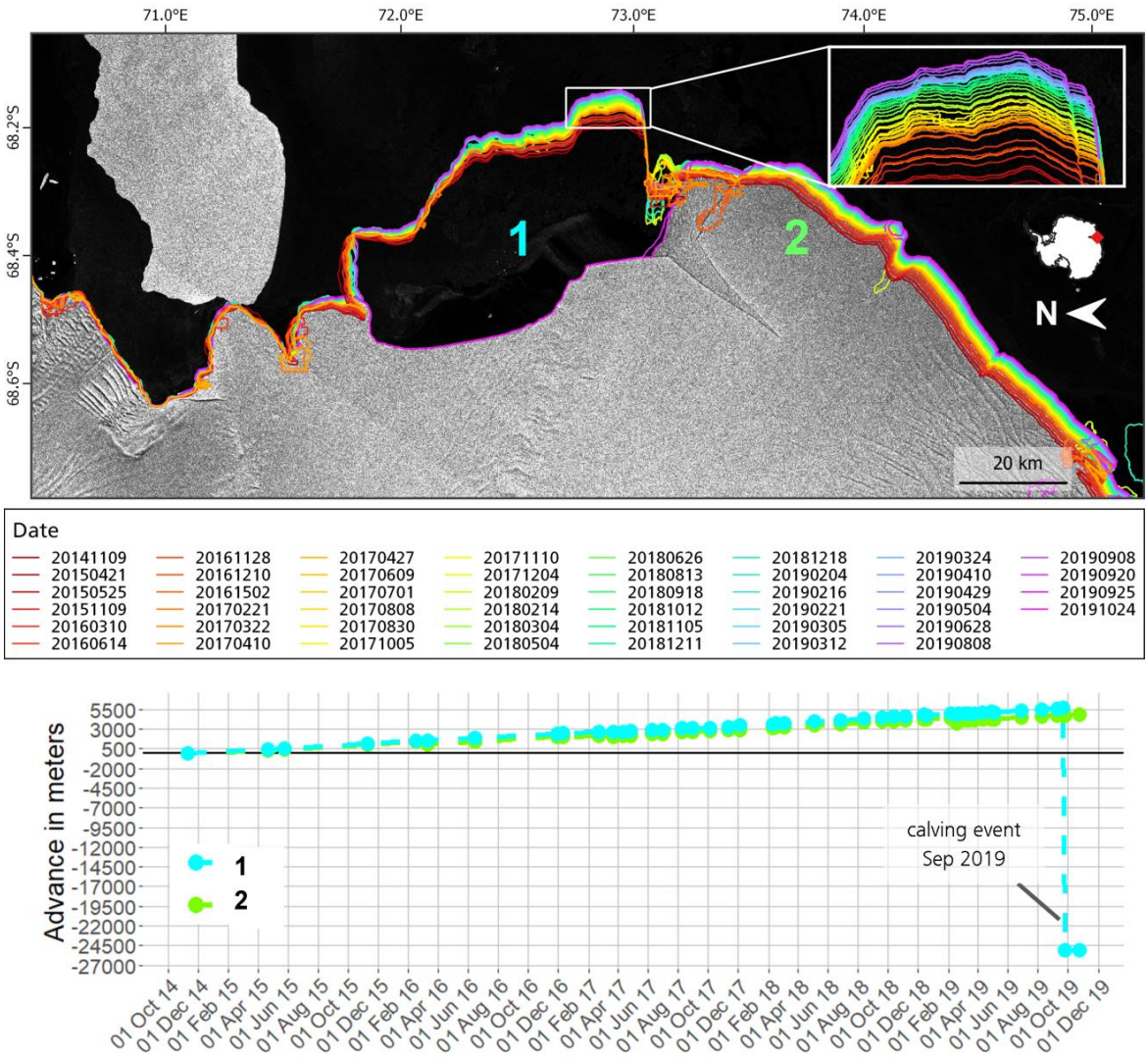

Figure 5.14: Calving front fluctuation of Amery Ice Shelf. The iceberg D-28 which calved in September 2019 is still visible in the picture. The ice shelf front change is given for the northern part of Amery Ice Shelf (1) and the southern part (2). Copernicus Sentinel-1 Data September 2019.

5.4.1.3 Amery Ice Shelf

The front of Amery Ice Shelf continuously advanced with 3.7 m/day since October 2014. The total advance of the ice shelf was 5.7 km on the northern front and 4.9 km on the southern front. The relatively stable advance was interrupted after summer melt with no advance in March 2016, March/April 2017 and February 2019. End of September 2019, the iceberg D-28 calved at the northern part of the ice shelf front (see Figure 5.14). At this point, the front retreated 31.4 km whereas the southern front continued to advance.

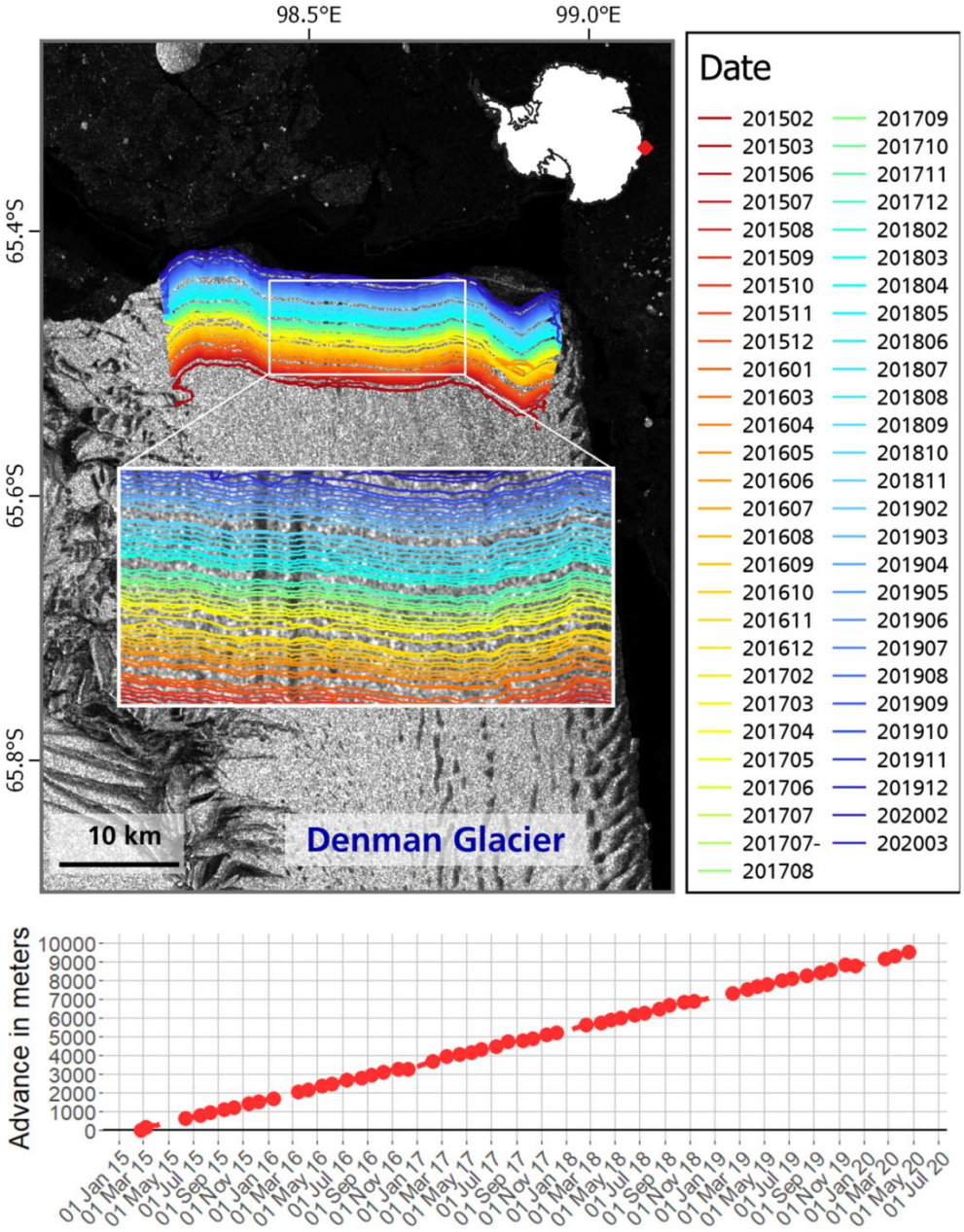

Figure 5.15: Glacier front advance of Denman Glacier since February 2015. Steady calving front advance (upper panel) and cumulative frontal change in meters (lower panel). Copernicus Sentinel-1 Data April 2020.

5.4.1.4 Denman Glacier

Denman Glacier (located right next to Shackleton Ice Shelf) is a steady advancing glacier with a very low lying bed. In total, the front of Denman Glacier advanced 9.5 km since February 2015 not experiencing any calving events (see Figure 5.15). In two cases the front position stayed in the same position and did not advance further. This was in December 2016 and 2018 when a slight melt occurred at the front. On average the calving front advanced with a daily rate of 5.0 m/day.

5.4.2 Intercomparison

Different intra-annual patterns of calving front change were identified ranging from continuous advance at Denman Glacier to commencing disintegration at Glenzer Glacier. Glacier and ice shelf front changes relative to the first CFL measurement are summarized in Figure 5.16 for intercomparison.

The highest advance rate experienced Denman Glacier with 5.0 m/day followed by the southern Amery Ice Shelf with 3.7 m/day. The front of the northern Amery Ice Shelf experienced the most extreme retreat with 31.4 km. The beginning disintegration of Glenzer Glacier measured just by frontal retreat was comparable small with 4.2 km. But in relation to the remaining ice bridge, the calving event was critical. Pine Island Glacier was characterized by the most dynamic glacier front. The total retreat of Pine Island Glacier was almost as high as the retreat of the northern Amery Ice Shelf even though Pine Island had several phases of advance in-between.

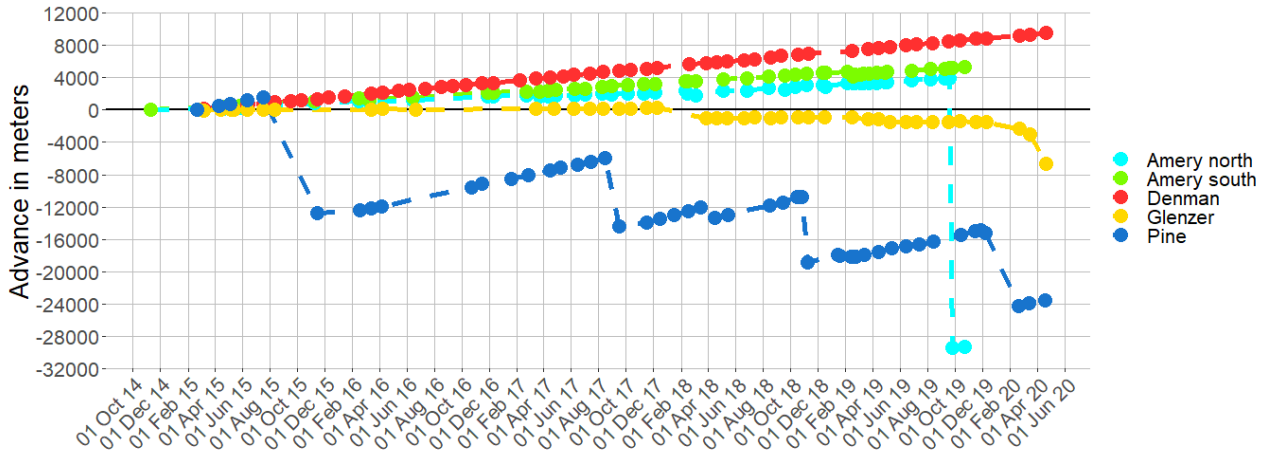

Figure 5.16: Comparison of glacier front changes for Amery Ice Shelf, Pine Island Glacier, Denman Glacier, and Glenzer Glacier

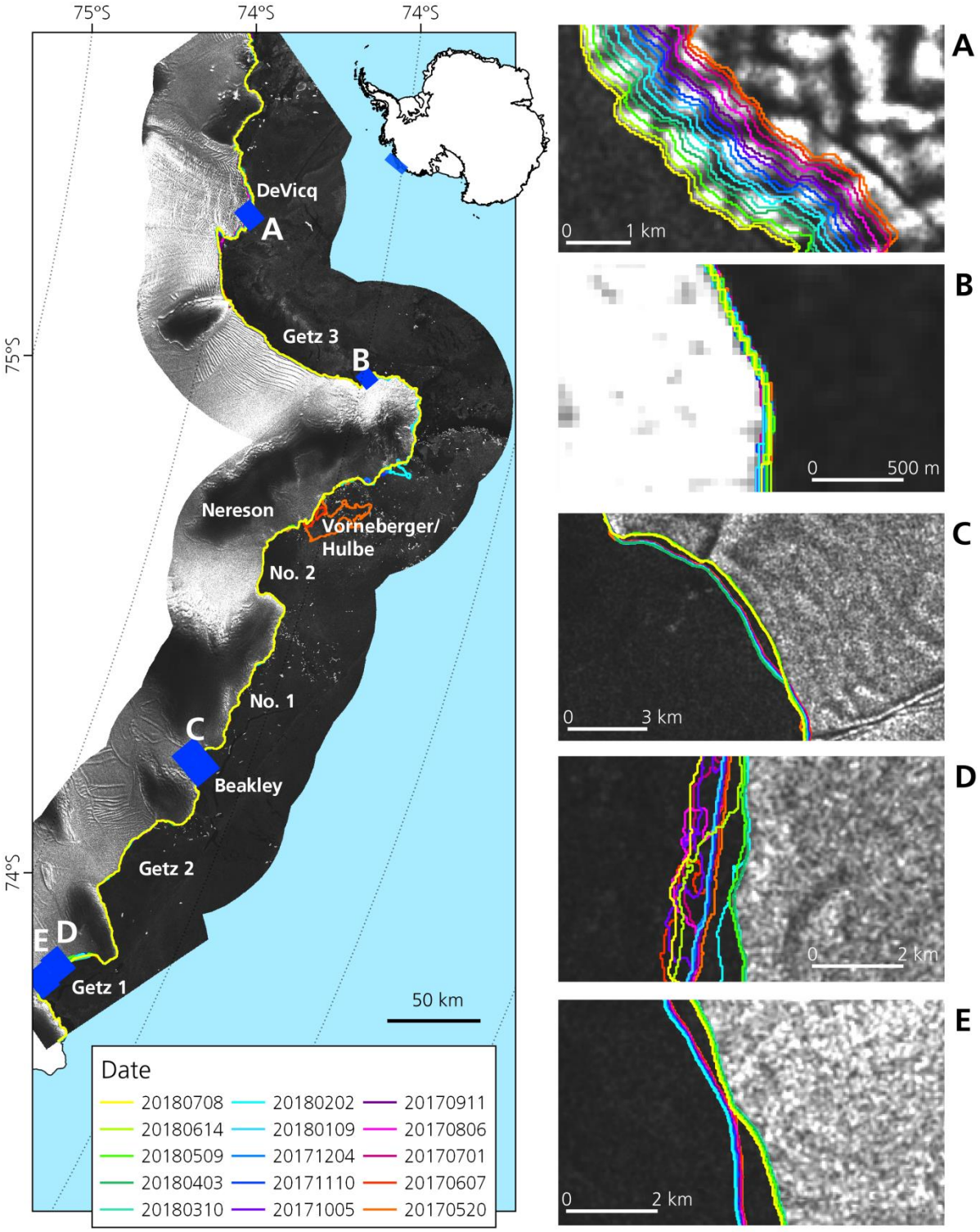

Figure 5.17: Calving front time series of Getz Ice Shelf. (a) Continuous advance of the DeVicq Glacier. (b) Part of a stable coastline. (c) Front of the Beakley Glacier showing a calving event. Front of Getz 1 with wrong delineation in (d) and calving event in (e). Sentinel-1 scene from 2018-07-08 in HH polarization.

5.4.3 Fully-Automated Calving Front Time Series

The fully automated creation of calving front time series including outlier detection was tested for Getz Ice Shelf. The time series for Getz Ice Shelf was created based on all available Sentinel-1 dual-pol EW scenes. Therefore, time series only covered the period May 2017 to July 2018 and is displayed in Figure 5.17. Figure 5.17 and the accompanying detailed displays show the accurate extracted front of Getz Ice Shelf with rare exceptions. The advance of DeVicq Glacier was captured in very detail with a front advancing around 1-2 pixels (40-80 m) per month (see Figure 5.17a). In Figure 5.17b an example of coastline extraction along a stable coastline is given. The lines almost overlap completely, hence errors along stable parts of the coastline due to extraction or orthorectification errors were negligibly small. At Beakley Glacier a small calving event was detected with a width of 315 m (see Figure 5.17c). The front of Getz 1 Ice Shelf was extracted perfectly in region E (Figure 5.17e) but diffused in the nearby Region D (Figure 5.17d). A further misclassification occurred for Verneberger/Hulbe Glacier during mélange at the glacier front in May and June 2017 (see Figure 5.17).

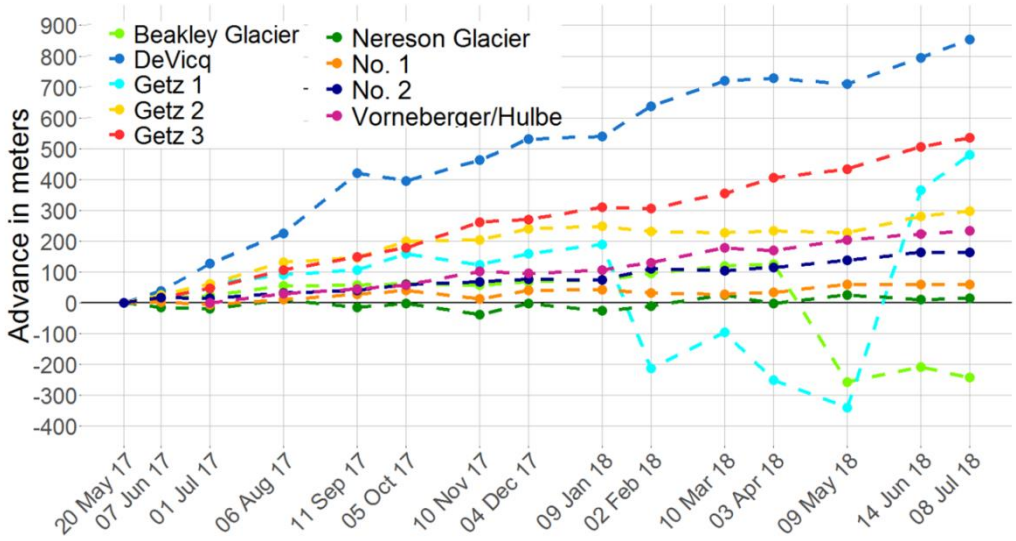

Figure 5.18: Calving front fluctuations in meters at Getz Ice Shelf relative to May 2017. Not the erroneously extracted front of Getz 1. All fronts advanced except the one of Beakley Glacier. Modified after Baumhoer et al. (2019).

The wrong extracted front at Vorneberger/Hulbe Glacier was excluded by the outlier detection as can be seen in the plotted calving front time series in Figure 5.18. Figure 5.18 presents the average calving front position change along Getz Ice Shelf for each front separately after the outlier detection was applied. The corresponding overall change rates and the linear regression coefficient are listed in Table 5.1. The strongest advance rate existed for DeVicq Glacier with 726±20 m/yr followed by the front of Getz 3 with 463±21 m/yr. Lowest advance rates were observed for Nereson Glacier (23±37 m/yr) and Glacier No. 1 (52±26 m/yr). The only fronts diverging from the overall trend of advance were

Beakley and Getz 1. As previously mentioned, the front of Getz 1 was not accurately extracted along the entire front and hence the calving front movement is not representative. The second misclassification at the front of Vorneberger/Hulbe was detected by the outlier detection and hence not included in the time series. Beakley Glacier was the only retreating glacier along Getz Ice Shelf with -170±29 m/yr. Linear glacier front advance was observed for the fronts of DeVicq, Getz 3 and No.2 with an R^2 of 0.95, 0.99 and 0.98, respectively. The fronts of Nereson and Beakley did not show linear front movement with R^2 of 0.23 and 0.24, respectively.

Table 5.1: Calving front change rates per year with mean standard deviation and R-square of linear regression for each calving front time series.

Glacier/Ice Shelf	m/yr	R^2
Beakley	**−170** ±29	0.24
DeVicq	**726** ± 20	0.95
Getz 1	**37** ± 518	0.00
Getz 2	**222** ± 33	0.82
Getz 3	**463** ± 21	0.99
Nereson	**23** ± 37	0.23
No. 1	**52** ± 26	0.77
No. 2	**141** ± 32	0.98
Vorneberger/Hulbe	**232** ± 39	0.98

5.4.4 Coastline Extraction Results

Examples of extracted coastlines are presented in Figure 5.19 and Figure 5.20 with detailed visualization of selected glaciers. Each of the overview maps visualizes the match between the manual (orange) and automated (turquoise) coastlines plotted on Sentinel-1 imagery. Due to a good overlap, deviations between the manual and automated delineations are difficult to visualize. Therefore, enlarged maps for selected glaciers are provided to present a more detailed view. The high accuracy of the results is represented by the almost overlapping coastlines with only minor deviations. A perfect overlap of the manual and automated coastline was achieved for Shackleton Ice Shelf in all areas. Along Wilkes Land, only slight deviations existed over areas with icebergs at the calving front. At Wilkes Land, the extraction of the front of Bell and Blair Glacier was most challenging due to the low backscatter over blue ice. The coastline along the area of Wordie Ice Shelf overlapped with the manual delineation in parts with a steep coastline. In the area of the former Wordie Ice Shelf, heavy mélange complicated the calving front delineation. The automated approach did not create accurate results in this area. The glaciers along Oates Land were extracted very accurately along the steeper coastline. Also, small glaciers were captured well. The only major deviation existed for one part of the Rennick Ice Shelf where a small part of the front was missed out (see Figure 5.20d).

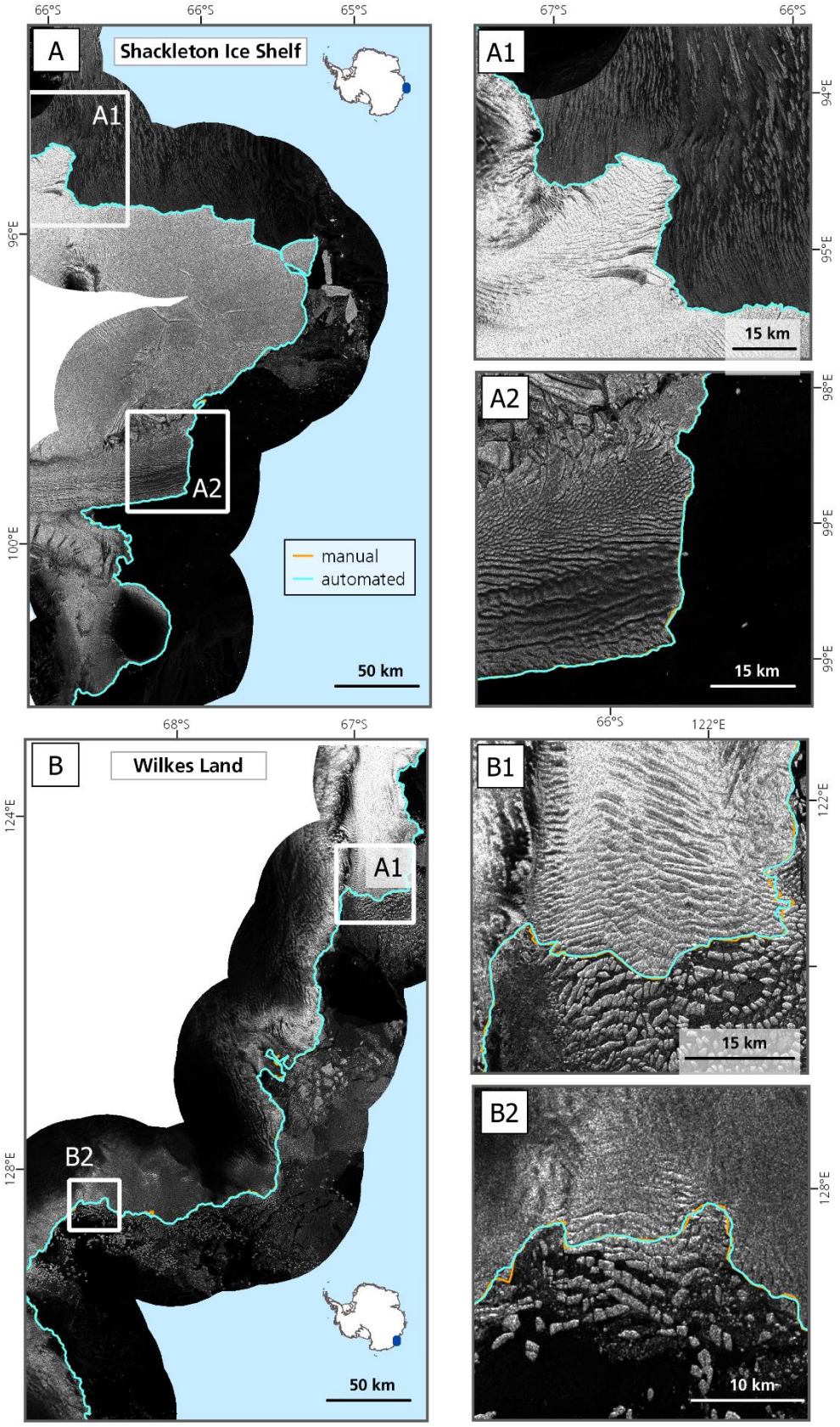

Figure 5.19: Calving front extraction results for Shackleton Ice Shelf (A) with detailed display of Roscoe Glacier (A1) and Denman Glacier (A2). (B) Results for Wilkes Land with detailed presentation of Moskow University Ice Shelf (B1) and DeHaven Glacier (B2).

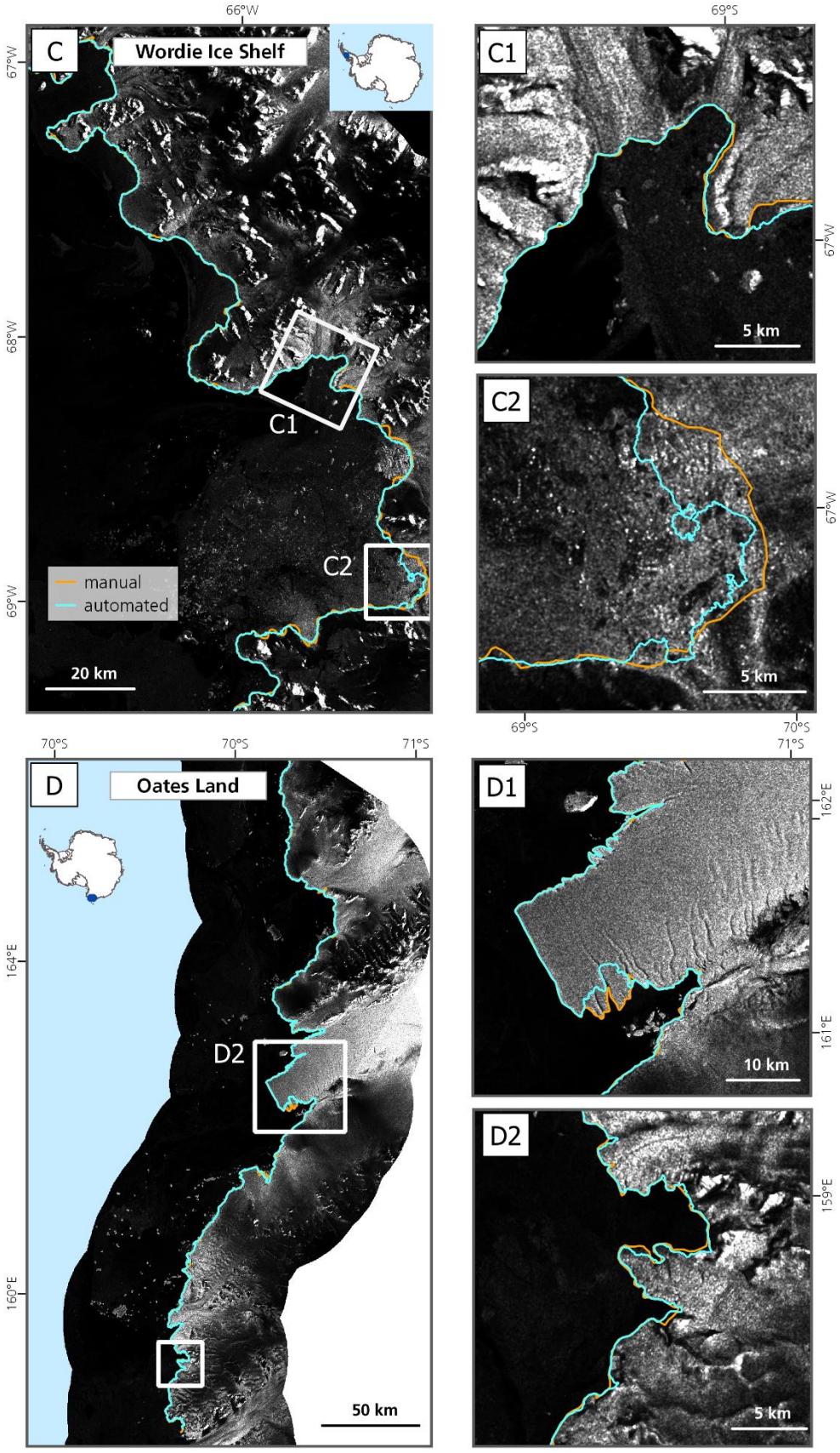

Figure 5.20: Results for the area around the former Wordie Ice Shelf (C) and Oates Land (D). Detailed displays of Hariot Glacier (C1) and the Wordie Bay (C2) covered by mélange. For Oates Land detailed displays of Rennick Ice Shelf (D1) and McLeod Glacier (D2) are presented.

5.5 Accuracy Assessment

The performance of the presented framework is tested in two ways as the results can be seen as the solution for a classification or delineation problem. Within the deep learning community, classification accuracies are used as an accuracy measure. In contrast, for coastal change and CFL studies, a distance measure is more suitable. The model was tested for eight areas (depicted in Figure 5.4, Chapter 5.2.4) in June 2018 (no data was used for training during this month) as this is the only month where additional manual delineated calving fronts from the ADD existed for an external reference. Four of the areas were also included for training but during different seasons. Hence, the temporal transferability was tested as done by Zhang et al. (2019b) and Mohajerani (2019). With the other four areas, the spatial transferability was tested by including new areas. Additionally, it is of interest to see whether differences in accuracy exist between areas included during training and completely new areas. The following sections describe the calculation of different accuracy measures as well as the calculated accuracies.

5.5.1 Calculating Accuracies

For calculating the classification accuracy, a 1 km buffer along the manually delineated coastline was created. Within this buffer, the classification accuracies were calculated. This was done as classification accuracies for the entire 100 km buffer were over 99 % and not precise enough to account for errors at the calving front. To measure accuracies, standard performance measures were chosen accounting for false positives (precision), true positives (recall), and the weighted average of both (f1-score).

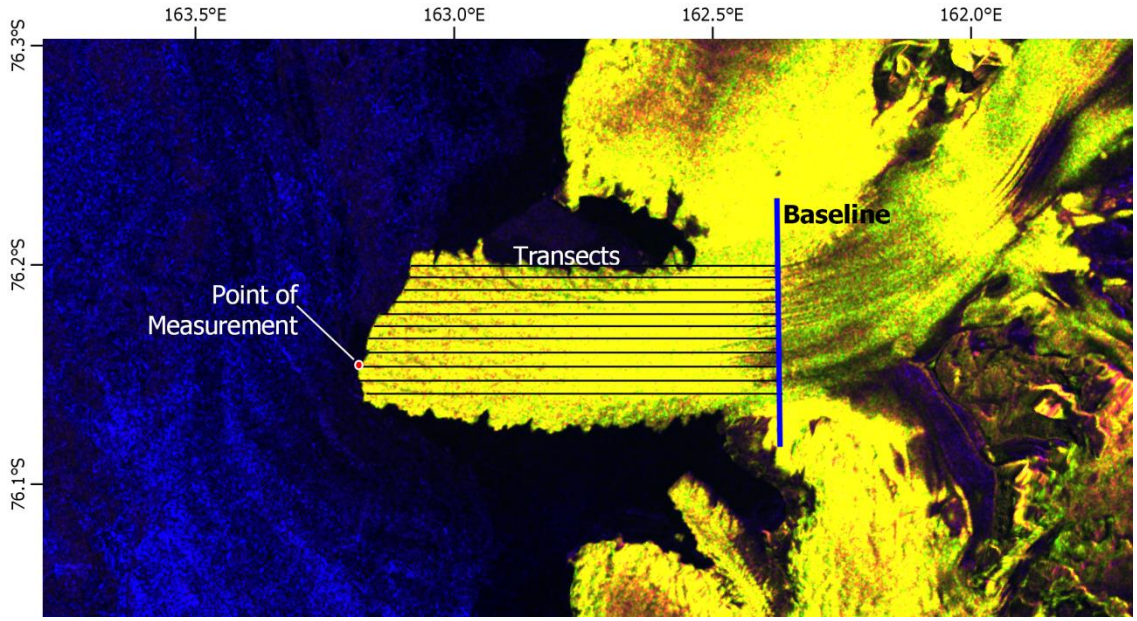

Figure 5.21: Schematic representation of transect measurements at Mawson Glacier. Point of measurement is the intersection between each transect and the glacier front.

The DSAS tool provided by USGS was used to measure the distance between manually delineated and automatically extracted fronts. It can also be used to track distance changes between several front delineations. This tool is freely available and the MATLAB based code can be integrated into ArcGIS. For each test site, a baseline was created. Along the baseline perpendicular transects were automatically created by the software (see Figure 5.21). Only in areas of overlapping and non-perpendicular transects manual corrections were necessary. Between transects a spacing of 1 km was chosen to keep the computational cost low but still achieve accurate results. The mean or median of all transect measurements was then used to estimate the average distance error. The distance differences were calculated in the Antarctic Polar Stereographic Projection.

Additionally, a second measurement to measure the distance deviation was applied. It is a simpler and more often applied approach (Zhang *et al.* 2019b, Krieger & Floricioiu 2017). The average distance deviation D was calculated as

$$D = \frac{A}{(F_{expert} + F_{automatic})/2}$$

where A is the enclosed area between both coastlines divided by the mean length F of the expert and automatically extracted front. This method (short A/F) is a quick way to measure the average distance difference but smooths out outliers.

5.5.2 Results of the Accuracy Assessment

The accuracy assessment was performed for the fully automatically extracted calving front time series at Getz Ice Shelf as well as the classification performance (Table 5.4) and the distance deviations (Table 5.5) for the coastline extraction. Accuracies for the intra-annual patterns of glacier and ice shelf front fluctuations were not calculated as manual corrections were applied and ensured results that are as accurate as manually delineated fronts.

5.5.2.1 Accuracies for Time Series

The first part of the accuracy assessment evaluates the accuracy of a fully automatic derived calving front time series. To assess the accuracy of an entire time series, the 15-month time series over Getz Ice Shelf was validated against five manual drawn ice shelf fronts. The five manual coastlines were drawn for May, July, and December 2017 as well as March and July 2018. Those dates cover the full time range of the automatically extracted time series. The distance error for five randomly selected dates compared to a manual coastline is given in Table 5.2 for the average absolute mean and in Table 5.3 for the median.

Table 5.2: Error calculation for the Getz time series with five manual reference coastlines. The distance to the reference coastlines is presented as the absolute mean of the measured transect values.

	distance (absolute mean) to manual reference (m)					abs. metrics (m)	
	05-2017	07-2017	12-2017	03-2018	07-2018	mean	sd
Beakley	34	41	71	98	56	**60**	**26**
DeVicq	43	185	91	87	91	**99**	**52**
Getz 1	72	237	433	1018	1103	**573**	**464**
Getz 2	36	23	101	79	79	**64**	**33**
Getz 3	48	31	76	44	53	**50**	**16**
Nereson	149	43	72	134	60	**92**	**47**
No. 1	44	29	63	61	82	**56**	**20**
No. 2	40	29	45	77	58	**50**	**18**
Vorneberger/Hulbe	-	156	193	164	132	**161**	**75**

Table 5.3: Error calculation for the Getz time series with five manual reference coastlines. The distance to the reference coastlines is presented as the median of the measured transect values

	distance (median) to manual reference (m)					abs. metrics (m)	
	05-2017	07-2017	12-2017	03-2018	07-2018	mean	sd
Beakley	−17	−30	−66	−91	−49	51	29
DeVicq	5	42	−24	−50	−52	35	20
Getz 1	−37	−50	−146	−75	−1231	308	518
Getz 2	−29	−9	−84	−78	−73	55	33
Getz 3	−20	8	−64	−36	−38	33	21
Nereson	−32	5	−43	−107	−49	47	37
No. 1	−23	−19	−71	−58	−71	48	26
No. 2	−12	9	−48	−71	−47	37	26
Vorneberger/Hulbe	-	−5	−97	−73	−65	60	39

The mean error compared between manual and automatic delineations accounted for 50 to 573 m. High accuracies existed for the fronts of Getz 3 and Glacier No. 2. Inaccuracies were high for the front of Getz 1 where the outlier detection did not remove the wrongly extracted fronts. The overall median error between the automatically and manually extracted fronts was smaller as the median is less sensitive for outliers. Calculated with the median, the deviation was between 37 and 60 m. Only for the front of Getz 1, the deviation was high with 308 m.

5.5.2.2 Classification Accuracies

The overall accuracy within a 1 km coastline buffer was 90 %. For the class ice the average f1-score was 90 % for training and 91% for test regions. For the class water the average f1-score was 89% and 90% respectively. Depending on the study region the accuracies varied. For Sulzberger Ice Shelf accuracies of 85 % (ice) and 83 % (water) were reached. Higher accuracies could be reached for Ekstromisen Ice Shelf (93 % ice and 92 % water) and Shackleton Ice Shelf (94 % for both classes). For the area of Wordie Ice Shelf, accuracies were lowest with 88 % for ice and 87 % for water. From those results, it is apparent that for the class ice the true positives were captured well (higher recall) but a

lower accuracy in precision indicates more false positives. Therefore, a slight over-classification for the class ice existed.

Table 5.4: Classification performance for all training and test sites (June 2018). Highest and lowest values are indicated in bold.

		Training Sites				Test Sites					
	Accuracy measure	Sulzberger	Victoria Land	Wilkes Land	Shackleton	Marie Byrd Land	Oats Land	Ekstromisen	Wordie	**mean train**	**mean test**
ice	precision	0.85	0.89	0.87	**0.92**	0.91	**0.92**	0.91	0.85	0.88	0.90
	recall	0.85	**0.98**	0.92	0.96	**0.94**	0.91	**0.94**	0.91	0.93	0.93
	f1-score	0.85	0.93	0.89	**0.94**	**0.93**	0.91	**0.93**	0.88	**0.90**	**0.91**
water	precision	0.79	0.97	0.91	**0.96**	0.92	0.91	**0.94**	0.90	0.91	0.92
	recall	0.86	0.87	0.86	**0.92**	0.90	**0.92**	0.90	0.84	0.88	0.89
	f1-score	0.83	0.92	0.88	**0.94**	0.91	0.91	**0.92**	0.87	**0.89**	**0.90**

5.5.2.3 Distance Measured Accuracies

The distance measured accuracies are presented in Table 5.5. Measurements are given for the transect method in mean and median as well as for the A/F measurement. Measured with the transects method, the manual delineation deviated on average 151 m over areas included during training and 154 m over completely new areas. In general, the accuracy over stable coastline areas was higher compared to accuracies for glacier fronts. Accuracies calculated with the A/F method were higher with deviations of less than 2 pixels (78 m) for areas included during training and 2.69 pixels (108 m) for test areas.

Table 5.5: Distance measured errors (in meters) along transects for frontal and stable coastline sections as well as the entire study region. An estimate for the difference between two manually delineated coastlines is given with the ADD (Antarctic Digital Database) coastline (mean error). A/F is the averaged width of the enclosed area between the automated and manual delineated coastline for each study region.

		Training Sites				Test Sites					
	measured coastline	Sulzberger	Victoria Land	Wilkes Land	Shackleton	Marie Byrd Land	Oats Land	Ekstromisen	Wordie	**mean train**	**mean test**
mean	complete	267	112	153	72	118	162	126	210	**151**	**154**
	front	421	174	208	80	171	119	172	338	221	200
	stable	46	68	127	49	53	70	62	235	73	105
median	complete	8	-31	-13	-27	-7	4	-8	3	-16	-2
	front	20	-56	19	-32	-9	1	6	2	-12	0
	stable	-2	-25	-61	-22	-4	5	-12	15	-28	1
ADD	complete	1539	-	-	-	416	-	-	-	-	-
	front	3098	-	-	-	313	-	-	-	-	-
	stable	**180**	-	-	-	**186**	-	-	-	-	-
A/F	complete	**121**	103	**35**	54	108	104	**66**	**153**	**78**	**108**

The following accuracy results are presented based on the A/F method to be comparable to other calving front extraction publications (Zhang *et al.* 2019b, Krieger & Floricioiu 2017). The coastline of Wilkes Land and Shackleton Ice Shelf were extracted most accurately with a mean deviation of 35 m and 54 m, respectively. High accuracy was also obtained for Ekstromisen Ice Shelf with 66 m. For Victoria Land, all glacier tongues were accurately extracted with a mean deviation of 103 m. Deviations of 2-3 pixels occurred at Oats Land, Victoria Land, Marie Byrd Land, and Sulzberger Ice Shelf with 103 m, 104 m, 108 m, and 121 m, respectively. Lowest accuracies occurred for the coastline along Wordie Ice Shelf with 153 m due to mélange in the Wordie Bay.

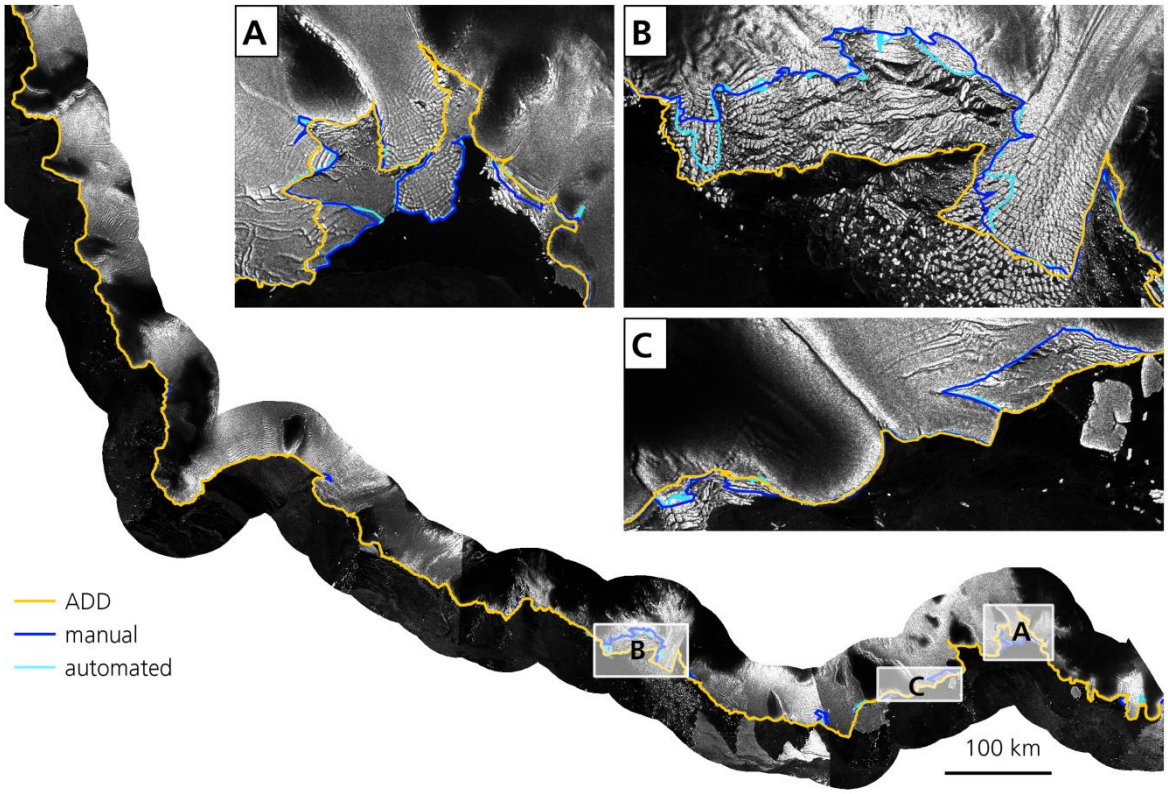

Figure 5.22: Comparison of the ADD coastline (orange) with the manual expert delineation (blue) and the automatically extracted one (turquoise). The ADD coastline includes fast ice areas over Swinburne Ice Shelf (A), at Land Glacier (B), and Sulzberger Ice Shelf (C). Background: Sentinel-1 Copernicus data 2018.

To draw a comparison between the automated derived results and an independent coastline, deviations were also calculated relative to the ADD coastline. This approach also provided the opportunity to assess deviations between two manual delineated coastlines. The ADD coastline of Marie Byrd Land was manually delineated by the ADD community based on the same Sentinel-1 scenes used for extracting the coastline for Marie Byrd Land in June. The second manual coastline was manually delineated with the approach described in Section 5.2.3. The deviations of both manual coastlines were higher than the differences between manual and automatic extracted coastlines. The reason is visible in Figure 5.22.

The ADD coastline mistakenly included calved glacier ice (Figure 5.22b) and fast ice (Figure 5.22c) but excluded parts of the glacier not yet calved (Figure 5.22a). This emphasizes the subjectivity of manual calving front extractions and the required expertise for glacier and ice shelf front delineations. The coastline products from Liu and Jezek (2004a) and Scambos et al. (Scambos *et al.* 2007) were closer to the automatic extracted and manual expert coastline than to the ADD coastline. Therefore, it was concluded that the ADD coastline was not a suitable accuracy measure in calving front areas and the calculated values (3098 m) clearly overestimate the real distance deviation for manual delineations. Instead, measured over stable coastline areas where delineation is far less subjective the fronts deviated 180 m and 186 m for Sulzberger Ice Shelf and Marie Byrd Land, respectively. Those values were more realistic estimates for deviations between manual delineations. Other studies published values between 38 m and 92.5 m for deviations in manual delineations (Mohajerani *et al.* 2019, Zhang *et al.* 2019b).

5.6 Implementation of *Antarctic*LINES for Circum-Antarctic Processing

This final subchapter on methodology explains the final automated implementation of the novel methodical framework for automatic calving front extraction at the DLR computing infrastructure. This allowed data processing for large-scale applications. Finally, the implementation was tested by extracting the entire Antarctic coastline for 2018.

5.6.1 General Implementation of AntarcticLINES

Figure 5.23 visualizes the implementation of *Antarctic*LINES and how it was used to extract Antarctic calving fronts from Sentinel-1 scenes. The implementation was designed for large data amounts either for dense calving front time series or large-scale applications.

The workflow can be described as following: First, a polygon over the area of interest (AOI) was created and stored in the WTK (Well Known Text) format. To acquire Sentinel-1 scenes different approaches existed depending on the amount of needed data. For quick data access, the ASF (Alaska Satellite Facility) portal was used for acquiring Sentinel-1 data. The ASF portal allowed to manually filter Sentinel-1 data by temporal and spatial coverage as well as product specifications. The final selection of scenes could be automatically downloaded via a provided python script. For bigger data amounts the internal data access (IDA) of DLR was used. Large amounts of data could be ordered over the area of interest for a selected time frame.

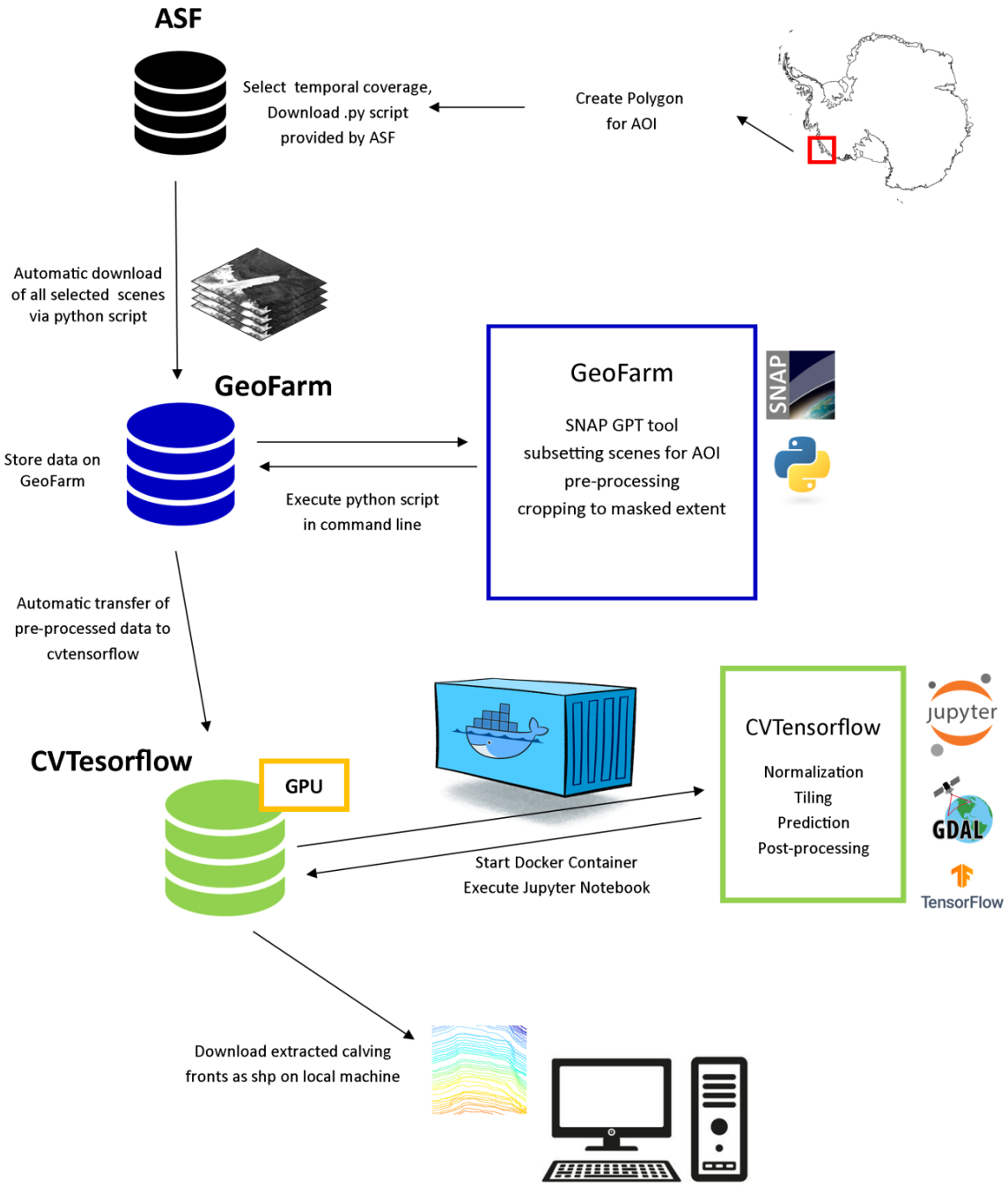

Figure 5.23: Implementation of AntarcticLINES. A methodical framework for automatic calving front extraction. Copyright for icons belongs to corresponding companies. ASF: Alaska Satellite Facility, SNAP: Sentinel Application Platform, GPT: Graph Processing Tool, AOI: Area of interest, shp: Shapefile.

The data was provided via an FTP server. Independently from the used data provider, the Sentinel-1 scenes were transferred to the processing infrastructure GeoFarm. At the virtual machine a single python command needed to be executed to trigger the sub-setting, pre-processing, and cropping of all Sentinel-1 scenes via GPT (Graph Processing Tool). GPT is a build-in function of the SNAP (Sentinel Application Platform) software provided by ESA which can directly be executed in the terminal for automated Sentinel-1 processing. In case an AOI was provided, automated sub-setting for the requested area was performed

before pre-processing. If the AOI was missing, the entire scene was processed which required higher computational costs. Afterwards, the no data area around the pre-processed Sentinel-1 scenes was cropped to minimize the data volume. The cropped scenes were automatically transferred to the GPU server CVTensorflow. This GPU cluster was optimized for deep learning applications with four GPUs. At CVTensorflow a docker container had to be created from an already created docker image. This enabled the use of a Jupyter Notebook with GPU processing. Before the code of the provided Jupyter Notebook was executed, the user was able to set user-specific preferences (path, overlap, etc.). The written code automatically normalized and tiled all pre-processed Sentinel-1 scenes before feeding them to the stored weights of the trained U-Net. Each image tile was segmented into land ice and ocean (see section 5.3.3). The subsequent post-processing re-assembled all tiles to a complete mosaic from which the coastline shapefile was extracted. Several output shapefiles were generated for various application requirements. First of all, the extracted coastline for each scene was provided. In case the AOI was covered by several scene extents, the average monthly extracted coastline could be derived. The more predictions were merged to one mosaic the higher was the final accuracy of the extracted front. Therefore, also the coastline for each season or the (semi) annual coastline was provided for download.

5.6.2 Circum-Antarctic Coastline Extraction

The above explained implementation was used to extract the Antarctic coastline for 2018. The first step for deriving the entire coastline was to split the area of interest to acquire Sentinel-1 data. In the case of deriving the entire Antarctic coastline smaller subsets had to be created. The Antarctic coastline was split into 18 zones (see Figure 5.24) based on ice sheet basin boundaries defined by Rignot et al. (2011). For each zone, Sentinel-1 scenes were selected during winter for the months of June, July, and August to avoid any melt events. In the best case, every zone was completely covered three times by dual-polarized satellite scenes. However, for zones 1,2 and 17 along the Bellingshausen Sea mostly single-polarized imagery existed and along Enderby Land (zone 11) scene availability was very limited sometimes only allowing single scene coverage. In total, 158 dual-pol and 17 single-pol scenes were used. The amounts of used scenes as well as zone boundaries are visualized in Figure 5.24.

For each zone, a polygon was created and stored in WTK (Well Known Text) format. For each zone, the coastline was extracted as described in the section above. To ensure the most reliable results for the entire Antarctic coastline, the mean of the classification probabilities for all three months was taken to extract the mean coastline during winter 2018. In zones with multiple scene coverage, more accurate results were derived as in overlapping areas prediction probabilities from several scenes went into the final extracted coastline. The

small gaps in the coastline between each zone had to be closed manually as line connecting algorithms did not work properly with the Polar Stereographic Projection. This resulted in the final coastline of Antarctica for winter 2018 which is presented in the following subchapter.

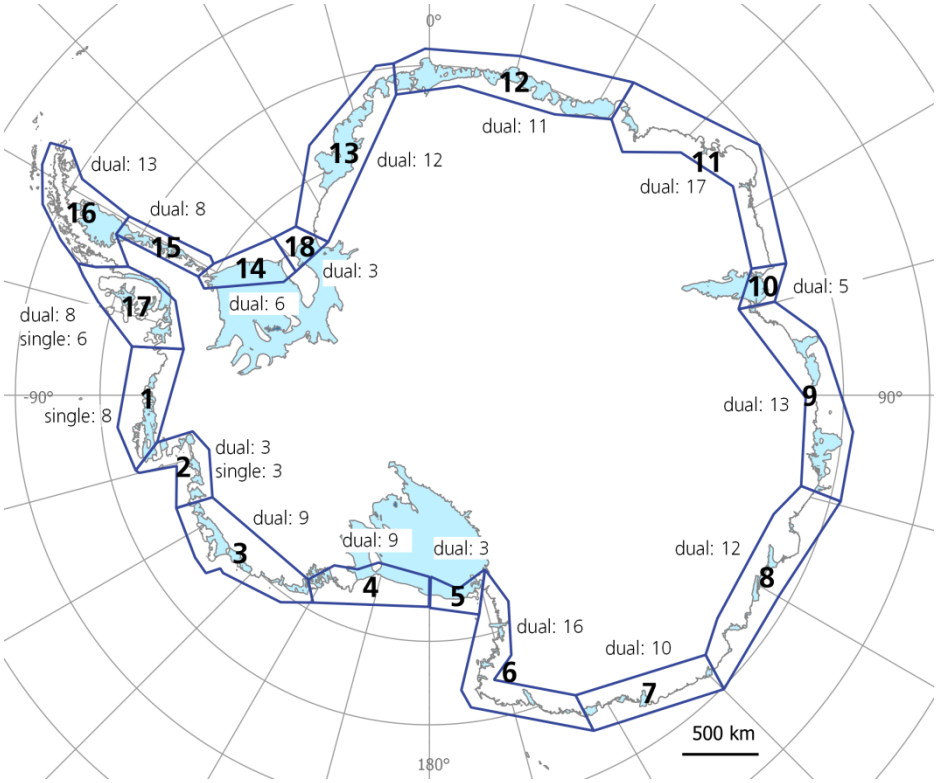

Figure 5.24: Antarctic coastline split into 18 zones. The amount and polarization of available Sentinel-1 scenes are indicated.

5.6.3 The Extracted Coastline 2018

Figure 5.25 shows the automatic extracted coastline 2018 in black. To get an impression of the accuracy of the extracted coastline, a manual corrected version of the automatically extracted coastline is also displayed in orange. Both coastlines overlap in most regions with minor deviations. The only obvious difference in the overview of Antarctica (see Figure 5.25, middle) is the island in front of Wilkins Ice Shelf. It was formerly connected to the Antarctic continent but the ice bridge of the ice shelf disintegrated. Hence, the island was correctly removed during post-processing. But it was included in the manual corrected version for later comparisons with other coastline products created before the disintegration of Wilkins Ice Shelf in 2008.

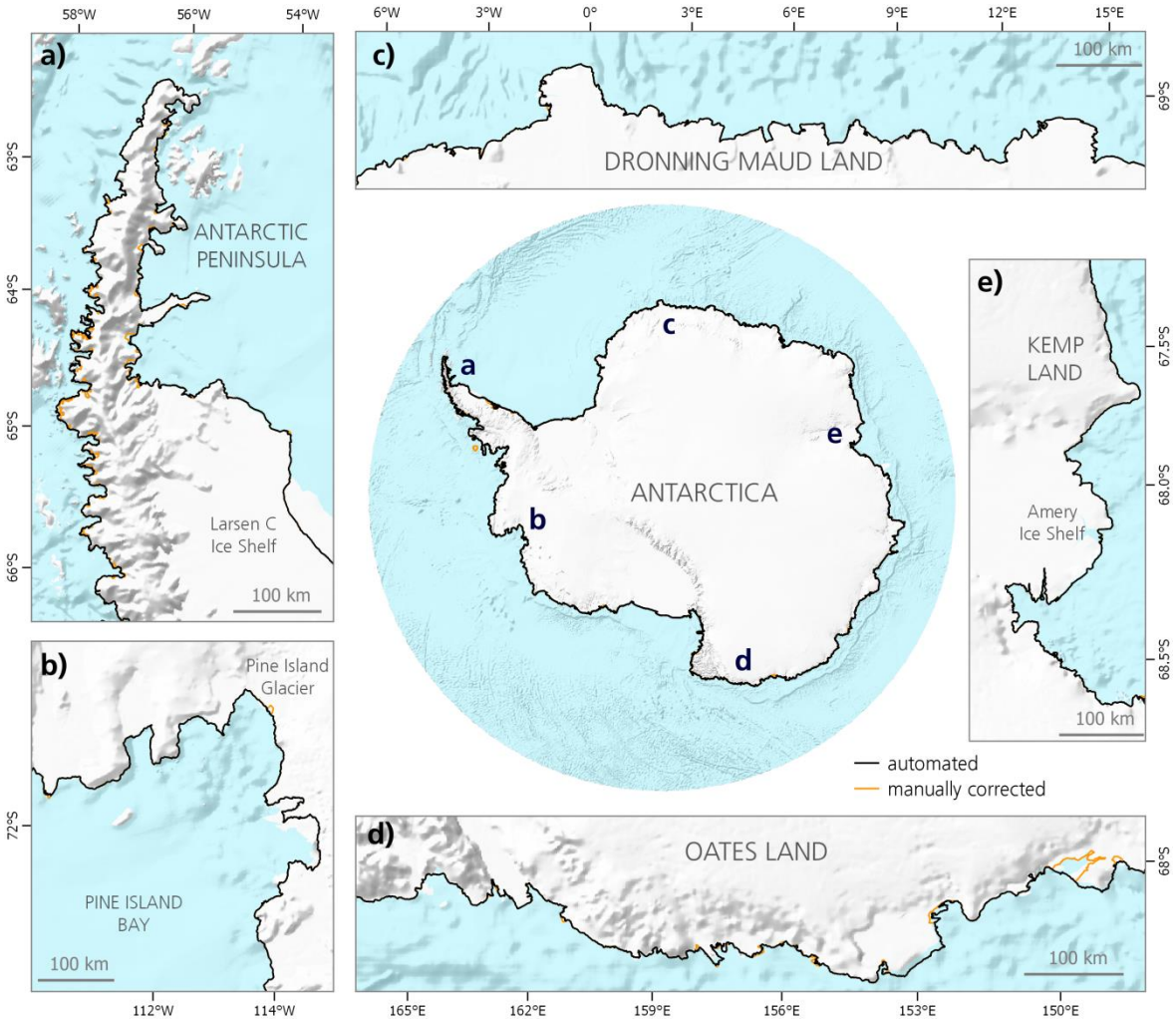

Figure 5.25: Automatically extracted coastline (black) in winter 2018 underlaid by the manually corrected coastline (orange). Enlarged views of the Antarctic Peninsula (a), Pine Island Bay (b), Dronning Maud Land (c), Oates Land (d), Kemp Land, and Amery Ice Shelf (e). Background: Hillshade of the Antarctic continent from ADD.

The enlarged views along the coastline emphasize the almost perfect overlap of the automatic and manual coastlines with slight deviations in Figure 5.25. Best results were obtained along Dronning Maud Land and Victoria Land. Most difficulties occurred along the steep coast of the Western Antarctic Peninsula. Additionally, fast ice areas at Shirase Glacier, Glenzer Glacier, and Larsen D made the coastline extraction more challenging. Areas with large ice shelves such as Shackleton, Dronning Maud Land and Getz Ice Shelf were perfectly delineated. Accurate results in coastal sectors with steep but straight coastlines (e.g. along Adélie, Kemp, and Enderby Land) were created. Floating glacier tongues frequently found along Victoria Land were extracted without any deviations.

Because a detailed representation of the entire Antarctic coastline in one Figure is difficult, a few representative subsets of the Antarctic coastline 2018 are presented in Figure 5.26. Figure 5.26 gives an impression of different coastline morphologies of Antarctica with the corresponding extracted and manually delineated coastlines

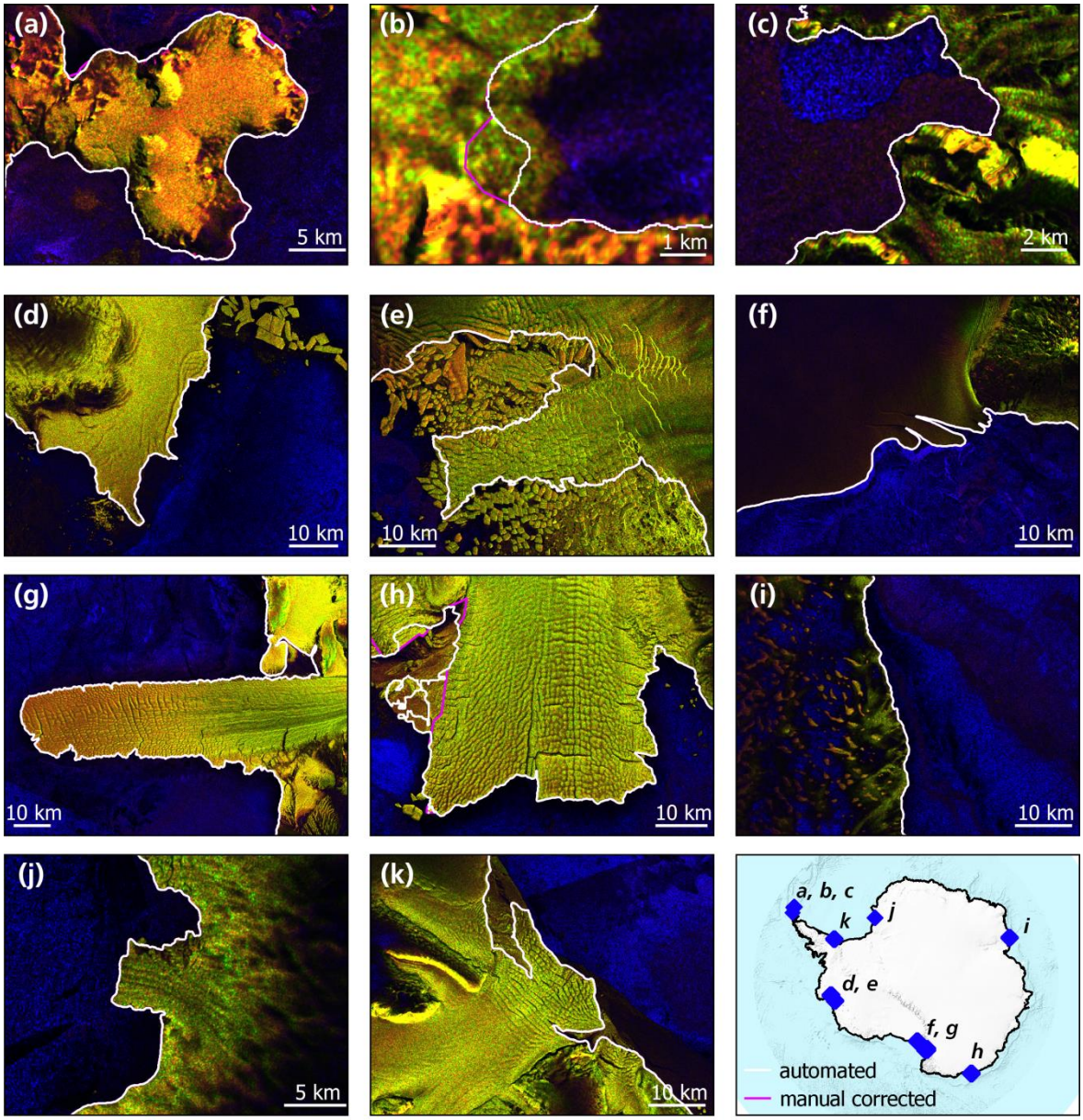

Figure 5.26: Exemplary displays of the extracted coastline 2018 for the Antarctic Peninsula (a-c), Pine Island Bay (d,e), Ross Ice Shelf (f), David Glacier (g), Mertz Glacier (h), Kemp Land (i), Hayes Glacier (j) and a part of Larsen D (k). Sentinel-1 Copernicus Data 2020.

The northern top of the Antarctic Peninsula was extracted accurately (Figure 5.26a) only smaller glaciers with mélange at the front complicated the coastline extraction. At the western part of the Peninsula (Figure 5.26c) steep slopes, small glaciers in deep valleys and rocky islands along the coast did not always allow accurate results. For Pine Island Bay, even for the very rugged Thwaites Glacier, the calving front was delineated correctly (Figure 5.26d and e). The contrast between ocean and ice sheet sometimes was really low due to thick and dry snow cover reducing the backscatter intensity. Still the results for Ross Ice Shelf and the coastline of Kemp Land were flawless (Figure 5.26f, i). Glacier tongues were mapped in every detail (Figure 5.26 g, j) and only fast ice areas could decrease the

accuracy as seen for Mertz Glacier (Figure 5.26h). In contrast, the southern Larsen D Ice Shelf was delineated exactly even though enclosed by fast ice (Figure 5.26k).

5.7 Discussion

The novel framework *Antarctic*LINES for glacier and ice shelf front extraction was developed by taking advantage of current improvements in computer vision as well as the all-day and all-weather imaging capability of Sentinel-1 data. The presented framework provides four major advantages compared to previously published approaches. First, calving front extraction was automatized by implementing the CNN U-Net which not only segments images based on pixel values but also considers the spatial context. Second, the workflow can be applied to any Sentinel-1 scene over the Antarctic coastline and is transferable in space and time. Third, for Antarctic glaciers and ice shelves calving front time series can be generated automatically. And last but not least, the large-scale applicability was proven by extracting the coastline for 2018. For the very first time, this development allows to assess glacier and ice shelf front dynamics on a continent-wide scale and to close gaps in calving front mapping previously identified by Baumhoer et al. (2018).

5.7.1 Performance

The presented methodology was tested for new satellite scenes over regions included during training and completely new test sites. One would have expected that calving front extraction results would have been better over areas included during training as the U-Net would have learned the specific shapes. But classification accuracies for training and test sites were almost similar. Measured with the transects method, the coastline deviated 151 m for training and 154 m for test areas. Calculated with the A/F method the difference is slightly higher with 78 m for training and 108 m for testing areas. For testing and training regions better results (e.g. Shackleton, Ekstromisen) and worse results (e.g. Sulzberger, Wordie) were obtained. This leads to the conclusion that the developed approach is very well spatially transferable and inaccuracies generally exist over more challenging regions as it is also the case for manual delineations (e.g. ADD coastline vs. MODIS and Radarsat). Challenging regions included fast ice areas, mélange, surface melt, and steep topography causing radar shadow. In contrast, for testing areas such as Ekstromisen, northern Marie Byrd Land, and Oats Land accurate results were obtained. In those regions calving fronts were clearly defined and only shape, size, and topography of the areas varied compared to areas used for training.

When speaking about the accuracy, it is important to mention that the method of accuracy measurement strongly influenced the calculated accuracy. This study presented for the first time three different approaches to measure calving front extraction accuracy and clearly highlights the differences in calculation. This can be best illustrated in

accuracies calculated for Wilkes Land. Measurements based on transects yielded a high deviation with 153 m. On the contrary, the deviations based on the A/F method was 35 m. This was only one-fourth of the originally calculated transect based deviation. Further, depending on using the median or mean of transects to estimate the deviation differences existed. Especially, when using the median the deviations were less than -31 to 8 m. Calculating the median for entire coastal sections might not be applicable as too many variations exist and outliers would not be considered. But for studies on single glacier fronts, the median can give a more accurate measure of calving front change averaged over the front.

Compared to existing studies, the here presented framework increased classification accuracies from 92.4% for training and 93.6% for validation (Mohajerani *et al.* 2019) to 98.1% and 98.2% respectively. Additionally, the number of input scenes could be reduced from 123 (Mohajerani *et al.* 2019) and 75 (Zhang *et al.* 2019b) images to only 38 by using different polarizations, bigger training areas and the higher proportional selection of input tiles covering frontal areas. The deviation distance to manual front delineations was comparable with previous studies using the A/F method. On average, deviations with 1.96 px (78 m) for training and 2.69 px (108 m) for testing areas were achieved. This is close to the results of Mohajerani et al. (2019) over Helheim glacier with 1.97 px (96.3 m). Zhang et al. (2019b) achieved comparable results with 104 m considered distance wise. In pixels, the deviation was much higher with 17.3 pixels. This clearly highlights that the usage of high resolution imagery does not improve the overall accuracy as a higher resolution lowers the spatial context within one tile. In comparison, Krieger et al. (2017) achieved slightly higher deviations with 159 m and 246 m compared to an expert delineated coastline. Partly this can be explained by the very difficult mélange conditions in their Greenlandic study area.

Overall, deviations between manual delineations range from 38 m (Zhang *et al.* 2019b) to 92.5 m (Mohajerani *et al.* 2019) and in Antarctica even up to 183 m (measured for entire Marie Byrd Land with the ADD coastline). In sum, the here developed novel automated approach extracted calving fronts within the typical variations of calving front delineation and provided a valuable tool to speed up glacier and ice shelf front delineation.

5.7.2 Intra-Annual Calving Front Fluctuations

Intra-annual patterns of glacier and ice shelf front fluctuations were presented for four glaciers and ice shelves with very different CFL changing patterns. The applied method for calving front time series generation proved to be a quick and effortless approach to generate dense monthly time series with around 50 valid measurements for each glacier or ice shelf. In general, Sentinel-1 scenes during the melt season between December and February could only sporadically be used depending on the area of interest and surface melt

intensity of the respective year. Backscatter over water is very low in radar imagery whereby the ocean and melting ice surface appear black not allowing any contrast between ice shelves and ocean. For approximately 14 % of the automatically extracted fronts, minor manual corrections were made to densify the calving front time series. Those front extractions could also have been excluded by the outlier detection (see Section 5.4.3) but would have minimized data availability which is crucial when observing calving events. Nevertheless, using only the valid automatically derived fronts would have provided sufficient data for calculating average rates of calving front change but not during the calving event.

Intra-annual measurements of Antarctic calving front fluctuations revealed that none of the investigated glaciers or ice shelves experienced annual recurring seasonal changes in calving front position as known for Greenlandic glaciers with retreat during summer and advance in winter (Moon *et al.* 2015, Schild & Hamilton 2013). But events reoccurring biennially were observed. Denman Glacier stopped to advance in December 2016 and 2018, both times at the beginning of the summer seasons with extreme surface melt. For the melt seasons 2017 and 2019 exceptional more melt was detected on Amery Ice Shelf (Dirscherl *et al.* 2020) also located close at the EAIS. Further investigations on surface melt on Denman Glacier should be undertaken and also long-term time series could help to explain whether slowdown events in the advance rate occur more often. In particular with respect to recently detected velocity increases, grounding line retreat of 5.4±0.3 km (1996-2017/18) (Brancato *et al.* 2020) and a retrograde bed potentially further destabilizing the glacier. For Amery Ice Shelf such events of no-advance occurred in late summer or early autumn in 2016, 2017, and 2019. In the radar imagery, clear melt was apparent in those scenes. The edge of the calving front appeared darker through melt and was mapped probably slightly more inwards. Hence, no advance was measured. The connection to melt is further strengthened as 2018 was a year of little melt at Amery Ice Shelf (Dirscherl *et al.* 2020) not causing the previously described effect. Even though no seasonality in the frontal movement of Amery Ice Shelf was noticed, seasonality in the rift propagation was detected by Walker et al. (2015). During summer rifts propagated strongly whereas during winter no rift propagation existed between 2002 and 2014. This raises the question of why this pattern is not visible in calving front change. Either the rift propagation pattern existed only until 2014 or the faster frontal advance could not be measured due to melt on the ice shelf. Besides, the calving of Amery Ice Shelf was predicted to occur in the mid-2020s or later. Hence, the calving event followed the natural calving cycle (65-70 years) of the Amery Ice Shelf and is probably not caused by climate change (Fricker *et al.* 2002).

Calving events at Glenzer Glacier occurred after mid-autumn in April but of very different magnitudes. The magnitude of melt intensity would be an interesting factor compared to calving amount or whether other factors influenced the calving. One possible

explanation could be higher ice flow velocities during summer (Ai *et al.* 2019, Liang *et al.* 2019) intensifying the stresses of the glacier pressing against the island. The widening crevasse clearly indicated increasing stresses. Further strong surface melt events could cause the complete disintegration of Glenzer Glacier as only a narrow ice bridge connects the opposite island which functions as a pinning point. Additionally, Glenzer already lost a tremendous amount of its floating tongue as can be seen from earlier coastlines from Radarsat and MODIS (Liu & Jezek 2004a, Scambos *et al.* 2007).

Pine Island Glacier attracted attention by its frequent calving events. Those calving events do not follow a seasonal pattern and occur every 1-2 years. Also, the duration between rift propagation and actual calving ranges broadly between 2 to 12 months. This emphasizes the very dynamic nature of Pine Island Glacier. The calving frequency between 1990 and 2011 was approximately 5-7 years (MacGregor *et al.* 2012) but now increased to annual or biennial. Increased calving frequency is consistent with recent changes happening at Pine Island Glacier. At least since 1992, Pine Island Glacier thinned (Dutrieux *et al.* 2013) and meltwater production increased by 50 % since 1994 (Jacobs *et al.* 2011). Also grounding line retreat is apparent which was most severe between 1994 and 2011 with 1.2 km of retreat (Milillo *et al.* 2017). Pine Island Glacier is causing a recent global sea-level rise contribution of ~ 5-10 % (Bingham *et al.* 2017). The Glacier accelerated 55 % between 2000 and 2010 with a short decrease between 2010-2013 before accelerating again in 2015 (Christianson *et al.* 2016, Han *et al.* 2016). Unfortunately, no surface velocity measurements exist for recent years which would have allowed a more concise interpretation of ice velocity changes in comparison to calving front retreat and whether increases in velocity caused calving or calving caused higher ice flow velocities.

5.7.3 Fully-Automated Calving Front Time Series

A 15-month calving front time series for Getz Ice Shelf was fully automatically extracted based on Sentinel-1 dual-pol imagery. On average, the automatically extracted fronts deviated 75±181 m. This mean deviation of about 2 pixels demonstrated the transferability in space and time of the developed method. The fronts of Getz Ice Shelf were accurately extracted in 7 of 9 cases. For two fronts additional challenges were faced that are discussed in the following. The high standard deviation of the mean error with 181 m can mostly be attributed to the wrongly delineated front at Getz 1. Probable causes for the miss-delineation might be radar shadow as the wrongly delineated part of Getz lies behind Wright Island and appears much darker than the correctly delineated part. As only a part of the front was wrongly delineated the outlier detection did not detect the erroneous fronts. Radar shadow also occurred at Siple Dome causing similar difficulties in case mélange was present at the glacier fronts. But in this case, the wrong front extraction was removed by the outlier detection as seen for the time series of Vorneberger/Hulbe. For

future improvements, a more robust outlier detection should be implemented to make a visual inspection of the extracted fronts unnecessary.

Very accurate delineations could be obtained for DeViqc Glacier where even small fontal changes of 1 pixel were extracted correctly. This would have been very difficult by manual delineations as inaccuracies in manual delineations are often higher than 40 m. Also, calving events of smaller size at Beakley Glacier were mapped in detail. Overall, the developed workflow allows the generation of calving front time series with smaller errors which can be spotted visually immediately. This automatization technique allows faster and very accurate extractions which would have been an endless manual task if at all possible at pixel level.

For Getz Ice Shelf all fronts showed advancing tendencies except Beakley Glacier which retreated. This is in some cases contrasting to previous observations. But it should also be mentioned that a 15-month time series is rather short to access calving front change. "The Getz Ice Shelf was described as a pretty stable ice shelf with phases of slight retreat and advance (Ferrigno *et al.* 2004). DeVicq Glacier is one of the fast-flowing glaciers along with Marie Byrd Land (Rosanova *et al.* 1998). Between 1973 and 1988, the glacier retreated 5 km (Rosanova *et al.* 1998), and 18.6 km between 1973 and 1997 (Ferrigno *et al.* 2004). Compared to available coastline products, the retreat from the maximum extent in 1973 decreased slightly in the 1980s and further until 1997. Since then, a phase of advance started until our last measurement in July 2018, when the maximum extent of 1973 was almost reached" (Baumhoer *et al.* 2019). Assuming the current speed of 726 ± 40 m/yr at DeVicq Glacier would continue, the maximum extent observed in the 1970s is reached in 2020. The front of Getz 2 is 2 km further land inwards compared to the maximum extent in the 70s. This is about the extent that was once reached in the 80s based on the USGS coastal change maps. The front of Getz 3 experienced retreat between the 70s until 2014. Since then, the front advanced. Even though changes in front position existed over the past years the fluctuations of the Getz fronts were little indicating a relatively stable ice shelf. Drivers of calving front change in the area of Getz Ice Shelf may have several origins. Very changeable ocean conditions and changes in sea ice conditions might belong to them (Jacobs *et al.* 2013, Miles *et al.* 2016).

5.7.4 Large-Scale Applicability

The performance of the framework *Antarctic*LINES was tested for large-scale applications by extracting the entire Antarctic coastline for winter 2018. The automatically extracted result compared to a manual corrected version illustrated the spatial transferability of *Antarctic*LINES and the applicability for circum-Antarctic applications. The implementation of *Antarctic*LINES in the processing infrastructure for automatic processing made the handling of large data volumes possible. The here presented

automatization of calving front extraction only required little manual work which will allow to extract the Antarctic coastline for additional seasons and years.

Still, in some areas, the accuracy of the coastline is not yet sufficient. An example was the Western Antarctic Peninsula where islands and steep valleys made the extraction more challenging. The model is not yet trained sufficiently for steep valleys and smaller outlet glaciers existing at the Antarctic Peninsula. In future applications further training areas should be included to improve the performance over the Antarctic Peninsula. Additional challenges were found in areas with fast ice with often similar backscatter characteristics as the enclosed glacier ice. Even manual delineations struggle to correctly delineate fast ice regions as has been seen for errors in the ADD coastline and the MODIS coastline products. But also examples to prove the opposite exists. Fast ice areas at the southern Larsen D Ice Shelf were correctly delineated as well as glaciers and ice shelves in Shirase Bay. Particularly accurate extracted was the calving front of Thwaites Glacier which is surrounded by icebergs and mélange. This proves the capability of the model to differentiate between shapes of a glacier compared to icebergs as both have the same backscatter characteristics but different morphologies. To further advance the performance for large-scale applications in the future, training areas over the Antarctic Peninsula should be added. The remaining manual efforts could be further reduced by implementing an algorithm for merging coastlines sections of the different coastal zones and to further automatize the selection of suitable Sentinel-1 scenes via ASF or IDA.

5.8 Summary

This chapter introduced a novel framework for automatic glacier and ice shelf front extraction. The approach intended to use improvements in computer vision to solve the challenging task of calving front extraction. Core of the presented method was the usage of a modified U-Net able to segment imagery based on pixel values and spatial context. The implementation of the complete workflow of *Antarctic*LINES was designed to be spatially and temporally transferable. By using free and open-source software and data as well as a Docker-based approach, the framework is easy to be implemented in other infrastructures. With *Antarctic*LINES a complete workflow from Sentinel-1 data download over pre-processing, segmentation, post-processing and the final retrieval of the extracted coastline was created. This allows for big data processing, and large-scale applications.

The presented results achieved similar or even better accuracies compared to errors in manually delineated coastlines. The average deviation was 78 m and 108 m for training and test areas, respectively. Best results were achieved for ice shelves with distinct fronts (e.g. Shackleton, Ekstromisen). Accuracies decreased slightly in areas with fast ice, mélange, and steep terrain (e.g. Wordie, Sulzberger). The presented workflow allowed fast

processing of monthly glacier and ice shelf front fluctuation time series which can be used for investigating CFL changes patterns, comparing them between different glaciers and interpreting glacier and calving dynamics. The time series generation was limited by melt during the summer months. Slight manual post-correction allowed densifying the automatically extracted time series by a few additional front positions. The presented workflow allowed for the first time to investigate almost monthly change patterns of four calving fronts with over 50 measurements for each investigated ice shelf. The fully automatically extracted calving front time series for the Getz Ice Shelf demonstrated the application possibilities without manual intervention. Nevertheless, automatic outlier detection could be improved to achieve even better results. Between May 2017 and July 2018, the Getz Ice Shelf experienced a phase of advance with DeVicq Glacier being the strongest advancing glacier with 726±20 m/yr.

In addition, this chapter demonstrated the spatial transferability and large-scale applicability of *Antarctic*LINES. The developed framework is an important contribution to the current Antarctic coastal change assessment. The coastline for 175 Sentinel-1 scenes was automatically extracted. Smaller manual corrections were necessary over fast ice areas and along the Western Antarctic Peninsula. For the remaining zones, accurate calving front positions were extracted not requiring any additional manual work. *Antarctic*LINES enables future monitoring of the Antarctic coastline with little effort.

In the future, this implementation for calving front extraction will contribute to circum-Antarctic glacier and ice shelf front monitoring due to its great spatial and temporal transferability. Further developments by integrating additional training areas and improving the outlier detection will even further improve the presented framework. For the first time, the implementation of *Antarctic*LINES enables frequent monitoring of intra-annual calving front fluctuations and calving events as well as the observation of the current state of the Antarctic coastline. Hence, this novel approach will help to bridge major gaps in the knowledge of current circum-Antarctic calving front dynamics which will reduce the inaccuracies in sea-level rise projections

Chapter 6

6 Environmental Drivers of Calving Front Change*

Glaciers and ice shelves are sensitive indicators of changing environmental conditions because they are in direct interaction with atmosphere and ocean (Vaughan & Doake 1996, Wouters *et al.* 2015). Nevertheless, ice shelf and glacier retreat can either be part of the natural cycle of glacier growth and decay (De Rydt *et al.* 2019, Hogg & Gudmundsson 2017) or the result of external environmental and mechanical forcing (Cook *et al.* 2005, Cook *et al.* 2016, Dutrieux *et al.* 2014, Thoma *et al.* 2008, Walker *et al.* 2013). Consequently, identifying the share of environmental driving forces of glacier and ice shelf retreat is challenging and has been subject to many discussions. Potential environmental driving forces range from rising air temperatures (Cook *et al.* 2005, Mercer 1978), ocean forcing (Cook *et al.* 2016, Wouters *et al.* 2015), decreases in sea ice cover (Miles *et al.* 2016) to surface melt and lake ponding (Scambos *et al.* 2000). This chapter explores circum-Antarctic changes in glacier and ice shelf extent in relation to changes in environmental conditions over two decades. Calving front change is assessed in decadal time steps (1997, 2009, and 2018) to reduce the effect of short-term glacier fluctuations. In addition to climate data, changes in Antarctic environmental conditions are assessed. The processed climate variables include air temperature, sea surface temperature, wind direction, snowmelt, and sea ice days. In combination, the data sets will help to identify environmental drivers of glacier and ice shelf front changes.

* Parts of this chapter are based on Baumhoer, C., Dietz, A., Kneisel, C., Paeth, H., and Kuenzer, C. (2021): Environmental drivers of circum-Antarctic glacier and ice shelf front retreat over the last two decades, The Cryosphere, 15, 2357–2381

6.1 Data Sets

In the following, all data sets used for the assessment of driving forces on calving front change are introduced. First, the assessment of circum-Antarctic coastal change is explained. Second, the processing of climate variables from ERA5 and remote sensing data is explained.

6.1.1 Coastlines

Decadal variations of glacier and ice shelf front change were assessed by comparing Antarctic coastline products. The earliest complete coastline product of Antarctica dates back to 1997 which was created by Liu and Jezek (2004a). Based on a Radarsat-1 Antarctic mosaic the authors created an automated approach to extract the Antarctic coastline from radar imagery by adaptive thresholding. Final manual correction of the extracted coastline created a very accurate result. The coastline was extracted from Radarsat imagery acquired between September and October 1997 with a spatial resolution of 25 m. The data set is freely available and can be downloaded from the National Snow and Ice Data Center (NSIDC) (1997). In approximate range for a decadal analysis, the MODIS coastline product from 2009 was selected. It was generated from MODIS optical satellite imagery in austral summer 2008/2009 (November to February). The spatial resolution is coarser with 125 m and inaccuracies exist over multi-year sea ice with snow cover (Scambos *et al.* 2007). The data set can be accessed at the NSIDC (2009). For the last approximate decadal step, the automatically extracted Antarctic coastline for 2018 was used. The coastline of 2018 was created with the novel developed framework *Antarctic*LINES as described in Section 5.6.

6.1.2 ERA5

For this study ERA5 data for Antarctic air temperature, zonal wind speed, and snowmelt was used. ERA5 is the state-of-the-art climate reanalysis product by the European Centre for Medium-Range Weather Forecasts (ECMWF) replacing the former ERA-Interim product. Several studies documented that the ERA5 product outperforms the former ERA-Interim product with regard to accuracy and resolution (Gossart *et al.* 2019, Tetzner *et al.* 2019). ERA5 provides hourly or monthly averaged estimates of atmospheric, land, and oceanic climate variables. For this study, ERA5-Land data were used which come at a 9 km spatial resolution and are available since 1981/82. This reanalysis product was chosen over in-situ measurements as ground truth observations over the Antarctic continent are too scarce for a circum-Antarctic and long-term analysis of environmental change. Even though ERA5 only provides estimated values of climate variables, the accuracy compared to in-situ observations is sufficient for large-scale analysis. ERA5 surface air temperature data (2 m temperature product) capture the annual variability and magnitude of temperature change over the Antarctic Ice Sheet (Gossart *et al.* 2019, Tetzner *et al.* 2019). On average

the mean absolute error is 2.0°C whereas temperature estimates along the Antarctic coastline are more accurate compared to estimates over the interior of the ice sheet (Gossart *et al.* 2019). Noticeably higher accuracies are reported by a study of Tetzner et al. (2019) with a mean error of -0.13° for the Antarctic Peninsula. For this study, temperature data along the coastline were used which allows the assumption that the accuracies of Tetzner et al. (2019) are more realistic. The variability of temperature change over Antarctica is captured accurately by ERA5 data. The Pearson correlation coefficient between in-situ observations and ERA5 data is better than 0.98 (Gossart *et al.* 2019, Tetzner *et al.* 2019). To assess not only changes in annual temperature changes, the data set was split into the warmer half of the year ("summer") from October to March and the cooler half ("winter) from April to September. This allowed analysing environmental forcing during different seasons.

ERA5-Land data provide modelled estimates on snowmelt at a spatial resolution of 9 km. ERA5 snowmelt data were processed for the austral summer months (December to February) to assess the magnitude of melt. Snowmelt data should be handled with care as no validation to ground truth measurements is provided by ECMWF. Only accuracies for ERA5 surface mass balance (SMB) data are available by Gossart et al. (2019). Data on SMB include snowmelt data but also other variables. Gossart et al. (2019) notice a small bias to in-situ measurements as ERA5 data slightly underestimate surface mass balance. The amount of snowmelt is provided in mm water equivalent per day (w. eq. per day).

ERA5 zonal wind speed data were taken as a proxy for CDW upwelling. Changes in wind direction from easterlies to westerlies at the Antarctic coastline cause upwelling of warm CDW (Hazel & Stewart 2019). For zonal wind (West to East) speed estimations, ERA5 monthly averaged data on single levels with an approximate spatial resolution of 31 km were used. The zonal wind speed is modelled 10 m above the surface. The study of Gossart et al. (2019) compared weather station wind speed measurements to the modelled near-surface wind speed of ERA5. They found that ERA5 data captured the spatial variability of near-surface winds well but strong and coastal winds were underestimated. The mean absolute error of ERA5 wind speed is 2.8 m/s with high variance in space and time but the annual variability is accurately represented (Gossart *et al.* 2019). Compared to ASCAT (Advanced Scatterometer) observations over the ocean, ERA5 mean zonal wind speed underestimates the actual wind speed (Belmonte Rivas & Stoffelen 2019). Mean zonal wind estimates were calculated for the summer months December to February as a strong trend in weakening easterly winds during summer was detected (Hazel & Stewart 2019). ERA5 data are freely available at the Copernicus Climate Change Service Climate Data Store (CDS) (C3S 2017).

6.1.3 Sea Ice Coverage

Sea ice coverage is measured as the amount of sea ice days per year. A day of sea ice occurred when a pixel had a sea ice concentration above 15 %, as suggested by previous studies (Massom *et al.* 2013, Miles *et al.* 2016). The most state-of-the-art sea ice concentration data (Global Sea Ice Concentration Data Record -Version 2) (Lavergne *et al.* 2019) are currently only available from the Ocean and Sea Ice Satellite Application Facility (Osisaf 2020). The data date back to 1981 and were derived from passive microwave data from Nimbus 7 and DMSP (Defense Meteorological Satellite Program) satellites. The spatial resolution is 25 km x 25 km. For the months with sea ice cover (April to October) the daily sea ice products OSI-450, OSI-430-b were downloaded. The calculation of sea ice days was especially challenging in the early acquisition years as gaps in the time series existed. Until mid-1987, only second-daily or less frequent data were available. In this case, the available acquisitions were used and multiplied to reach the amount of total days within a month, hence 30 or 31. For the year 1986, only a very limited amount of measurements existed which was not enough to calculate the mean amount of annual sea ice days. Therefore, it was decided to exclude sea ice data of the year 1986. The accuracy of the OSI products was assessed by a comparison to sea ice chart products. The standard deviation of mismatch between OSI products and ice chart analysis on sea ice concentration is 8 % for ice and open water during winter (JJA). From both products a similar trend in sea ice extent was calculated leading to the assumption that the OSI sea ice concentration measurements are very accurate (Brandt-Kreiner *et al.* 2019).

6.1.4 Sea Surface Temperature

Sea surface temperature (SST) data were downloaded from the CDS (C3S 2017). The most recent SST product consists of an ensemble of multiple satellite observations and is listed as “Level-4 spatially complete global SST product based on data from multiple sensors” (Version 2) (C3S 2017). Satellite observations were acquired from NOAA (National Oceanic and Atmospheric Administration), ERS (European Remote Sensing Satellite), Envisat, and Sentinel-3 satellites. The product is available at a 0.05° gridded resolution (approx. 5.5 km). Sea surface temperature was only calculated for months with little sea ice cover (October to March) as measurements over sea ice are noisy due to changing sea ice thickness and concentration (Kwok & Comiso 2002). Depending on year and latitude of measurement, the accuracies of the Level 4 SST data vary. Before 1996, the difference between Level 4 SST data and in-situ measurements is up to -0.4 K for low latitudes. Earlier measurements only deviated up to -0.1 K from in-situ measurements. The trend of the Level 4 SST product is very stable with a maximum trend of 0.01 K per year (Embury 2019). A summary of all processed climate variables is provided in Table 6.1.

Table 6.1: Summary of processed climate variable data sets. Modified after Baumhoer et al. (2021).

Climate Variable	Time Span	Season	Spatial Resolution	Accuracy	Data	Data Provider
Air Temperature	1982-2018	Summer (Oct-Mar) Winter (Apr-Sep)	9 km	-0.13 – 2.0 °C	modelled	CDS
Snowmelt	1982-2018	Dec-Feb	9 km	-	modelled	CDS
Zonal Wind	1982-2018	Dec-Feb	31 km	2.8 m/s	modelled	CDS
Sea Ice Days	1982-2018 (not 1986)	Apr-Oct	25 km	8 % std to ice chart	modelled + satellite	Osisaf
Sea Surface Temperature	1982-2018	Oct-Mar	~5.5 km	-0.1 to -0.4 °C	multiple satellites	CDS

6.2 Study Design

This chapter explains the calculation of calving front change from coastline products. Further on, the correlation of all processed climate variables with glacier and ice shelf front change is described.

6.2.1 Calculating Calving Front Change

The total amount of decadal calving front change was estimated by calculating the area change between three stages of the Antarctic coastline. Calving front change of the first decade was assessed from 1997 to 2008 and for the second decade from 2009 to 2018. Hereafter, it is referred to as the first (1997-2008) and the second (2009-2018) decade, even though the time periods are 11 and 9 years, limited by the availability of coastline products.

The origin of all three Antarctic coastline products was different which caused discrepancies due to different image sources (optical, radar) and subjectivity of coastline delineation. To align all three coastline products, the coastlines were manually corrected. Especially over fast ice, blue ice, and mélange errors in the coastline products existed. Hence, the coastline products were aligned based on the original satellite imagery and satellite image mosaics from which the coastlines were originally extracted. Little errors occurred for the Radarsat coastline whereas the MODIS coastline experienced major errors over snow covered sea ice. This was mainly owed to the lower spatial resolution and the use of optical imagery. The automatically extracted coastline from Sentinel-1 imagery had errors along the Western Antarctic Peninsula and over fast ice areas. The manual adjustment and correction removed all mismatches between the coastline products. After manual correction, area changes between the coastline products could be attributed to glacier and ice shelf front change.

To calculate area changes, each coastline shapefile was rasterized at a 40 km x 40 km resolution and combined into a raster stack. For each of the three resulting raster layers, a specific value was assigned for ice covered area. By summing up the raster stack, each

raster pixel had a specific value allowing conclusions on land ice cover for the according year. The area change was calculated by drawing polygons over all major glaciers and ice shelves wider than 3 km. Within the polygon, the area of advance and retreat for each year was calculated. For a basin-wide consideration, the area change values were summed up based on the Antarctic basins defined by Mouginot (2017).

In order to measure the accuracy of the manual adjusted coastlines, 30 randomly picked polygons over stable coastline areas were created. In those stable regions, no area change should have occurred between the three coastline products. The error in each of those 30 areas was calculated relative to a change over the coastline of 1 km length. On average, the coastlines deviated by ± 1.2 px per kilometer along the coastline. This error was caused by differences in image resolution, orthorectification errors, and the limits of manual correction. The error of 1.2 pixels per kilometer was calculated for each glacier front relative to the glacier front length.

6.2.2 Climate Data Correlation

In order to identify drivers of glacier and ice shelf retreat, the percentage of retreat and advance for each glacier/ice shelf basin (as defined by Mouginot (2017)) was spatially correlated with the selected climate variables. As Antarctic glaciers and ice shelves have very different basin sizes and calving front lengths only the percentage of retreat and advance per basin was used instead of the absolute value of change. The 37-year climate data record was averaged for the three time periods 1997-2008, 2009-2018, and 1982-1996. This allowed correlating the climate variables with the same time spans as the calculated glacier retreat. Additionally, the long-term mean (1982-1996) was subtracted from the first and second decade to assess relative changes in climate variables to previous times. Mean values of zonal wind, sea ice days, and sea surface temperature were calculated within a 100 km seawards buffer in front of each glacier or ice shelf. Mean air temperature was calculated within a 100 km landwards buffer to asses direct temperature changes over the ice shelves and glaciers. Surface melt only occurs at the edges of the ice sheet and was therefore calculated within the 100 km landwards buffer. The climate variables were correlated with the percentage of retreat and advance using a Pearson correlation. The input data for the correlation were 14 different variables which were spatially correlated with each other based on 188 observations (N=188). The number of observations was composed of 94 assessed glacier basins with variable averages for two different decades (1997-2008 and 2009-2018).

6.3 Results

Results are presented for changes in glacier and ice shelf extent as well as for climate variables. The results are presented for the two decades 1997-2009 and 2009-2018. For climate variables, also relative changes to the long-term mean (1982-1996) are presented.

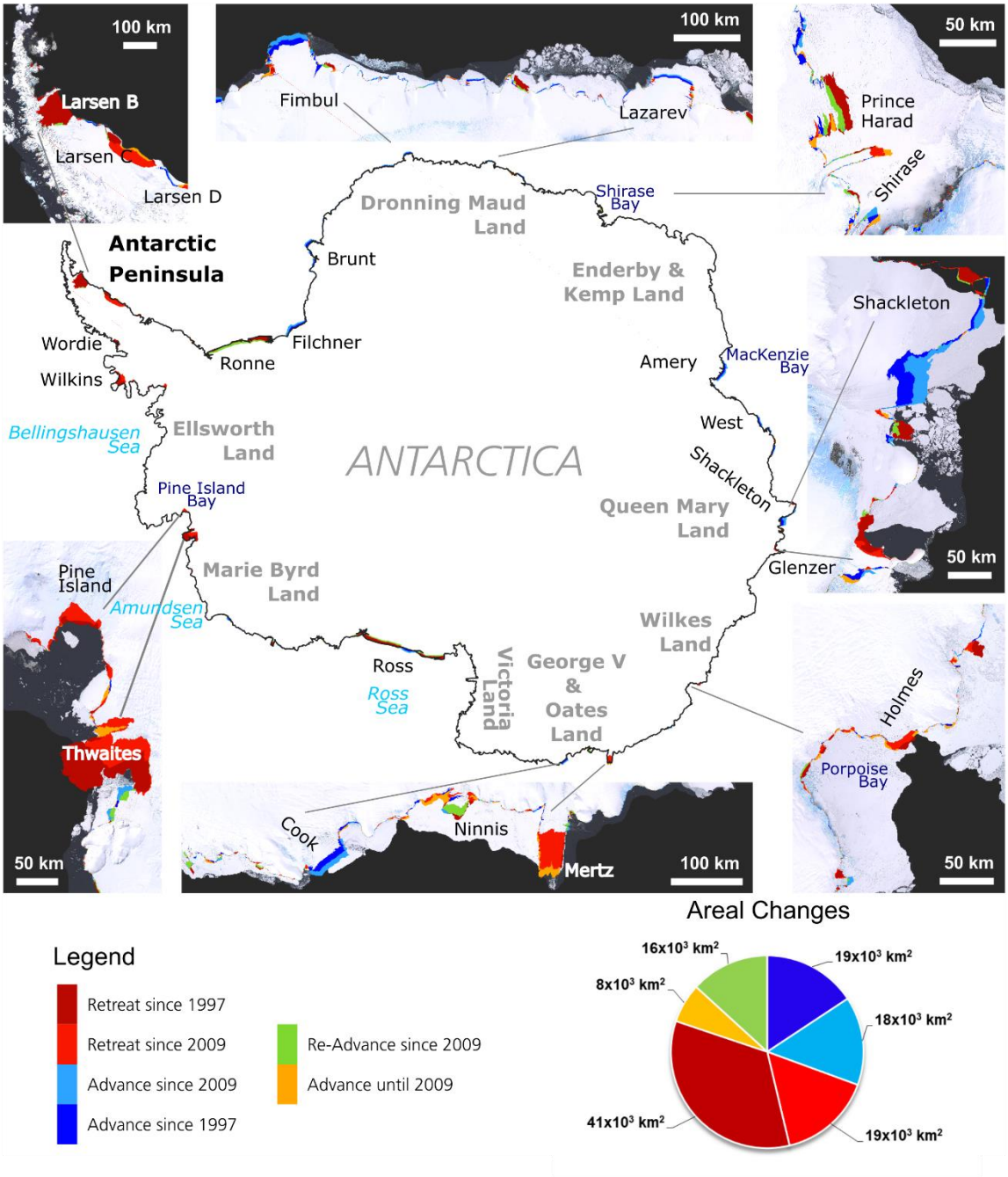

Figure 6.1: Two decades of Antarctic coastal change from 1997 to 2018. Map in the center: Overview of entire Antarctica. Enlarged displays (counter-clockwise) for Larsen Ice Shelf, Pine Island Bay, George V Land, Wilkes Land, Shirase Bay, and Dronning Maud Land. Background: LIMA Landsat Mosaic. Source: Baumhoer et al. (2021).

6.3.1 Antarctic Coastal Change

Antarctic coastal change can best be visualized by presenting the summed raster stack of all three coastline products for 1997, 2009, and 2018 (see Figure 6.1). Red colors indicate retreat whereas blue colors indicate advance. The darker the color, the longer the glacier retreat or advance lasted. For example, dark red areas indicate retreat between 1997 and 2018. Additionally, glacier fronts that did not show a continuous trend in retreat or advance are indicated in green and orange. The green color describes glaciers retreating before 2009 and starting to re-advance since then. Orange color stands for the opposite where glaciers first advanced and then started to retreat since 2009. Strong glacier and ice shelf retreat was observed along the Antarctic Peninsula and in West Antarctica. Fluctuations in ice shelf extent were most obvious for Ronne and Ross Ice Shelf. Advancing fronts were located along East Antarctica's ice shelves such as Filchner, Amery, Cook, Brunt and Fimbul Ice Shelf. Very evident was the breakup of the Mertz Glacier Tongue at George V Land, as can be seen in Figure 6.1.

6.3.2 Advance and Retreat of Antarctic Glaciers and Ice Shelves

Retreat and advance of Antarctic glaciers and ice shelves is summarized in Table 6.2. The table summarizes retreat and advance rates per decade for AP, WAIS, and EAIS. Additionally, the change rates are provided for each major ice sheet basin, as defined by Rignot et al. (2011) (see Figure 6.2 for basin boundaries). The table also summarizes the total changes in glacier and ice shelf extent per decade.

From 1997 to 2008, the extent of the Antarctic Ice Sheet decreased by -29,618±1193 km^2. During this time period, 69 % of ice shelf and glacier extent was lost whereas 31 % was gained. The opposite was measured for the period from 2009 to 2018 where the ice sheet increased its area by 7,108±1029 km^2. 44 % of the total ice shelf and glacier extent decreased and 56 % increased. The main areas of retreat and advance were located at similar locations during both decades. The only exceptions were the Ronne and Ross ice shelves. Both retreated between 1997 and 2008 and advanced within the second decade. This switch from retreat to advance was mainly responsible for a shrinking ice sheet during the first and a growing ice sheet during the second decade.

Continuous glacier and ice shelf retreat was observed for the Antarctic Peninsula over both decades. During the first decade (1997-2008), the disintegration events of the Larsen B, Wilkins, and Wordie Ice Shelf caused a 37 % higher calving amount as during the second decade. The second decade was characterized by the breakup of iceberg A-68 from the Larsen C Ice Shelf and the further disintegration of Wilkins Ice Shelf. The only exception from the overall retreat was the Larsen D Ice Shelf which advanced. Summed up, the retreat of glaciers and ice shelves along the Antarctic Peninsula was 5-6 times higher than the advance over the last two decades.

At the WAIS, the retreat of the Ronne and Ross ice shelves accounted for 75 % of the total ice shelf and glacier retreat area between 1997 and 2008. This resulted in a three times higher retreat within the first decade compared to 2009-2018. The pattern of glacier front change along the West Antarctic coastline was different when excluding the Ronne and Ross ice shelves from the calculation. Then glacier retreat dominates during both decades. Especially the Pine Island and Thwaites Glacier retreated continuously. The retreat of Getz and Abbot Ice Shelf started within the second decade.

Table 6.2: Area change rates in glacier and ice shelf front extent between 1997 and 2018 (upper table). Total lost and gained ice shelf/glacier area per decade (lower table). For basin abbreviations see Figure 6.2.Modified after Baumhoer et al. (2021).

		1997-2008		2009-2018		1997-2018	
	basin	*advance* [km²/yr]	*retreat*	*advance* [km²/yr]	*retreat*	*advance* [km²/yr]	*retreat*
EAIS	A-Ap	249±14.9	164±17.4	295±27.5	112±13	215±11.8	85±6.5
	Ap-B	62±4.8	89±5.6	80±8.9	53±4.2	34±3.8	36±2.1
	B-C	187±1.9	4±2.2	186±3.5	20±1.6	179±1.5	4±0.8
	C-Cp	380±7.7	167±9	363±14.2	153±6.7	323±6.1	111±3.3
	Cp-D	49±4.6	58±5.4	45±8.6	97±4.1	23±3.7	51±2
	D-Dp	154±5	64±5.8	156±9.2	317±4.3	85±3.9	111±2.2
	Dp-E	68±9.5	58±11.1	74±17.5	81±8.3	34±7.5	32±4.1
	E-Ep	6±3	411±3.5	156±5.5	8±2.6	5±2.4	154±1.3
	Jpp-K	163±2.1	2±2.4	252±3.8	2±1.8	203±1.6	1±0.9
	K-A	306±7.8	23±9.1	285±14.3	82±6.8	270±6.2	24±3.4
	EAIS	**1,626±61.1**	**1,040±71.4**	**1,894±112.9**	**926±53.4**	**1,370±48.6**	**607±26.6**
AP	Hp-I	20±4.5	328±5.3	25±8.4	305±4	11±3.6	306±2
	I-Ipp	87±3.9	938±4.6	59±7.2	592±3.4	12±3.1	715±1.7
	Ipp-J	91±4.5	67±5.3	118±8.4	75±4	71±3.6	38±2
	AP	**198±13**	**1333±15.2**	**202±24**	**972±11.4**	**94±10.3**	**1,060±5.7**
WAIS	Ep-F	160±7.7	868±8.9	452±14.1	74±6.7	136±6.1	341±3.3
	F-G	103±5.2	101±6.1	73±9.7	106±4.6	59±4.2	73±2.3
	G-H	40±3.6	371±4.2	49±6.7	369±3.2	14±2.9	340±1.6
	H-Hp	26±3.7	35±4.3	6±6.8	97±3.2	3±2.9	51±1.6
	J-Jpp	29±5.8	1127±6.8	643±10.7	26±5.1	13±4.6	317±2.5
	WAIS	**358±26**	**2,502±30.4**	**1,222±48**	**672±22.7**	**225±20.7**	**1,121±11.3**

Total glacier and ice shelf extent loss/gain [km²]

	1997-2008		2009-2018		1997-2018	
	advance	*retreat*	*advance*	*retreat*	*advance*	*retreat*
WAIS	3,942±286	27,525±334	11,612±456	6382±216	4,617±424	22,970±232
AP	2,178±143	14,660±167	1920±228	9232±36	19,29±212	21,722±116
EAIS	17,886±672	11,439±785	17,990±1072	8801±51	28,089±997	12,453±545
AIS	24,006±1100	5,3624±1286	31,522±1756	24414±303	34,636±1632	57,146±893
total	**-29,618±1193**		**7,108±1029**		**-22,510±1263**	

The East Antarctic Ice Sheet was characterized by glacier and ice shelf advance for both decades. During the second decade the advance rate was higher by 268 km² per year compared to 1997-2008. Continuous advance was observed for Amery and Filchner Ice Shelf and along Dronning Maud and Queen Mary Land. Wilkes Land as well as Victoria Land had an almost equal share of retreat and advance within the first decade. In the second decade, Wilkes Land as well as George V and Adélie Land started to retreat predominantly

whereas Enderby Land started to advance. The area changes are summarized in Table 6.2 for all major ice sheet basins and visualized in Figure 6.2 on glacier basin scale.

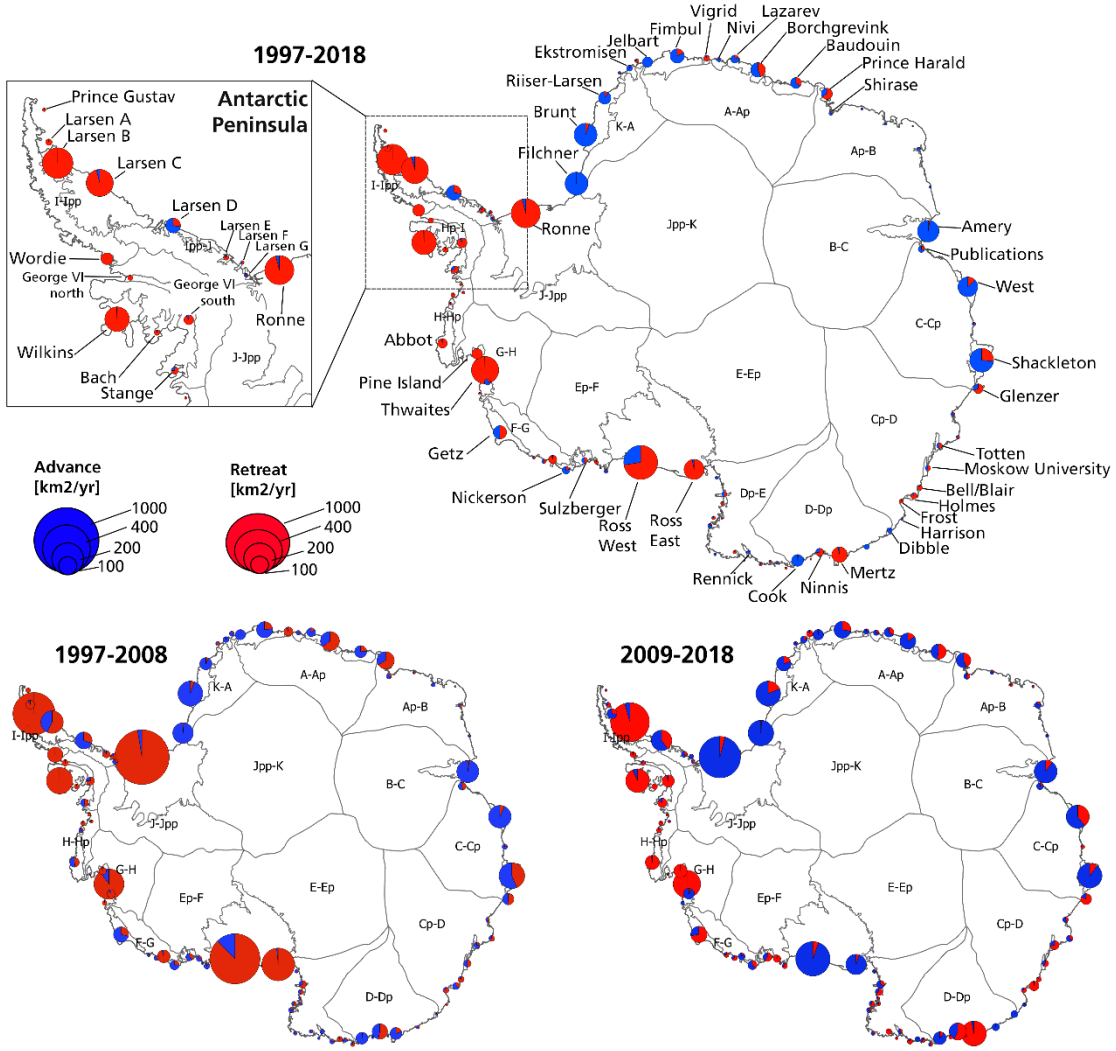

Figure 6.2: Glacier and ice shelf extent changes between 1997-2008, 2009-2018, and 1997-2018. Source: Baumhoer et al. (2021)

6.3.3 Air Temperature

In Figure 6.3, absolute and relative air temperatures over the Antarctic continent derived from the ERA5-Land product are depicted. The absolute air temperatures of Antarctica have a clear distribution of warmer temperatures along the coastline and a colder interior of the ice sheet. The absolute air temperatures in Figure 6.3 also clearly highlight the temperature difference between Oct-Mar and Apr-Sep. Highest air temperatures were reached over the Antarctic Peninsula. West Antarctica experienced warmer air temperatures than East Antarctica, especially along the Bellingshausen Sea and in the interior of the ice sheet.

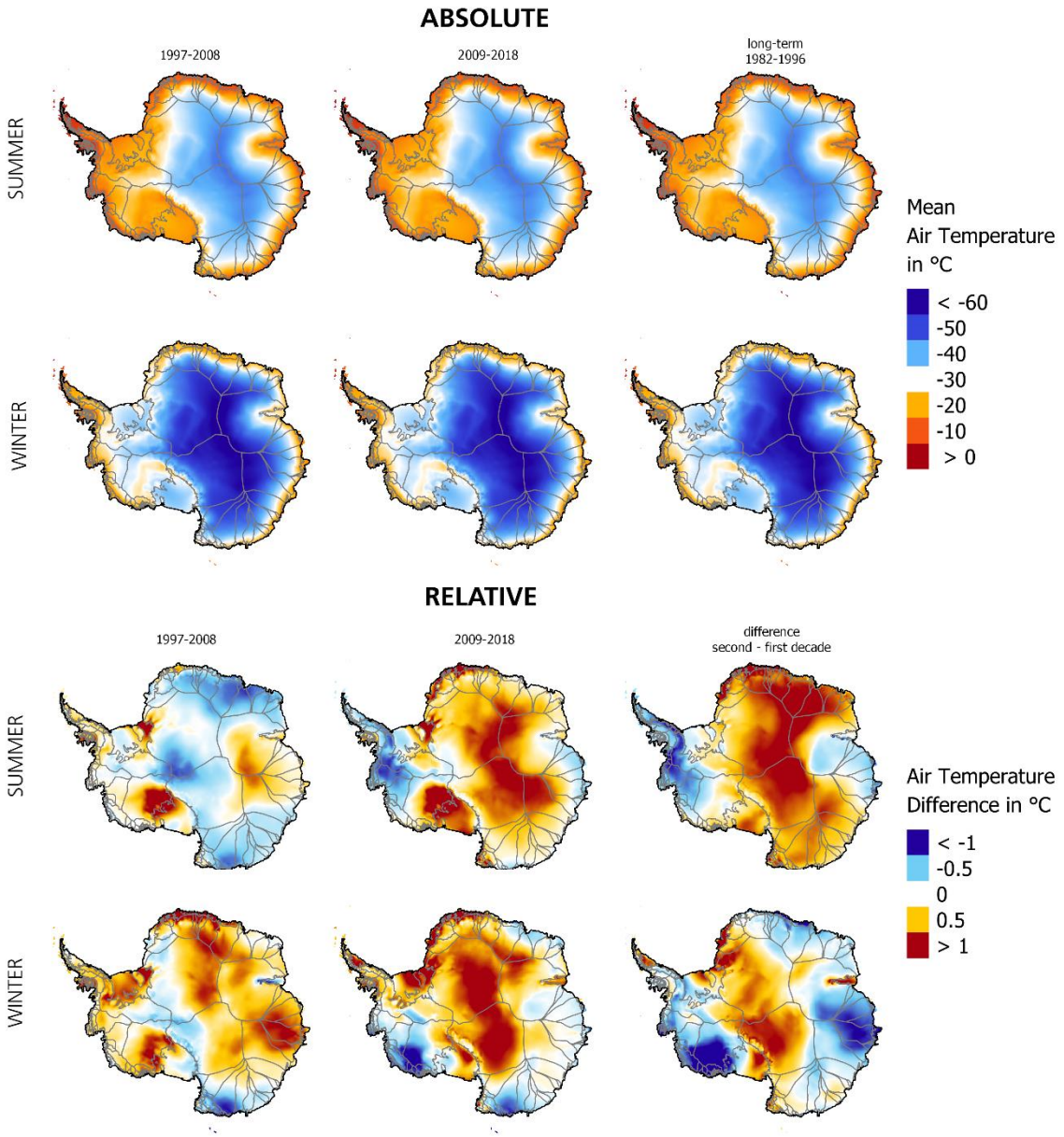

Figure 6.3: Absolute (upper) and relative (lower) air temperatures over the Antarctic continent in summer (Oct-Mar) and winter (Apr-Sep). Data: C3S (2017)

Relative changes in air temperature were calculated by subtracting the long-term mean (1982-1996) from the decadal means. Within the last two decades, the mean Antarctic air temperature did not change in the colder half of the year (Apr-Sep, "winter") but during the warmer half (Oct-Mar, "summer"). Over the Antarctic continent, the mean air temperature during summer increased by 0.6°C from the first to the second decade. This temperature increase occurred over the interior of the ice sheet where warming of >1° was measured whereas the Antarctic Peninsula cooled between 0.5-1°C depending on region. Even though, the overall mean temperature did not change during winter, greater regional differences in temperature change existed. The interior of the ice sheet warmed during winter within the second decade but less strong than during summer. From the first to the

second decade, the mean air temperature decreased over West Antarctica and the Antarctic Peninsula except over the Larsen C Ice Shelf. Over the Larsen C Ice Shelf, an air temperature increase during winter existed. During the second decade, the air temperature compared to the long-term mean (1982-1996) increased during winter over the interior of the ice sheet and especially over the ice shelves of Dronning Maud Land with up to 1.8°C.

6.3.4 Sea Ice Days

Sea ice cover around the Antarctic continent usually exists between April and October. Longer sea ice cover durations were measured close to the coastline and shorter durations in the open ocean (see Figure 6.4, upper panel). The maximum of sea ice days between April and October added up to 214 days. This maximum sea ice cover was almost reached close to the Antarctic coastline. Especially long sea ice cover exists for the Weddell and Ross Sea surrounding the Ronne, Filchner, and Ross ice shelves. Generally, the duration of sea ice cover was longer close to the Antarctic coastline. The only exception existed along the Western Antarctic Peninsula.

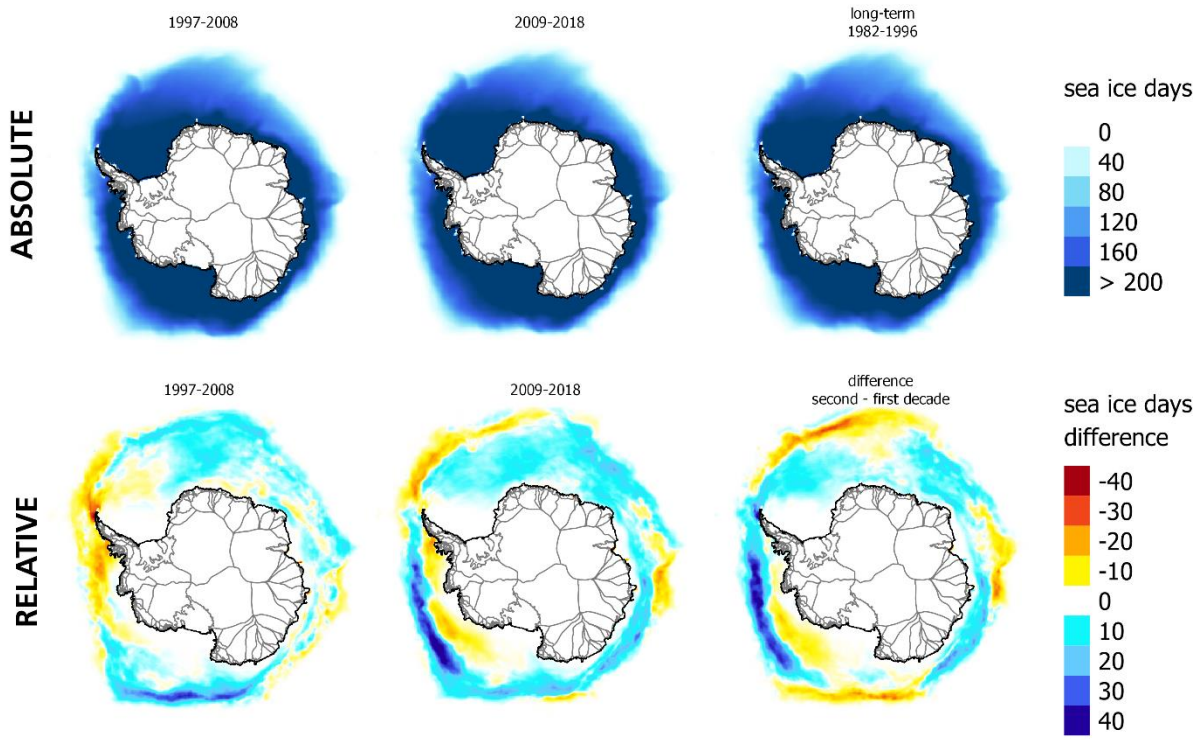

Figure 6.4: Sea ice days around the Antarctic continent measured during April to October for each year. Absolute sea ice days (upper panel) and relative mean sea ice days compared to the long-term mean (lower) per year. Also, the difference of mean annual sea ice days between both decades is given.

The difference in the number of mean annual sea ice days per year changed compared to the long-term mean. The general pattern of change indicated an increase in sea ice days along the EAIS and a decrease in the Amundsen and Bellingshausen Sea. The most extreme decrease in sea ice days occurred at the tip of the Antarctic Peninsula. Here, mean sea ice

days decreased up to 40 days in the first decade compared to the long-term mean. The strongest increase in mean sea ice days occurred in the outer boundaries of the Bellingshausen and Amundsen Sea within the second decade compared to the long-term mean. Slighter decreases were observed along Wilkes Land (approx. -5 days) during the first decade. Increases in sea ice days were only of low magnitude with less than 5 days along Dronning Maud and Oates Land. During 2009-2018, the tendency of a decreasing sea ice cover continued in the Bellingshausen Sea and extended further to the Amundsen Sea. Along the Antarctic Peninsula, sea ice days increased slightly by up to 10 days from the first to the second decade. At the top of the Peninsula, the decrease in sea ice days continued but was less severe with decreases up to -10 days instead of -40 days within the second decade compared to the long-term mean. Within the second decade, the increase in sea ice days along the entire EAIS continued. An increase between 7 to 25 days occurred. Also, along Wilkes Land, the sea ice cover duration started to increase again in the second decade.

6.3.5 Sea Surface Temperature

The sea surface temperature was measured in the warmer half of the year with lower sea ice cover (October to March). The coolest mean sea surface temperature reached -1.8°C close to the Antarctic coastline. In general, sea surface temperatures were below zero around the Antarctic coastline except for the Western Antarctic Peninsula (see Figure 6.5, upper panel). In further distance to the coastline, the sea surface temperatures increased. Cold sea surface temperatures along the Ross and Weddell Sea extended far seawards. In contrast, sea surface temperatures increased more quickly in seaward direction around Wilkes Land, the Western Antarctic Peninsula, and Dronning Maud Land.

Figure 6.5 displays relative changes in sea surface temperature revealing greater regional differences. Compared to the long-term mean, little temperature differences existed between 1997 and 2008 (first decade). Increases below 0.2°C occurred along the Bellingshausen Sea and the Western Antarctic Peninsula. Along the EAIS, cooling sea surface temperatures with less than -0.2°C were observed compared to 1982-1996. For 2009-2018, stronger changes in sea surface temperatures were detected. In the Bellingshausen and Amundsen Sea, increases of up to 0.4°C compared to the long-term mean occurred. The cooling effect along East Antarctica was still apparent but lowered almost to zero degrees.

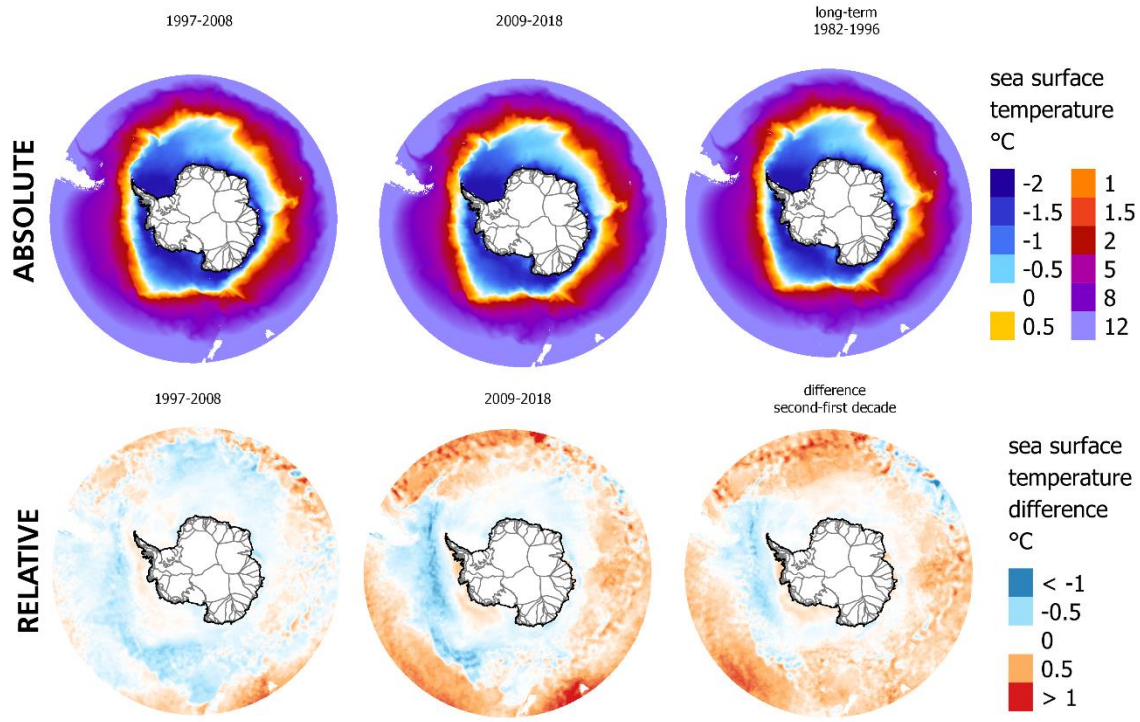

Figure 6.5: Sea surface temperature of the Southern Ocean from October to March. Absolute sea surface temperature (upper panel) and relative changes to the long-term mean (lower panel).

6.3.6 Snowmelt

Snowmelt over Antarctica occurs mostly during the summer months from December to February. The Antarctic Peninsula is the most melt affected area. In general, snowmelt was more intense during the reference period 1982-1996 compared to the last two decades which explains the negative snowmelt values over the Antarctic Peninsula (see Figure 6.6). Melt peaks occurred over the Larsen B ice shelf with 5 mm w. eq. per day. Melt increases during recent decades were less extensive and occurred over more selective areas. Especially over Wilkins, Larsen B, and the northern Antarctic Peninsula, melt increased point-wise compared to the long-term mean. Within the first decade, snowmelt expanded to Pine Island Bay, Getz Ice Shelf, and Ross Ice Shelf as well as along Wilkes, George V, and Dronning Maud Land. Even though the melt area increased in those regions, the magnitude was very low with 0.1 mm w. eq. per day. Snowmelt increased by 0.1 mm w. eq. over George V, Oates, and parts of Wilkes Land as well as over Getz and Sulzberger Ice Shelf in the second decade. The previously detected melt over Pine Island and Dronning Maud Land disappeared in the second decade.

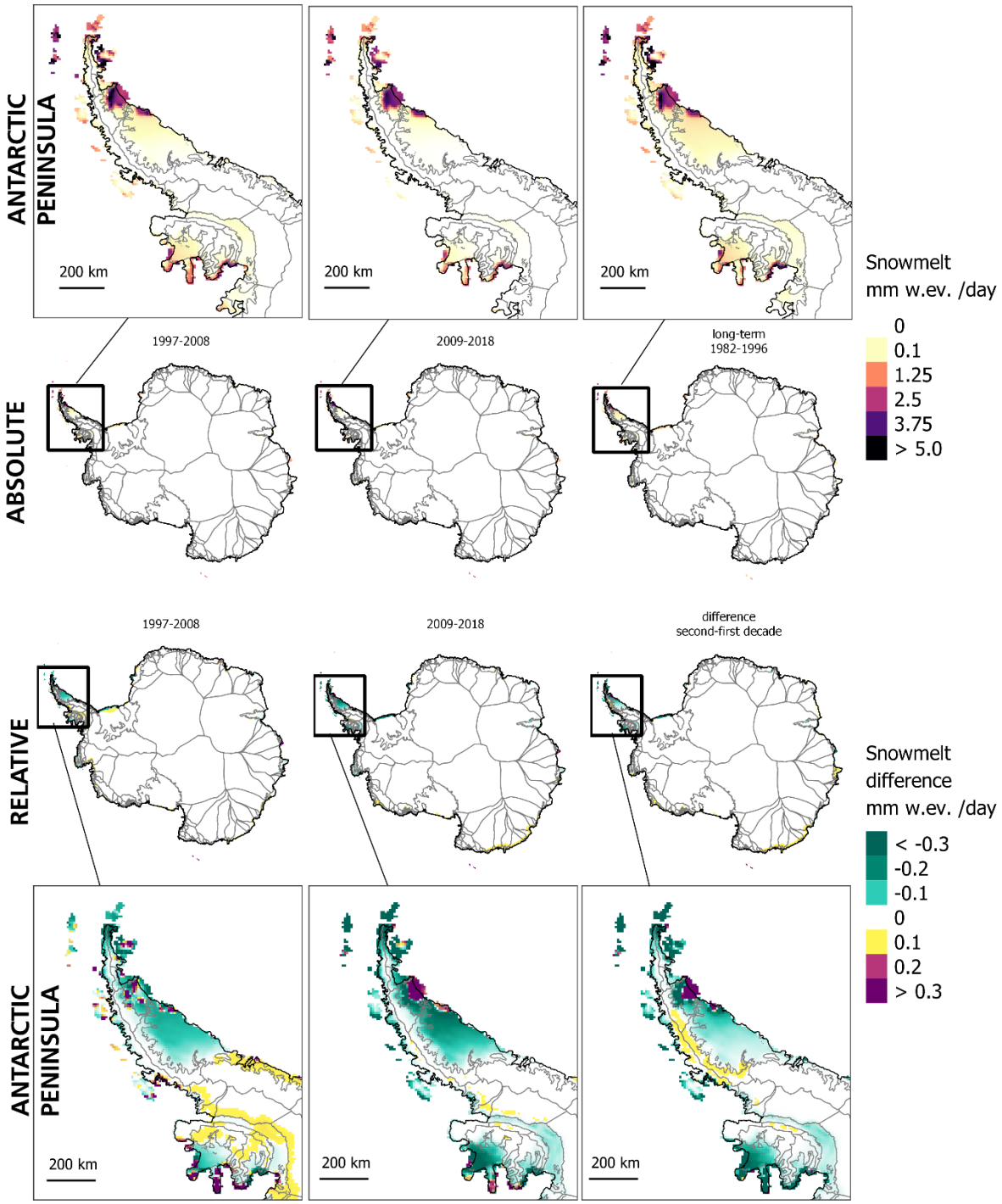

Figure 6.6: Mean absolute snowmelt in mm water equivalent per day between 1997-2008 and 2009-2018 (upper panel) and relative to the long-term mean (1982-1996). The enlarged panels show absolute and relative snowmelt amount over the Antarctic Peninsula. Source: Baumhoer et al. (2021)

6.3.7 Wind Direction

"The Antarctic continent is circled by weak and irregular easterly winds driven by high-pressure areas over the interior of the Antarctic continent created by cold and dry air. Easterlies weaken in the case of a positive Southern Annular Mode (SAM) as the west wind drift shifts poleward." (Baumhoer *et al.* 2021). This overall pattern existed during summer

months as can be seen in Figure 6.7 (upper panel). Easterlies were strongest along the EAIS with up to 3 m/s and lowest at the Peninsula with less than 1 m/s.

During the first decade (1997-2008), mean zonal wind speed increased (compared to the long-term mean) along the Peninsula (> 1 m/s), the Bellingshausen and Amundsen Sea (~0.5 m/s) and along the coastline between Wilkes Land and Queen Mary Land (~0.2 m/s). Westerlies got even stronger along the East Antarctic coast from Oates Land to Kemp Land (+ 1.3 m/s) in 2009-2018. In contrast, easterlies started to strengthen again in the second decade along the Amundsen and Bellingshausen Sea compared to 1997-2008 with +0.15 m/s. The only exception was the area around Pine Island Bay where westerlies strengthened further compared to the first decade with +0.4 m/s. During the second decade, dominating easterlies developed along Dronning Maud Land with up to ~0.75 m/s compared to the long-term mean.

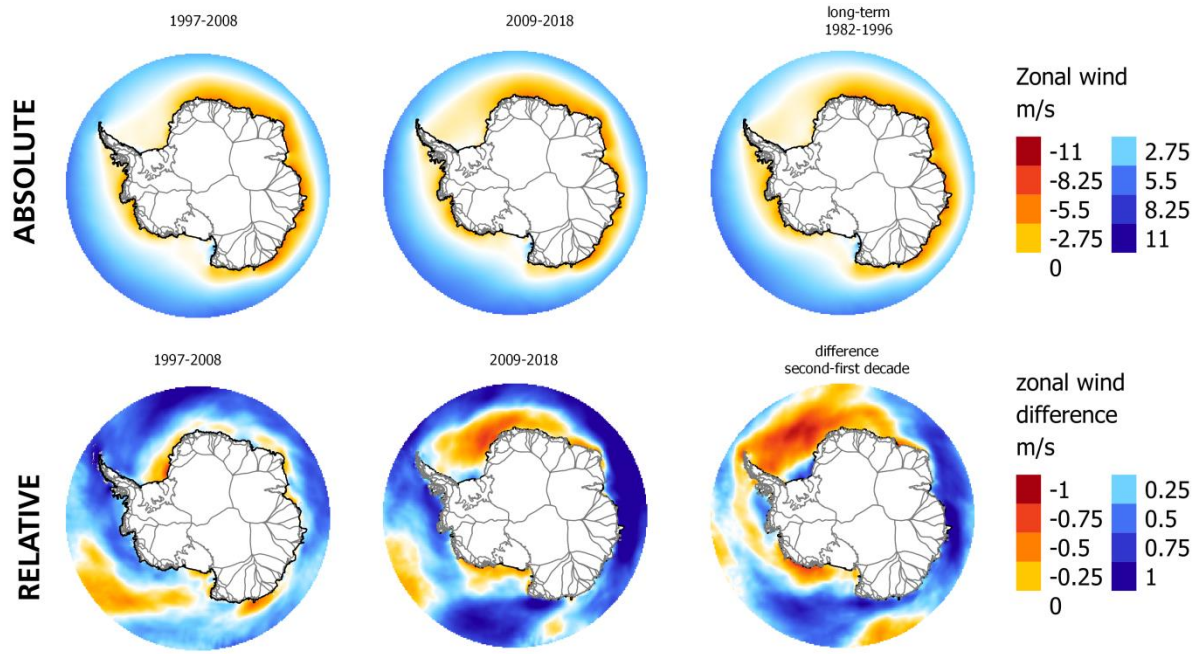

Figure 6.7: Zonal (West to East) wind speed (m/s) during summer months Dec-Feb. Positive absolute wind speed indicates dominating westerlies, negative speed dominating easterlies. Relative changes show changes in wind speed compared to the long-term mean.

6.3.8 Correlation Matrix

To identify potential drivers of calving front change, the percentage of retreat or advance was correlated with investigated climate variables. The results of the Pearson correlation are displayed in Figure 6.8. Darker blue colors indicate strong positive correlations whereas dark red colors signalize strong negative correlations. The bigger the circle, the higher was the magnitude of positive or negative correlation. A significant Pearson correlation is marked with stars for p=0.05 (*), 0.01 (**) and 0.001(***). Positive significant correlations existed between glacier retreat and absolute air temperature in

summer and winter, snowmelt, relative sea surface temperature, and relative zonal wind. Negative correlations existed only for absolute and relative sea ice days. Correlations for retreat and advance are counterparts. Hence, correlations with retreat or advance were of the same magnitude for each climate variable but with reversed sign. Overall, weak to moderate correlations existed with strong significance except for snowmelt with p=0.05. The strongest linear relationship with r=0.44 existed between glacier retreat and relative sea surface temperature. Weaker correlations occurred between calving front retreat and air temperature. The relationship with absolute summer air temperature on the ice shelf surface was slightly weaker with r_{summer}=0.18 and r_{winter}=0.23. Relative changes in zonal wind correlated with glacier retreat with r=0.30. The absolute wind speed of zonal winds did not correlate with calving front change. The lowest positive but significant correlation existed between the absolute amount of snowmelt and glacier retreat with r=17. A negative correlation between glacier retreat and an increase in sea ice days occurred for absolute and relative values (r_{abs}=0.33, r_{rel}=0.27).

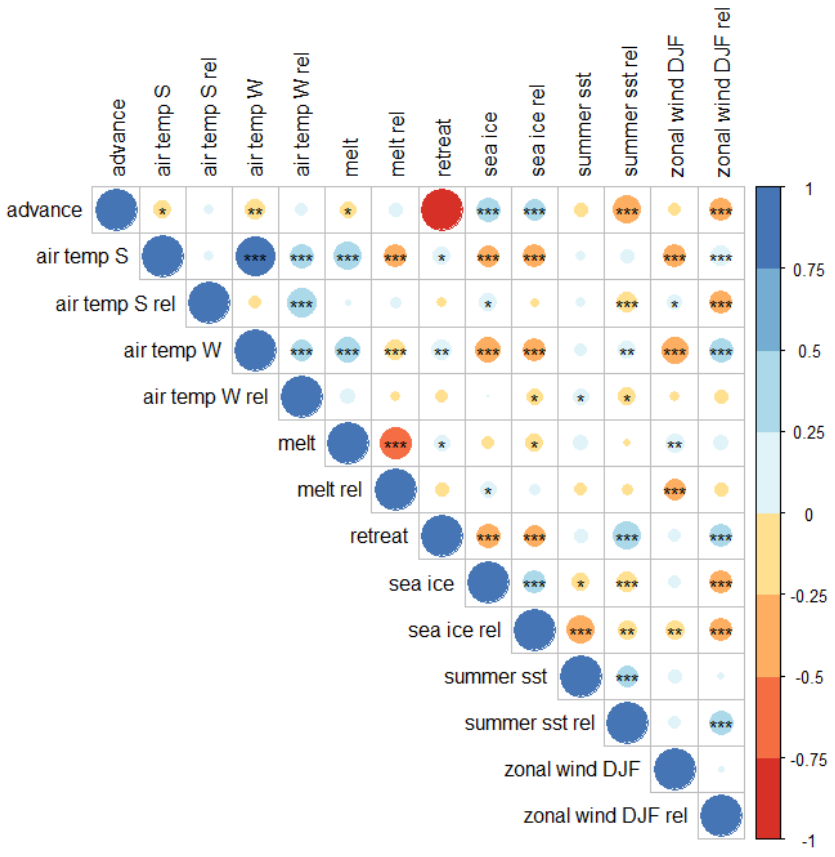

Figure 6.8: Correlation between glacier and ice shelf change and the analysed climate variables winter/summer air temperature, snowmelt, sea ice days, summer sea surface temperatures, and zonal wind speed. Colour and circle size indicate the correlation coefficient. Stars indicate significance levels for p=0.05 (*), 0.01 (**) and 0.001(***). S: summer, W: winter, rel: relative to 1982-1996, DJF: Dec-Feb. Source: Baumhoer et al. (2021)

6.4 Discussion

The results section presented glacier and ice shelf front changes over the last two decades as well as changes in climate variables. A spatial relationship between calving front retreat and strengthening westerlies, intense snowmelt, decreasing sea ice cover, and rising sea surface temperature was indicated by the correlation analysis. Now it has to be discussed to what extent environmental factors were responsible for the observed calving front retreat. This question is not easy to address as a significant correlation between calving front retreat/advance and climate variables cannot alone provide conclusive evidence of a causal link. Additionally, the possibility of calving front retreat due to internal glaciological factors has to considered as well. Therefore, previous observed calving events are discussed in combination with measured changes in climate variables as well as scientific publications to find solid evidence for drivers of glacier and ice shelf retreat.

6.4.1 Antarctic Peninsula

The Antarctic Peninsula experienced a strong decrease in glacier and ice shelf extent within the last two decades. Major events included the disintegration of Larsen B, Wordie, and Wilkins Ice Shelf as well as the retreat of Larsen C Ice Shelf. Wordie Ice Shelf had a major calving event during the first decade (1997-2008) where more positive zonal winds during summer were observed compared to the reference period (+0.62 m/s) and to 2009-2018 (+ 0.28 m/s). This poleward shift of the westerlies during the first decade can cause upwelling of warm CDW and enhance basal melt at the ice shelf bottom. The poleward shift of westerlies is linked to positive SAM years (Marshall 2003). Figure 6.9 displays the progression of SAM since 1970 during summer months (DJF) and annually. Additionally, the five-year moving average of the annual SAM is plotted. An extreme positive SAM year occurred in summer 1998/99 which could have triggered the disintegration of Wordie Ice Shelf. A major calving event occurred in 1998/99 (Friedl *et al.* 2018) and later calculated basal melt rates for the remaining parts of Wordie Ice Shelf (Depoorter *et al.* 2013, Rignot *et al.* 2013) indicate the ice shelf's vulnerability to basal melt. CDW upwelling was particularly strong at Wordie Ice Shelf between 2008 and 2011 due to a positive SAM (Walker & Gardner 2017). Besides, it should be emphasized that a retrograde bed in a subglacial trough further destabilized Wordie Ice Shelf which resulted in grounding line retreat in 2010/2011 (Friedl *et al.* 2018). Additionally, a 14-day decrease (compared to 1982-1996) in sea ice days occurred in the Wordie Bay during the disintegration period which further destabilized the Wordie Ice Shelf. So far, the effect of decreasing sea ice at Wordie Ice Shelf has not been discussed in literature but very likely added additional forcing.

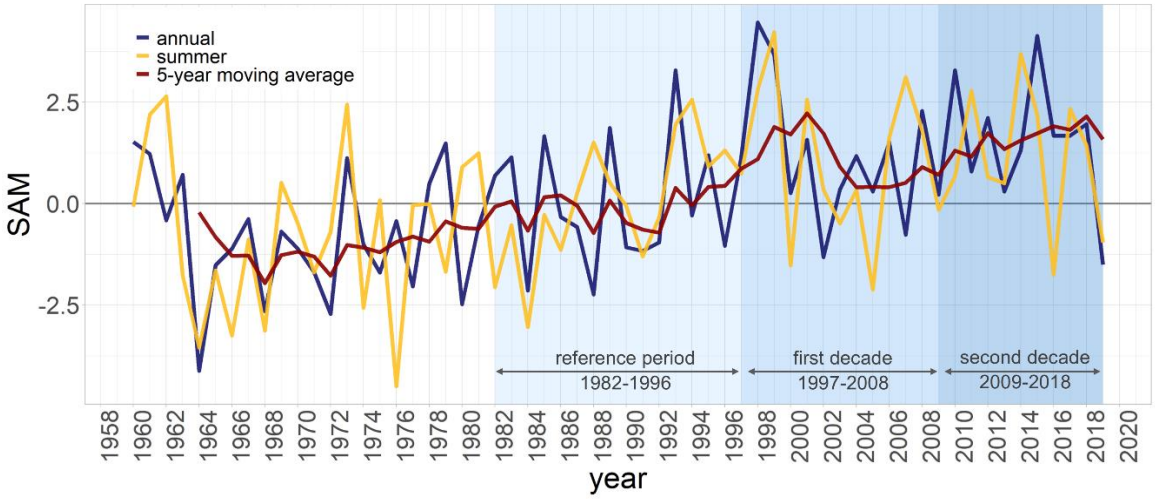

Figure 6.9: Southern Annular Mode (SAM) since 1960. Values are given for the annual SAM (blue), SAM during summer (orange), and a 5-year moving average for the annual SAM (red). The dashed grey lines indicate the investigated periods 1997/08 and 2009/18, as delimited by the available coastline data. For SAM during summer (Dec-Feb), the beginning of austral summer (hence December) indicates the year of the peak. Data: Marshall et al. (2003). Source: Baumhoer et al. (2021).

Wilkins Ice Shelf disintegrated in two phases in 1998 and further in 2008 (Rankl *et al.* 2017). Within this time span, an increase in zonal winds (+0.47 m/s) was measured. In addition, a decrease of 9 mean sea ice days and up to +1°C warmer winter air temperatures occurred. The first break up event in 1998 coincides with an exceptional positive SAM which increased basal melt rates by upwelling CDW. In summer 2007/08, the SAM index was positive but not of exceptional magnitude. Indeed, the first calving event in the beginning of 2008 was associated with surface melt (Scambos *et al.* 2009). Neither an increase in melt days (-4 days) nor an increase in the amount of melt (±0 mm w. eq.) was observed. This means that either a peak melt event triggered the disintegration which is not represented in the calculated mean over a decade or the accuracy of modelled ERA5 snowmelt data is too low over Antarctic ice shelves. It is more likely that the combination of forcing factors resulted in the disintegration of the ice shelf. For example, the second disintegration event in winter 2008 was likely caused by internal forces through bending stresses created by unequal decreases in ice thickness (Braun *et al.* 2009) and enhanced strong winds (Humbert *et al.* 2010).

During the disintegration event of Larsen B Ice Shelf an increase in zonal winds of +0.33 m/s (1997-2008) was calculated compared to the long-term mean. During the disintegration in 2002, a very positive SAM anomaly was recorded during summer. At Larsen B Ice Shelf, strengthening westerlies are not associated with upwelling CDW but with increasing temperatures at the Peninsula, warm föhn winds and surface melt (Rack & Rott 2004). Recent studies found that a series of years with increases in föhn days during positive SAM years significantly increased surface melt (Cape *et al.* 2015, Leeson *et al.* 2017). This is in

line with the strong mean snowmelt rate of 5.5 mm w. eq per day measured between 1997 and 2008. This strong melt caused increased supraglacial lake formation. Right before the disintegration of Larsen B lake drainage was observed. But so far it is unsolved whether lake drainage is a cause or effect of ice shelf collapse (Leeson *et al.* 2020).

The calving event of the Larsen C Ice shelf was not accompanied by strong changes in environmental forces. Snowmelt days decreased by 8 days compared to the long-term mean and the melt rate was -0.2 mm w. eq. per day, and hence lower than during the long-term mean. Zonal winds were slightly higher compared to the long-term mean with +0.1 m/s (2009-2018) but lower than in the previous decade with +0.54 m/s (1997-2008). Also, no change in sea ice days was recorded. All in all, this strengthens the hypothesis of Hogg and Gudmundsson (2017) of a natural calving event without external forces triggering the event. Nevertheless, the Larsen C Ice Shelf is not untouched by environmental forcing. Negative thickness changes of the ice shelf were detected between 1994 and 2012 (Paolo *et al.* 2015). The only Larsen Ice Shelf still gaining ice shelf area is the Larsen D Ice Shelf. The ice shelf was not affected by surface melt as the Larsen B and Larsen C Ice Shelf and strengthening zonal winds did not reach the Larsen D Ice Shelf. The Larsen D is a stable ice shelf gaining ice thickness (Paolo *et al.* 2015) and having a positive (Gardner *et al.* 2018) or slightly negative mass balance (Rignot *et al.* 2019) not comparable with the strong mass losses along the Antarctic Peninsula.

On the Western Antarctic Peninsula, George VI and Stange Ice Shelf were relatively stable during the first decade and started to retreat in the second decade. During the second decade (compared to 1982-1996), summer sea surface temperatures increased by +0.62°C and +0.38°C for George VI south and Stange. Slightly strengthening westerlies (+0.25 m/s) but almost no melt (0.02 mm w. eq. per day) existed. Over the entire observation period, George VI south showed constant retreat of low magnitude and is not expected to disintegrate rapidly (Holt *et al.* 2013). But recently many supraglacial lakes were found on the ice shelf (Dirscherl *et al.* 2020) and moderate basal melt occurred (Paolo *et al.* 2015) which is why it might be worth to reconsider this assumption.

6.4.2 West Antarctica

West Antarctica was mostly affected by calving front retreat at Pine Island Bay as well as at Ronne and Ross West Ice Shelf accounting for the strongest retreat between 1997 and 2008 with 1,098±0.91 km^2/yr and -732±0.73 km^2/yr, respectively. Even though, those are the highest retreat rates measured for single ice shelves, the calving area is small compared to the size of both ice shelves. The entire Ross Ice Shelf has an area of 481,298 km^2 and the Ronne-Filchner Ice Shelf of 437,008 km^2 (Griggs & Bamber 2011). Both ice shelves had their maximum extent around 1997 (Ferrigno *et al.* 2005, Ferrigno *et al.* 2007) with calving front positions further landwards before and after. This indicates that the

calving event was part of the natural calving cycle. The ice shelf front of Ross West Ice Shelf had almost the same position in 1962 as in 2004 after the major calving event (Ferrigno *et al.* 2007). The same was observed for Ronne Ice Shelf with a minimum extent in 1974 similar to 2004 (Ferrigno *et al.* 2005). Further indicators of a usual calving cycle were no noticeable changes in environmental conditions. Neither zonal winds strengthened (-0.15 m/s) nor sea surface temperatures (+0.02 °C) or sea ice days changed compared to the long-term mean. Only, melt was detected on the calving front of the Ronne Ice Shelf in 1997-2008 (0.5 mm w. eq. per day) but was less than during the reference period. But future environmental forcing might also affect the Ronne Ice Shelf through increasing basal melt, changing sea ice conditions and changing winds as assumed by Darelius et al. (2016).

During the entire observational period (2997-2018), the Pine Island Glacier and the Thwaites Glacier retreated by 40±0.15 km^2/yr and 288±0.77km^2/yr, respectively. Potential forcing included strengthening westerlies with +0.28 m/s (1997-2008) and +0.25 m/s (2009-2018) compared to 1982-1996. The rate of retreat was the same for the Thwaites Glacier but tripled for the Pine Island Glacier from the first to the second decade. Notable changes for Pine Island Glacier were a rise in sea surface temperature by 0.28°C from 1997-2008 to 2009-2018 but only by 0.11°C for Thwaites Glacier. It is difficult to assess whether this temperature increase directly affected the retreat rate as both glaciers have very different dynamics and morphologies. In addition, the Pine Island Glacier lies on a deeper subglacial bed probably more prone to basal melt. Additionally, land fast ice persistency and hydrofracture affected both glaciers differently (Miles *et al.* 2020, Milillo *et al.* 2017, Seroussi *et al.* 2017, Yu *et al.* 2017).

Pine Island Bay touches the Abbot Ice Shelf in the east and Getz Ice Shelf in the west, both very stable with little changing fronts. No strong increases in sea surface temperature occurred for both ice shelves with +0.13°C between both decades. In the first decade, the sea surface temperature did not change compared to 1982-1996. Basal melt probably increased for Abbot Ice Shelf as zonal winds increased by +0.45 m/s in 1997-2008 and by +0.68 m/s in 2009-2018 compared to the long-term mean. The Getz Ice Shelf only experienced stronger westerlies in the first decade with +0.39 m/s but not in the second (-0.02 m/s) relative to 1982-1996. Sea ice days did not vary with ±1 day for both ice shelves. Even though strong basal melt rates through upwelling CDW exist for both ice shelves with basal melt rates of 1.5 m/decade (Abbot) and 66.5 m/decade (Getz) (Paolo *et al.* 2015), the oceanic forcing had only minor effects on their calving fronts so far. The Abbot Ice Shelf was stable in the first decade and retreated by 73 km^2/yr in the second. The Getz Ice Shelf advanced in 1997-2008 by 38 km^2/yr and retreated afterwards by -41 km^2/yr (2009-2018). The explanation why both ice shelves only slightly retreated over the last two decades despite strong ocean forcing could be their low ice flow velocities (Mouginot *et al.* 2019), stabilizing pinning points, a more stable initial setting of the ice shelves, and completely

different bed topographies than for glaciers in Pine Island Bay. The bed below Abbot Ice Shelf is situated at around -200 m with only a small trough reaching below 500 m, while the Getz Ice Shelf's bed lies like a barrier around 400 m before deepening closer to the grounding line up to 700 m. In comparison, the bed of Pine Island Glacier reaches depths around 700-1000 m (Fretwell *et al.* 2013). The higher beds may have protected the ice shelves more effectively from upwelling CDW in combination with stabilizing ice rises as pinning points. Future calving front retreat can be expected if ocean forcing continues. Basal melt has already forced grounding line retreat since 2008 (Chuter *et al.* 2017).

West Antarctica's most stable ice shelves were Nickerson and Sulzberger with almost no change in frontal position. They experienced no environmental forcing over the last two decades and do not experience basal melt as they are located in the cooler Ross Sea (Paolo *et al.* 2015, Rignot *et al.* 2013).

6.4.3 East Antarctica

Most recent mass balance estimates for the EAIS reveal that the paradigm of an invulnerable East Antarctica not prone to environmental forcing might be wrong. Mass balance estimates based on the mass budget method revealed mass loss over the EAIS since 1979 with increasing loss since 1999 (Rignot *et al.* 2019). On the contrary, mass balance estimates based on altimeter measurements still report a stable mass balance since 1992 (IMBIE 2018). Glacier and ice shelf retreat along the East Antarctic coastline was little compared to the WAIS and the Peninsula. Calving front advance still dominated the EAIS over the last two decades which strengthens the hypothesis of a stable East Antarctic Ice Sheet. Nevertheless, in a few cases glacier retreat appeared on the EAIS which will be assessed regarding potential driving forces starting counter-clockwise at Victoria Land.

Glacier fronts along Victoria Land were equally balanced in retreat and advance overt the last two decades. External environmental forcing was not observed. The only remarkable change in climate variables was an increase in summer air temperatures of up to 1.7°C. But as relative changes in air temperature were not identified as driving forces in the correlation matrix it is concluded that Victoria Land was not suspect to environmental forcing. This is in line with previous studies mentioning the healthy state of those glaciers (Fountain *et al.* 2017). Glacier type and topography accounted for changes in glacier extent instead of climate forcing (Lovell *et al.* 2017). Along Oates and George V Land, only the retreat of Mertz Glacier is unusual as the remaining glaciers advanced (e.g. Cook Ice Shelf) or fluctuated (e.g. Ninnis Glacier). No increase in driving factors for glacier retreat could be observed for Oates and George V Land except for slightly less sea ice days (< 3 days) in the second decade compared to 1997-2008. The break-up event of Mertz Glacier was externally forced by an iceberg (broken off from the Ross Ice Shelf) colliding with Mertz

Glacier Tongue in 2010. This decreased polynya activity after calving resulted in a decrease in sea ice cover (Tamura *et al.* 2012).

Wilkes Land was identified as the only Antarctic region where several glaciers retreated simultaneously between 2009 and 2018. Previously, glacier retreat in Wilkes Land was linked to a decrease in sea ice days between 2000 and 2012 (Miles *et al.* 2016). In this study, no decrease in sea ice days was observed during the second decade (2009-2018), where most glaciers of Wilkes Land retreated. Only a slight decrease of ~5 days was measured in the first decade where glacier retreat and advance of Wilkes Land was rather balanced. This leads to the conclusion that only an exceptional decrease in sea ice days (~34 days in the study of Miles et al. (2016)) drives calving front retreat, but not the observed minor changes in sea ice days (±5 days). Hence, there might be additional causes for glacier retreat in Wilkes Land. It is suggested that stronger zonal winds with up to +0.44m/s during the second decade compared to the long-term mean induced basal melt by upwelling CDW. Forcing through increased sea surface temperatures and enhanced snowmelt was not observed.

Glenzer Glacier was also affected by strengthening westerlies beginning in 1997 with +0.32 m/s in the first and +1.23 m/s in the second decade. During the first decade, melt was higher than during the reference period with 7 mm w. eq. per day. Glenzer Glacier retreated over the last two decades which might be ongoing as an important pinning point was lost in 2004 and the remaining ice bridge to the last pinning point is narrowing down (see Section 5.4.1.2).

The three biggest ice shelves between Queen Mary and Kemp Land did not experience major calving events even though, West and Shackleton Ice Shelf experienced a major increase of strengthening westerlies with +0.97 m/s in the first and +1.2 m/s in the second decade compared to the long-term mean. Depending on study, those ice shelves experienced slight basal melt (Rignot *et al.* 2013) or a slight gain in ice thickness (Paolo *et al.* 2015). Potential explanations for advancing ice shelf fronts despite forcing westerlies could either be that basal melt needs to continue longer than two decades to trigger calving or that forcing by basal melt alone is not strong enough to result in ice shelf front retreat. Also tidal forcing can reduce the effect of upwelling CDW (Stewart *et al.* 2018). Similarly, Amery Ice Shelf experienced stronger zonal winds between 2009 and 2018 (+0.26 m/s). Over the two last decades, snowmelt increased (+ 0.23 mm w. eq. per day) on the northern part of Amery Ice Shelf whereas melt decreased (- 0.1 mm w. eq. per day) in the southern part of the ice shelf. The part affected by surface melt calved in 2019. A natural calving event at Amery Ice Shelf was expected earliest in 2025 as the calving cycle of the ice shelf is about 65-70 years (Fricker *et al.* 2002). “Still, it remains unclear if the observed increase in surface melt influenced the rift propagation in the Loose Tooth region. Prior to 2006, the rift propagation was not influenced by environmental forcing, but Bassis et al. (2008) did

not exclude the potential influence of surface melt if the mean air temperature would rise above zero" (Baumhoer *et al.* 2021).In addition, the fast ice sitting in the middle crack of Amery Ice Shelf started to disappear which might have further weakened the front. Fast ice was earlier reported as an stabilizing factor for calving fronts (Larour 2004).

Very contrasting glacier retreat appeared in Shirase Bay where Prince Harald Ice Shelf retreated by with 39 km^2/yr between 1997 and 2008 while Shirase Glacier advanced. In the following decade, the opposite was the case. This contrary pattern was already mentioned by Jezek (2002b). During the calving event, stronger mean snowmelt with an increase of 1 mm w. eq. per day (relative to 1982-1996) occurred at the front of Prince Harald Ice Shelf where no melt was detected for Shirase Glacier. Melt decreased in the second decade at Prince Harald Ice Shelf. For Shirase Glacier no external forcing was observed which leads to the conclusion that rather the very specific glacier shape influences calving cycles (Nakamura *et al.* 2007).

Dronning Maud Land was dominated by advancing ice shelves experiencing no basal melt (Paolo *et al.* 2015). During the first decade, a few calving events occurred in the eastern part of Dronning Maud Land where sea ice days decreased about -5 days. Also, winter air temperatures warmed by 1.78°C compared to 1982-1996 not affecting ice shelf advance. Other potential drivers like strengthening westerlies, surface melt, and rising sea surface temperatures did not occur. The health of the ice shelves along Dronning Maud Land was also confirmed by historical calving front data. In this region phases of retreat and advance are common. Phases of retreat occurred in 1963 and the 1970s whereas advance dominates since the 1990s (Kim *et al.* 2001, Miles *et al.* 2016).

6.4.4 A Circum-Antarctic Perspective

The above discussed circum-Antarctic ice shelf and glacier front changes linked calving front retreat to snowmelt, strengthening westerlies, decreasing sea ice days, and rising sea surface temperatures. The identified drivers did not only correlate with glacier retreat but also among each other. Hence, they are closely connected and changes in one climate variable can force changes in another variable that can force glacier retreat. Therefore, feedbacks between all assessed variables have to be considered.

Forced glacier retreat occurred when at least one of the listed drivers strengthened compared to the long-term mean. A cyclic calving event was identified when glacier retreat occurred without any forcing. This was further proven by a comparison with historic front positions. An exception of this overall pattern was observed at the West and Shackleton Ice Shelf where westerlies strengthened but no frontal retreat occurred. This suggests that either the duration of forcing westerly winds was too short to result in immediate calving front retreat or upwelling CDW did not increase the basal melt rate. Strong tidal forcing occurs at the area of both ice shelves which prevents CDW from reaching the ice shelf bottom

(Hazel & Stewart 2019, Stewart *et al.* 2018). Additionally, the combination of forcing factors can play a crucial role. For example, rising ocean temperatures and surface runoff in Greenland have a linear relationship with tidewater glacier retreat (Cowton *et al.* 2018). For Greenlandic glaciers, the combination of atmospheric and ocean forcing had the highest impact on glacier retreat and not a single driver. "For example, catchment-wide melt and the resulting runoff had a higher impact on the retreat of Greenlandic glaciers than local air temperatures (Cowton *et al.* 2018). Howat et al. (2008) found that peak events in air temperature and sea surface temperature can initialize glacier retreat. " (Baumhoer *et al.* 2021).

In this study, only a low correlation between snowmelt and calving front retreat was observed. The connection between surface melt and glacier retreat might be much stronger as the here used melt data were often inaccurate and low in resolution not able to represent surface hydrology accurately. The missing accuracy assessment of ERA5 snowmelt data further limited the trust in data quality and makes the reanalysis data prone to potentially large biases. Therefore, it is suggested to create a more detailed study on glacier retreat and surface melt with more accurate high-resolution surface melt data, as was previously published by Trusel et al. (2013). In this study, only average amounts of melt were used not able to account for extreme melt events. Further studies should also assess the effect of peak melt events on glacier calving. Surface melt can affect ice sheet stability in many ways. For example, lake ponding on the ice shelf surface effects ice shelf vulnerability (Joughin & Alley 2011), and the drainage of lakes might be connected to calving (Leeson *et al.* 2020) which requires further studies. In this study, only melt during the summer months was measured but recent studies showed, that also in the remaining seasons surface melt occurs (Kuipers Munneke *et al.* 2018, Zheng *et al.* 2020) which might be worth to consider in future assessments.

Ocean forcing for Antarctica could best be estimated by sea surface temperatures and changes in zonal wind as a proxy for upwelling CDW (Spence *et al.* 2014). Still, it is difficult to determine the magnitude of wind forcing necessary to induce calving front retreat. In Pine Island Bay, increases in positive wind speed by 0.25 m/s in combination with increasing sea surface temperatures and decreasing sea ice days came along with glacier retreat. In contrast, strengthening westerlies with increases of up to 1.2 m/s in one decade did not create such a strong ocean forcing that Shackleton, West, Abbot, and Getz Ice Shelf retreated significantly. This might have several reasons. First, ocean forcing on previously stable ice shelves with low ice flow velocities might not produce enough basal melt to cause calving due to a thinning ice shelf. Hence, forcing over several decades would be necessary to see effects at the calving front in those cases. Second, strengthening westerlies are only a proxy for basal melt. The actual basal melt rates below the ice shelves might vary strongly. The topography of the ocean floor and the specific bed topography of

each glacier can regulate the amount of warm upwelling CDW at the ice shelf bottom as well as tidal forcing. A retrograde bed will further destabilize the glacier at the grounding line (Scheuchl *et al.* 2016). Additionally, the amount of basal melt has no linear relationship with ocean temperature. Only a small increase in ocean temperature can cause four times as much basal melt (Jenkins *et al.* 2018). Consequently, there might be a tipping point where only a small increase in upwelling CDW might cause very high basal melt rates weakening the glacier. Third, the combination of environmental forcing determines the timing and magnitude of calving rather than a pinpointed amount of forcing. Fourth, the internal ice dynamics and morphology of glaciers and ice shelves will always influence glacier retreat. And last but not least, the ERA5 wind speed data underestimate the actual wind speed measured by weather stations and overestimate the wind speed over the ocean (Gossart *et al.* 2019, Belmonte Rivas & Stoffelen 2019). Hence the measured magnitude of wind speed data is not always realistic when compared for different coastal sectors. But the time series modelled at the same location are very consistent and accurately capture the inter-annual variability of wind speed (Gossart *et al.* 2019). To conclude, positive zonal winds can be a proxy for basal melt but to calculate the actual basal melt rate many more parameters have to be considered.

For the first time, a strong relationship of a relative rise in sea surface temperatures and calving front retreat was observed. Sea surface temperature changes occurred with glacier retreat when temperatures increased between 0.15 to 0.6°C. Those values were below the trend uncertainty stability of 0.01 °C per year (Embury 2019). Warming sea surface temperatures can cause melt at the margins of the glacier and reduce stabilizing fast ice (Larour 2004). This weakens the calving front and results in calving. Additionally, recently it was found, that warm sea surface temperatures melt the glacier front at the waterline and weaken the ice cliff stability. This results in the collapse of the ice cliff and glacier retreat (Mosbeux *et al.* 2020b).

Interestingly, higher mean air temperatures with an increase of up to 1.8°C observed in Victoria Land, Dronning Maud Land, and parts of the Antarctic Peninsula did not affect the calving front negatively. This suggests that rather temperature extreme events and above zero-degree days might be better parameters to assess atmospheric forcing. Further research is necessary to ascertain the connection between rising air temperatures, surface melt, and the subsequent effect on the glaciers and ice shelves. Decreasing sea ice days could be identified as destabilizing mechanism for the calving front but only if sea ice days decreased significantly (> 10 days) within the decade which might be of importance in the future. Just recently, the turning point in the so far increasing Antarctic sea ice extent was reached (Parkinson 2019).

The overall effect of a positive SAM on driving forces for glacier retreat should be considered. All identified drivers such as wind direction, sea surface temperatures, föhn, snowmelt, and sea ice cover change with variations in SAM (Verdy *et al.* 2006, Kwok & Comiso 2002, Marshall 2007, Tedesco & Monaghan 2009, Cape *et al.* 2015). Extreme positive peaks of SAM influence ice shelf disintegration, as shown for the Wordie Ice Shelf. Rising greenhouse gases and ozone depletion will cause a trend to more positive phases of SAM (Wang *et al.* 2014, Paeth & Pollinger 2010) which will further strengthen forcing factors of glacier retreat in the future.

6.5 Summary

This chapter for the first time presented a circum-Antarctic record on calving front change for the last two decades. The Antarctic Ice Sheet shrank by 29,618±1193 km^2 in extent between 1997-2008 and gained an area of 7,108±1029 km^2 between 2009-2018. Glacier retreat concentrated along the Antarctic Peninsula and West Antarctica. The only East Antarctic coastal sector experiencing simultaneous calving front retreat was Wilkes Land in 2009-2018.

This analysis was limited to two decades of calving front change restricted by three time steps of available coastline data. Even though this study identified numerous drivers of calving front retreat, the results might be biased by the strong inter-annual variability of assessed climatic and cryospheric change. Global warming and the natural cycle of glacier calving persist on longer time scales that could not be entirely covered by this study as data availability delimited the study design. Nevertheless, this study for the first time revealed drivers for circum-Antarctic calving front changes on an inter-annual time scale. It was found that strengthening westerlies, snowmelt, rising sea surface temperatures, and decreasing sea ice cover forced glacier retreat whereas relative changes in air temperature did not. Nevertheless, it should be remembered that calving front retreat is often not forced by a single driver but the result of an interaction between internal ice dynamics, bed topography, external mechanical and environmental forcing.

The strengthening of identified environmental drivers was closely connected to positive phases of SAM. With regard to increasing greenhouse gases and ozone depletion, positive phases of SAM will occur more often and force glacier retreat even further in the future. To better assess the vulnerability of glaciers and ice shelves to external forcing in the future, it is essential to better understand surface melt processes, the effect of ponding and lake drainage at the ice shelf surface, runoff, and the effect of peak melt events. Equally important is the understanding of upwelling CDW caused by poleward shifting westerlies. More in-situ ocean temperature measurements could help to calibrate models using indirect measurements like wind direction to better predict basal melt. Being able to use easy-to-

access remote sensing and climate data to predict ice shelf and glacier front retreat can help to better parametrize sea level-rise-models in the future.

Chapter 7

7 Synthesis & Outlook

This final chapter presents a brief summary on the results of this dissertation. The final conclusive findings are outlined in regard to the research questions and objectives defined in the introduction of this thesis. Further on, the future potential of earth observation is discussed with respect to the extraction and monitoring of Antarctic glacier and ice shelf fronts. Recommendations on future research projects and further development potentials of *Antarctic*LINES are presented.

7.1 Conclusive Findings

Global sea-level rise will have severe effects on coastal regions in the future. Especially in coastal megacities, millions of people are exposed to storm floods and rising sea levels. The Antarctic Ice Sheet will be the major contributor of sea-level rise after the 21th century (Bamber *et al.* 2019, Pfeffer *et al.* 2008). Glacier and ice shelf extents control the ice flow of the Antarctic Ice Sheet by creating buttressing effects. This safety band largely affects the magnitude of Antarctica's contribution to global sea-level rise. Recent disintegration events of Antarctic ice shelves along the Antarctic Peninsula and massive glacier retreat in West Antarctica raise questions on the stability of the Antarctic safety band and potential effects of climate change on calving fronts. Earth observation offers the only opportunity for frequent and large-scale monitoring of glacier and ice shelf retreat in remote areas like Antarctica.

This dissertation addressed the urgent need for frequent mapping of circum-Antarctic calving front positions by providing a framework for automatic calving front extraction. Sentinel-1 satellite imagery provides an abundance of data which can only be analysed by an automatized big data approach transferable in space and time. The overall goal of this

thesis was not only to present *Antarctic*LINES as a framework for calving front extraction, but also to assess current changes in glacier and ice shelf front location and identify potential drivers of glacier retreat.

In the beginning of this thesis (see chapter 1) the main research questions and objectives were defined and subsequently addressed in the chapters 3-6. A final answer for each research question is provided in the following.

Research Question 1:

What is the relevance of Antarctic glacier and ice shelf fronts? Which calving and disintegration events were observed in the past? How good is the circum-Antarctic data availability of glacier and ice shelf front positions?

Antarctic glacier and ice shelf fronts are of great societal relevance as they influence the magnitude of sea-level rise contribution from Antarctica. The greater the extent of ice shelves or glaciers is, the higher are the buttressing effects decreasing ice discharge. Furthermore, information on glacier and ice shelf front fluctuations can help to better understand ice dynamics. Changes in calving front position in combination with ice flow velocities, thickness changes, grounding line position, bed topography and the hydrology of a glacier can help to understand glacier dynamics especially in regard to a changing climate. A comprehensive review on remote sensing of Antarctic glacier and ice shelf front dynamics was conducted as defined by objective 1. This revealed that seven out of twelve ice shelves of the Antarctic Peninsula already disintegrated. Further on, strong glacier retreat occurred at Pine Island Bay in West Antarctica. Pine Island and Thwaites Glacier alone have contributed to global sea-level rise almost twice as much as the entire Antarctic Peninsula. That signalises that the retreat of single glaciers can have tremendous effects. The East Antarctic Ice Sheet was found to be relatively stable except for Wilkes Land where glaciers and ice shelves started to disintegrate simultaneously. Major gaps in the circum-Antarctic calving front record were identified. Earliest records of calving front position existed since first ship expeditions in the 19th century. Later records were limited by the availability of remote sensing imagery dating back to 1947 for the Antarctic Peninsula and to the 1970s for East Antarctica. For the WAIS, only short glacier and ice shelf front records existed often not dating back further than 25 years. Most studies on glacier and ice shelf fronts were conducted along the Antarctic Peninsula and Victoria Land whereas West Antarctica, Wilkes Land and Dronning Maud Land were studied less. The majority of glacier fronts were studied less than three times, often only once. Only ice shelves and glaciers that experienced major disintegration events and retreat were studied more often such as the Larsen B, Wilkins and Wordie Ice Shelf and the Pine Island and Thwaites Glacier. The review identified a lack of gapless calving front records created from continuous and comparable observations. Calving front locations were often mapped per

decade and in rare cases inter-annually. To assess seasonal fluctuations in glacier and ice shelf fronts, intra-annual measurements are necessary. With the current state of existing calving front studies, it is not possible to assess recent circum-Antarctic calving front location changes on a frequent and comparable basis and requests frequent and standardized large-scale mapping of the Antarctic coastline.

Research Question 2:

What is the potential of earth observation for the assessment of Antarctic calving fronts? What are the advantages and challenges of remote sensing based calving front studies? Which methods exist to extract calving fronts and what technical innovations can be achieved by integrating big data and artificial intelligence approaches?

In remote areas like Antarctica the in-situ large-scale monitoring of glaciers and ice shelves would be very time and cost intensive. Therefore, earth observation provides continuous and reliable observations from space which could not be achieved by ground truth data from field work. Nowadays, even medium resolution satellite images are freely available almost at real-time. This allows inexpensive and near-term analysis for large-scale regions. Current developments in remote sensing ensure precise orthorectification enabling accurate measurements of even small positional changes in calving front movement. A comprehensive literature review revealed that calving fronts were mostly mapped on the basis of optical airborne and space-borne imagery. Optical imagery is easy to handle as only little pre-processing is required and the contrast between ice and ocean is mostly clearly visible allowing a straightforward delineation of the calving front. Even though, clouds and polar darkness limit the data availability of optical imagery, Landsat satellite imagery was the most applied data source for calving front mapping. Data from ERS and Radarsat satellites were the second most applied imagery sources. SAR data requires expert knowledge for calving front delineation but allows the generation of continuous time series of glacier and ice shelf front movement due to all-weather imaging capabilities. Limitations only exist during phases of strong surface melt in summer. A review on existing calving front extraction methods found that in 85 % of all studies time intensive manual delineation was used to extract glacier fronts. Today's amount of Antarctic satellite imagery is beyond the scope of manual delineations. Consequently, the abundance of remote sensing data requires a big data-oriented processing chain with an automated algorithm for glacier front extraction. In 7 % of the studies (semi-)automatic approaches were developed but a fully automated calving front extraction processing chain did not exist. Artificial intelligence (AI) could be an enormous gain to tackle the challenge of automated calving front extraction. The ability of AI algorithms to learn from data can be used to train an algorithm on selected manual delineated glacier and ice shelf fronts over the Antarctic coastline. Antarctica is geographically limited and shapes of glaciers and ice shelves are similar in appearance in different coastal sectors. Hence, training an AI

algorithm only on selected glaciers could yield an algorithm that is transferable in space and time for entire Antarctica. A big data based approach, including the usage of server infrastructures, is needed as weekly (or more frequent) radar satellite acquisitions over the entire Antarctic coastline would overload a desktop based processing infrastructure.

Research Question 3:

How can dense Sentinel-1 time series support the monitoring of calving front fluctuations? How can deep learning be used to automatically extract Antarctic glacier and ice shelf fronts? How can a novel fully-automated framework for circum-Antarctic calving front extraction be implemented that is transferable in space and time?

The literature review identified a need for continuous and seasonal time series of calving front fluctuations. Previously used satellite image sources were either limited by polar darkness and weather or by high acquisition costs. Since 2014, Sentinel-1A provides dual-polarized SAR satellite data over the Antarctic coastline with a revisit time of < 12 days. Since the launch of Sentinel-1B in 2016, the revisit time even decreased to < 6 days which allows the tracking of calving events near real-time. For the first time, Sentinel-1 data allows the monitoring of the Antarctic coastline with open access medium resolution imagery perfectly applicable for creating continuous dense time series on glacier and ice shelf front fluctuations.

Previously, the automatization of calving front extraction for SAR data was not possible due to changing sea ice conditions, icebergs, mélange, wind-roughened ocean and surface melt. Especially similar backscatter values of different surface materials made the simple classification of ice and ocean impossible as rather the shape of a feature is decisive for locating the calving front. At this point, current developments in computer vison on deep learning for image processing tasks leveraged the automatization of calving front extraction. Image segmentation techniques not only considering pixel values but the spatial context of an image were able to outperform traditional image processing techniques. As a result, the deep learning architecture U-Net was selected to extract calving fronts based on their unique shape instead of just backscatter characteristics. The U-Net is a well-known architecture for image segmentation especially useful for low contrast images and little training data. Chapter 5 of this dissertation presented how the U-Net was integrated in a fully-automated processing chain from downloading Sentinel-1 data to a final extracted calving front. For all test and training regions an overall classification accuracy of 0.90 was achieved. The automatic extracted fronts compared to manual delineations deviated between 35 m and 153 m depending on assessed glacier/ice shelf. The developed methodical framework *Antarctic*LINES did not only prove to create accurate calving front extractions but also the ability to generate monthly time series of glacier front movements. Planned launches of Sentinel-1 C and D will allow the future monitoring of Antarctic calving front dynamic with the presented method. Additionally, the modification of

*Antarctic*LINES for ERS and Envisat data can prolong the time series until the early 1990s. Taken together, this abundance of data can provide 40-50 years of circum-Antarctic glacier and ice shelf front dynamics in the future.

Research Question 4:

Which different patterns in intra-annual calving front fluctuations can be observed? Which circum-Antarctic patterns of glacier and ice shelf front change occurred over the last two decades and what were potential driving forces?

In chapter 5 intra-annual time series for four glaciers and ice shelves were presented. Each of them had very individual calving front dynamics - reaching from steady advance at Denman Glacier, frequent calving at Pine Island Glacier, a major calving event at Amery Ice Shelf to the potential disintegration of Glenzer Glacier. Seasonality in glacier and ice shelf front fluctuations as known for Greenland could not be observed. Rather bi-annual events either due to intense surface melt or calving were apparent. Surface melt made the exact location of the front position difficult and could have distorted results during summer months. The overall rate of calving front movement over the entire observation period was not affected by missing measurements during summer.

Finally, the literature review emphasized gaps in the circum-Antarctic calving front position data set compiled from all existing CFL measurements. Especially, measurements were not of comparable time spans and methods for calving front position change varied. To address this problem, *Antarctic*LINES was used to extract the entire Antarctic coastline for 2018. The coastline 2018 was compared to previous coastline products from 1997 and 2009 in order to calculate two decades of long-term calving front change in Antarctica. The results revealed that the Antarctic Ice Sheet shrank 29,618±1193 km^2 in extent between 1997-2008-2008 and gained an area of 7,108±1029 km^2 between 2009-2018. Retreat dominated the first decade as the largest ice shelves Ross and Ronne experienced major calving events. Further retreat over both decades was observed for the Antarctic Peninsula and West Antarctica. East Antarctica's glacier and ice shelves were relatively stable experiencing occasional calving within the natural cycle of advance and retreat. The only exception was Wilkes Land where almost all glaciers retreated between 2009 and 2018.

To identify potential environmental drivers of glacier retreat, changes in glacier and ice shelf extent over the last two decades were correlated with changes in climate variables. The outcome was that strengthening westerlies, snowmelt, rising sea surface temperatures and decreasing sea ice cover forced glacier retreat whereas relative changes in mean air temperature did not. Hence, the connection between calving front retreat and atmospheric forcing could not be entirely revealed and further analysis regarding threshold behaviour regarding extreme events are necessary. Furthermore, this study demonstrated the influence of environmental drivers of calving front retreat but also revealed that mostly a combination

of factors such as internal ice dynamics, bed topography, glacier morphology as well as external mechanical and environmental cause calving front change. It should be considered that the study design was limited to three time steps of available coastline data and the accuracy of modelled climate variables. Calving cycles and climate warming might persist for longer time scales than this study covered. Nevertheless, for the first time this analysis assessed circum-Antarctic calving front change and identified drivers of glacier retreat for two decades.

The Southern Annular Mode was identified to be of overriding importance as positive years of SAM intensify the forcing of the identified drives. Hence, the SAM could be the overall driving force of glacier retreat. In regard to rising CO_2 concentrations and ozone depletion, positive SAM years might increase in the future and put additional pressure on Antarctic glaciers and ice shelves causing further glacier retreat and ice shelf disintegration.

7.2 Towards the Monitoring of Antarctic Calving Fronts

Glacier and ice shelf fronts are sensitive indicators of environmental change. Monitoring changes in calving front position can provide valuable information on changing boundary conditions impacting the Antarctic Ice Sheet. The framework *Antarctic*LINES was designed to create Antarctic glacier and ice shelf front time series. This novel framework has a great potential to be integrated in a web service to provide Antarctic calving front data to the scientific community. The open access policy of Copernicus Sentinel data allows the continuous use of acquisitions over the Antarctic coastline. The satellite data archives for Sentinel-1 data will grow within the next decade as mission continuity is ensured by the future launch of Sentinel-1C and 1D. Building a completely autonomous monitoring for monthly circum-Antarctic calving front positions would require further improvements. Training data over the Western Antarctic Peninsula should be included to achieve more accurate results for smaller glaciers and steep rock coast. To prolong time series, SAR data from ERS and Envisat missions can be included for training. So far, over 10,000 scenes acquired between 1991 and 2011 have been sighted in the DLR archives. Further on, a data integrity check for extracted glacier fronts should be integrated to guarantee the exclusion of acquisitions during summer melt. The final extracted calving front time series for major glaciers and ice shelves could then be provided to the scientific community via web services in near real-time. The incorporation of statistics on calving front advance and retreat rates could allow a better assessment of tendencies in glacier and ice shelf front fluctuations. Additionally, an alert system for major calving events could provide almost real-time information on ice shelf disintegration.

The results of this dissertation made an important step towards the automated monitoring of Antarctic calving fronts. For the first time circum-Antarctic changes in

glacier and ice shelf extent over the last two decades were presented. Potential drivers of glacier retreat were identified, thus providing important information for future changes in the Antarctic coastline. The spatial and temporal transferability of the presented framework *Antarctic*LINES was used to assess seasonal changes in calving front movement and will be extended to a circum-Antarctic glacier and ice shelf front monitoring system which will provide essential information for modelling calving processes and the future contribution of the Antarctic Ice Sheet to global sea level rise.

8 References

ADD. 2020. Antarctic Digital Database Available at: https://www.add.scar.org/ [Accessed February 3, 2020].

AI, S., WANG, S., LI, Y., MOHOLDT, G., ZHOU, C., LIU, L. & YANG, Y. 2019. High-precision ice-flow velocities from ground observations on Dalk Glacier, Antarctica. *Polar Science*, **19**, 13–23, 10.1016/j.polar.2018.09.003.

ALBRECHT, T. & LEVERMANN, A. 2014. Spontaneous ice-front retreat caused by disintegration of adjacent ice shelf in Antarctica. *Earth and Planetary Science Letters*, **393**, 26–30, 10.1016/j.epsl.2014.02.034.

ALLEY, R.B., HORGAN, H.J., JOUGHIN, I., CUFFEY, K.M., DUPONT, T.K., PARIZEK, B.R., ANANDAKRISHNAN, S. & BASSIS, J. 2008. A simple law for ice-shelf calving. *Science*, **322**, 1344–1344.

AMRC. 2020. The Antarctic Meteorological Research Center. *Automatic Weather Station (AWS) Program* Available at: http://amrc.ssec.wisc.edu/ [Accessed May 14, 2020].

ANDERSON, R., JONES, D.H. & GUDMUNDSSON, G.H. 2014. Halley Research Station, Antarctica: calving risks and monitoring strategies. *Natural Hazards and Earthsystem Sciences*, **14**, 917–927, 10.5194/nhess-14-917-2014}.

ATCM. 2017. *Antarctic Treaty Consultative Meeting. Compilation of Key Documents of the Antarctic Treaty System. Third edition.* 3rd ed. Buenos Aires: Secretariat of the Antarctic Treaty.

AUDEBERT, N., LE SAUX, B. & LEFÈVRE, S. 2016. Semantic Segmentation of Earth Observation Data Using Multimodal and Multi-scale Deep Networks. *In* Computer Vision – ACCV 2016. Springer, Cham, 180–196., 10.1007/978-3-319-54181-5_12.

BAMBER, J.L., OPPENHEIMER, M., KOPP, R.E., ASPINALL, W.P. & COOKE, R.M. 2019. Ice sheet contributions to future sea-level rise from structured expert judgment. *Proceedings of the National Academy of Sciences*, **116**, 11195–11200, 10.1073/pnas.1817205116.

BAMBER, J.L., WESTAWAY, R.M., MARZEION, B. & WOUTERS, B. 2018. The land ice contribution to sea level during the satellite era. *Environmental Research Letters*, **13**, 063008, 10.1088/1748-9326/aac2f0.

BASSIS, J.N. 2011. The statistical physics of iceberg calving and the emergence of universal calving laws. *Journal of Glaciology*, **57**, 3–16.

BASSIS, J.N., FRICKER, H.A., COLEMAN, R. & MINSTER, J.-B. 2008. An investigation into the forces that drive ice-shelf rift propagation on the Amery Ice Shelf, East Antarctica. *Journal of Glaciology*, **54**, 17–27.

BAUMHOER, C.A., DIETZ, A.J., KNEISEL, C. & KUENZER, C. 2019. Automated Extraction of Antarctic Glacier and Ice Shelf Fronts from Sentinel-1 Imagery Using Deep Learning. *Remote Sensing*, **11**, 2529, 10.3390/rs11212529.

BAUMHOER, C.A., DIETZ, A.J., KNEISEL, C., PAETH, H. & KUENZER, C. 2021. Environmental drivers of circum-Antarctic glacier and ice shelf front retreat over the last two decades. *The Cryosphere*, **15**, 2357–2381, 10.5194/tc-15-2357-2021.

BAUMHOER, DIETZ, A., DECH, S. & KUENZER, C. 2018. Remote Sensing of Antarctic Glacier and Ice-Shelf Front Dynamics—A Review. *Remote Sensing*, **10**, 1445, 10.3390/rs10091445.

BELMONTE RIVAS, M. & STOFFELEN, A. 2019. Characterizing ERA-Interim and ERA5 surface wind biases using ASCAT. *Ocean Science*, **15**, 831–852, 10.5194/os-15-831-2019.

BENN, D.I., WARREN, C.R. & MOTTRAM, R.H. 2007. Calving processes and the dynamics of calving glaciers. *Earth-Science Reviews*, **82**, 143–179.

BEVAN, S.L., LUCKMAN, A.J. & MURRAY, T. 2012. Glacier dynamics over the last quarter of a century at Helheim, Kangerdlugssuaq and 14 other major Greenland outlet glaciers. *The Cryosphere*, **6**, 923–937.

BINDOFF, N.L., STOTT, P.A., ACHUTARAO, K.M., ALLEN, M.R., GILLETT, N., GUTZLER, D., HANSINGO, K., et al. 2013. Detection and attribution of climate change: from global to regional. *In Climate Change 2013: The Physical Science Basis. Contribution of Working Group I to the Fifth Assessment Report of the Intergovernmental Panel on Climate Change*. Cambridge, United Kingdom and New York, NY, USA: Cambridge University Pres.

BINDSCHADLER, R.A. 1998. Monitoring ice sheet behavior from space. *Reviews of Geophysics*, **36**, 79–104.

BINGHAM, R.G., VAUGHAN, D.G., KING, E.C., DAVIES, D., CORNFORD, S.L., SMITH, A.M., ARTHERN, R.J., et al. 2017. Diverse landscapes beneath Pine Island Glacier influence ice flow. *Nature Communications*, **8**, 1618, 10.1038/s41467-017-01597-y.

BOGDANOV, A.V., SANDVEN, S., JOHANNESSEN, O.M., ALEXANDROV, V.Y. & BOBYLEV, L.P. 2005. Multisensor approach to automated classification of sea ice image data. *IEEE Transactions on geoscience and remote sensing*, **43**, 1648–1664.

BOZKURT, D., BROMWICH, D.H., CARRASCO, J., HINES, K.M., MAUREIRA, J.C. & RONDANELLI, R. 2020. Recent Near-surface Temperature Trends in the Antarctic Peninsula from Observed, Reanalysis and Regional Climate Model Data. *Advances in Atmospheric Sciences*, **37**, 477–493, 10.1007/s00376-020-9183-x.

BRANCATO, V., RIGNOT, E., MILILLO, P., MORLIGHEM, M., MOUGINOT, J., AN, L., SCHEUCHL, B., et al. 2020. Grounding Line Retreat of Denman Glacier, East Antarctica, Measured With COSMO-SkyMed Radar Interferometry Data. *Geophysical Research Letters*, **47**, 10.1029/2019GL086291.

BRANDT-KREINER, M., LAVELLE, J., TONBOE, R., HOWE, E., LAVERGNE, T., KILLIE, M.A., SORENSEN, A., EASTWOOD, S. & NEUVILLE, A. 2019. Global Sea Ice ConcentrationClimate Data RecordValidation Report. OSI-450 and OSI-430-b. (1.1) Available at: http://osisaf.met.no/docs/osisaf_cdop3_ss2_valrep_sea-ice-conc-climate-data-record_v1p1.pdf.

BRAUN, M., HUMBERT, A. & MOLL, A. 2009. Changes of Wilkins Ice Shelf over the past 15 years and inferences on its stability. *The Cryosphere*, **3**, 41–56, 10.5194/tc-3-41-2009.

BROMWICH, D.H., NICOLAS, J.P. & MONAGHAN, A.J. 2011. An Assessment of Precipitation Changes over Antarctica and the Southern Ocean since 1989 in Contemporary Global Reanalyses. *Journal of Climate*, **24**, 4189–4209, 10.1175/2011JCLI4074.1.

BROMWICH, D.H., NICOLAS, J.P., MONAGHAN, A.J., LAZZARA, M.A., KELLER, L.M., WEIDNER, G.A. & WILSON, A.B. 2013. Central West Antarctica among the most rapidly warming regions on Earth. *Nature Geoscience*, **6**, 139–145, 10.1038/ngeo1671.

C3S. 2017. Copernicus Climate Change Service. ERA5: Fifth generation of ECMWF atmospheric reanalyses of the global climate. *Copernicus Climate Change Service Climate Data Store (CDS)* Available at: https://cds.climate.copernicus.eu/cdsapp#!/home [Accessed February 5, 2020].

CAPE, M.R., VERNET, M., SKVARCA, P., MARINSEK, S., SCAMBOS, T.A. & DOMACK, E. 2015. Foehn winds link climate-driven warming to ice shelf evolution in Antarctica: Foehn winds link climate driven warming. *Journal of Geophysical Research: Atmospheres*, **120**, 11,037-11,057, 10.1002/2015JD023465.

CASPAR, C., COLIN, O., LAUR, H., TELL, B.R., MATHOT, E., TANDURELLA, G., GONCALVES, P. & BRITO, F. 2007. Generation of ENVISAT ASAR mosaics accessible on-line. *In IEEE International Geoscience and Remote Sensing Symposium*. 1405–1408.

CATANIA, G.A., STEARNS, L.A., SUTHERLAND, D.A., FRIED, M.J., BARTHOLOMAUS, T.C., MORLIGHEM, M., SHROYER, E. & NASH, J. 2018. Geometric Controls on Tidewater Glacier Retreat in Central Western Greenland. *Journal of Geophysical Research: Earth Surface*, **123**, 2024–2038, 10.1029/2017JF004499.

CHRISTIANSON, K., BUSHUK, M., DUTRIEUX, P., PARIZEK, B.R., JOUGHIN, I.R., ALLEY, R.B., SHEAN, D.E., et al. 2016. Sensitivity of Pine Island Glacier to observed ocean forcing: PIG response to ocean forcing. *Geophysical Research Letters*, **43**, 10,817-10,825, 10.1002/2016GL070500.

CHUTER, S.J., MARTÍN-ESPAÑOL, A., WOUTERS, B. & BAMBER, J.L. 2017. Mass balance reassessment of glaciers draining into the Abbot and Getz Ice Shelves of West Antarctica: Getz and Abbot Mass Balance Reassessment. *Geophysical Research Letters*, **44**, 7328–7337, 10.1002/2017GL073087.

CIA. 2020. The World Fact Book -Antarctica. *Central Intelligence Agency, Antarctica* Available at: https://www.cia.gov/library/publications/the-world-factbook/geos/ay.html [Accessed May 13, 2020].

CLEM, K.R., RENWICK, J.A. & MCGREGOR, J. 2017. Large-Scale Forcing of the Amundsen Sea Low and Its Influence on Sea Ice and West Antarctic Temperature. *Journal of Climate*, **30**, 8405–8424, 10.1175/JCLI-D-16-0891.1.

CLEM, K.R., RENWICK, J.A., MCGREGOR, J. & FOGT, R.L. 2016. The relative influence of ENSO and SAM on Antarctic Peninsula climate: Antarctic Peninsula Climate Variability. *Journal of Geophysical Research: Atmospheres*, **121**, 9324–9341, 10.1002/2016JD025305.

COMISO, J.C. 2000. Variability and Trends in Antarctic Surface Temperatures from In Situ and Satellite Infrared Measurements. *Journal of Climate*, **13**, 1674–1696.

COMISO, J.C., GERSTEN, R.A., STOCK, L.V., TURNER, J., PEREZ, G.J. & CHO, K. 2017. Positive Trend in the Antarctic Sea Ice Cover and Associated Changes in Surface Temperature. *Journal of Climate*, **30**, 2251–2267, 10.1175/JCLI-D-16-0408.1.

COMISO, J.C. & STEFFEN, K. 2001. Studies of Antarctic sea ice concentrations from satellite data and their applications. *Journal of Geophysical Research: Oceans*, **106**, 31361–31385, 10.1029/2001jc000823.

CONMAP. 2020. Antarctic Facilities. *Antarctic Facilities, Council of Managers of National Antarctic Programs* Available at: https://github.com/PolarGeospatialCenter/comnap-antarctic-facilities/blob/master/dist/COMNAP_Antarctic_Facilities_Master.xls [Accessed May 13, 2020].

COOK, A.J., FOX, A.J., VAUGHAN, D.G. & FERRIGNO, J.G. 2005. Retreating glacier fronts on the Antarctic Peninsula over the past half-century. *Science*, **308**, 541–544.

COOK, A.J., HOLLAND, P.R., MEREDITH, M.P., MURRAY, T., LUCKMAN, A. & VAUGHAN, D.G. 2016. Ocean forcing of glacier retreat in the western Antarctic Peninsula. *Science*, **353**, 283–286.

COOK, A.J. & VAUGHAN, D.G. 2010. Overview of areal changes of the ice shelves on the Antarctic Peninsula over the past 50 years. *The Cryosphere*, **4**, 77–98, 10.5194/tc-4-77-2010.

COWTON, T.R., SOLE, A.J., NIENOW, P.W., SLATER, D.A. & CHRISTOFFERSEN, P. 2018. Linear response of east Greenland's tidewater glaciers to ocean/atmosphere warming. *Proceedings of the National Academy of Sciences*, **115**, 7907–7912, 10.1073/pnas.1801769115.

DARELIUS, E., FER, I. & NICHOLLS, K.W. 2016. Observed vulnerability of Filchner-Ronne Ice Shelf to wind-driven inflow of warm deep water. *Nature Communications*, **7**, 12300, 10.1038/ncomms12300.

DAVIES, B.J., CARRIVICK, J.L., GLASSER, N.F., HAMBREY, M.J. & SMELLIE, J.L. 2012. Variable glacier response to atmospheric warming, northern Antarctic Peninsula, 1988-2009. *The Cryosphere*, **6**, 1031–1048, 10.5194/tc-6-1031-2012}.

DE RYDT, J., GUDMUNDSSON, G.H., NAGLER, T. & WUITE, J. 2019. Calving cycle of the Brunt Ice Shelf, Antarctica, driven by changes in ice shelf geometry. *The Cryosphere*, **13**, 2771–2787, 10.5194/tc-13-2771-2019.

DE RYDT, J., GUDMUNDSSON, G.H., ROTT, H. & BAMBER, J.L. 2015. Modeling the instantaneous response of glaciers after the collapse of the Larsen B Ice Shelf. *Geophysical Research Letters*, **42**, 5355–5363, 10.1002/2015GL064355}.

DEB, P., ORR, A., BROMWICH, D.H., NICOLAS, J.P., TURNER, J. & HOSKING, J.S. 2018. Summer Drivers of Atmospheric Variability Affecting Ice Shelf Thinning in the Amundsen Sea Embayment, West Antarctica. *Geophysical Research Letters*, **45**, 4124–4133, 10.1029/2018GL077092.

DECONTO, R.M. & POLLARD, D. 2016. Contribution of Antarctica to past and future sea-level rise. *Nature*, **531**, 591–597, 10.1038/nature17145.

DEPOORTER, M.A., BAMBER, J.L., GRIGGS, J.A., LENAERTS, J.T.M., LIGTENBERG, S.R.M., VAN DEN BROEKE, M.R. & MOHOLDT, G. 2013. Calving fluxes and basal melt rates of Antarctic ice shelves. *Nature*, **502**, 89–89, 10.1038/nature12567.

DIETZ, A.J., KUENZER, C., GESSNER, U. & DECH, S. 2012. Remote sensing of snow--a review of available methods. *International Journal of Remote Sensing*, **33**, 4094–4134, 10.1080/01431161.2011.640964.

DIRSCHERL, M., DIETZ, A.J., KNEISEL, C. & KUENZER, C. 2020. Automated Mapping of Antarctic Supraglacial Lakes Using a Machine Learning Approach. *Remote Sensing*, **12**, 1203, 10.3390/rs12071203.

DOAKE, C.S.M., CORR, H.F.J., ROTT, H., SKVARCA, P. & YOUNG, N.W. 1998. Breakup and conditions for stability of the northern Larsen Ice Shelf, Antarctica. *Nature*, **391**, 778–780.

DODDS, K. 2010. Governing Antarctica: Contemporary Challenges and the Enduring Legacy of the 1959 Antarctic Treaty. *Global Policy*, **1**, 108–115, 10.1111/j.1758-5899.2009.00006.x.

DOMACK, E., DURAN, D., LEVENTER, A., ISHMAN, S., DOANE, S., MCCALLUM, S., AMBLAS, D., RING, J., GILBERT, R. & PRENTICE, M. 2005. Stability of the Larsen B ice shelf on the Antarctic Peninsula during the Holocene epoch. *Nature*, **436**, 681–685, 10.1038/nature03908.

DUTRIEUX, P., DE RYDT, J., JENKINS, A., HOLLAND, P.R., HA, H.K., LEE, S.H., STEIG, E.J., DING, Q., ABRAHAMSEN, E.P. & SCHRODER, M. 2014. Strong Sensitivity of Pine Island Ice-Shelf Melting to Climatic Variability. *Science*, **343**, 174–178, 10.1126/science.1244341.

DUTRIEUX, P., VAUGHAN, D.G., CORR, H.F.J., JENKINS, A., HOLLAND, P.R., JOUGHIN, I. & FLEMING, A.H. 2013. Pine Island glacier ice shelf melt distributed at kilometre scales. *CRYOSPHERE*, **7**, 1543–1555, 10.5194/tc-7-1543-2013}.

DWD. 2020. Deutscher Wetterdienst. Klimadatenwelt Antarktis Available at: https://www.dwd.de/DE/leistungen/klimadatenwelt/antarktis/stationen /stationen_node.html [Accessed May 18, 2020].

EMBURY, O. 2019. Product Quality Assessment Report. Sea Surface Temperature. Available at: http://datastore.copernicus-climate.eu/c3s/published-forms/c3sprod/satellite-sea-surface-temperature/documentation/v2.0/D2.SST.2-v2.1_PQAR_of_v2SST_products_v3.1_APPROVED_Ver1.pdf [Accessed September 28, 2019].

ESA. 2020a. European Space Agency. Aquisition Segments Archive. Available at: https://sentinel.esa.int/web/sentinel/missions/sentinel-1/observation-scenario/acquisition-segments/archive [Accessed May 26, 2020].

ESA. 2020b. European Space Agency. Observation Scenario Archive. Available at: https://sentinels.copernicus.eu/web/sentinel/missions/sentinel-1/observation-scenario/archive [Accessed May 26, 2020].

ESA. 2012. *European Space Agency. Sentinel-1: ESA's radar observatory mission for GMES operational services*. Noordwijk, The Netherlands: ESA Communications, 86 pp.

ESA. 2020c. European Space Agency. Sentinel-1 SAR Technical Guide.

FAHNESTOCK, M., BINDSCHADLER, R.A., KWOK, R. & JEZEK, K. 1993. Greenland ice sheet surface properties and ice dynamics from ERS-1 SAR imagery. *Science*, **262**, 1530–1534.

FERRIGNO, FOLEY, K.M., SWITHINBANK, C. & WILLIAMS JR, R.S. 2007. Coastal-Change and Glaciological Mapof the Northern Ross Ice Shelf Area,Antarctica: 1962–2004. *USGS coastal change maps*, 1–11.

FERRIGNO, FOLEY, K.M., SWITHINBANK, C., WILLIAMS JR, R.S. & DAILIDE, L. 2005. Coastal-Change And Glaciological Map Of The Ronne Ice Shelf Area,Antarctica: 1974–2002. *USGS coastal change maps*, **I-2600-D**, 1–11.

FERRIGNO, J.G., COOK, A.J., MATHIE, A., WILLIAMS, R., SWITHINBANK, C., FOLEY, K.M., FOX, A.J., THOMSON, J.W. & SIEVERS, J. 2009. *Coastal-change and Glaciological Map of the Palmer Land Area, Antarctica, 1947-2009. Geologic Investigations Series Map I–2600–C.* Virginia: US Department of the Interior, US Geological Survey.

FERRIGNO, J.G. & GOULD, W.G. 1987. Substantial changes in the coastline of Antarctica revealed by satellite imagery. *Polar Record*, **23**, 577–583, 10.1017/s003224740000807x.

FERRIGNO, J.G., WILLIAMS JR, R.S., ROSANOVA, C.E., LUCCIIITTA, B.K. & SWITHINBANK, C. 1998. Analysis of coastal change in Marie Byrd Land and Ellsworth Land, West Antarctica, using Landsat imagery. *Annals of Glaciology*, **27**, 33–40.

FERRIGNO, J.G., WILLIAMS, R.S. & FOLEY, K.M. 2004. Coastal-change and glaciological map of the Saunders Coast area, Antarctica: 1972-97. *In* Jacka, J., *ed.* ANNALS OF GLACIOLOGY, VOL 39, 2004. 245–250., 10.3189/172756404781814285.

FOUNTAIN, A.G., GLENN, B. & SCAMBOS, T.A. 2017. The changing extent of the glaciers along the western Ross Sea, Antarctica. *Geology*, **45**, 927–930.

FOX, A.J. & COOPER, R. 1994. Measured properties of the Antarctic ice sheet derived from the SCAR Antarctic digital database. *Polar Record*, **30**, 201–206.

FRETWELL, P., PRITCHARD, H.D., VAUGHAN, D.G., BAMBER, J.L., BARRAND, N.E., BELL, R., BIANCHI, C., et al. 2013. Bedmap2: improved ice bed, surface and thickness datasets for Antarctica. *The Cryosphere*, **7**.

FREZZOTTI, M. 1997. Ice front fluctuation, iceberg calving flux and mass balance of Victoria Land glaciers. *Antarctic Science*, **9**, 61–73.

FREZZOTTI, M., GIMBELLI, A. & FERRIGNO, J.G. 1998. Ice-front change and iceberg behaviour along Oates and George V Coasts, Antarctica, 1912-96. *Annals of Glaciology*, **27**, 643–650.

FREZZOTTI, M. & POLIZZI, M. 2002. 50 years of ice-front changes between the Adélie and Banzare Coasts, East Antarctica. *Annals of Glaciology*, **34**, 235–240–235–240, 10.3189/172756402781817897.

FRICKER, H.A., YOUNG, N.W., ALLISON, I. & COLEMAN, R. 2002. Iceberg calving from the Amery Ice Shelf, East Antarctica. *Annals of Glaciology*, **34**, 241–246–241–246, 10.3189/172756402781817581.

FRIEDL, P., SEEHAUS, T.C., WENDT, A., BRAUN, M.H. & HÖPPNER, K. 2018. Recent dynamic changes on Fleming Glacier after the disintegration of Wordie Ice Shelf, Antarctic Peninsula. *The Cryosphere*, **12**, 1347–1365, 10.5194/tc-12-1347-2018.

FRIELER, K., CLARK, P.U., HE, F., BUIZERT, C., REESE, R., LIGTENBERG, S.R.M., VAN DEN BROEKE, M.R., WINKELMANN, R. & LEVERMANN, A. 2015. Consistent evidence of increasing Antarctic accumulation with warming. *Nature Climate Change*, **5**, 348–352, 10.1038/nclimate2574.

FUKUDA, T., SUGIYAMA, S., SAWAGAKI, T. & NAKAMURA, K. 2014. Recent variations in the terminus position, ice velocity and surface elevation of Langhovde Glacier, East Antarctica. *Antarctic Science*, **26**, 636–645.

FÜRST, J.J., DURAND, G., GILLET-CHAULET, F., TAVARD, L., RANKL, M., BRAUN, M. & GAGLIARDINI, O. 2016. The safety band of Antarctic ice shelves. *Nature Climate Change*, **6**, 479–482.

GAGLIARDINI, O., DURAND, G., ZWINGER, T., HINDMARSH, R.C.A. & LE MEUR, E. 2010. Coupling of ice-shelf melting and buttressing is a key process in ice-sheets dynamics. *Geophysical Research Letters*, **37**, 10.1029/2010gl043334.

GAGNÉ, M.-È., GILLETT, N.P. & FYFE, J.C. 2015. Observed and simulated changes in Antarctic sea ice extent over the past 50 years. *Geophysical Research Letters*, **42**, 90–95, 10.1002/2014GL062231.

GALLAHER, D.W., CAMPBELL, G.G. & MEIER, W.N. 2014. Anomalous Variability in Antarctic Sea Ice Extents During the 1960s With the Use of Nimbus Data. *IEEE Journal of Selected Topics in Applied Earth Observations and Remote Sensing*, **7**, 881–887, 10.1109/JSTARS.2013.2264391.

GAO, B.-C., HAN, W., TSAY, S.C. & LARSEN, N.F. 1998. Cloud detection over the Arctic region using airborne imaging spectrometer data during the daytime. *Journal of Applied Meteorology*, **37**, 1421–1429.

GARDNER, A.S., MOHOLDT, G., SCAMBOS, T.A., FAHNSTOCK, M., LIGTENBERG, S., VAN DEN BROEKE, M. & NILSSON, J. 2018. Increased West Antarctic and unchanged East Antarctic ice discharge over the last 7 years. *The Cryosphere*, **12**, 521–547, 10.5194/tc-12-521-2018.

GILES, A.B. 2017. The Mertz Glacier Tongue, East Antarctica. Changes in the past 100 years and its cyclic nature - Past, present and future. *Remote Sensing of Environment*, **191**, 30–37, 10.1016/j.rse.2017.01.003}.

GLASSER, N.F. & SCAMBOS, T.A. 2008. A structural glaciological analysis of the 2002 Larsen B ice-shelf collapse. *Journal of Glaciology*, **54**, 3–16–3–16, 10.3189/002214308784409017.

GOLDBERG, D., HOLLAND, D.M. & SCHOOF, C. 2009. Grounding line movement and ice shelf buttressing in marine ice sheets. *Journal of Geophysical Research: Earth Surface*, **114**, 10.1029/2008jf001227.

GOSSART, A., HELSEN, S., LENAERTS, J.T.M., BROUCKE, S.V., VAN LIPZIG, N.P.M. & SOUVERIJNS, N. 2019. An Evaluation of Surface Climatology in State-of-the-Art Reanalyses over the Antarctic Ice Sheet. *Journal of Climate*, **32**, 6899–6915, 10.1175/JCLI-D-19-0030.1.

GRIGGS, J.A. & BAMBER, J.L. 2011. Antarctic ice-shelf thickness from satellite radar altimetry. *Journal of Glaciology*, **57**, 485–498.

HALLEGATTE, S., GREEN, C., NICHOLLS, R.J. & CORFEE-MORLOT, J. 2013. Future flood losses in major coastal cities. *Nature Climate Change*, **3**, 802–806, 10.1038/nclimate1979.

HAN, H., IM, J. & KIM, H. 2016. Variations in ice velocities of Pine Island Glacier Ice Shelf evaluated using multispectral image matching of Landsat time series data. *Remote Sensing of Environment*, **186**, 358–371, 10.1016/j.rse.2016.09.001.

HANNA, E., NAVARRO, F.J., PATTYN, F., DOMINGUES, C.M., FETTWEIS, X., IVINS, E.R., NICHOLLS, R.J., et al. 2013. Ice-sheet mass balance and climate change. *Nature*, **498**, 51–59.

HANSON, S., NICHOLLS, R., RANGER, N., HALLEGATTE, S., CORFEE-MORLOT, J., HERWEIJER, C. & CHATEAU, J. 2011. A global ranking of port cities with high exposure to climate extremes. *Climatic Change*, **104**, 89–111, 10.1007/s10584-010-9977-4.

HAZEL, J.E. & STEWART, A.L. 2019. Are the Near-Antarctic Easterly Winds Weakening in Response to Enhancement of the Southern Annular Mode? *Journal of Climate*, **32**, 1895–1918, 10.1175/JCLI-D-18-0402.1.

HILL, E.A., CARR, J.R., STOKES, C.R. & GUDMUNDSSON, G.H. 2018. Dynamic changes in outlet glaciers in northern Greenland from 1948 to 2015. *The Cryosphere Discussions*, 1–39, 10.5194/tc-2018-17.

HOESER, T. & KUENZER, C. 2020. Object Detection and Image Segmentation with Deep Learning on Earth Observation Data: A Review-Part I: Evolution and Recent Trends. *Remote Sensing*, **12**, 1667, 10.3390/rs12101667.

HOGG, A.E. & GUDMUNDSSON, G.H. 2017. Impacts of the Larsen-C Ice Shelf calving event. *Nature Climate Change*, **7**, 540–542, 10.1038/nclimate3359.

HOLLAND, M.M. & BITZ, C.M. 2003. Polar amplification of climate change in coupled models. *Climate Dynamics*, **21**, 221–232, 10.1007/s00382-003-0332-6.

HOLT, T.O., GLASSER, N.F., QUINCEY, D.J. & SIEGFRIED, M.R. 2013. Speedup and fracturing of George VI Ice Shelf, Antarctic Peninsula. *The Cryosphere*, **7**, 373–417.

HOWAT, I.M., JOUGHIN, I., FAHNESTOCK, M., SMITH, B.E. & SCAMBOS, T.A. 2008. Synchronous retreat and acceleration of southeast Greenland outlet glaciers 2000–06: ice dynamics and coupling to climate. *Journal of Glaciology*, **54**, 646–660, 10.3189/002214308786570908.

HOWAT, I.M., PORTER, C., SMITH, B.E., NOH, M.-J. & MORIN, P. 2019. The Reference Elevation Model of Antarctica. *The Cryosphere*, **13**, 665–674, 10.5194/tc-13-665-2019.

HUGHES, T. 1981. The weak underbelly of the West Antarctic ice sheet. *Journal of Glaciology*, **27**, 518–525.

HUMBERT, A., GROSS, D., MÜLLER, R., BRAUN, M., VAN DE WAL, R.S.W., VAN DEN BROEKE, M.R., VAUGHAN, D.G. & VAN DE BERG, W.J. 2010. Deformation and failure of the ice bridge on the Wilkins Ice Shelf, Antarctica. *Annals of Glaciology*, **51**, 49–55–49–55, 10.3189/172756410791392709.

IMBIE. 2018. Mass balance of the Antarctic Ice Sheet from 1992 to 2017. *Nature*, **558**, 219–222, 10.1038/s41586-018-0179-y.

IMBIE. 2020. Mass balance of the Greenland Ice Sheet from 1992 to 2018. *Nature*, **579**, 233–239, 10.1038/s41586-019-1855-2.

JACOBS, S., GIULIVI, C., DUTRIEUX, P., RIGNOT, E., NITSCHE, F. & MOUGINOT, J. 2013. Getz Ice Shelf melting response to changes in ocean forcing. *Journal of Geophysical Research: Oceans*, **118**, 4152–4168, 10.1002/jgrc.20298.

JACOBS, S.S. 1991. On the nature and significance of the Antarctic Slope Front. *Marine Chemistry*, **35**, 9–24, 10.1016/S0304-4203(09)90005-6.

JACOBS, S.S., JENKINS, A., GIULIVI, C.F. & DUTRIEUX, P. 2011. Stronger ocean circulation and increased melting under Pine Island Glacier ice shelf. *Nature Geoscience*, **4**, 519–523.

JENKINS, A., SHOOSMITH, D., DUTRIEUX, P., JACOBS, S., KIM, T.W., LEE, S.H., HA, H.K. & STAMMERJOHN, S. 2018. West Antarctic Ice Sheet retreat in the Amundsen Sea driven by decadal oceanic variability. *Nature Geoscience*, **11**, 733–738, 10.1038/s41561-018-0207-4.

JEZEK, K.C. 2002a. RADARSAT-1 Antarctic Mapping Project: change-detection and surface velocity campaign. *Annals of Glaciology*, **34**, 263–268.

JEZEK, K.C. 2002b. RADARSAT-1 Antarctic Mapping Project: change-detection and surface velocity campaign. *Annals of Glaciology*, **34**, 263–268.

JONES, J.M., GILLE, S.T., GOOSSE, H., ABRAM, N.J., CANZIANI, P.O., CHARMAN, D.J., CLEM, K.R., et al. 2016. Assessing recent trends in high-latitude Southern Hemisphere surface climate. *Nature Climate Change*, **6**, 917–926, 10.1038/nclimate3103.

JONES, M., BROMWICH, D.H., NICOLAS, J.P., CARRASCO, J., PLAVCOVÁ, E., ZOU, X. & WANG, S.H. 2019. Sixty Years of Widespread Warming in the Southern Middle and High Latitudes (1957–2016). *Journal of Climate*, **32**, 6875–6898, 10.1175/JCLI-D-18-0565.1.

JOUGHIN, I. & ALLEY, R.B. 2011. Stability of the West Antarctic ice sheet in a warming world. *Nature Geoscience*, **4**, 506–513.

JOUGHIN, I. & MACAYEAL, D.R. 2005. Calving of large tabular icebergs from ice shelf rift systems. *Geophysical Research Letters*, **32**, L02501, 10.1029/2004GL020978.

KENNICUTT, M.C., CHOWN, S.L., CASSANO, J.J., LIGGETT, D., PECK, L.S., MASSOM, R., RINTOUL, S.R., et al. 2015. A roadmap for Antarctic and Southern Ocean science for the next two decades and beyond. *Antarctic Science*, **27**, 3–18–3–18, 10.1017/S0954102014000674.

KEYS, H.J.R., JACOBS, S.S. & BRIGHAM, L.W. 1998. Continued northward expansion of the Ross Ice Shelf, Antarctica. *Annals of Glaciology*, **27**, 93–98.

KIM, K., JEZEK, K.C. & LIU, H. 2007. Orthorectified image mosaic of Antarctica from 1963 Argon satellite photography: image processing and glaciological applications. *International Journal of Remote Sensing*, **28**, 5357–5373.

KIM, K.T., JEZEK, K.C. & SOHN, H.G. 2001. Ice shelf advance and retreat rates along the coast of Queen Maud Land, Antarctica. *JOURNAL OF GEOPHYSICAL RESEARCH-OCEANS*, **106**, 7097–7106, 10.1029/2000JC000317}.

KLINGER, T., ZIEMS, M., HEIPKE, C., SCHENKE, H.W. & OTT, N. 2011. Antarctic Coastline Detection using Snakes. *Photogrammetrie-Fernerkundung-Geoinformation*, **2011**, 421–434.

KÖNIG, M., WINTHER, J.-G. & ISAKSSON, E. 2001. Measuring snow and glacier ice properties from satellite. *Reviews of Geophysics*, **39**, 1–27, 10.1029/1999rg000076.

KONRAD, H., SHEPHERD, A., GILBERT, L., HOGG, A.E., MCMILLAN, M., MUIR, A. & SLATER, T. 2018. Net retreat of Antarctic glacier grounding lines. *Nature Geoscience*, **11**, 258–258.

KRIEGER, L. & FLORICIOIU, D. 2017. Automatic calving front delienation on TerraSAR-X and Sentinel-1 SAR imagery. *In IEEE International Geoscience and Remote Sensing Symposium (IGARSS)*.

KUENZER, C., OTTINGER, M., WEGMANN, M., GUO, H., WANG, C., ZHANG, J., DECH, S. & WIKELSKI, M. 2014. Earth observation satellite sensors for biodiversity monitoring: potentials and bottlenecks. *International Journal of Remote Sensing*, **35**, 6599–6647, 10.1080/01431161.2014.964349.

KUIPERS MUNNEKE, P., LUCKMAN, A.J., BEVAN, S.L., SMEETS, C.J.P.P., GILBERT, E., VAN DEN BROEKE, M.R., WANG, W., et al. 2018. Intense Winter Surface Melt on an Antarctic Ice Shelf. *Geophysical Research Letters*, **45**, 7615–7623, 10.1029/2018GL077899.

KUSAHARA, K. & HASUMI, H. 2013. Modeling Antarctic ice shelf responses to future climate changes and impacts on the ocean. *Journal of Geophysical Research: Oceans*, **118**, 2454–2475.

KUSSUL, N., LAVRENIUK, M., SKAKUN, S. & SHELESTOV, A. 2017. Deep Learning Classification of Land Cover and Crop Types Using Remote Sensing Data. *IEEE Geoscience and Remote Sensing Letters*, **14**, 778–782, 10.1109/LGRS.2017.2681128.

KWOK, R. & COMISO, J.C. 2002. Spatial patterns of variability in Antarctic surface temperature: Connections to the Southern Hemisphere Annular Mode and the Southern Oscillation: Antarctic Surface Temperature. *Geophysical Research Letters*, **29**, 50-1-50–54, 10.1029/2002GL015415.

KWOK, R., RIGNOT, E., HOLT, B. & ONSTOTT, R. 1992. Identification of sea ice types in spaceborne synthetic aperture radar data. *Journal of Geophysical Research: Oceans*, **97**, 2391–2402.

LAROUR, E. 2004. Modelling of rift propagation on Ronne Ice Shelf, Antarctica, and sensitivity to climate change. *Geophysical Research Letters*, **31**, L16404, 10.1029/2004GL020077.

LAVERGNE, T., SØRENSEN, A.M., KERN, S., TONBOE, R., NOTZ, D., AABOE, S., BELL, L., et al. 2019. Version 2 of the EUMETSAT OSI SAF and ESA CCI sea-ice concentration climate data records. *The Cryosphere*, **13**, 49–78, 10.5194/tc-13-49-2019.

LEA, J.M. 2018. The Google Earth Engine Digitisation Tool (GEEDiT) and the Margin change Quantification Tool (MaQiT) – simple tools for the rapid mapping and quantification of changing Earth surface margins. *Earth Surface Dynamics*, **6**, 551–561, 10.5194/esurf-6-551-2018.

LEA, J.M., MAIR, D.W.F. & REA, B.R. 2014. Evaluation of existing and new methods of tracking glacier terminus change. *Journal of Glaciology*, **60**, 323–332.

LEE, J., JIN, Y.K., HONG, J.K., YOO, H.J. & SHON, H. 2008. Simulation of a tidewater glacier evolution in Marian Cove, King George Island, Antarctica. *Geosciences Journal*, **12**, 33–39.

LEESON, A.A., FORSTER, E., RICE, A., GOURMELEN, N. & WESSEM, J.M. 2020. Evolution of Supraglacial Lakes on the Larsen B Ice Shelf in the Decades Before it Collapsed. *Geophysical Research Letters*, **47**, 10.1029/2019GL085591.

LEESON, A.A., VAN WESSEM, J.M., LIGTENBERG, S.R.M., SHEPHERD, A., VAN DEN BROEKE, M.R., KILLICK, R., SKVARCA, P., MARINSEK, S. & COLWELL, S. 2017. Regional climate of the Larsen B embayment 1980–2014. *Journal of Glaciology*, **63**, 683–690, 10.1017/jog.2017.39.

LI, R., LIU, W., YANG, L., SUN, S., HU, W., ZHANG, F. & LI, W. 2018. DeepUNet: A Deep Fully Convolutional Network for Pixel-Level Sea-Land Segmentation. *IEEE Journal of Selected Topics in Applied Earth Observations and Remote Sensing*, **11**, 3954–3962, 10.1109/JSTARS.2018.2833382.

LI, Y, ZHANG, H., XUE, X., JIANG, Y. & SHEN, Q. 2018. Deep learning for remote sensing image classification: A survey. *Wiley Interdisciplinary Reviews: Data Mining and Knowledge Discovery*, **0**, e1264, 10.1002/widm.1264.

LIANG, Q., ZHOU, C., HOWAT, I.M., JEONG, S., LIU, R. & CHEN, Y. 2019. Ice flow variations at Polar Record Glacier, East Antarctica. *Journal of Glaciology*, **65**, 279–287, 10.1017/jog.2019.6.

LIPOVSKY, B.P. 2020. Ice shelf rift propagation: stability, three-dimensional effects, and the role of marginal weakening. *The Cryosphere*, **14**, 1673–1683, 10.5194/tc-14-1673-2020.

LIU, H. & JEZEK, K.C. A complete high-resolution coastline of Antarctica extracted from orthorectified Radarsat SAR imagery. *Photogrammetric Engineering & Remote Sensing*, **70**, 605–616, 10.14358/pers.70.5.605.

LIU, H. & JEZEK, K.C. 2004a. A complete high-resolution coastline of Antarctica extracted from orthorectified Radarsat SAR imagery. *Photogrammetric Engineering & Remote Sensing*, **70**, 605–616, 10.14358/pers.70.5.605.

LIU, H. & JEZEK, K.C. 2004b. Automated extraction of coastline from satellite imagery by integrating Canny edge detection and locally adaptive thresholding methods. *International Journal of Remote Sensing*, **25**, 937–958, 10.1080/0143116031000139890.

LIU, H., WANG, L. & JEZEK, K.C. 2006. Automated delineation of dry and melt snow zones in Antarctica using active and passive microwave observations from space. *IEEE transactions on geoscience and remote sensing*, **44**, 2152–2163.

LIU, X., DENG, Z. & YANG, Y. 2018. Recent progress in semantic image segmentation. *Artificial Intelligence Review*, 10.1007/s10462-018-9641-3.

LIU, Y., MOORE, J.C., CHENG, X., GLADSTONE, R.M., BASSIS, J.N., LIU, H., WEN, J. & HUI, F. 2015. Ocean-driven thinning enhances iceberg calving and retreat of Antarctic ice shelves. *Proceedings of the National Academy of Sciences*, **112**, 3263–3268.

LONG, J., SHELHAMER, E. & DARRELL, T. 2015. Fully convolutional networks for semantic segmentation. *In IEEE Conference on Computer Vision and Pattern Recognition* – IEEE Conference on Computer Vision and Pattern Recognition. 3431–3440.

LOVELL, A.M., STOKES, C.R. & JAMIESON, S.S.R. 2017. Sub-decadal variations in outlet glacier terminus positions in Victoria Land, Oates Land and George V Land, East Antarctica (1972–2013). *Antarctic Science*, **29**, 468–483–468–483, 10.1017/S0954102017000074.

LUCKMAN, A., BENN, D.I., COTTIER, F., BEVAN, S., NILSEN, F. & INALL, M. 2015. Calving rates at tidewater glaciers vary strongly with ocean temperature. *Nature communications*, **6**.

LUDESCHER, J., YUAN, N. & BUNDE, A. 2019. Detecting the statistical significance of the trends in the Antarctic sea ice extent: an indication for a turning point. *Climate Dynamics*, **53**, 237–244, 10.1007/s00382-018-4579-3.

MACGREGOR, J.A., CATANIA, G.A., MARKOWSKI, M.S. & ANDREWS, A.G. 2012. Widespread rifting and retreat of ice-shelf margins in the eastern Amundsen Sea Embayment between 1972 and 2011. *JOURNAL OF GLACIOLOGY*, **58**, 458–466, 10.3189/2012JoG11J262}.

MAGGIORI, E., TARABALKA, Y., CHARPIAT, G. & ALLIEZ, P. 2017. Convolutional neural networks for large-scale remote-sensing image classification. *IEEE Transactions on Geoscience and Remote Sensing*, **55**, 645–657.

MARSHALL, G.J. 2007. Half-century seasonal relationships between the Southern Annular mode and Antarctic temperatures. *International Journal of Climatology*, **27**, 373–383, 10.1002/joc.1407.

MARSHALL, G.J. 2003. Trends in the Southern Annular Mode from Observations and Reanalyses. *Journal of Climate*, **16**, 10.

MARSHALL, G.J., THOMPSON, D.W.J. & BROEKE, M.R. 2017. The Signature of Southern Hemisphere Atmospheric Circulation Patterns in Antarctic Precipitation. *Geophysical Research Letters*, **44**, 11,580-11,589, 10.1002/2017GL075998.

MASON, D.C. & DAVENPORT, I.J. 1996. Accurate and efficient determination of the shoreline in ERS-1 SAR images. *IEEE Transactions on Geoscience and Remote Sensing*, **34**, 1243–1253.

MASSOM, R., REID, P., STAMMERJOHN, S., RAYMOND, B., FRASER, A. & USHIO, S. 2013. Change and Variability in East Antarctic Sea Ice Seasonality, 1979/80–2009/10 Strutton, P., *ed. PLoS ONE*, **8**, e64756, 10.1371/journal.pone.0064756.

MASSOM, R.A., GILES, A.B., WARNER, R.C., FRICKER, H.A., LEGRESY, B., HYLAND, G., LESCARMONTIER, L. & YOUNG, N. 2015. External influences on the Mertz Glacier Tongue (East Antarctica) in the decade leading up to its calving in 2010. *Journal of Geophysical Research: Earth Surface*, **120**, 490–506, 10.1002/2014JF003223}.

MASSOM, R.A., SCAMBOS, T.A., BENNETTS, L.G., REID, P., SQUIRE, V.A. & STAMMERJOHN, S.E. 2018. Antarctic ice shelf disintegration triggered by sea ice loss and ocean swell. *Nature*, **558**, 383–389, 10.1038/s41586-018-0212-1.

MATSUOKA, K., HINDMARSH, R.C.A., MOHOLDT, G., BENTLEY, M.J., PRITCHARD, H.D., BROWN, J., CONWAY, H., et al. 2015. Antarctic ice rises and rumples: Their properties and significance for ice-sheet dynamics and evolution. *Earth-Science Reviews*, **150**, 724–745, 10.1016/j.earscirev.2015.09.004.

MAZLOFF, M.R., HEIMBACH, P. & WUNSCH, C. 2010. An Eddy-Permitting Southern Ocean State Estimate. *Journal of Physical Oceanography*, **40**, 880–899, 10.1175/2009JPO4236.1.

MEDLEY, B. & THOMAS, E.R. 2019. Increased snowfall over the Antarctic Ice Sheet mitigated twentieth-century sea-level rise. *Nature Climate Change*, **9**, 34–39, 10.1038/s41558-018-0356-x.

MERCER, J.H. 1978. West Antarctic ice sheet and CO2 greenhouse effect: a threat of disaster. *Nature*, **271**, 321–325.

MEREDITH, M.P., SOMMERKORN, M., CASSOTTA, C., DERKSEN, A., EKAYKIN, A., HOLLOWED, G. & ET AL. In press. Special Report on the Ocean and Cryosphere in a Changing Climate. *In IPCC* Available at: https://www.ipcc.ch/site/assets/uploads/sites/3/2019/11/07_SROCC_Ch03_FINAL.pdf.

MILES, B.W.J., STOKES, C.R. & JAMIESON, S.S.R. 2016. Pan–ice-sheet glacier terminus change in East Antarctica reveals sensitivity of Wilkes Land to sea-ice changes. *Science Advances*, **2**, e1501350, 10.1126/sciadv.1501350.

MILES, B.W.J., STOKES, C.R. & JAMIESON, S.S.R. 2017. Simultaneous disintegration of outlet glaciers in Porpoise Bay (Wilkes Land), East Antarctica, driven by sea ice break-up. *The Cryosphere*, **11**, 427–442, 10.5194/tc-11-427-2017.

MILES, B.W.J., STOKES, C.R., JENKINS, A., JORDAN, J.R., JAMIESON, S.S.R. & GUDMUNDSSON, G.H. 2020. Intermittent structural weakening and acceleration of the Thwaites Glacier Tongue between 2000 and 2018. *Journal of Glaciology*, 1–11, 10.1017/jog.2020.20.

MILES, B.W.J., STOKES, C.R., VIELI, A. & COX, N.J. 2013. Rapid, climate-driven changes in outlet glaciers on the Pacific coast of East Antarctica. *Nature*, **500**, 563–566.

MILILLO, P., RIGNOT, E., MOUGINOT, J., SCHEUCHL, B., MORLIGHEM, M., LI, X. & SALZER, J.T. 2017. On the Short-term Grounding Zone Dynamics of Pine Island Glacier, West Antarctica, Observed With COSMO-SkyMed Interferometric Data: PIG Grounding Line Dynamics. *Geophysical Research Letters*, **44**, 10,436-10,444, 10.1002/2017GL074320.

MOEN, M.-A., DOULGERIS, A.P., ANFINSEN, S.N., RENNER, A.H.H., HUGHES, N., GERLAND, S. & ELTOFT, T. 2013. Comparison of feature based segmentation of full polarimetric SAR satellite sea ice images with manually drawn ice charts. *The Cryosphere*, **7**, 1693–1705, 10.5194/tc-7-1693-2013.

MOHAJERANI, Y., WOOD, M., VELICOGNA, I. & RIGNOT, E. 2019. Detection of Glacier Calving Margins with Convolutional Neural Networks: A Case Study. *Remote Sensing*, **11**, 1–13, 10.3390/rs11010074.

MONAGHAN, A.J. 2006. Insignificant Change in Antarctic Snowfall Since the International Geophysical Year. *Science*, **313**, 827–831, 10.1126/science.1128243.

MOON, T. & JOUGHIN, I. 2008. Changes in ice front position on Greenland's outlet glaciers from 1992 to 2007. *Journal of Geophysical Research: Earth Surface*, **113** Available at: http://dx.doi.org/10.1029/2007JF000927.

MOON, T., JOUGHIN, I. & SMITH, B. 2015. Seasonal to multiyear variability of glacier surface velocity, terminus position, and sea ice/ice mélange in northwest Greenland. *Journal of Geophysical Research: Earth Surface*, **120**, 818–833, 10.1002/2015JF003494.

MOSBEUX, C., WAGNER, T.J.W., BECKER, M.K. & FRICKER, H.A. 2020a. Viscous and elastic buoyancy stresses as drivers of ice-shelf calving. *Journal of Glaciology*, 1–15, 10.1017/jog.2020.35.

MOSBEUX, C., WAGNER, T.J.W., BECKER, M.K. & FRICKER, H.A. 2020b. Viscous and elastic buoyancy stresses as drivers of ice-shelf calving. *Journal of Glaciology*, 1–15, 10.1017/jog.2020.35.

MOUGINOT, J. 2017. MEaSURES Antarctic Boundaries for IPY 2007-2009 from Satellite Radar, Version 2, 10.5067/AXE4121732AD.

MOUGINOT, J., RIGNOT, E. & SCHEUCHL, B. 2019. Continent-Wide, Interferometric SAR Phase, Mapping of Antarctic Ice Velocity. *Geophysical Research Letters*, **46**, 9710–9718, 10.1029/2019GL083826.

NAKAMURA, K., DOI, K. & SHIBUYA, K. 2007. Why is Shirase Glacier turning its flow direction eastward? *Polar Science*, **1**, 63–71, 10.1016/j.polar.2007.09.003.

NAYLOR, S., SIEGERT, M., DEAN, K. & TURCHETTI, S. 2008. Science, geopolitics and the governance of Antarctica. *Nature Geoscience*, **1**, 143–143.

NICHOLLS, K.W., ØSTERHUS, S., MAKINSON, K., GAMMELSRØD, T. & FAHRBACH, E. 2009. Ice-ocean processes over the continental shelf of the southern Weddell Sea, Antarctica: A review. *Reviews of Geophysics*, **47**.

NSIDC. 1997. *National Snow and Ice Data Center. RAMP AMM-1 SAR Image Mosaic of Antarctica, Version 2* Available at: https://nsidc.org/data/NSIDC-0103/versions/2 [Accessed January 3, 2020].

NSIDC. 2009. *National Snow and Ice Data Center. MODIS Mosaic of Antarctica 2008-2009 (MOA2009) Image Map, Version 1* Available at: https://nsidc.org/data/NSIDC-0593/versions/1 [Accessed May 3, 2020].

OSISAF. 2020. Ocean and Sea Ice Satellite Application Facility. High Latitude Products. Sea Ice Concentration. Available at: http://osisaf.met.no/p/ice/ [Accessed February 3, 2020].

PAETH, H. & POLLINGER, F. 2010. Enhanced evidence in climate models for changes in extratropical atmospheric circulation. *Tellus A: Dynamic Meteorology and Oceanography*, **62**, 647–660, 10.1111/j.1600-0870.2010.00455.x.

PALERME, C., CLAUD, C., DUFOUR, A., GENTHON, C., WOOD, N.B. & L'ECUYER, T. 2017. Evaluation of Antarctic snowfall in global meteorological reanalyses. *Atmospheric Research*, **190**, 104–112, 10.1016/j.atmosres.2017.02.015.

PAOLO, F.S., FRICKER, H.A. & PADMAN, L. 2015. Volume loss from Antarctic ice shelves is accelerating. *Science*, **348**, 327–331.

PARKINSON, C.L. 2019. A 40-y record reveals gradual Antarctic sea ice increases followed by decreases at rates far exceeding the rates seen in the Arctic. *Proceedings of the National Academy of Sciences*, **116**, 14414–14423, 10.1073/pnas.1906556116.

PARTINGTON, K.C. 1998. Discrimination of glacier facies using multi-temporal SAR data. *Journal of Glaciology*, **44**, 41–53.

PFEFFER, W.T., HARPER, J.T. & O'NEEL, S. 2008. Kinematic Constraints on Glacier Contributions to 21st-Century Sea-Level Rise. *Science*, **321**, 1340–1343, 10.1126/science.1159099.

PRITCHARD, HD., LIGTENBERG, S.R.M., FRICKER, H.A., VAUGHAN, D.G., VAN DEN BROEKE, M.R. & PADMAN, L. 2012. Antarctic ice-sheet loss driven by basal melting of ice shelves. *Nature*, **484**, 502–505, 10.1038/nature10968.

PRITCHARD, H.D. & VAUGHAN, D.G. 2007. Widespread acceleration of tidewater glaciers on the Antarctic Peninsula. *Journal of Geophysical Research: Earth Surface*, **112**, 10.1029/2006JF000597}.

RACK, W. & ROTT, H. 2004. Pattern of retreat and disintegration of the Larsen B ice shelf, Antarctic Peninsula. *Annals of Glaciology*, **39**, 505–510.

RADIĆ, V., BLISS, A., BEEDLOW, A.C., HOCK, R., MILES, E. & COGLEY, J.G. 2014. Regional and global projections of twenty-first century glacier mass changes in response to climate scenarios from global climate models. *Climate Dynamics*, **42**, 37–58, 10.1007/s00382-013-1719-7.

RANKL, M., FÜRST, J.J., HUMBERT, A. & BRAUN, M.H. 2017. Dynamic changes on the Wilkins Ice Shelf during the 2006--2009 retreat derived from satellite observations. *The Cryosphere*, **11**, 1199–1211, 10.5194/tc-11-1199-2017.

RAPHAEL, M.N., MARSHALL, G.J., TURNER, J., FOGT, R.L., SCHNEIDER, D., DIXON, D.A., HOSKING, J.S., JONES, J.M. & HOBBS, W.R. 2016. The Amundsen Sea Low: Variability, Change, and Impact on Antarctic Climate. *Bulletin of the American Meteorological Society*, **97**, 111–121, 10.1175/BAMS-D-14-00018.1.

RAU, F., BRAUN, M., SAURER, H., GOßMANN, H., KOTHE, G., WEBER, F., EBEL, M. & BEPPLER, D. 2000. Monitoring multi-year snow cover dynamics on the Antarctic Peninsula using SAR imagery. *Polarforschung*, **67**, 27–40.

RAU, F., MAUZ, F., DE ANGELIS, H., JAÑA, R., NETO, J.A., SKVARCA, P., VOGT, S., SAURER, H. & GOSSMANN, H. 2004. Variations of glacier frontal positions on the northern Antarctic Peninsula. *Annals of Glaciology*, **39**, 525–530–525–530, 10.3189/172756404781814212.

RESSEL, R., FROST, A. & LEHNER, S. 2015. Comparing automated sea ice classification on single-pol and dual-pol terrasar-x data. *In Geoscience and Remote Sensing Symposium (IGARSS), 2015 IEEE International* – Geoscience and Remote Sensing Symposium (IGARSS), 2015 IEEE International. 3442–3445.

RIGNOT, E. 2002. Ice-shelf changes in Pine Island Bay, Antarctica, 1947-2000. *Journal of Glaciology*, **48**, 247–256, 10.3189/172756502781831386.

RIGNOT, E., JACOBS, S., MOUGINOT, J. & SCHEUCHL, B. 2013. Ice-Shelf Melting Around Antarctica. *Science*, **341**, 266–270, 10.1126/science.1235798.

RIGNOT, E., MOUGINOT, J. & SCHEUCHL, B. 2011. Ice Flow of the Antarctic Ice Sheet. *Science*, **333**, 1427–1430, 10.1126/science.1208336.

RIGNOT, E., MOUGINOT, J., SCHEUCHL, B., VAN DEN BROEKE, M., VAN WESSEM, M.J. & MORLIGHEM, M. 2019. Four decades of Antarctic Ice Sheet mass balance from 1979–2017. *Proceedings of the National Academy of Sciences*, **116**, 1095–1103, 10.1073/pnas.1812883116.

RIGNOT, E., VAUGHAN, D.G., SCHMELTZ, M., DUPONT, T. & MACAYEAL, D. 2002. Acceleration of Pine Island and Thwaites Glaciers, West Antarctica. *Annals of Glaciology*, **34**, 189–194, 10.3189/172756402781817950.

RIZZOLI, P., MARTONE, M., GONZALEZ, C., WECKLICH, C., BORLA TRIDON, D., BRÄUTIGAM, B., BACHMANN, M., et al. 2017. Generation and performance assessment of the global TanDEM-X digital elevation model. *ISPRS Journal of Photogrammetry and Remote Sensing*, **132**, 119–139, 10.1016/j.isprsjprs.2017.08.008.

ROBEL, A.A. 2017. Thinning sea ice weakens buttressing force of iceberg mélange and promotes calving. *Nature Communications*, **8**, 14596, 10.1038/ncomms14596.

RONNEBERGER, O., FISCHER, P. & BROX, T. 2015. U-Net: Convolutional Networks for Biomedical Image Segmentation. *In* Navab, N., Hornegger, J., Wells, W.M. & Frangi, A.F., *eds. Medical Image Computing and Computer-Assisted Intervention – MICCAI 2015*. Cham: Springer International Publishing, 234–241., 10.1007/978-3-319-24574-4_28.

ROSANOVA, C.E., LUCCHITTA, B.K. & FERRIGNO, J.G. 1998. Velocities of Thwaites Glacier and smaller glaciers along the Marie Byrd Land coast, West Antarctica. *Annals of Glaciology*, **27**, 47–53.

ROSE, G. & MCELROY, C.T. 1987. Coal potential of Antarctica. Australia Bureau of Mineral Resources. *Geology and Geophysics*.

ROSS, J.C. 1847. *A Voyage of Discovery and Research in the Southern and Antarctic Regions, during the Years 1839-43*. John Murray.

ROTT, H., RACK, W., NAGLER, T. & SKVARCA, P. 1998. Climatically induced retreat and collapse of northern Larsen Ice Shelf, Antarctic Peninsula Budd, W.F., *ed. Annals of Glaciology*, **27**, 86–92.

ROYSTON, S. & GUDMUNDSSON, G.H. 2016. Changes in ice-shelf buttressing following the collapse of Larsen A Ice Shelf, Antarctica, and the resulting impact on tributaries. *Journal of Glaciology*, **62**, 905–911.

RÜCKAMP, M., BRAUN, M., SUCKRO, S. & BLINDOW, N. 2011. Observed glacial changes on the King George Island ice cap, Antarctica, in the last decade. *Global and Planetary Change*, **79**, 99–109.

SAT. 2020. Secretariat of the Antarctic Treaty. *Secretariat of the Antarctic Treaty* Available at: https://www.ats.aq/index_e.html [Accessed May 13, 2020].

SCAMBOS, T.A., BELL, R.E., ALLEY, R.B., ANANDAKRISHNAN, S., BROMWICH, D.H., BRUNT, K., CHRISTIANSON, K., et al. 2017. How much, how fast?: A science review and outlook for research on the instability of Antarctica's Thwaites Glacier in the 21st century. *Global and Planetary Change*, **153**, 16–34, 10.1016/j.gloplacha.2017.04.008.

SCAMBOS, T.A., BOHLANDER, J.A., SHUMAN, C.A. & SKVARCA, P. 2004. Glacier acceleration and thinning after ice shelf collapse in the Larsen B embayment, Antarctica. *Geophysical Research Letters*, **31**, 10.1029/2004GL020670}.

SCAMBOS, T.A., FRICKER, H.A., LIU, C.-C., BOHLANDER, J., FASTOOK, J., SARGENT, A., MASSOM, R. & WU, A.-M. 2009. Ice shelf disintegration by plate bending and hydro-fracture: Satellite observations and model results of the 2008 Wilkins ice shelf break-ups. *Earth and Planetary Science Letters*, **280**, 51–60, 10.1016/j.epsl.2008.12.027.

SCAMBOS, T.A., HARAN, T.M., FAHNESTOCK, M.A., PAINTER, T.H. & BOHLANDER, J. 2007. MODIS-based Mosaic of Antarctica (MOA) data sets: Continent-wide

surface morphology and snow grain size. *Remote Sensing of Environment*, **111**, 242–257, 10.1016/j.rse.2006.12.020.

SCAMBOS, T.A., HULBE, C., FAHNESTOCK, M. & BOHLANDER, J. 2000. The link between climate warming and break-up of ice shelves in the Antarctic Peninsula. *Journal of Glaciology*, **46**, 516–530, 10.3189/172756500781833043.

SCHEUCHL, B., MOUGINOT, J., RIGNOT, E., MORLIGHEM, M. & KHAZENDAR, A. 2016. Grounding line retreat of Pope, Smith, and Kohler Glaciers, West Antarctica, measured with Sentinel-1a radar interferometry data. *Geophysical Research Letters*, **43**, 8572–8579, 10.1002/2016GL069287.

SCHILD, K.M. & HAMILTON, G.S. 2013. Seasonal variations of outlet glacier terminus position in Greenland. *Journal of Glaciology*, **59**, 759–770.

SCHODLOK, M.P., MENEMENLIS, D. & RIGNOT, E. 2016. Ice shelf basal melt rates around Antarctica from simulations and observations. *Journal of Geophysical Research: Oceans*, **121**, 1085–1109.

SCHOOF, C. 2007. Ice sheet grounding line dynamics: Steady states, stability, and hysteresis. *Journal of Geophysical Research: Earth Surface*, **112**.

SEALE, A., CHRISTOFFERSEN, P., MUGFORD, R.I. & O'LEARY, M. 2011. Ocean forcing of the Greenland Ice Sheet: Calving fronts and patterns of retreat identified by automatic satellite monitoring of eastern outlet glaciers. *Journal of Geophysical Research: Earth Surface*, **116**.

SEROUSSI, H., NAKAYAMA, Y., LAROUR, E., MENEMENLIS, D., MORLIGHEM, M., RIGNOT, E. & KHAZENDAR, A. 2017. Continued retreat of Thwaites Glacier, West Antarctica, controlled by bed topography and ocean circulation. *Geophysical Research Letters*, **44**, 6191–6199, 10.1002/2017GL072910.

SHEPHERD, A., GILBERT, L., MUIR, A.S., KONRAD, H., MCMILLAN, M., SLATER, T., BRIGGS, K.H., SUNDAL, A.V., HOGG, A.E. & ENGDAHL, M. 2019. Trends in Antarctic Ice Sheet Elevation and Mass. *Geophysical Research Letters*, **0**, 10.1029/2019GL082182.

SHEPHERD, A., IVINS, E.R., GERUO, A., BARLETTA, V.R., BENTLEY, M.J., BETTADPUR, S., BRIGGS, K.H., et al. 2012. A reconciled estimate of ice-sheet mass balance. *Science*, **338**, 1183–1189.

SHEPHERD, A., WINGHAM, D., WALLIS, D., GILES, K., LAXON, S. & SUNDAL, A.V. 2010. Recent loss of floating ice and the consequent sea level contribution. *Geophysical Research Letters*, **37**.

SIMÕES, J.C., BREMER, U.F., AQUINO, F.E. & FERRON, F.A. 1999. Morphology and variations of glacial drainage basins in the King George Island ice field, Antarctica. *Annals of Glaciology*, **29**, 220–224–220–224, 10.3189/172756499781821085.

SKVARCA, P., RACK, W., ROTT, H. & DONÁNGELO, T.I. 1999. Climatic trend and the retreat and disintegration of ice shelves on the Antarctic Peninsula: an overview. *Polar Research*, **18**, 151–157.

SLATER, T., LAWRENCE, I.R., OTOSAKA, I.N., SHEPHERD, A., GOURMELEN, N., JAKOB, L., TEPES, P., GILBERT, L. & NIENOW, P. 2021. Review article: Earth's ice imbalance. *The Cryosphere*, **15**, 233–246, 10.5194/tc-15-233-2021.

SLATER, T., SHEPHERD, A., MCMILLAN, M., MUIR, A., GILBERT, L., HOGG, A.E., KONRAD, H. & PARRINELLO, T. 2018. A new digital elevation model of Antarctica derived from CryoSat-2 altimetry. *The Cryosphere*, **12**, 1551–1562, 10.5194/tc-12-1551-2018.

SMITH, B., FRICKER, H.A., GARDNER, A.S., MEDLEY, B., NILSSON, J., PAOLO, F.S., HOLSCHUH, N., et al. 2020. Pervasive ice sheet mass loss reflects competing ocean and atmosphere processes. *Science*, eaaz5845, 10.1126/science.aaz5845.

SOHN, H.-G. & JEZEK, K.C. 1999. Mapping ice sheet margins from ERS-1 SAR and SPOT imagery. *International Journal of Remote Sensing*, **20**, 3201–3216.

SPENCE, P., GRIFFIES, S.M., ENGLAND, M.H., HOGG, A.MCC., SAENKO, O.A. & JOURDAIN, N.C. 2014. Rapid subsurface warming and circulation changes of Antarctic coastal waters by poleward shifting winds: Antarctic subsurface ocean warming. *Geophysical Research Letters*, **41**, 4601–4610, 10.1002/2014GL060613.

STEIG, E.J., DING, Q., WHITE, J.W.C., KÜTTEL, M., RUPPER, S.B., NEUMANN, T.A., NEFF, P.D., et al. 2013. Recent climate and ice-sheet changes in West Antarctica compared with the past 2,000 years. *Nature Geoscience*, **6**, 372–375, 10.1038/ngeo1778.

STEIG, E.J., SCHNEIDER, D.P., RUTHERFORD, S.D., MANN, M.E., COMISO, J.C. & SHINDELL, D.T. 2009. Warming of the Antarctic ice-sheet surface since the 1957 International Geophysical Year. *Nature*, **457**, 459–462, 10.1038/nature07669.

STEPHENSON, S. & ZWALLY, H.J. 1989. Ice-shelf topography and structure determined using satellite-radar altimetry and Landsat imagery. *Annals of Glaciology*, **12**, 162–169.

STEWART, A.L., KLOCKER, A. & MENEMENLIS, D. 2018. Circum-Antarctic Shoreward Heat Transport Derived From an Eddy- and Tide-Resolving Simulation. *Geophysical Research Letters*, **45**, 834–845, 10.1002/2017GL075677.

STUECKER, M.F., BITZ, C.M., ARMOUR, K.C., PROISTOSESCU, C., KANG, S.M., XIE, S.-P., KIM, D., et al. 2018. Polar amplification dominated by local forcing and feedbacks. *Nature Climate Change*, **8**, 1076–1081, 10.1038/s41558-018-0339-y.

SWITHINBANK, C. 1993. Airborne tourism in the Antarctic. *Polar Record*, **29**, 103–110.

SWITHINBANK, C., CHINN, T.J., WILLIAMS, R.S. & FERRIGNO, J.G. 1988. Satellite image atlas of glaciers of the world: Antarctica. U.S. Geological Survey Professional Paper 1386-B Available at: https://pubs.usgs.gov/pp/p1386b/.

SWITHINBANK, C., WILLIAMS JR., R.S., FERRIGNO, J.G., SEEKINS, B.A., LUCCHITA, B.K. & ROSANOVA, C.E. 1997. Coastal-change and glaciological map of the Bakutis Coast, Antarctica Available at: http://pubs.er.usgs.gov/publication/i2600F_ED1 [Accessed August 1, 2018].

TAMURA, T., WILLIAMS, G.D., FRASER, A.D. & OHSHIMA, K.I. 2012. Potential regime shift in decreased sea ice production after the Mertz Glacier calving. *Nature Communications*, **3**, 826, 10.1038/ncomms1820.

TEDESCO, M. 2014. *Remote sensing of the cryosphere*. John Wiley & Sons.

TEDESCO, M. & MONAGHAN, A.J. 2009. An updated Antarctic melt record through 2009 and its linkages to high-latitude and tropical climate variability. *Geophysical Research Letters*, **36**, L18502, 10.1029/2009GL039186.

TETZNER, D., THOMAS, E. & ALLEN, C. 2019. A Validation of ERA5 Reanalysis Data in the Southern Antarctic Peninsula—Ellsworth Land Region, and Its Implications for Ice Core Studies. *Geosciences*, **9**, 289, 10.3390/geosciences9070289.

THOMA, M., JENKINS, A., HOLLAND, D. & JACOBS, S. 2008. Modelling Circumpolar Deep Water intrusions on the Amundsen Sea continental shelf, Antarctica. *Geophysical Research Letters*, **35**, L18602, 10.1029/2008GL034939.

THOMPSON, D.W.J., SOLOMON, S., KUSHNER, P.J., ENGLAND, M.H., GRISE, K.M. & KAROLY, D.J. 2011. Signatures of the Antarctic ozone hole in Southern Hemisphere surface climate change. *Nature Geoscience*, **4**, 741–749, 10.1038/ngeo1296.

TINGEY, R.J. 1991. *Schematic Geological Map of Antarctica*. 1st ed. Canberra: Australien Government Publishing Service.

TRUSEL, L.D., FREY, K.E., DAS, S.B., MUNNEKE, P.K. & VAN DEN BROEKE, M.R. 2013. Satellite-based estimates of Antarctic surface meltwater fluxes: Satellite-Based Antarctic Melt Fluxes. *Geophysical Research Letters*, **40**, 6148–6153, 10.1002/2013GL058138.

TURNER, J. 2004. The El Niño–southern oscillation and Antarctica. *International Journal of Climatology*, **24**, 1–31, 10.1002/joc.965.

TURNER, J., ANDERSON, P., LACHLAN-COPE, T., COLWELL, S., PHILLIPS, T., KIRCHGAESSNER, A., MARSHALL, G.J., et al. 2009a. Record low surface air temperature at Vostok station, Antarctica. *Journal of Geophysical Research*, **114**, D24102, 10.1029/2009JD012104.

TURNER, J., BINDSCHADLER, R.A., CONVEY, P., DI PRISCO, G., FAHRBACH, E., GUTT, J., HODGSON, D.A., MAYEWSKI, P.A. & SUMMERHAYES, C. 2009b. *Antarctic Climate Change and the Environment*. Cambridge, UK: Scientific Committee on Antarctic Research (SCAR) Available at: https://www.scar.org/library/scar-publications/occasional-publications/3508-antarctic-climate-change-and-the-environment-1/file/.

TURNER, J., LU, H., WHITE, I., KING, J.C., PHILLIPS, T., HOSKING, J.S., BRACEGIRDLE, T.J., MARSHALL, G.J., MULVANEY, R. & DEB, P. 2016. Absence of 21st century warming on Antarctic Peninsula consistent with natural variability. *Nature*, **535**, 411–415, 10.1038/nature18645.

VAUGHAN, D.G., COMISO, J.C., ALLISON, I., CARRASCO, J., KASER, G., KWOK, R., MOTE, P., et al. 2013. Observations: cryosphere. *Climate change*, **2103**, 317–382.

VAUGHAN, D.G. & DOAKE, C.S.M. 1996. Recent atmospheric warming and retreat of ice shelves on the Antarctic Peninsula. *Nature*, **379**, 328–328.

VERDY, A., MARSHALL, J. & CZAJA, A. 2006. Sea surface temperature variability along the path of the Antarctic Circumpolar Current. *Journal of physical oceanography*, **36**, 1317–1331.

WALKER, C.C., BASSIS, J.N., FRICKER, H.A. & CZERWINSKI, R.J. 2015. Observations of interannual and spatial variability in rift propagation in the Amery Ice Shelf, Antarctica, 2002-14. *Journal of Glaciology*, **61**, 243–252, 10.3189/2015JoG14J151}.

WALKER, C.C., BASSIS, J.N., FRICKER, H.A. & CZERWINSKI, R.J. 2013. Structural and environmental controls on Antarctic ice shelf rift propagation inferred from satellite monitoring: Antarctic Ice Shelf Rifting. *Journal of Geophysical Research: Earth Surface*, **118**, 2354–2364, 10.1002/2013JF002742.

WALKER, C.C. & GARDNER, A.S. 2017. Rapid drawdown of Antarctica's Wordie Ice Shelf glaciers in response to ENSO/Southern Annular Mode-driven warming in the Southern Ocean. *Earth and Planetary Science Letters*, **476**, 100–110, 10.1016/j.epsl.2017.08.005.

WANG, G., CAI, W. & PURICH, A. 2014. Trends in Southern Hemisphere wind-driven circulation in CMIP5 models over the 21st century: Ozone recovery versus greenhouse forcing. *Journal of Geophysical Research: Oceans*, **119**, 2974–2986, 10.1002/2013JC009589.

WANG, L., SCOTT, K.A., XU, L. & CLAUSI, D.A. 2016. Sea Ice Concentration Estimation During Melt From Dual-Pol SAR Scenes Using Deep Convolutional Neural Networks: A Case Study. *IEEE Transactions on Geoscience and Remote Sensing*, **54**, 4524–4533, 10.1109/TGRS.2016.2543660.

WESCHE, C. & DIERKING, W. 2014. From ice shelves to icebergs: Classification of calving fronts, iceberg monitoring and drift simulation. *In Geoscience and Remote Sensing Symposium (IGARSS), IEEE International* – Geoscience and Remote Sensing Symposium (IGARSS), 2014 IEEE International. 274–277.

WESCHE, C. & DIERKING, W. 2012. Iceberg signatures and detection in SAR images in two test regions of the Weddell Sea, Antarctica. *Journal of Glaciology*, **58**, 325–339.

WESCHE, C., JANSEN, D. & DIERKING, W. 2013. Calving Fronts of Antarctica: Mapping and Classification. *Remote Sensing*, **5**, 6305–6322, 10.3390/rs5126305.

WILLIAMS, R.S., FERRIGNO, J.G., SWITHINBANK, C., LUCCHITTA, B.K. & SEEKINS, B.A. 1995. Coastal-change and glaciological maps of Antarctica. *Annals of Glaciology*, **21**, 284–290.

WINKELMANN, R., LEVERMANN, A., MARTIN, M.A. & FRIELER, K. 2012. Increased future ice discharge from Antarctica owing to higher snowfall. *Nature*, **492**, 239–242, 10.1038/nature11616.

WOUTERS, B., MARTIN-ESPANOL, A., HELM, V., FLAMENT, T., VAN WESSEM, J.M., LIGTENBERG, S.R.M., VAN DEN BROEKE, M.R. & BAMBER, J.L. 2015. Dynamic thinning of glaciers on the Southern Antarctic Peninsula. *Science*, **348**, 899–903, 10.1126/science.aaa5727.

WRIGHT, N.A. & WILLIAMS, P.L. 1974. Mineral resources of Antarctica. U.S. Department of the Interior. Geological Survey. *705*.

WU, S.Y. & LIU, A.K. 2003. Towards an automated ocean feature detection, extraction and classification scheme for SAR imagery. *International Journal of Remote Sensing*, **24**, 935–951, 10.1080/01431160210144606.

WUITE, J., NAGLER, T., GOURMELEN, N., ESCORIHUELA, M.J., HOGG, A.E. & DRINKWATER, M.R. 2019. Sub-Annual Calving Front Migration, Area Change and Calving Rates from Swath Mode CryoSat-2 Altimetry, on Filchner-Ronne Ice Shelf, Antarctica. *Remote Sensing*, **11**, 2761, 10.3390/rs11232761.

YU, H., RIGNOT, E., MORLIGHEM, M. & SEROUSSI, H. 2017. Iceberg calving of Thwaites Glacier, West Antarctica: full-Stokes modeling combined with linear elastic fracture mechanics. *CRYOSPHERE*, **11**, 1283–1296, 10.5194/tc-11-1283-2017}.

ZEMP, M., HUSS, M., THIBERT, E., ECKERT, N., MCNABB, R., HUBER, J., BARANDUN, M., et al. 2019. Global glacier mass changes and their contributions to sea-level rise from 1961 to 2016. *Nature*, **568**, 382–386, 10.1038/s41586-019-1071-0.

ZENG, Q., CAO, M., FENG, X., LIANG, F., CHEN, X. & SHENG, W. 1984. A study of spectral reflection characteristics for snow, ice and water in the north of China. *Hydrological applications of remote sensing and remote data transmission*, **145**, 451–462.

ZHANG, E., LIU, L. & HUANG, L. 2019a. Automatically delineating the calving front of Jakobshavn Isbræ from multi-temporal TerraSAR-X images: a deep learning approach. *The Cryosphere Discussions*, 1–20, https://doi.org/10.5194/tc-2019-14.

ZHANG, E., LIU, L. & HUANG, L. 2019b. Automatically delineating the calving front of Jakobshavn Isbræ from multitemporal TerraSAR-X images: a deep learning approach. *The Cryosphere*, **13**, 1729–1741, 10.5194/tc-13-1729-2019.

ZHENG, L., ZHOU, C. & WANG, K. 2020. Enhanced winter snowmelt in the Antarctic Peninsula: Automatic snowmelt identification from radar scatterometer. *Remote Sensing of Environment*, **246**, 111835, 10.1016/j.rse.2020.111835.

ZHU, X.X., TUIA, D., MOU, L., XIA, G.-S., ZHANG, L., XU, F. & FRAUNDORFER, F. 2017. Deep Learning in Remote Sensing: A Comprehensive Review and List of Resources. *IEEE Geoscience and Remote Sensing Magazine*, **5**, 8–36, 10.1109/MGRS.2017.2762307.

ZWALLY, H.J., BECKLEY, M.A., BRENNER, A.C. & GIOVINETTO, M.B. 2002. Motion of major ice-shelf fronts in Antarctica from slant-range analysis of radar altimeter data, 1978–98. *Annals of Glaciology*, **34**, 255–262–255–262, 10.3189/172756402781817653.

Eidesstattliche Erklärung

Versicherung an Eides Statt

Ich, Celia Baumhoer, wohnhaft in der Fabrikstr. 17, 81245 München mit der Matrikel-Nr. 2497130 versichere an Eides Statt durch meine Unterschrift, dass ich die Dissertation „*Glacier Front Dynamics of Antarctica - Analysing Changes in Glacier and Ice Shelf Front Position based on SAR Time Series*“ selbständig und ohne fremde Hilfe angefertigt, alle Stellen, die ich wörtlich oder dem Sinne nach aus Veröffentlichungen entnommen habe, als solche kenntlich gemacht und ich auch keine anderen als die von mir angegebenen Quellen und Hilfsmittel benutzt habe. Ich versichere an Eides Statt durch meine Unterschrift, dass ich die Regeln der Universität Würzburg über gute wissenschaftliche Praxis eingehalten habe, insbesondere, dass ich die Gelegenheit zum Promotionsvorhaben nicht kommerziell vermittelt bekommen und insbesondere nicht eine Person oder Organisation eingeschaltet habe, die gegen Entgelt Betreuer bzw. Betreuerinnen für die Anfertigung von Dissertationen sucht.

Ich versichere an Eides Statt, dass ich die vorgenannten Angaben nach bestem Wissen und Gewissen gemacht habe und dass die Angaben der Wahrheit entsprechen und ich nichts verschwiegen habe. Die Strafbarkeit einer falschen eidesstattlichen Versicherung ist mir bekannt, namentlich die Strafandrohung gemäß § 156 StGB bis zu drei Jahren Freiheitsstrafe oder Geldstrafe bei vorsätzlicher Begehung der Tat bzw. gemäß § 161 Abs. 1 StGB bis zu einem Jahr Freiheitsstrafe oder Geldstrafe bei fahrlässiger Begehung.

München, 18.08.2020

Ort, Datum

Unterschrift

Curriculum Vitae – C. Baumhoer

PERSÖNLICHE DATEN

Name:	Celia Amélie Baumhoer
Geburtsdatum/-ort:	
Anschrift:	
Telefon:	
E-Mail:	celia.baumhoer@dlr.de

BERUFLICHER WERDEGANG

ab 09/2020 — **Wissenschaftliche Mitarbeiterin**
am Deutschen Zentrum für Luft- und Raumfahrt (DLR), Abteilung Dynamik der Landoberfläche
Mitarbeit am AI-CORE Projekt
Künstliche Intelligenz für die Kryosphärenforschung

09/2017 – 08/2020 — **Promotion/ Wissenschaftliche Mitarbeiterin**
am Deutschen Zentrum für Luft- und Raumfahrt (DLR), Oberpfaffenhofen, Abteilung Dynamik der Landoberfläche
Automatisierte Ableitung von Antarktischen Gletscherfronten

04/2017 – 07/2017 — **European Space Imaging, München**
Kunden Support: Technische Angestellte

10/2016 – 03/2017 — **Masterarbeit**
am Deutschen Zentrum für Luft- und Raumfahrt (DLR), Oberpfaffenhofen, Abteilung Georisiken und zivile Sicherheit
Automatisierte Abschätzung von Hochwasservolumina

11/2014 – 02/2016 — **Studentische Hilfskraft am Geographischen Institut Bonn**
AG Klimatologie & Ökologie
Dendroecology of alpine shrubs & climate change

03/2015 – 09/2015 — **Studentische Hilfskraft am Geographischen Institut Bonn**
AG Paläohydrologie & Geomorphologie

10/2012 – 06/2014 — **Studentische Hilfskraft am Geographischen Institut Erlangen**
Isotopenlabor & Dendroökologie

SCHULISCHE und AKADEMISCHE AUSBILDUNG

09/2017 – 05/2021 — **Promotion**
Lehrstuhl für Fernerkundung, Universität Würzburg in Kooperation mit dem Deutschen Zentrum für Luft- und Raumfahrt (DLR)
Titel: Glacier front dynamics of Antarctica – Analysing changes in glacier and ice shelf front position based on SAR time-series

10/2014 – 03/2017	**Master of Science in Geographie, Friedrich-Wilhelms Universität Bonn** (Note: 1.2) **Masterarbeit**: An automated approach to estimate large-scale flood volumes based on SAR satellite imagery and different DEMs – a risk management support
10/2011 – 08/2014	**Bachelor of Science in physischer Geographie, Friedrich-Alexander Universität Erlangen-Nürnberg** (Note: 1.5) **Bachelorarbeit**: Glacier Velocities in the Mt Everest Area derived from different SAR Missions
05/2011	**Abitur am Gymnasium Grafing**

PRAKTIKA

05/2016 – 06/2016	**Remote Sensing Solutions (RSS), München** Wetland dynamics with SAR and optical imagery, land cover classification (Sentinel-2, Landsat-8), fire scar detection
03/2016 – 04/2016	**DLR, Oberpfaffenhofen** Abteilung für Georisiken und zivile Sicherheit Hochwassererkennung und -volumenberechnung
07/2014 – 08/2014	**Praktikum an der University of Louisiana at Lafayette** „How do trees respond to climate change“ (Stipendium)

AUSZEICHNUNGEN/BERUFLICHE WEITERBILDUNG

seit 10/2017	DLR Graduate Program
10/2018	ASTO Förderpreis
09/2018	Wissenschaftliche Anwendungen in Python, Aufbaukurs
06/2018	Remote Sensing Summer School, ESA, Spitzbergen
09/2017	Image Processing in Python – Advanced Course
07/2014	DAAD Rise Stipendium

SPRACHKENNTNISSE

Deutsch:	Muttersprache
Englisch	fließend in Sprache und Schrift (Au Pair in Dublin 2011, Praktikum in den USA)
Französisch	Grundkenntnisse

INTERESSEN

Taekwondo (Schwarzer Gürtel, 2. Dan), Leiten von Hochtourenkursen & Führen von alpinen Bergtouren (Trainer C Bergsteigen), Ballett (ehem. Trainerin an der FAU Erlangen), Reisen, Exkursionen, Bergsteigen in Hochgebirgsregionen z.B. Himalaya, Anden, Kaukasus, Zentralasien (Pamir & Tien Shan), Alpen etc.